Toward a Coherent Framework for the Control of Planar Biped Locomotion

by

Eric R. Westervelt

A dissertation submitted in partial fulfillment
of the requirements for the degree of
Doctor of Philosophy
(Electrical Engineering: Systems)
in The University of Michigan
2003

Doctoral Committee:
Professor Jessy W. Grizzle, Co-Chair
Professor Daniel E. Koditschek, Co-Chair
Assistant Professor R. Brent Gillespie
Associate Professor Arthur D. Kuo
Professor N. Harris McClamroch

ABSTRACT

Toward a Coherent Framework for the Control of Planar Biped Locomotion

by

Eric R. Westervelt

Co-Chairs: Jessy W. Grizzle and Daniel E. Koditschek

Planar, underactuated, biped walkers form an important domain of application for hybrid dynamical systems.

This dissertation presents the design of controllers that induce exponentially stable dynamic walking for general planar biped robots that have one degree of freedom greater than the number of available actuators during the single support phase. The within-step control action creates an attracting invariant set—a two-dimensional zero dynamics submanifold of the full hybrid model—whose restriction dynamics admits a scalar linear time invariant return map. Exponentially stable periodic orbits of the zero dynamics correspond to exponentially stabilizable orbits of the full model. Thus, walking controllers may be designed via the two-dimensional zero dynamics. A convenient parameterization of the hybrid zero dynamics is imposed through the choice of a class of output functions. Parameter optimization is used to tune the hybrid zero dynamics in order to achieve closed-loop, exponentially stable walking with low energy consumption, while meeting natural kinematic and dynamic constraints. Two additional control features are developed: 1) the ability to compose controllers that induce walking at a fixed average walking rate to obtain walking at several, discrete average walking rates with guaranteed stability during the transitions; and 2) the ability to regulate the average walking rate to a continuum of values. The general theory developed in the dissertation is experimentally verified on a five-link prototype walker, consisting of a torso and two legs with knees.

In loving memory of my grandmother, Annette Focarelli.

ACKNOWLEDGEMENTS

The process of obtaining a Ph.D. is better characterized as a group endeavor than an individual effort. I wish to express my sincere thanks to the many who made the successful completion of this work possible.

Foremost on the list is my primary advisor, Jessy Grizzle. From my very first visit to the University of Michigan he has worked tirelessly to engineer my graduate career into a success. For his patience, kindness and undeserved generosity I am deeply grateful. While this dissertation bears only my name it is truly the result of a collaboration lead by his vision and genius.

The second on the list and major contributer to this work is my co-advisor, Dan Koditschek. Dan's involvement in this work precedes my own. If it had not been for him encouraging Jessy to begin this line of work in 1998, I dare say that this dissertation would have never been. Dan's enthusiasm and never-ending stream of ideas have been an encouragement for which I am grateful.

Our collaborators in France have contributed to this dissertation both in intellectual and material ways. Carlos Canudas-de-Wit generously hosted us during our research visits, giving us free reign of his laboratory. In addition, it was on Carlos's suggestion that the output function parameter adjustment work was begun. Christine Chevallereau's mechanical insight has helped guide our understanding of what the geometry of the hybrid zero dynamics told us. Without the dedication and talent of Gabriel Buche, the experimental portion of this dissertation would have not been possible. The ideas of Franck Plestan, Yannick Aoustin, and Gabriel Abba have also contributed to this work.

My many conversations with the fellow student denizens of the Advanced Technology Laboratories (ATL) have not only been educational and pleasurable, but have also con-

tributed to this work's intellectual content. I thank Noah Cowan for his encouragement and apt mentorship right from my first days in the ATL. I am grateful for the untold hours of conversation with Rick Groff in his gentle, generous manner that have taught me an amount that is likely equal to the sum of what I learned in courses while at Michigan. His friendship and example will be sorely missed. I am thankful to Greg Sharp for freely lending his masterful programming skills, for his generous nature, and for his refreshing view of graduate school. I thank Even Leung for his programming diligence in helping me with the numerical work of this dissertation. Additional thanks are due to Richard Altendorfer, Haldun Komsuoğlu, Pei-Chun Lin, and Uluç Saranlı.

Special thanks are due to Dominic Di Toro, my uncle, who, over many years of holiday meal conversations, worked to help me understand the life of an academic. Without his encouragement, I probably never would have considered graduate school.

I thank my mother for her years of nurturing and love. Her unwavering belief in my ability has helped me through many trying times. I thank my father for instilling in me a love for investigation and a strong work ethic. Our years in the garage and basement together were the true beginning of my engineering education. I thank my entire immediate family, which also includes Krista and Mark Levesque, Jessica and Don Lussier, Sara Westervelt, and Lindsay Hanson, for their support and patience with me during my years of overusing the "I'm just a student" excuse.

I am forever in debt to Mark and Pam Douglas, Rachel Cieslak, and James MacKay, among others, for their patience and love during my investigation of Christianity. Their light lead to an effective call and subsequent justification which has been my strength through this dissertation and graduate school. I also wish to thank Bob Adgate and Chuck Roeper for their discipleship, and Donald Gray and David Plate for being the brothers I never had.

To Heather Holleman I give thanks for lending her keen eye and grammar expertise in proofreading this dissertation.

Finally, I wish to register my sentiment expressed in the words of David,

> O taste and see that the Lord is good;
> How blessed is the man who takes refuge in Him!
>
> Psalm 34:8 (NASB)

TABLE OF CONTENTS

LIST OF TABLES

Table

LIST OF FIGURES

Figure

LIST OF APPENDICES

APPENDIX

NOTATION

Modeling

N	number of robot links; also the dimension of configuration space
$\mathcal{Q}$	configuration space
$T\mathcal{Q}$	state space
$(q, \dot{q})$	generalized coordinates on $T\mathcal{Q}$
$D_{\mathrm{e}}, q_{\mathrm{e}}$, etc.	"e" denotes objects related to the extended model
π^{-1}	map from the full to reduced coordinates
x^+, q^+, etc.	"+" denotes objects related to the beginning of the stance phase
x^-, q^-, etc.	"−" denotes objects related to the end of the stance phase
K	kinetic energy
V	potential energy
L	Lagrangian
g_0	gravitation constant
Δ	impact map relating pre- and post-impact state
R	circular matrix representing the coordinate relabeling at impact
S	impact surface; also the Poincaré section
$(\hat{F}_2^{\mathrm{T}}, \hat{F}_2^{\mathrm{N}})$	impulsive forces on the swing leg end
$(F_1^{\mathrm{T}}, F_1^{\mathrm{N}})$	forces on the stance leg end
$(p_{\mathrm{H}}^{\mathrm{h}}, p_{\mathrm{H}}^{\mathrm{v}})$	Cartesian position of the hip
$(p_1^{\mathrm{h}}, p_1^{\mathrm{v}})$	Cartesian position of the stance leg end
$(p_2^{\mathrm{h}}, p_2^{\mathrm{v}})$	Cartesian position of the swing leg end
$(p_{\mathrm{COM}}^{\mathrm{h}}, p_{\mathrm{COM}}^{\mathrm{v}})$	Cartesian position of the center of mass

Zero dynamics

zero	denotes an object related to the zero dynamics
$\tilde{\mathcal{Q}}$	subset of $\mathcal{Q}$ where the decoupling matrix is invertible
Z	zero dynamics manifold
κ_i	i^{th} component of the zero dynamics vector field
ξ_i	i^{th} coordinate on the zero dynamics manifold
θ	monotonically increasing functional on $T\mathcal{Q}$
γ	functional on $T\mathcal{Q}$ such that $L_g\gamma = 0$
$\bar{\nu}$	average walking rate
P	Poincaré map
ρ	Poincaré map restricted to $S \cap Z$
σ	diffeomorphism from $S \cap Z$ to $\mathbb{R}$
z^*, ζ^*, etc.	"$*$" denotes objects related to a fixed point
M	Bézier polynomial order
α	matrix in $\mathbb{R}^{(N-1)\times(M+1)}$ of output function parameters

Additional tools

$\mathcal{D}$	domain of attraction of ρ in $S \cap Z$
invar	denotes an object related to parameters used to ensure invariance
free	denotes an object related to parameters that may be freely chosen
$\bar{\alpha}, \bar{A}$, etc.	"$\bar{\cdot}$" indicates objects related to regular parameters
A	space of all α equal to $\mathbb{R}^{(N-1)\times(M+1)}$
π	fiber bundle projection, $\pi : A \times T\mathcal{Q} \to A$
$\mathcal{S}$	fiber bundle of α with the associated Poincaré sections
$\mathcal{Z}$	fiber bundle of α with the associated zero dynamics manifolds

HYPOTHESES

The hypotheses of Chapter 2 and Chapter 3 are reproduced here for convenience.

Robot hypotheses: (page 19) The robot is assumed to be:

RH1) comprised of N rigid links with mass, connected by revolute joints with no closed kinematic chains;

RH2) planar, with motion constrained to the sagittal plane;

RH3) bipedal, with symmetric legs connected at a common point called the hips;

RH4) actuated at each joint;

RH5) unactuated at the point of contact between the stance leg and ground; and

RH6) (page 37) the model is expressed in $N-1$ *relative* angular coordinates, $(q_1, \cdots, q_{N-1})$, plus one *absolute* angular coordinate, q_N.

Gait hypotheses: (page 19) A simple walking gait satisfies that:

GH1) there are alternating phases of single support and double support;

GH2) during the single support phase, the stance leg acts as a pivot joint, that is, throughout the contact, it can be guaranteed that the vertical component of the ground reaction force is positive and that the ratio of the horizontal component to the vertical component does not exceed the coefficient of static friction;

GH3) the double support phase is instantaneous and can be modeled as a rigid contact [HM94];

GH4) at impact, the swing leg neither slips nor rebounds;

GH5) in steady state, successive phases of single support are symmetric with respect to the two legs;

GH6) walking is from left to right, so that the swing leg starts from behind the stance leg and is placed strictly in front of the stance leg at impact.

Impact model hypotheses: (page 22) The impact model of [HM94] is used under the following assumptions:

IH1) the contact of the swing leg with the ground results in no rebound and no slipping of the swing leg;

IH2) at the moment of impact, the stance leg lifts from the ground without interaction;

IH3) the impact is instantaneous;

IH4) the external forces during the impact can be represented by impulses;

IH5) the impulsive forces may result in an instantaneous change in the velocities, but there is no instantaneous change in the configuration; and

IH6) the actuators cannot generate impulses and hence can be ignored during impact.

Output function hypotheses: (page 35) A smooth output h is selected so that:

HH1) h is a function of only the configuration coordinates;

HH2) there exists an open set $\tilde{\mathcal{Q}} \subset \mathcal{Q}$ such that for each point $q \in \tilde{\mathcal{Q}}$, the decoupling matrix $L_g L_f h(q)$ is square and invertible (i.e., the dimension of u equals the dimension of y, and h has vector relative degree $(2, \ldots, 2)'$);

HH3) there exists a smooth real valued function $\theta(q)$ such that $(h(q)', \theta(q))' : \tilde{\mathcal{Q}} \to \mathbb{R}^N$ is a diffeomorphism onto its image (see Figure 6.6 for an example $\theta(q)$);

HH4) there exists at least one point in $\tilde{\mathcal{Q}}$ where h vanishes; and

HH5) (page 42) there exists a unique point $q_0^- \in \tilde{\mathcal{Q}}$ such that $(h(q_0^-), p_2^{\mathrm{v}}(q_0^-)) = (0,0)$, $p_2^{\mathrm{h}}(q_0^-) > 0$ and the rank of $[h' \; p_2^{\mathrm{v}}]'$ at q_0^- equals N.

Controller Hypotheses: (page 50) For the closed-loop chain of double integrators, $\ddot{y} = v(y, \dot{y})$,

CH2) solutions globally exist on $\mathbb{R}^{2N-2}$, and are unique;

CH3) solutions depend continuously on the initial conditions;

CH4) the origin is globally asymptotically stable, and convergence is achieved in finite time;

CH5) the settling time function[1], $T_{\mathrm{set}} : \mathbb{R}^{2N-2} \to \mathbb{R}$ by

$$\begin{aligned} T_{\mathrm{set}}(y_0, \dot{y}_0) \quad := \quad & \inf\{t > 0 \mid (y(t), \dot{y}(t)) = (0,0), \\ & (y(0), \dot{y}(0)) = (y_0, \dot{y}_0)\} \end{aligned}$$

depends continuously on the initial condition, $(y_0, \dot{y}_0)$.

[1] That is, the time it takes for a solution initialized at $(y_0, \dot{y}_0)$ to converge to the origin. The terminology is taken from [BB98].

CHAPTER 1

Introduction

Locomotion, the ability for a body to move from one place to another, is a defining characteristic of animal life. Without it, most animals could not gather food, escape danger, or mate. In the natural setting, locomotion takes on many forms, whether its in swimming amoebas, flying fruit flies, or walking humans. The diversity of animal locomotion is truly astounding and surprisingly complex [CCS00]. Yet whether by plasmasol,[1] wings, or legs, locomotion is accomplished through manipulating the body with respect to the environment. In each case, the means of locomotion is appropriate for the morphology, scale, and environment of the organism. The same is true in an artificial setting. Man-made machines that locomote are designed with their purposes and operating environments in mind: planes have wings that create lift for flight, tanks have tracks for traversing uneven terrain, automobiles have wheels for rolling efficiently, etc. In the case of environments with discontinuous ground support, such as a rocky slope or a flight of stairs, it is arguable that the most appropriate and versatile means for locomotion is legs. Legs enable the avoidance of support discontinuities in the environment by stepping over them. Moreover, legs are the obvious choice for locomotion in environments designed for humans.

[1] Plasmasol is the fluid state of cytoplasm in an amoeba. Within its body the amoeba moves plasmasol to change its shape, thereby enabling locomotion [vE01].

1.1 A brief introduction to legged locomotion

The research into legged locomotion is long and interesting, with the motivations for research varying from pure scientific inquiry [DFF+00], to advertising [Hon03]. Legged locomotion was investigated as early as 350 B.C. with Aristotle in his work *Progression of Animals* [Bar84] where he asked such questions as, "why are man and bird bipeds, but fish footless?" Evidence of the study of legged machines can be found as early as the late nineteenth century with Rygg's mechanical horse [Ryg93] that used a gear and lever system to generate a fixed gait actuated by a bicycle-like crank system. Since Aristotle and Rygg, research on legged locomotion has grown into a multidisciplinary field spanning physiology, dynamics, computer science, and robotics. Despite such great interest, there are almost no legged machines in use today, and those in use are for entertainment purposes only. Some of the industries, other than entertainment, that would benefit from legged machines are prosthetics, orthotics, defense, mining, agriculture, forestry, nuclear facilities inspection, and planetary exploration. With such a long list, why is there no proliferation of legged machines for work, i.e., for purposes other than entertainment?

The lack of legged machines for work is certainly not due to a lack of prototype development. In the past 40 years there have been hundreds of prototypes constructed, from lumbering polypeds to hopping monopeds. To give a sense of the development effort, a few of the pioneering, non-biped examples will now be highlighted; a more thorough discussion of biped prototypes will follow later. One of the earliest legged machine success stories is the quadrupedal General Electric Walking Truck constructed by Mosher [LR68] in the late 1960s. Weighing in at 1400 kg, it required an external power source to drive its hydraulic actuation. It carried a single operator who was responsible for controlling each of the twelve servo loops that controlled the legs. It was capable of a top speed of 2.2 m/s and could carry a 220 kg payload. In the early 1980s Odetics, Inc. constructed a series of electro-mechanically powered, autonomous, i.e., untethered, hexapeds serially named the Odex-1, Odex-2, and Odex-3 Functionoids. The Odex-1 weighed 160 kg and had a top speed of about 0.5 m/s [Rus83, CB87]. Also constructed in the early 1980s was Raibert's dynamically balancing monoped hopper [Rai84, Rai86]. It was capable of a top speed of 1.2

m/s and weighed 8.6 kg (neglecting the weight of the boom used to constrain the hopper's motions to be planar and the weight of the external power source and computation). Raibert also built a very successful three-dimensional version of his monoped hopper, as well as polypedal versions with two and four legs. Constructed in the mid 1980s and weighing in at 2700 kg, one of the largest legged machines is Ohio State's hexapedal, hydraulicly actuated Adaptive Suspension Vehicle (ASV) [SW89]. It operated autonomously with a top speed of 3.6 m/s and could carry a 220 kg payload. In contrast to Mosher's Walking Truck, the ASV utilized digital feedback control to ease the burden on the operator. In addition to this list of pioneering machines there have been a host of others developed. For more complete treatments of legged machine history see [Tod85, Rai86, KW89, Ros94, Ber03, VBSS90].

Despite the nearly half-century of design efforts, no legged machines have made their way into sectors where their utility exceeds their novelty. It is conjectured here that the main factor contributing to the slow development of usable legged machines is the difficulty of simultaneously achieving energy efficiency and stability,[2] both important attributes for an autonomous vehicle.

For autonomous vehicles, greater energy efficiency translates into the ability to travel farther and longer. Energy efficiency may be achieved in two ways: by machine design and by using (automatic) control to maximize the machine's potential for efficiency. For example, consider the modern automobile. In the years since the Model T, both redesign and control have been used to improve fuel economy. Modern automobiles are lighter, more aerodynamic, and have more efficient engines. To boost fuel economy modern automobiles also use control to regulate spark timing, meter fuel, etc. The same idea applies to legged machines. Legged machines can be made efficient through the use of light materials, efficient actuators, and improved mechanical design. Through the use of control, a legged machine's gait may be designed and tuned to yield efficient locomotion.

Stability is also of great concern. A vehicle that overturns may damage itself and whatever it falls onto. Of course, any autonomous vehicle will overturn given sufficiently unfavorable circumstances. The objective of vehicle design and control is to maximize

[2]Until later in the discussion, "stability" is used to mean that the machine does not overturn. By "more stable" it is meant that the machine is further, in some sense, from overturning, and by "less stable" it is meant that the machine is closer, in some sense, to overturning.

stability, that is, to minimize the chance of overturning.

Again, consider the evolution of the modern automobile. Stability is increased by using suspensions with designs and components that maintain the wheels in contact with the driving surface. Also in use are stability control systems that use the braking system to prevent side-skidding and wheel slippage. In a similar way, legged machines may be designed to have morphologies that enhance stability, for example, feet can be made larger and the number of legs increased. Control may be used to impose gaits that, under some assumptions, have guarantees of stability. Typically, this has been accomplished by controlling the machine's motion to be slow. Slowing the motion minimizes inertial effects so that quasi-static stability measures may be used.

The slow development of legged machines for work arises because machine and control design choices that ensure stability tend not to be ones that give energy efficiency, and vice versa. For example, consider a person walking with snowshoes on fresh, powdery snow. The snowshoes help prevent tipping over by increasing the snowshoer's support polygon.[3] Also to prevent tipping over, the snowshoer uses a slower, more laborious gait than he would if he were walking on a hard surface. By using slower motions and a broader support polygon he is able to maintain stability by keeping his center of pressure[4] (COP) within his support polygon. The same principles are at work in the General Electric Walking Truck, the Odex Functionoids, the Adaptive Suspension Vehicle, and many of the bipeds to be described shortly. Stability is maintained simply by ensuring that the COP is within the support polygon. In the case of polypeds with four or more legs, the support polygon is usually large because of sprawled posture and enough legs to maintain a support tripod; however, as speed increases or the support polygon decreases in size, the COP generally leaves the support polygon making stability difficult to assess. This is the case with bipeds that walk with dynamic gaits and the reason, among others, why almost no biped robots currently walk with such gaits.

[3]The support polygon is the convex hull of the vehicle's ground contact points.

[4]The center of pressure is defined as the point on the ground where the resultant of the ground-reaction force acts [Gos99]. In the legged robotics literature, the COP is often referred to as the Zero Moment Point (ZMP) [VBSS90].

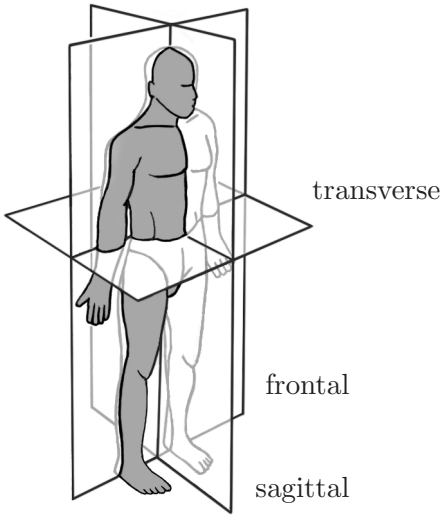

Figure 1.1: The human planes of section. The sagittal plane is the longitudinal plane that divides the body into right and left sections. The frontal plane is the plane parallel to the long axis of the body and perpendicular to the sagittal plane that separates the body into front and back portions. A transverse plane is a plane perpendicular to sagittal and frontal plane.

1.2 Robotic biped locomotion

The subject of this dissertation is the design of controllers to regulate dynamic gaits with *a priori* known stability properties in a class of biped robots. By "*a priori*" it is meant that the closed-loop system's stability is known—under certain assumptions—before the control is simulated or implemented. This section will proceed by first establishing some nomenclature and then by giving an overview of the biped robot prototype and control development efforts.

Here, a biped is a kinematic chain consisting of two sub-chains called *legs* and, often, a sub-chain called the *torso*, all connected at a common point called the *hip*. One or both of the legs may be in contact with the ground. When only one leg is in contact with the ground, the contacting leg is called the *stance leg* and the other is called the *swing leg*. The end of a leg, whether it has links constituting a foot or not, will often be referred to as a *foot*. *Single support* or *swing phase* is defined to be the phase of locomotion where only one

foot is on the ground. Conversely, *double support* is the phase where both feet are on the ground. *Walking* is then defined as alternating phases of single and double support.

The *sagittal plane* is the longitudinal plane that divides the body into right and left sections. The *frontal plane* is the plane parallel to the long axis of the body and perpendicular to the sagittal plane that separates the body into front and back portions. A *transverse plane* is a plane perpendicular to sagittal and frontal plane. See Figure 1.1 for an illustration of these planes of section. A *planar* biped is a biped with motions taking place only in the sagittal plane. Whereas a three-dimensional walker has motions taking place in both the sagittal and frontal planes. A *statically stable* gait is one where the biped's COM does not leave the support polygon. A *quasi-statically stable* gait is one where the biped's COP does not leave the support polygon. Loosely, a *dynamically stable* gait is a periodic gait where the biped's COP leaves the support polygon and yet the biped does not overturn.

In recent years, there has been a large effort in the development of biped robot prototypes and in the control and analysis of biped robot gaits. An overview of the literature on biped robot prototypes and control and analysis will now be given. The literature may be largely divided into two categories: the analysis of passive walking—walking where gravity alone powers the walking motion—and the analysis and control of non-passive walking—walking that requires an external power source. The presentation will begin with work on passive, or semi-passive walking, then continue with a presentation on the development of non-passive walkers and conclude with a presentation of the various control schemes proposed.

The work on passive walking is motivated by the drive for energy efficiency. In passive walking, dissipation due to impacts or damping is offset by the use of potential energy supplied by walking down a slope. Research in passive walking appears to have originated by McGeer in the late 1980s [McG90, McG93]. In his seminal work, McGeer built a four-link planar passive walker and performed a detailed parameter variation and stability analysis. McGeer's mechanism featured locking knees to prevent leg collapse and circular feet to give a rolling ground contact. It weighed 3.5 kg, was 0.5 m tall, and could stably walk down a 1.4 degree slope at about 0.4 m/s. Garcia, Chatterjee, and Ruina [GCR00] duplicated McGeer's mechanism and performed detailed analysis of its dynamics and the dynamics of several other passive walkers with similar morphologies. In the late 1990s Goswami, Espiau,

and Keramane [GEK96] showed that the so-called compass gait walker, a two-link planar passive walker with prismatic legs, can also exhibit stable gaits. By adding a torque acting between the legs and adding control to regulate the biped's total energy, they were able to increase the passive gait's basin of attraction. Also for the compass gait walker, Thuilot, Goswami, and Espiau [TGE97] showed that this model can exhibit gait bifurcations and apparent chaos under certain conditions. For a model similar to the compass gait walker but with circular feet and fixed damping and adjustable compliance in series with the stance leg, van der Linde [van98] showed that by actively adjusting the leg compliance, the magnitude of the velocity discontinuities which occur upon swing leg touchdown may be reduced. Howell and Baillieul [HB98] investigated a planar, semi-passive three-link model with two legs and a torso. With a single actuator to hold the torso parallel to the ground, they found that this model can also exhibit gait bifurcations. As an approximation to walking in three-dimensions, Smith and Berkemeier [SB98] studied a three-dimensional, spoked, rimless wheel of finite width rolling down a slope. They showed that this tinker toy-like model is capable of an asymptotically stable rolling motion. At the end of the 1990s, Collins built a three-dimensional version of McGeer's passive walker. Collin's walker weighed 4.8 kg and measured 0.85 m in height [CWR01]. With carefully designed feet and pendular arms, it was able to walk down a 3.1 degree slope at about 0.5 m/s. Most recently, Adolfsson, Dankowicz and Nordmark [ADN01] studied a passive, three-dimensional model by beginning with McGeer's planar model and gradually transforming the model into a ten-DOF, three-dimensional model. In this way, stable gaits of the three-dimensional model were found. Gait stability under parameter variations was also investigated. Though it is important and interesting to investigate the properties of passive bipeds and their gaits, any practical biped will require energy input.

In recent years, there has been a large effort in the development of non-passive biped robot prototypes lead by the Japanese. Some of the more noteworthy walkers reported in the literature will now be highlighted in rough chronological order. The first reported biped capable of walking is the WL-5, a three-dimensional, 11-DOF walker constructed by Kato and Tsuiki at Waseda University in Japan in 1972 [KT72]. By the mid-1980s, the same group developed the WL-10RD, a three-dimensional, a 12-DOF walker weighing 80 kg and

capable of walking at about 0.1 m/s [TIYK85]. In the mid-1980s, Miura and Shimoyama [MS84] constructed a series of bipeds, Biper-1 through Biper-5, that—at least some of which—were capable of walking. The bipeds ranged in complexity from planar walkers, Biper-1 and Biper-2, to a three-dimensional walker with all computational facilities on board, Biper-5. Both Biper-3 and Biper-4 weighed about 3 kg and were 0.3 m in height; presumably the rest of the bipeds, which were not documented, were about the same scale. Also in the mid-1980s, Furusho and Masubuchi [FM86] constructed Kenkyaku, a planar, five-link biped weighing about 23 kg and measuring 0.7 m in height. Kenkyaku had four actuators, at the hip and knees, with no actuation provided between the ground and the biped. It was reported to be able to walk at 0.8 m/s. In the late 1980s, Furusho and Sano constructed BLR-G2, a nine-link, three-dimensional biped [FS90, SF90]. It weighted 25 kg and was 0.97 m in height. It was capable of walking at 0.18 m/s. Early in the 1990s, Kajita and Tani built Meltran II, a planar, four-DOF biped weighing 4.7 kg and 0.45 m in height [KYK92, KT96]. It was capable of walking successfully over small obstacles at a speed of 0.2 m/s. In the late 1990s, Pratt, at the MIT Leg Lab, built a planar, seven-link walker with feet named Spring Flamingo. It weighed 14 kg and measured 1.2 m in height [PCT$^+$01, Pra00]. Spring Flamingo was capable of walking at 1.2 m/s, traversing a sloped terrain and featured series elasticity purposefully included in between the actuator and load [PW95]. Also in the late 1990s, the Technical University of Munich began development of Johnnie, a 23-DOF, three-dimensional walker weighing 40 kg and measuring 1.8 m in height [GLP00, PLG02]. To date, Johnnie has been able to walk at approximately 0.4 m/s. Beginning in the mid-1990s, a French group at INRIA constructed BIP, a 15-DOF, three-dimensional walker weighing about 100 kg and measuring 1.7 m in height [Esp97]. Currently, BIP is unable to walk. In the late-1990s, the CNRS and the French National Research Council constructed RABBIT, a five-DOF, planar walker weighing 32 kg and measuring 1.2 m in height [CAA$^+$02]. RABBIT's stated purpose is to serve as a test bed for the study of control issues related to biped walking and running: impacts, limit cycles, and hybrid systems. RABBIT is the prototype on which the experiments in Chapter 6 were performed. Following in the series of prototypes that began with the WL-5, the Humanoid Robotics Institute formed at Waseda University in 2000 has most recently developed WABIAN [HNK$^+$98,

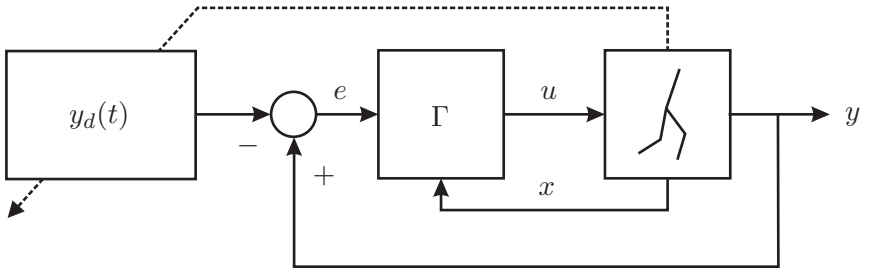

Figure 1.2: Block diagram of a trajectory tracking controller. The controller Γ forces the error $e = y - y_d$ to zero so that output y tracks the desired trajectory $y_d(t)$. The dashed line indicates that the trajectories $y_d(t)$ may be modified through some heuristic based upon the robot's state.

TTN+99, YSIT99]. WABIAN is a three-dimensional biped weighing 107 kg and measuring 1.84 m in height. It has 52-DOF and is capable of walking at 0.21 m/s. By far the most impressive biped to date is ASIMO (standing for Advanced Step in Innovation MObility) developed by the Honda Corporation [Hon03, HHHT98]. ASIMO is an autonomous three-dimensional walker with 26-DOF weighing 43 kg and measuring 1.2 m in height and is capable of walking at 0.3 m/s on level ground and climbing and descending stairs. ASIMO's development began in the mid-1980s and continues to the present day. The development has involved ten generations of prototypes, named E0 through E6 and P1 through P3, and has cost tens of millions of dollars. Following Honda's success, the Japanese government began the Humanoid Robot Project (HRP) in an attempt to grow Japan's service robot sector. Most recently, the HRP project has produced HRP-2, a three-dimensional, 30-DOF biped weighing 54.1 kg and measuring 1.55 m in height [KKK+02b, KKK+02a]. With the recent flurry of activity in Europe and Japan, it will be exciting to see what the prototype development effort produces.

An integral but unseen component of each non-passive biped is its control. From the literature, several categories of control algorithms appear. They fall into two groups: time-dependent and time-invariant algorithms. By far, the most popular algorithms are time-dependent and involve the tracking of pre-computed trajectories, see Figure 1.2. To control dynamic walking in Biper-3, Miura and Shimoyama [MS84] approximated the biped as a linearized inverted pendulum and used trajectory tracking. The dynamic walking this

approach produced might best be described as a shuffle. Katoh and Mori [KM84] demonstrated numerically that using PID control to track refence trajectories generated by a van der Pol's oscillator induced walking in a model of BIPMAN, a planar, four-DOF biped with prismatic legs. Upon implementation, BIPMAN is reported to have only successfully taken one step. Using PID control, Furusho and Masubuchi [FM86] were able to control walking in Kenkyaku by tracking piecewise linear joint reference trajectories. Furusho and Sano [FS90, SF90] were able to control walking in the three-dimensional BLR-G2 by using decoupled control for the frontal and sagittal planes. In the frontal, plane PID control was used to stabilize the upright configuration. In the sagittal plane, joint trajectory tracking was used regulate the robot's angular momentum to be that of an inverted pendulum. To control walking in Meltran II, Kajita et al. [KYK92, KT96] used PID control to track trajectories generated by a length varying inverted pendulum. The pendulum's length was varied to maintain the biped's COM a constant height above the walking surface. To control walking in a three-link, three-DOF planar biped with telescoping legs, Grishin et al. [GFLZ94] used PID control to track pre-computed trajectories that were modified online. To control walking in a planar, five-DOF biped, Mitobe et al. [MMAN95] used computed torque to regulate the biped's COM and swing leg end position. To control walking in a planar, five-DOF biped, Raibert, Tzafestas, and Tzafestas [RTT93] compared in simulation the performance of 1) PID, 2) computed torque, and 2) sliding mode control in the tracking of piecewise linear joint trajectories. In simulation, Fujimoto [FOK98, FK98] used trajectory tracking augmented with foot force control to control walking in a three-dimensional, 20 axis biped. In simulation, to control walking in a three-dimensional biped, Park and Kim [PK98] used computed torque with gravity compensation to track reference trajectories generated by a length varying inverted pendulum. In a similar scheme, Kajita et al. [KKK$^+$01, KKK$^+$02a] tracked trajectories generated by an inverted pendulum to control walking in HRP-2. To simplify the analysis, the pendulum height was constrained to be constant. One of the most pervasive schemes used to augment trajectory tracking controllers or to analyze their stability is the so-called Zero Moment Point (ZMP) criterium [VBSS90]. The ZMP is defined to be the point on the ground where the resultant of the ground-reaction force acts and is, consequently, always contained in the robot's support

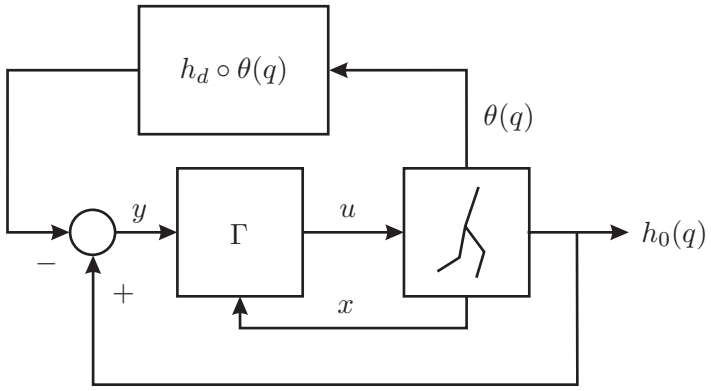

Figure 1.3: Block diagram of a time invariant controller. The controller Γ forces the signal $y = h_0(q) - h_d \circ \theta(q)$ to zero so that the signal $h_0(q)$ tracks the function $h_d \circ \theta(q)$.

polygon [Gos99]. The ZMP criterium states that when the ZMP is contained within the interior of the support polygon, the robot is stable, i.e., will not topple. The ZMP criterium has been used to augment trajectory tracking in WABIAN [LYT00, YSIT99] and ASIMO [HHHT98]. The ZMP criteria has also been used to analyze the stability of the control algorithms of [KKK$^+$01, KKK$^+$02a, PK98].

In addition to the various time-dependent trajectory tracking algorithms, there have been several other time-invariant control schemes proposed, see Figure 1.3 for an example. In simulation, Hürmüzlü [Hür93a, Hür93b] constrained the motion of a planar, five-link biped by imposing various constraints parameterized by the robot's state. This permitted a detailed study of the resulting gait and its stability properties. To control dynamic walking in Spring Flamingo, Pratt et al. [PCT$^+$01] used what they termed "virtual model control." Virtual model control uses intuitive constraints designed *ad hoc* that are switched according to a state machine driven by the robot's state. The results of this approach are impressive, but it is unclear how stability is achieved or how to improve robustness or energy efficiency. For the compass gait walker, Spong [Spo99] used a potential energy shaping, passivity-based feedback to render passive gaits slope invariant. Spong and Bullo [Spo99, SB02] then extended the result to a class of three-dimensional walkers of arbitrary DOF. Ono, Takahashi, and Shimada [OTS01] successfully controlled dynamic walking in a four-link, planar biped with locking knees by using the single actuator at the hip to slave the crotch

angle (the angle between the legs) to be a function of the swing leg tibia angle (see also [OYI01] where this idea is applied to the Acrobot). Using this algorithm, the 0.8 m biped walked at a 0.29 m/s. In simulation, Chevallereau [Che03b] controlled walking in RABBIT by using essentially a trajectory tracking scheme but with the important difference that the feedback's dependence on time was removed by time-scaling the pre-computed trajectories. In pursuit of analytical rigor, Grizzle, Abba, and Plestan [GAP01] controlled walking in a planar, three-link five-DOF model with no feet and no actuation between the biped and ground by imposing holonomic constraints on the robot's configuration parameterized by a monotonically increasing function of the robot's state. In doing so, the stability analysis problem was reduced from a 5-dimensional to a scalar Poincaré return map. This dissertation generalizes and extends this approach. Finally, note that nearly all the time-dependent trajectory tracking algorithms that were successfully applied to prototypes induce quasi-statically stable walking, while the two time-invariant schemes [GAP01, PCT$^+$01, OTS01] induce dynamic walking.

Comparing the relatively slow development of algorithms that control dynamic walking with the rapid development of sophisticated prototypes makes one wonder why this discrepancy exists when control is an integral aspect of a functioning biped. Given the sophistication of prototypes like ASIMO and HRP-2, it would seem appropriate to expect a coherent framework for the control of dynamic walking which is able to balance the tradeoff between stability and energy efficiency. It is conjectured here that this has not happened for five reasons that are *inherent* to dynamic biped walking. The five difficulties are divided into two groups. The first three difficulties are common to all aspects of biped walking while the final two are common only to dynamic biped walking.

The first difficulty is *limb coordination*. Bipeds are typically high DOF mechanisms but the task of biped walking is inherently a low DOF task. That is, bipeds typically have many links and joints that must be coordinated to achieve locomotion—the moving of the robot's COM from one point to another. The second difficulty is *effective underactuation* during the phase of single support. Unlike traditional robotic manipulators which are securely fastened to the environment, bipeds are designed to move with respect to the environment. Unilateral constrains severely limit the amount of torque that may be supplied at the stance leg ankle

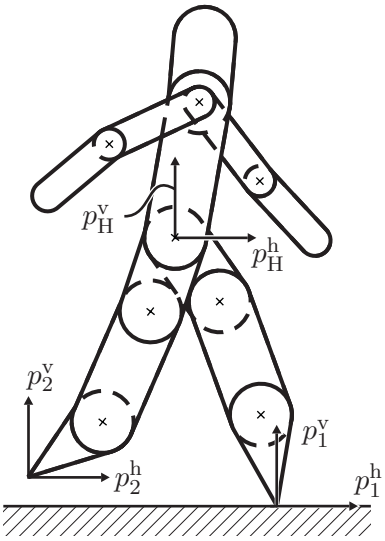

Figure 1.4: A higher DOF planar robot model. Cartesian coordinates are indicated at the hip and the leg ends.

joint; because of finite foot size, too large a torque supplied at the angle joint results in foot roll-over. This has been recognized in [FS90, HKK+99, KT96, Gos99]. The third difficulty is *hybrid dynamics*. The presence of impacts and changing dynamic constraints during the walking cycle due to foot touchdown and lift-off necessarily lead to models that are hybrid.

The final two difficulties are common only to dynamic biped walking. The first is *static instability* of the biped during portions of the walking cycle. That is, in dynamic walking the projection of the biped's COM—and usually the COP—onto the walking surface is outside of the biped's polygon of support during portions of the walking cycle. This prohibits the use of the popular ZMP criterium to ensure stability. The second, and final, difficulty is the *design of limit cycles*. Dynamically stable walking corresponds to the existence of limit cycles in the biped's state space. The design of controllers that induce limit cycles, while a challenge in its own right, is made significantly more difficult by the first four difficulties and by the need for energy efficiency.

Following Grizzle, Abba, and Plestan [GAP01], the approach of this dissertation has been to study a class of bipeds robots whose model is only as complex as required to capture these inherent difficulties. The class of bipeds are planar bipeds consisting of a rigid, N-link open kinematic chain and thus have N-DOF during the stance phase (see Figure 1.4).

Restricting attention to the sagittal plane is reasonable since the sagittal plane dynamics are almost decoupled from those in the frontal plane in the sense that stability in the frontal plane can be achieved with only frontal plane control actions, such as step width control [FS90, Kuo99, BK00]. Therefore, it seems reasonable to expect that a control algorithm to stabilize walking in the sagittal plane may be coupled with an algorithm to stabilize motions in the frontal plane to achieve stable three-dimensional walking. The class of robots studied here are assumed to have point feet with no actuation between the stance leg end and the ground, and actuation at all internal joints is assumed. By this assumption, static, or quasi-static walking is nearly impossible[5] thus requiring any walking to be dynamic. The model for the swing phase of walking is therefore that of an underactuated mechanical system and is not locally controllable. Developing controllers to regulate walking in a robot without feet is interesting since a controller designed in this way may be used as an inner control loop for a robot with feet. An outer control loop can then be designed to exploit the additional torque available at the ankle to improve the robustness properties of the overall closed-loop system. Finally, the phase of double support is assumed to be instantaneous and modeled by a rigid contact model [HM94].

1.3 Contributions

This dissertation introduces an important improvement over the work of Grizzle, Abba, and Plestan [GAP01] by giving a common framework for stability analysis and performance enhancement. The framework provides systematic design of feedback controllers that achieve exponentially stable walking motions in the class of planar biped models described above while affording adjustment of additional figures of merit—for example, energy consumption—as well. Specifically, a within-step controller is devised whose closed loop incorporates a two-dimensional submanifold—the zero set of an appropriately parameterized output map—that is an attracting invariant set with respect to the full hybrid model. The selection of this zero dynamics through the choice of output map parameters enables the

[5]The only class of gaits where static walking would be possible are ones where the biped's COP is over the stance leg end for the entire phase of single support and the double support phase is assumed to be of finite duration, i.e., non-instantaneous.

choice of practicable kinematic, torque, and power ranges, all while respecting the guarantee of an exponentially stable step. Two additional features are developed: 1) the ability to compose the above controllers to obtain walking at several discrete average walking rates with guaranteed stability during the transitions, and 2) use of an event-based PI controller that acts step-to-step giving the ability to regulate the robot's average walking rate to a continuum of values and to reject disturbances.

In the broader spectrum of dynamically dexterous machines, this work builds on the ideas of Koditschek et al. [NFK00, BKK90, KB91, RK96] where the goal is not to prescribe the dynamics of systems via reference trajectories—as is often done in the control of legged locomotion—but rather to encode the dynamic task via a lower dimensional target, itself represented by a set of differential equations. Given the demonstrated appearance of internal dynamical models in the animal nervous system [Kaw99], and the emerging evidence that these models incorporate a state-event based (as opposed to explicit time-dependent) representations of the plant [CMI99], it seems plausible to hypothesize that task encoding via internal target dynamics may also play a significant role in animal motor control [FK99]. Previous work on legged locomotion has attempted to encode the task of walking via internal target dynamics without clearly articulating or exploiting its full potential. Sano and Furusho [SF90] regulated angular momentum as a means of inducing locomotion; Goswami, Espiau, and Keramane [GEK96] regulated total energy; and Kajita and Tani [KT96] approximated the robot as an inverted pendulum, regulating its center of mass. Ono, Takahashi, and Shimada [OTS01] slave the control to one of the states of the system, instead of time. Pratt et al. [PCT$^+$01, PP98] achieved a reduction in complexity through their virtual model control. Although in that work, the "target" is first order (gradient) dynamics, the leg transitions are imposed by event-driven logic, and it is unclear over what range of initial conditions and perturbations the physical second order hybrid closed loop system may ultimately succeed in maintaining a stable gait. In all such approaches, mechanisms comparable to those developed here impose kinematic or dynamic constraints, enforcing, over the Lagrangian (i.e., away from impact conditions) portion of the state space, low dimensional attracting submanifolds. Here, in contrast, as in [BKK90, RK96, NFK00], the attracting submanifold is also designed to be an invariant set

of the Lagrangian portion of the closed-loop system whose restriction dynamics (the zero dynamics in this dissertation) emerge from the robot's motion itself. However, unlike any previous work, in this dissertation, the full hybrid zero dynamics (i.e., the entire reduced order motion of the mechanism including both the Lagrangian and the impact portions) is rendered invariant. In this sense, the present results combine the analytical machinery developed in [GAP01, PGWA01] with the notion of a dynamically targeted postural prescription [SSK98, NFK00] to provide the first rigorous methodology for a lower-dimensional hybrid target dynamics. Note that [Spo99] can be interpreted as providing a similar result for fully actuated systems and a target dynamics having the same dimension as the system being controlled.

The notion of hybrid zero dynamics is an extension of the notion of zero dynamics for systems described by ordinary differential equations. While the zero dynamics for a system modeled by ordinary differential equations is a well known [Isi95] and increasingly used concept, [BF99, IMT00, Spo95, RFAGCL00], the hybrid zero dynamics is a novel notion developed in this dissertation to deal with the impact map that is common in legged locomotion models. The hybrid zero dynamics may be defined analogously to the zero dynamics: the largest internal dynamics compatible with the output being identically zero. A central contribution of the dissertation is to establish a constructive approach to the definition of *hybrid* zero dynamics resulting in useful controllers for robotic walking. The zero dynamics of the swing phase portion of the model have been previously studied in [MS01] in the context of trajectory planning and tracking for an underactuated biped.

The theoretical framework was experimentally verified on the planar biped prototype RABBIT. The ability to systematically generate controllers with desired kinematic and dynamic properties enabled the direct implementation of controllers that successfully induced stable walking.

1.4 Organization of dissertation

Chapter 2 introduces the class of models treated by this dissertation. Chapter 3 casts the gait coordination problem as an output function design problem which results in nontrivial

zero dynamics. The model's impact map is incorporated into the notion of zero dynamics resulting in the definition of the hybrid zero dynamics. The Poincaré return map for the hybrid zero dynamics is calculated. Chapter 4 makes the results of Chapter 3 practicable by specializing the outputs to an almost linear structure utilizing Bézier polynomials. The use of polynomials finitely parameterizes the outputs which enables them to be automatically designed using standard parameter optimization techniques. Chapter 5 provides two additional control features: 1) the ability to compose controllers that induce walking at a fixed average walking rate to obtain walking at several, discrete average walking rates with guaranteed stability during the transitions; and 2) the ability to regulate the average walking rate to a continuum of values. Chapter 6 describes the experimental verification of the theoretical framework developed in Chapters 2–5 on a prototype biped, RABBIT. Chapter 7 is the conclusion. Appendix A gives the equations of motion of a 4-DOF model of a 2-link walker. Appendix B gives pseudocode for the implementation of the optimization scheme given in Chapter 4. Appendix C presents a novel means of proving decoupling matrix invertibility in an open set about the robot's trajectories. Appendix D gives the equations of motion of a 5-DOF model of the prototype biped RABBIT. Appendix E gives an overview of the method of Lagrange for deriving the swing phase equations of motions. Appendix F gives a convenient scheme for the automatic generation of `m`-files from symbolic MATLAB code. Appendix G describes the effect of gear reducers on the robot's swing phase model. Appendix H are the plots for the experiments described in Chapter 6. Finally, Appendix I gives some preliminary results on running.

Note that the main results of Chapters 3 and 4 have been published in [WGK03], and the main results of Chapter 5 have been published in [WGCdW03].

CHAPTER 2

Modeling

This chapter introduces the class of biped walking models treated in this dissertation. The class consists of planar open kinematic chain robots comprised of two symmetric open sub-chains called the legs and a third sub-chain called the torso all connected at a single joint called the hip. As depicted in Figure 1.4, intentionally suggestive of a human figure, conditions that guarantee the torso remains free in the air, while the legs alternate in ground contact will be imposed. All motions will be assumed to take place in the sagittal plane and consist of successive phases of single support and double support.

The two phases of the walking cycle naturally lead to a mathematical model of the biped consisting of two parts: the differential equations describing the dynamics during the single support phase, and a model of the dynamics of the double support phase. To avoid the "stiffness" associated with including a second differential equation to model the rapid evolution of the robot's state at the impact time [Bro96, MO96, Rou98], it will be assumed that the transition from one leg to another takes place in an infinitesimal length of time [EG94, SG92]; this assumption entails the use of a rigid contact model to describe the impulsive nature of the impact of the swing leg with the ground. The rigid contact model effectively collapses the double support phase to an instant in time and allows a discontinuity in the velocity component of the state, with the configuration remaining continuous. The biped model is thus *hybrid* in nature, consisting of a continuous dynamics and a re-initialization rule at the contact event.

An important source of complexity in a biped system is the degree of actuation of the

system, or more precisely, the degree of *underactuation* of the system. It will be assumed that there is no actuation at the end of the stance leg. Thus the system is underactuated during walking, as opposed to fully actuated (a control at each joint and at the contact point with the ground).

A complete list of hypotheses assumed for the robot model and the desired walking gaits is now enumerated.

Robot hypotheses

The robot is assumed to be:

RH1) comprised of N rigid links with mass, connected by revolute joints with no closed kinematic chains;

RH2) planar, with motion constrained to the sagittal plane;

RH3) bipedal, with symmetric legs connected at a common point called the hip;

RH4) actuated at each joint; and

RH5) unactuated at the point of contact between the stance leg and ground.

Gait hypotheses

Conditions on the controller will be imposed and shown to ensure that the robot's consequent motion satisfies the following properties consistent with the intuitive notion of a simple walking gait:

GH1) there are alternating phases of single support and double support;

GH2) during the single support phase, the stance leg acts as a pivot joint, that is, throughout the contact, it can be guaranteed that the vertical component of the ground reaction force is positive and that the ratio of the horizontal component to the vertical component does not exceed the coefficient of static friction;

GH3) the double support phase is instantaneous and can be modeled as a rigid contact [HM94];

GH4) at impact, the swing leg neither slips nor rebounds;

GH5) in steady state, successive phases of single support are symmetric with respect to the two legs;

GH6) walking is from left to right, so that the swing leg starts from behind the stance leg and is placed strictly in front of the stance leg at impact.

RH1) and RH2) imply the robot has $(N+2)$-degrees of freedom (DOF) (N joint angles plus the Cartesian coordinates of the hip, for example). RH4), RH5) and GH2) imply that when walking the robot has one degree of underactuation, i.e., one less control than DOF. It is worth noting that even if there were actuation between the stance leg end and ground, it would be worthwhile to first design a controller under hypothesis RH5) and then add an outer control loop to exploit the torque available at the ankle to improve the convergence rate of walking to a desired average walking rate or to enlarge the region of attraction of the inner controller.

2.1 Swing phase model

Under GH2) the dynamic model of the robot during the swing phase has N-DOF. Let $q := (q_1, \cdots, q_N)'$ be a set of angular coordinates describing the configuration of the robot with respect to a world reference frame. Since only symmetric gaits are of interest here, the same model can be used irrespective of which leg is the stance leg if the coordinates are re-labeled after each phase of double support. Forming the Lagrangian,

$$L(q, \dot{q}) := K(q, \dot{q}) - V(q). \tag{2.1}$$

were K and V are the kinetic and potential energy of the robot, respectively, and applying the method of Lagrange (see Appendix E), the model is written in the form

$$D(q)\ddot{q} + C(q, \dot{q})\dot{q} + G(q) = Bu. \tag{2.2}$$

The matrix D is the inertia tensor; C is the Coriolis matrix; G is gravity vector; and B is a linear map from joint torques to configuration variables.

In accordance with RH4) and RH5), torques $u_i,\ i = 1$ to $N-1$ are applied between each connection of two links, *but not between the stance leg and ground*. The model is written in state space form by defining

$$\dot{x} = \begin{bmatrix} \dot{q} \\ D^{-1}(q)\left[-C(q,\dot{q})\dot{q} - G(q) + Bu\right] \end{bmatrix} \tag{2.3}$$

$$=: f(x) + g(x)u \tag{2.4}$$

where $x := (q', \dot{q}')'$. The state space of the model is taken as $T\mathcal{Q} := \{x := (q', \dot{q}')' \mid q \in \mathcal{Q},\ \dot{q} \in \mathbb{R}^N\}$, where $\mathcal{Q}$ is a simply-connected, open subset of $[0, 2\pi)^N$ corresponding to physically reasonable configurations of the robot (for example, with the exception of the end of the stance leg, all points of the robot being above the walking surface; one could also impose that the knees are not bent backward, etc.). An alternate approach, not used here, would be to define the admissible states through *viability* constraints [Bab98, Bro96].

2.2 Impact model

An impact occurs when the swing leg touches the walking surface, also called the ground. The impact between the swing leg and the ground is modeled as a contact between two rigid bodies. In addition to modeling the change in state of the robot, the impact model accounts for the relabeling of the robot's coordinates that occurs after each phase of double support. The development of the impact model requires the full $(N+2)$-DOF of the robot. By adding Cartesian coordinates $(p_{\mathrm{H}}^{\mathrm{h}}, p_{\mathrm{H}}^{\mathrm{v}})$ to the hip (see Figure 1.4), the following extended model is easily obtained through the method of Lagrange,

$$D_{\mathrm{e}}(q_{\mathrm{e}})\ddot{q}_{\mathrm{e}} + C_{\mathrm{e}}(q_{\mathrm{e}}, \dot{q}_{\mathrm{e}})\dot{q}_{\mathrm{e}} + G_{\mathrm{e}}(q_{\mathrm{e}}) = B_{\mathrm{e}}u + \delta F_{\mathrm{ext}}, \tag{2.5}$$

with $q_{\mathrm{e}} := (q_1, q_2, \ldots, q_N, p_{\mathrm{H}}^{\mathrm{h}}, p_{\mathrm{H}}^{\mathrm{v}})'$ and where δF_{ext} represents the vector of external forces acting on the robot at the contact point. If the stance leg end is in contact with the ground and not slipping, the extended coordinates q_{e} and their velocities $\dot{q}_{\mathrm{e}}$ are related to q and $\dot{q}$ by

$$q_{\mathrm{e}} = \pi^{-1}(q) \quad \text{and} \quad \dot{q}_{\mathrm{e}} = \frac{\partial \pi^{-1}(q)}{\partial q}\,\dot{q}, \tag{2.6}$$

where $\pi^{-1}(q) := (q', p_{\mathrm{H}}^{\mathrm{h}}(q), p_{\mathrm{H}}^{\mathrm{v}}(q))'$, and $p_{\mathrm{H}}^{\mathrm{h}}(q)$ and $p_{\mathrm{H}}^{\mathrm{v}}(q)$ are the horizontal and vertical positions of the hip, respectively.

Impact model hypotheses

The impact model of [HM94] is used under the following assumptions:

IH1) the contact of the swing leg with the ground results in no rebound and no slipping of the swing leg;

IH2) at the moment of impact, the stance leg lifts from the ground without interaction;

IH3) the impact is instantaneous;

IH4) the external forces during the impact can be represented by impulses;

IH5) the impulsive forces may result in an instantaneous change in the velocities, but there is no instantaneous change in the configuration;[1] and

IH6) the actuators cannot generate impulses and hence can be ignored during impact.

IH1)–IH6) imply total angular momentum is conserved [HM94] and therefore

$$D_{\mathrm{e}}(q_{\mathrm{e}}^-)\dot{q}_{\mathrm{e}}^- = \left(\frac{\partial E(q_{\mathrm{e}})}{\partial q_{\mathrm{e}}}\right)'\Big|_{q_{\mathrm{e}}=q_{\mathrm{e}}^-} \begin{bmatrix} \hat{F}_2^{\mathrm{T}} \\ \hat{F}_2^{\mathrm{N}} \end{bmatrix} + D_{\mathrm{e}}(q_{\mathrm{e}}^+)\dot{q}_{\mathrm{e}}^+ \tag{2.12}$$

[1] To aid in understanding this assumption, consider the following scalar, second order system with an impulsive input at $t = t_0$,

$$\ddot{x}(t) + a\dot{x}(t) + bx(t) = c\delta(t - t_0) \tag{2.7}$$

where δ is the unit impulse, $t_0 > 0$, and $a, b, c \in \mathbb{R}$. Integrating (2.7) once yields

$$\dot{x}(t) = \dot{x}(0) + \int_0^t \left(-a\dot{x}(\tau) - bx(\tau) + c\delta(\tau - t_0)\right) d\tau \tag{2.8}$$

$$= \dot{x}(0) - ax(t) + ax(0) - \int_0^t bx(\tau)d\tau + cu(t - t_0) \tag{2.9}$$

where u is the unit step function and hence $\dot{x}(t)$ is discontinuous at $t = t_0$. Integrating (2.9) yields

$$x(t) = x(0) + \int_0^t \left(\dot{x}(0) - ax(\sigma) + ax(0) - \int_0^\sigma bx(\tau)d\tau + cu(\sigma - t_0)\right) d\sigma \tag{2.10}$$

$$= x(0) + (\dot{x}(0) + ax(0))\, t - \int_0^t ax(\sigma)d\sigma - \int_0^t \int_0^\sigma bx(\tau)d\tau d\sigma + c(t - t_0)u(t - t_0). \tag{2.11}$$

Notice that $x(t_0^+) - x(t_0^-) = 0$ whereas $\dot{x}(t_0^+) - \dot{x}(t_0^-) = c$, the magnitude of the impulsive input, where t_0^- and t_0^+ are respectively the times just before and just after the impulsive input is applied.

where $\hat{F}_2^{\mathrm{T}}$ and $\hat{F}_2^{\mathrm{N}}$ are, respectively, the integral of the tangential and normal forces acting on the swing leg end at touchdown, $E(q_{\mathrm{e}}) = (p_2^{\mathrm{h}}(q_{\mathrm{e}}), p_2^{\mathrm{v}}(q_{\mathrm{e}}))'$ is the Cartesian coordinates of the swing leg end (see Figure 1.4), and $\dot{q}_{\mathrm{e}}^-$ (resp. $\dot{q}_{\mathrm{e}}^+$) is the velocities of the robot just before (resp. just after without relabeling) impact. Hypothesis IH1) also implies

$$\left.\frac{\partial E(q_{\mathrm{e}})}{\partial q_{\mathrm{e}}}\right|_{q_{\mathrm{e}}=q_{\mathrm{e}}^+} = 0. \tag{2.13}$$

By hypothesis IH5) $q_{\mathrm{e}}^- = q_{\mathrm{e}}^+$ and hence the following expression relating the velocity of the robot just before impact to the velocity just after (without relabeling) may be written as

$$\Pi^{-1}(q_{\mathrm{e}}^-) \begin{bmatrix} \dot{q}_{\mathrm{e}}^+ \\ \hat{F}_2^{\mathrm{T}} \\ \hat{F}_2^{\mathrm{N}} \end{bmatrix} = \begin{bmatrix} D_{\mathrm{e}}(q_{\mathrm{e}}^-)\dot{q}_{\mathrm{e}}^- \\ 0 \end{bmatrix} \tag{2.14}$$

where

$$\Pi(q_{\mathrm{e}}) := \begin{bmatrix} D_{\mathrm{e}}(q_{\mathrm{e}}) & -\left(\dfrac{\partial E(q_{\mathrm{e}})}{\partial q_{\mathrm{e}}}\right)' \\ \dfrac{\partial E(q_{\mathrm{e}})}{\partial q_{\mathrm{e}}} & 0 \end{bmatrix}^{-1}, \tag{2.15}$$

Due to its block-triangular structure and the positive definiteness of D_{e}, the matrix Π is invertible whenever $\partial E/\partial q_{\mathrm{e}}$ is full rank[2] which will be the case whenever the robot is not in a kinematic singular configuration [MLS93, p. 123].

Solving (2.14) yields

$$\begin{bmatrix} \dot{q}_{\mathrm{e}}^+ \\ \hat{F}_2^{\mathrm{T}} \\ \hat{F}_2^{\mathrm{N}} \end{bmatrix} = \Pi(q_{\mathrm{e}}^-) \begin{bmatrix} D_{\mathrm{e}}(q_{\mathrm{e}}^-)\dot{q}_{\mathrm{e}}^- \\ 0 \end{bmatrix}. \tag{2.16}$$

The map from $\dot{q}_{\mathrm{e}}^-$ to $\dot{q}_{\mathrm{e}}^+$, that is, the map from velocities just prior to impact to just after impact (without relabeling), is obtained by partitioning $\Pi(q_{\mathrm{e}}^-)$ as

$$\dot{q}_{\mathrm{e}}^+ = \Pi_{11}(q_{\mathrm{e}}^-) D_{\mathrm{e}}(q_{\mathrm{e}}^-)\dot{q}_{\mathrm{e}}^- \tag{2.17}$$

$$\begin{bmatrix} \hat{F}_2^{\mathrm{T}} \\ \hat{F}_2^{\mathrm{N}} \end{bmatrix} = \Pi_{21}(q_{\mathrm{e}}^-) D_{\mathrm{e}}(q_{\mathrm{e}}^-)\dot{q}_{\mathrm{e}}^-. \tag{2.18}$$

[2]Suppose that Π is not invertible. Then, there exists $(\dot{q}_{\mathrm{e}}', \hat{F}_2^{\mathrm{T}}, \hat{F}_2^{\mathrm{N}})' \neq 0$ such that $\Pi^{-1}(\dot{q}_{\mathrm{e}}', \hat{F}_2^{\mathrm{T}}, \hat{F}_2^{\mathrm{N}})' = 0$. This implies $\dot{q}_{\mathrm{e}} = D_{\mathrm{e}}^{-1}(\partial E/\partial q_{\mathrm{e}})'(\hat{F}_2^{\mathrm{T}}, \hat{F}_2^{\mathrm{N}})'$ and $(\partial E/\partial q_{\mathrm{e}})\dot{q}_{\mathrm{e}} = 0$, which implies $(\partial E/\partial q_{\mathrm{e}})D_{\mathrm{e}}^{-1}(\partial E/\partial q_{\mathrm{e}})'(\hat{F}_2^{\mathrm{T}}, \hat{F}_2^{\mathrm{N}})' = 0$. By Sylvester's inequality [Che84, p. 31], this implies $(\hat{F}_2^{\mathrm{T}}, \hat{F}_2^{\mathrm{N}})' = 0$ which implies $\dot{q}_{\mathrm{e}} = 0$. Hence, Π is invertible.

Combining (2.6) with (2.17) and (2.18) results in an expression for the velocities of the robot just after impact and the integral of the forces experienced by the end of the swing leg at impact. At impact, it is assumed that the swing leg becomes the new stance leg, so the coordinates must be relabeled. Express the relabeling of the states as a linear transformation matrix, R with the property that $RR = I$, i.e., R is a circular matrix. The result of the impact and relabeling of the states is then an expression

$$x^+ = \Delta(x^-) \tag{2.19}$$

where $x^+ := (q^+, \dot{q}^+)$ (resp. $x^- := (q^-, \dot{q}^-)$) is state value just after (resp. just before) impact and

$$\Delta(x^-) := \begin{bmatrix} \Delta_q \, q^- \\ \\ \Delta_{\dot{q}}(q^-) \, \dot{q}^- \end{bmatrix} \tag{2.20}$$

where

$$\Delta_q := R \tag{2.21}$$

and

$$\Delta_{\dot{q}}(q^-) := [R \;\; 0\,] \, \Pi_{11} \circ \pi^{-1}(q^-) D_{\mathrm{e}} \circ \pi^{-1}(q^-) \left. \frac{\partial \pi^{-1}(q)}{\partial q} \right|_{q=q^-}. \tag{2.22}$$

2.3 Plant model: a hybrid nonlinear underactuated control system

With the addition of an appropriately chosen switching set, the swing phase model can be combined with the impact model and expressed as a nonlinear system with impulse effects [YMH98, GAP01]

$$\begin{aligned} \dot{x} &= f(x) + g(x)u \qquad && x^- \notin S \\ x^+ &= \Delta(x^-) && x^- \in S, \end{aligned} \tag{2.23}$$

where the switching set is chosen to be

$$S := \{(q, \dot{q}) \in T\mathcal{Q} \mid p_2^{\mathrm{v}}(q) = 0, \; p_2^{\mathrm{h}}(q) > 0\}, \tag{2.24}$$

and $x^-(t) := \lim_{\tau \nearrow t} x(\tau)$. The value of $p_2^{\mathrm{h}}(q)$ is taken to be positive so that for $x \in S$ the swing leg end is in front of the stance leg as per GH6). In Chapter 3 the set S will be

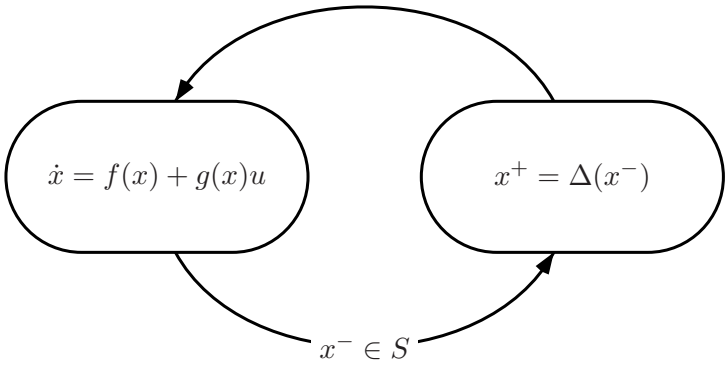

Figure 2.1: A graphical representation of the hybrid model for walking.

chosen as the Poincaré section. Figure 2.1 gives a graphical representation of this discrete event system. Solutions are taken to be right continuous and must have finite left and right limits at each impact event (see [GAP99] for details).

Informally, a *step* of the robot is a solution of (2.23) that starts with the robot in double support, ends in double support with the configurations of the legs swapped, and contains only one impact event. This is more precisely defined as follows. Let $\varphi(t, x_0)$ be a maximal solution of the swing phase dynamics (2.4) with initial condition x_0 at time $t_0 = 0$.

Definition 2.1. [GAP99] The *time to impact* function, $T_I : T\mathcal{Q} \to \mathbb{R} \cup \{\infty\}$, by

$$T_I(x_0) := \begin{cases} \inf\{t \geq 0 \mid \varphi(t, x_0) \in S\} & \text{if } \exists\ t \text{ s.t. } \varphi(t, x_0) \in S \\ \infty & \text{otherwise} \end{cases} \tag{2.25}$$

Let $x_0 \in S$ be such that $T_I \circ \Delta(x_0) < \infty$.

Definition 2.2. A *step* of the robot is the solution of (2.23) defined on the half-open interval $[0, T_I \circ \Delta(x_0))$ with initial point x_0. Any point $x_0 \in S$ such that $T_I \circ \Delta(x_0) < \infty$ is said to result in the robot taking a step.

Definition 2.3. *Walking* is defined as successive steps.

2.4 The Acrobot as a walker: a two-link example model

This section presents a simple biped model that will be used to illustrate key points developed in later chapters. The model consists of two symmetric links with a single actuator

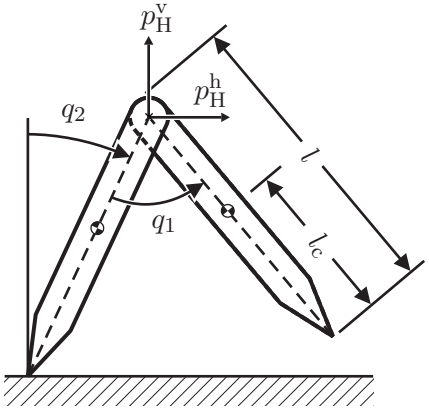

Figure 2.2: Schematic of the two-link walker with measurement conventions. Note that the legs are symmetric.

at the link connection point, the hip; see Figure 2.2. In the swing phase, the model corresponds to that of the Acrobot [Spo95, BF98, GEK96] with symmetric links. It is almost the simplest walking model of Garcia et al. [GCRC98] but with the exception that the mass is distributed as opposed to being concentrated at the hip.

With its simple morphology, however, this is not a physically realizable model of biped walking. With equal leg lengths, the swing foot will scuff, i.e., prematurely contact the walking surface. Usual arguments for overcoming this deficiency are assumptions of small, retractable leg ends which allow the swing leg to be shortened enough to achieve ground clearance [GAP01], or, that in three-dimensions, frontal plane hip sway would allow foot clearance [Kuo99]. The interest here is not the physical realizability of this model, but in its illustrative utility since it is the simplist model for walking which satisfies RH1)–RH5).

The equations of motion during the swing phase are (2.4) with

$$
\begin{aligned}
(D(q_1))_{1,1} &= l_{\mathrm{c}}^2 m + ml^2 + 2(l - l_{\mathrm{c}})ml\cos(q_1) + m(l - l_{\mathrm{c}})^2 + 2I && (2.26)\\
(D(q_1))_{1,2} &= (l - l_{\mathrm{c}})ml\cos(q_1) + m(l - l_{\mathrm{c}})^2 + I && (2.27)\\
(D(q_1))_{2,1} &= (l - l_{\mathrm{c}})ml\cos(q_1) + m(l - l_{\mathrm{c}})^2 + I && (2.28)\\
(D(q_1))_{2,2} &= m(l - l_{\mathrm{c}})^2 + I, && (2.29)
\end{aligned}
$$

$$
\begin{aligned}
(C(q_1, \dot{q}_1))_{1,1} &= -(l - l_{\mathrm{c}})ml\sin(q_1)\dot{q}_1 && (2.30)\\
(C(q_1, \dot{q}_1, \dot{q}_2))_{1,2} &= -(l - l_{\mathrm{c}})ml\sin(q_1)(\dot{q}_1 + \dot{q}_2) && (2.31)
\end{aligned}
$$

Model parameter	Units	Label	Value
Leg mass	kg	m	1
Leg length	m	l	1
Leg COM position	m	l_{c}	0.5
Leg Inertia	$\mathrm{m}^2\mathrm{kg}$	I	0

Table 2.1: Parameter values for the two-link walker.

$$(C(q_1, \dot{q}_2))_{2,1} = (l - l_{\mathrm{c}})ml\sin(q_1)\dot{q}_2 \tag{2.32}$$

$$(C)_{2,2} = 0 \tag{2.33}$$

$$(G(q_1, q_2))_1 = g_0 m(-2l\sin(q_2) + l_{\mathrm{c}}\sin(q_2) + (l - l_{\mathrm{c}})\sin(q_2 - q_1)) \tag{2.34}$$

$$(G(q_1, q_2))_2 = -g_0 m(l - l_{\mathrm{c}})\sin(q_2 - q_1), \tag{2.35}$$

and

$$B = \begin{bmatrix} 0 \\ 1 \end{bmatrix} \tag{2.36}$$

The state space is taken as $T\mathcal{Q} := \{x := (q_1, q_2, \dot{q}_1, \dot{q}_2)' \mid (q_1, q_2) \in \mathcal{Q},\ (\dot{q}_1, \dot{q}_2) \in \mathbb{R}^2\}$ where $\mathcal{Q}$ is an open subset of $(0, 2\pi) \times (-\pi/2, \pi/2)$. The parameter values are given in Table 2.1. Note that D is independent of q_2. This will be the case for any N-link robot satisfying RH1)–RH5) when the coordinates are chosen as $(N-1)$ shape (relative) coordinates plus one absolute coordinate, i.e., a coordinate referencing the angle of a point on the robot to a world coordinate frame. This is due to the invariance of the kinetic energy under the group action of $SO(2)$, i.e., planar rotations, and will be important for the zero dynamics development in Chapter 3. The impact map requires the full 4-DOF model which is given in Appendix A.

CHAPTER 3

Zero dynamics

The method of computed torque or inverse dynamics is ubiquitous in the field of robotics [SV89, MLS93, Cra89]. It consists of defining a set of outputs, equal in number to the inputs, and then designing a feedback controller that asymptotically drives the outputs to zero. The robot's task is encoded into the set of outputs in such a way that the nulling of the outputs is (asymptotically) equivalent to achieving the task, whether the task be asymptotic convergence to an equilibrium point, a surface, or a time trajectory. For a system modeled by ordinary differential equations (in particular, no impact dynamics), the *maximal internal dynamics* of the system that are *compatible with the output being identically zero* is called the *zero dynamics* [Isi95, IM88, Nv89]. Hence, the method of computed torque, which is asymptotically driving a set of outputs to zero, is indirectly designing a set of zero dynamics for the robot. Since in general the dimension of the zero dynamics is considerably less than the dimension of the model itself, the task to be achieved by the robot has been *implicitly* encoded into a lower dimensional system.

One of the main points of this chapter is that this process can be *explicitly* exploited in the design of feedback controllers for walking mechanisms *even in the presence of impacts*. Here, the outputs will be thought of as imposing virtual constraints—holonomic constraints parameterized by the system state imposed via a feedback. As opposed to physical mechanical constraints—constraints imposed with, for example, a geared mechanism that are, consequently, not easily reconfigured—virtual constraints may be easily redefined (reconfigured). Section 3.1 gives two examples which introduce the concepts of zero dynam-

ics and virtual constrains. Section 3.2 will introduce a class of outputs for which the swing phase zero dynamics can be readily identified and analyzed. Section 3.4 will derive natural conditions under which the swing phase zero dynamics become compatible with the impact model, thereby leading to the notion of a hybrid zero dynamics for the complete model of the biped.

3.1 Zero dynamics and virtual constraints

This section introduces zero dynamics and virtual constraints via two examples.

3.1.1 A simple zero dynamics example

Consider the single-input, single-output linear system described by the transfer function

$$H(s) = \frac{s+\alpha}{s^2 - s - 6} \tag{3.1}$$

where $\alpha \in \mathbb{R}$. $H(s)$ has a zero at $-\alpha$ and poles at 3 and -2 and thus the origin is not stable in the sense of Lyapunov. A state space realization of $H(s)$ is

$$\begin{bmatrix} \dot{x}_1 \\ \dot{x}_2 \end{bmatrix} = \begin{bmatrix} 0 & 1 \\ 6 & 1 \end{bmatrix} \begin{bmatrix} x_1 \\ x_2 \end{bmatrix} + \begin{bmatrix} 0 \\ 1 \end{bmatrix} u \tag{3.2}$$

$$y = \begin{bmatrix} \alpha & 1 \end{bmatrix} \begin{bmatrix} x_1 \\ x_2 \end{bmatrix}. \tag{3.3}$$

The output dynamics

$$\dot{y} = \alpha\dot{x}_1 + \dot{x}_2 \tag{3.4}$$

$$= 6x_1 + (1+\alpha)x_2 + u \tag{3.5}$$

may be stabilized by choosing

$$u = -6x_1 - (1+\alpha)x_2 - y \tag{3.6}$$

which results in

$$\dot{y} = -y. \tag{3.7}$$

Suppose that $y \equiv 0$, i.e., $x_2 \equiv -\alpha x_1$. Under this constraint, the system state must evolve on the set

$$Z := \{x \in \mathbb{R}^2 \mid \alpha x_1 + x_2 = 0\} \tag{3.8}$$

called the zero dynamics manifold. The maximal internal dynamics compatible with the output being identically zero, called the zero dynamics, are[1]

$$\begin{aligned} \dot{x}_2 &= -\alpha \dot{x}_1 && (3.9) \\ &= -\alpha x_2. && (3.10) \end{aligned}$$

The input compatible with $x \in Z$ is

$$\begin{aligned} u^* &= -6x_1 - (1+\alpha)x_2 && (3.11) \\ &= -(\alpha^2 + \alpha + 6)x_1 && (3.12) \end{aligned}$$

Notice that 1) the input u^* is *independent* of the input chosen to stabilize the output dynamics (3.5), 2) that $y \equiv 0$ implies $u \equiv u^*$, and 3) the zero dynamics, (3.10), are invariant with respect to choice of u.

The parameter α can be thought of as a design parameter which selects the zero dynamics manifold along with the corresponding zero dynamics. Figure 3.1 gives the vector fields for (3.2) in closed loop with (3.6) for two values of α. For both values of α, the output dynamics (3.5) with (3.6) are stable; however with $\alpha = 1$ the zero dynamics are stable while with $\alpha = -2$, the zero dynamics are unstable. It is important to note that different choices of α lead to zero dynamics with different zero dynamics manifolds and with different stability properties. For a thorough discussion of zero dynamics, see [Kha96, Isi95].

3.1.2 The idea of virtual constraints

As seen in the previous section, the choice of the output specifies the zero dynamics. This simple idea may be exploited for the design of walking motions in the following way: consider the two-link biped presented in Section 2.4. Suppose that the hip joint angle, q_2,

[1] It is no accident that the eigenvalue of (3.10) corresponds to the zero of $H(s)$. For a linear system, it is always the case that the eigenvalues of the zero dynamics correspond to the zeros of the corresponding transfer function [Isi95].

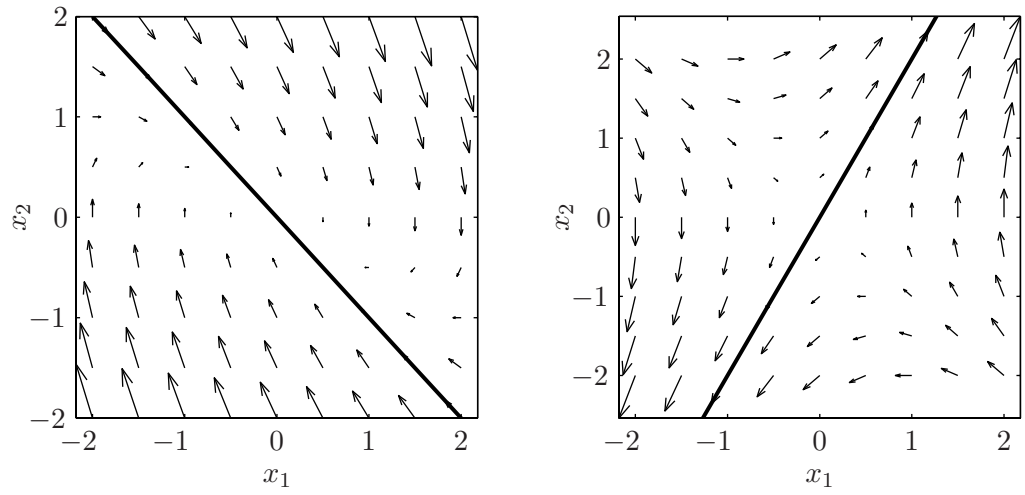

(a) Stable zero dynamics ($\alpha = 1$)

(b) Unstable zero dynamics ($\alpha = -2$)

Figure 3.1: Vector fields for a zero dynamics example using a second order linear system. Vector fields for (3.2) in closed loop with (3.6) for two values of α. The bold line corresponds to the zero dynamics manifold, $Z := \{x \in \mathbb{R}^2 \mid \alpha x_1 + x_2 = 0\}$.

is constrained to be a function of the absolute angle q_1,

$$q_2 = h_d(q_1). \tag{3.13}$$

Under appropriate conditions to be detailed in the next section, the output

$$y = q_2 - h_d(q_1) \tag{3.14}$$

being identically zero leads to second order zero dynamics which evolve on a two-dimensional embedded sub-manifold of the biped's state space. These zero dynamics only describe, however, the behavior of the robot during the swing phase (when the dynamics are continuous). One of the main contributions of this dissertation, addressed in Section 3.4, is understanding how the discontinuities created by impacts may be incorporated into the notion of the zero dynamics. See Section 4.3.1 for an investigation of the two-link model with an output of the form (3.14).

The constraint (3.13) can be thought of as imposing a virtual constraint that may be reconfigured electronically via change in feedback law as opposed to a physical mechanical

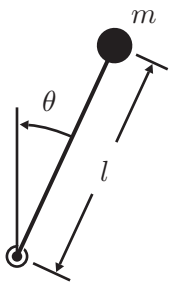

Figure 3.2: A horizontal, variable length pendulum used to explain virtual constraints.

constraint implemented with, for example, a geared mechanism. It is important to note that while virtual constraints and physical constraints impose the same kinematic behavior, the resulting dynamic behavior is different.

To understand this difference, consider the horizontal variable length pendulum depicted in Figure 3.2. The distance from the point mass m to the rotation point is l and may vary. Since the pendulum is horizontal, its Lagrangian is equal to the kinetic energy,

$$L = K = \frac{1}{2}m\left(\dot{l}^2 + l^2\dot{\theta}^2\right). \tag{3.15}$$

Two different scenarios will be considered. First, the length, l, will be constrained to be a function of θ via a physical constraint. Second, l will be constrained via a virtual constraint.

In the first case, suppose that a physical constraint is designed such that $l = l_d(\theta)$. The Lagrangian (3.15) then becomes

$$L = \frac{1}{2}m\left(\left(\frac{\partial l_d(\theta)}{\partial\theta}\right)^2 + l_d(\theta)^2\right)\dot{\theta}^2. \tag{3.16}$$

The equation of motion is therefore

$$m\left(\left(\frac{\partial l_d(\theta)}{\partial\theta}\right)^2 + (l_d(\theta))^2\right)\ddot{\theta} + m\frac{\partial l_d(\theta)}{\partial\theta}\left(\frac{\partial^2 l_d(\theta)}{\partial\theta^2} + l_d(\theta)\right)\dot{\theta}^2 = 0. \tag{3.17}$$

Now suppose that l is constrained via a virtual constraint. In this case, the length l is treated as a controlled quantity and the equations of motion may be calculated from the Lagrangian (3.15) to be

$$\ddot{\theta} = -\frac{2}{l}\dot{l}\dot{\theta} \tag{3.18}$$

$$\ddot{l} = l\dot{\theta}^2 + \frac{1}{m}u \tag{3.19}$$

where u is an input used to control the length l. Paralleling the development of the previous section, form an output on the system (3.18) and (3.19) as

$$y = l - l_d(\theta) \tag{3.20}$$

such that $y \equiv 0$ implies $l \equiv l_d(\theta)$. As long as $\partial l_d(\theta)/\partial\theta \neq 0$, the output (3.20) is of relative degree two. Hence, differentiating twice yields

$$\begin{aligned} \ddot{y} &= \ddot{l} - \frac{\partial l_d^2(\theta)}{\partial\theta^2}\dot{\theta}^2 - \frac{\partial l_d(\theta)}{\partial\theta}\ddot{\theta} && (3.21)\\ &= l\dot{\theta}^2 - \frac{\partial l_d^2(\theta)}{\partial\theta^2}\dot{\theta}^2 + \frac{2}{l}\frac{\partial l_d(\theta)}{\partial\theta}\dot{l}\dot{\theta} + \frac{1}{m}u && (3.22)\end{aligned}$$

The output dynamics (3.22) may be stabilized with

$$u = m\left(-l\dot{\theta}^2 + \frac{\partial l_d^2(\theta)}{\partial\theta^2}\dot{\theta}^2 - \frac{2}{l}\frac{\partial l_d(\theta)}{\partial\theta}\dot{l}\dot{\theta} - K_D\dot{y} - K_P y\right) \tag{3.23}$$

for $K_D, K_P > 0$. Under the constraint $l \equiv l_d(\theta)$, the system state must evolve on the set[2]

$$Z := \{(\theta, \dot{\theta}, l, \dot{l}) \in \mathrm{S} \times \mathbb{R}^3 \mid l - l_d(\theta) = 0\}. \tag{3.24}$$

The maximal internal dynamics compatible with the output being identically zero, the zero dynamics, are

$$m\left(l_d(\theta)\right)^2\ddot{\theta} + 2m\frac{\partial l_d(\theta)}{\partial\theta}l_d(\theta)\dot{\theta}^2 = 0 \tag{3.25}$$

and the unique control required to enforce $l \equiv l_d(\theta)$ is

$$u^* = ml_d(\theta)\left(-\left(l_d(\theta)\right)^2 + l_d(\theta)\frac{\partial l_d^2(\theta)}{\partial\theta^2} - 2\left(\frac{\partial l_d(\theta)}{\partial\theta}\right)^2\right)\dot{\theta}^2. \tag{3.26}$$

While the kinematic behavior of the zero dynamics resulting from the virtual constraint $l = l_d(\theta)$ is identical to that resulting from the physical constraint $l = l_d(\theta)$ their dynamic behavior is quite different, cf. (3.25) and (3.17). Figure 3.3 illustrates this difference for the constraint $l_d = \sin(\theta) + 1.5$. For this example, $m = 1$ and the system (3.17) was initialized with $(\theta, \dot{\theta}) = (0, 1)$ and the system (3.25) was initialized with $(\theta, \dot{\theta}, l, \dot{l}) = (0, 1, 1.5, 1) \in Z$. The difference between these two realizations lies in u^*, the energy entering the system in the virtual constraint realization which does not appear in the physical constraint realization.

[2]Here S is the topological space the unit circle, not the walking surface; see Section 2.3.

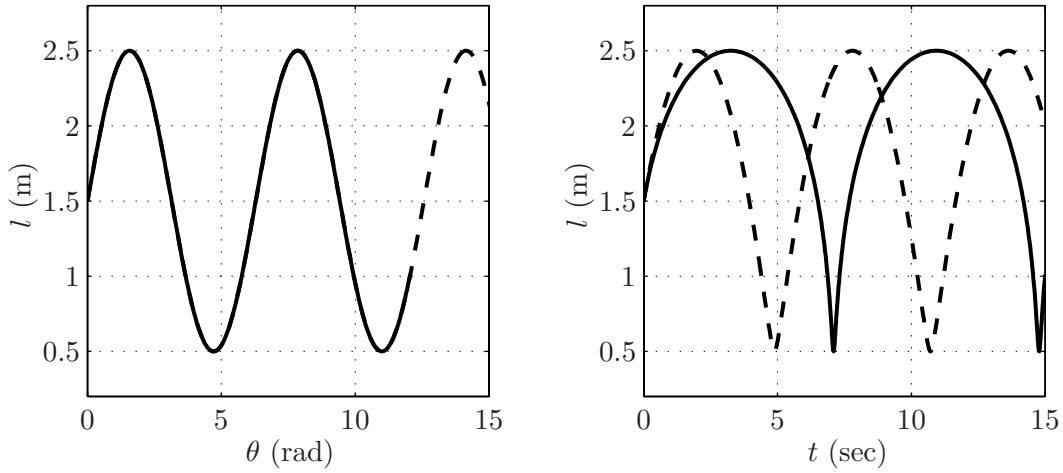

(a) Kinematic behavior

(b) Dynamic behavior

Figure 3.3: Kinematic and dynamic behaviors of the horizontal pendulum. The dashed lines correspond to the constraint $l = \sin(\theta) + 1.5$ imposed via a physical constraint, whereas the solid corresponds to the same constraint imposed via a virtual constraint.

3.2 Swing phase zero dynamics

This section identifies the swing phase zero dynamics for a particular class of outputs that have proven useful in constructing feedback controllers for bipedal walkers [GAP01, PGWA01]. Since no impact dynamics are involved, the work here is simply a specialization of the general results in [Isi95] to the model (2.4). The results summarized here will form the basis for defining a zero dynamics of the complete hybrid model of the planar biped walker, which is the desired object for study.

Note that if an output $y = h(q)$ depends only on the configuration variables, then, due to the second order nature of the robot model, the derivative of the output along solutions of (2.4) does not depend directly on the inputs,

$$\frac{dy}{dt} = \frac{\partial h}{\partial x}\dot{x} \tag{3.27}$$

$$= \begin{bmatrix} \frac{\partial h}{\partial q} & \frac{\partial h}{\partial \dot{q}} \end{bmatrix} \left[\underbrace{\begin{bmatrix} \dot{q} \\ D^{-1}\left[-C\dot{q} - G\right] \end{bmatrix}}_{f} + \underbrace{\begin{bmatrix} 0 \\ D^{-1}B \end{bmatrix}}_{g} u \right] \tag{3.28}$$

$$= \underbrace{\begin{bmatrix} \frac{\partial h}{\partial q} & 0 \end{bmatrix} \begin{bmatrix} \dot{q} \\ D^{-1}\left[-C\dot{q} - G\right] \end{bmatrix}}_{L_f h} + \underbrace{\begin{bmatrix} \frac{\partial h}{\partial q} & 0 \end{bmatrix} \begin{bmatrix} 0 \\ D^{-1}B \end{bmatrix}}_{L_g h} u \tag{3.29}$$

$$= L_f h. \tag{3.30}$$

Hence its relative degree is at least two. Differentiating the output once again computes the accelerations, resulting in

$$\frac{d^2 y}{dt^2} = \begin{bmatrix} \frac{\partial}{\partial q}\left(\frac{\partial h}{\partial q}\dot{q}\right) & \frac{\partial h}{\partial q} \end{bmatrix} \left[\begin{bmatrix} \dot{q} \\ D^{-1}\left[-C\dot{q} - G\right] \end{bmatrix} + \begin{bmatrix} 0 \\ D^{-1}B \end{bmatrix} u \right] \tag{3.31}$$

$$= \underbrace{\begin{bmatrix} \frac{\partial}{\partial q}\left(\frac{\partial h}{\partial q}\dot{q}\right) & \frac{\partial h}{\partial q} \end{bmatrix} \begin{bmatrix} \dot{q} \\ D^{-1}\left[-C\dot{q} - G\right] \end{bmatrix}}_{L_f^2 h} + \underbrace{\frac{\partial h}{\partial q} D^{-1} B}_{L_g L_f h} u \tag{3.32}$$

$$= L_f^2 h(q, \dot{q}) + L_g L_f h(q) u. \tag{3.33}$$

The matrix $L_g L_f h(q)$ is called the decoupling matrix and depends only on the configuration variables. A consequence of the general results in [Isi95] is that the invertibility of this matrix at a given point assures the existence and uniqueness of the zero dynamics in a neighborhood of that point. With a few extra hypotheses, these properties can be assured on a given open set.

Lemma 3.1. (Swing phase zero dynamics) *Suppose that a smooth function h is selected so that*

HH1) h is a function of only the configuration coordinates;

HH2) there exists an open set $\tilde{\mathcal{Q}} \subset \mathcal{Q}$ such that for each point $q \in \tilde{\mathcal{Q}}$, the decoupling matrix $L_g L_f h(q)$ is square and invertible (i.e., the dimension of u equals the dimension of y, and h has vector relative degree $(2, \ldots, 2)'$);

HH3) there exists a smooth real valued function $\theta(q)$ such that $(h(q)', \theta(q))' : \tilde{\mathcal{Q}} \to \mathbb{R}^N$ is a diffeomorphism onto its image (see Figure 6.6 for an example $\theta(q)$);

HH4) there exists at least one point in $\tilde{\mathcal{Q}}$ where h vanishes.

Then,

1. *the manifold*

$$Z := \{x \in T\tilde{\mathcal{Q}} \mid h(x) = 0, L_f h(x) = 0\} \tag{3.34}$$

is a smooth two-dimensional sub-manifold of $T\mathcal{Q}$; and

2. *the feedback control*

$$u^*(x) = -(L_g L_f h(x))^{-1} L_f^2 h(x) \tag{3.35}$$

renders Z invariant under the swing dynamics; that is, for every $z \in Z$,

$$f_{\text{zero}}(z) := f(z) + g(z)u^*(z) \in T_z Z. \tag{3.36}$$

Z is called the zero dynamics manifold and $\dot{z} = f_{\text{zero}}(z)$ is called the zero dynamics.

Lemma 3.1 follows immediately from general results in [Isi95]; a few of the details are outlined here for later use. From hypotheses HH1) and HH3), $\Phi(q) := [h', \theta(q)]'$ is a valid coordinate transformation on $\tilde{\mathcal{Q}}$, and thus

$$\begin{aligned} \eta_1 &= h(q), \quad \eta_2 = L_f h(q, \dot{q}), \\ \xi_1 &= \theta(q), \quad \xi_2 = L_f \theta(q, \dot{q}), \end{aligned} \tag{3.37}$$

is a coordinate transformation on $T\tilde{\mathcal{Q}}$. In these coordinates, the system takes the form

$$\begin{aligned} \dot{\eta}_1 &= \eta_2, \quad \dot{\eta}_2 = L_f^2 h + L_g L_f h u, \\ \dot{\xi}_1 &= \xi_2, \quad \dot{\xi}_2 = L_f^2 \theta + L_g L_f \theta u, \\ y &= \eta_1 \end{aligned} \tag{3.38}$$

where $(q, \dot{q})$ is evaluated at

$$q = \Phi^{-1}(\eta_1, \xi_1) \tag{3.39}$$

$$\dot{q} = \left(\frac{\partial \Phi}{\partial q}\right)^{-1} \begin{bmatrix} \eta_2 \\ \xi_2 \end{bmatrix}. \tag{3.40}$$

Enforcing $y \equiv 0$ results in $(\eta_1 = h = 0, \eta_2 = L_f h = 0)$, u^* as in (3.35), and the zero dynamics becoming

$$\begin{aligned} \dot{\xi}_1 &= \xi_2 \\ \dot{\xi}_2 &= L_f^2 \theta + L_g L_f \theta u^*. \end{aligned} \tag{3.41}$$

While it is useful to know that the zero dynamics can be expressed as a second order system, this form of the equations is very difficult to compute directly due to the need to invert the decoupling matrix. However, this can be avoided. Indeed, since the columns of g in (2.4) are involutive, by [Isi95, p. 222], in a neighborhood of any point where the decoupling matrix is invertible, there exists a smooth scalar function γ such that

$$\begin{aligned} \eta_1 &= h(q), \quad \eta_2 = L_f h(q, \dot{q}), \\ \xi_1 &= \theta(q), \quad \xi_2 = \gamma(q, \dot{q}), \end{aligned} \tag{3.42}$$

is a valid coordinate transformation and

$$L_g \gamma = 0. \tag{3.43}$$

Moreover, by applying the constructive proof of the Frobenius theorem of [Isi95, p. 23] in a set of coordinates for the robot such that

RH6) the model is expressed in $N-1$ *relative* angular coordinates, $(q_1, \ldots, q_{N-1})$, plus one *absolute* angular coordinate, q_N,

one obtains that γ can be explicitly computed to be the last entry of $D(q)\dot{q}$, and hence it can be assumed that $\gamma(q, \dot{q})$ has the form $\gamma_0(q)\,\dot{q}$; it follows that (3.42) is a valid coordinate change on all of $T\tilde{\mathcal{Q}}$.

In the coordinates (3.42), the zero dynamics become

$$\begin{aligned} \dot{\xi}_1 &= L_f \theta \\ \dot{\xi}_2 &= L_f \gamma \end{aligned} \tag{3.44}$$

where the right hand side is evaluated at

$$q = \Phi^{-1}(0, \xi_1) \tag{3.45}$$

$$\dot{q} = \begin{bmatrix} \frac{\partial h}{\partial q} \\ \gamma_0 \end{bmatrix}^{-1} \begin{bmatrix} 0 \\ \xi_2 \end{bmatrix}. \tag{3.46}$$

Theorem 3.1. (Swing phase zero dynamics form) *Under the hypotheses of Lemma 3.1,* $(\xi_1, \xi_2) = (\theta(q), \gamma_0(q)\,\dot{q})$ *is a valid set of coordinates on* Z*, and in these coordinates the*

zero dynamics take the form

$$\dot{\xi}_1 = \kappa_1(\xi_1)\xi_2 \tag{3.47}$$

$$\dot{\xi}_2 = \kappa_2(\xi_1). \tag{3.48}$$

Moreover, if the model (2.4) is expressed in coordinates satisfying RH6), the following interpretations can be given for the various functions appearing in the zero dynamics:

$$\xi_1 = \theta|_Z \tag{3.49}$$

$$\xi_2 = \left.\frac{\partial K}{\partial \dot{q}_N}\right|_Z \tag{3.50}$$

$$\kappa_1(\xi_1) = \left.\frac{\partial \theta}{\partial q}\begin{bmatrix} \frac{\partial h}{\partial q} \\ \gamma_0 \end{bmatrix}^{-1}\begin{bmatrix} 0 \\ 1 \end{bmatrix}\right|_Z \tag{3.51}$$

$$\kappa_2(\xi_1) = -\left.\frac{\partial V}{\partial q_N}\right|_Z, \tag{3.52}$$

where $K(q,\dot{q}) = \frac{1}{2}\dot{q}'D(q)\dot{q}$ is the kinetic energy of the robot, $V(q)$ is its potential energy, and γ_0 is the last row of D, the inertia matrix.

Proof. The form of (3.47) is immediate by the form of (3.44) and (3.46) since both h and γ_0 are functions of q, and hence when restricted to Z, are functions of ξ_1 only.

Suppose now that the model (2.4) is expressed in coordinates satisfying RH6). Since the kinetic energy of the robot, $K(q,\dot{q})$, is independent of the choice of world coordinate frame [SV89, p. 140], and since q_N fixes this choice, $K(q,\dot{q})$ is independent of q_N (i.e., q_N is a cyclic coordinate). Since $D := \partial\left[(\partial K/\partial\dot{q})'\right]/\partial\dot{q}$ [SV89, p. 141], it follows that $\partial D/\partial q_N = 0$. Let D_N, C_N, and G_N be the last rows of D, C, and G, respectively. Then $\xi_2 = \gamma_0(q)\,\dot{q}$ is equal to $D_N(q)\,\dot{q}$ [GAP01], and thus is equal to $\partial K/\partial\dot{q}_N$ since $K = \frac{1}{2}\dot{q}'D\dot{q}$. Continuing, $\dot{\xi}_2 := L_f\gamma$ becomes

$$L_f\gamma = \begin{bmatrix} \dot{q}'\dfrac{\partial D_N'}{\partial q} & D_N \end{bmatrix}\begin{bmatrix} \dot{q} \\ -D^{-1}\left[C\dot{q}+G\right] \end{bmatrix} \tag{3.53}$$

$$= \dot{q}'\frac{\partial D_N'}{\partial q}\dot{q} - C_N\dot{q} - G_N. \tag{3.54}$$

Noting that (see [SV89, p. 142])

$$C_N = \dot{q}'\frac{\partial D_N'}{\partial q} - \frac{1}{2}\dot{q}'\frac{\partial D}{\partial q_N}, \tag{3.55}$$

(3.54) becomes $L_f\gamma = -G_N = -\partial V/\partial q_N$, which, when evaluated on Z, is a function of ξ_1 only. □

Remark 3.1. *[CAA+02] The second state of the zero dynamics, (3.48), can also be derived directly from the Lagrangian. If the robot's Lagrangian, L, is expressed in coordinates satisfying RH6), then since q_N is unactuated*

$$\frac{d}{dt}\frac{\partial L}{\partial \dot{q}_N} - \frac{\partial L}{\partial q_N} = 0. \tag{3.56}$$

Since q_N is a cyclic coordinate (i.e., $\partial K/\partial q_N = 0$), (3.56) reduces to

$$\frac{d}{dt}\frac{\partial K}{\partial \dot{q}_N} = -\frac{\partial V}{\partial q_N}. \tag{3.57}$$

3.3 Interpreting the swing phase zero dynamics

Much in the way that it has been proposed that the spring loaded inverted pendulum is a template for running [Rai86, Sch98], it has been proposed, though less formally, that an inverted pendulum is the template for walking [FS90, KYK92, KT96, PK98, KKK+02a]. Hence, it may, and should, be asked whether the swing phase zero dynamics, (3.47) and (3.48), are those of an inverted pendulum or of a similar mechanical variant thereof. They are not.

Using the angular momentum balance theorem [RP], the rate of change of the angular momentum of the robot about the stance leg end during the swing phase, $\dot{\xi}_2$, is equal to the external applied torque,

$$\dot{\xi}_2 = g_0\, M p^{\mathrm{h}}_{\mathrm{COM}} \tag{3.58}$$

where g_0 is the acceleration due to gravity, M is the robot's mass and $p^{\mathrm{h}}_{\mathrm{COM}}$ is the horizontal position of the robot's center of mass (see Figure 3.4). Suppose ξ_1 is defined as in Figure 3.4. Then, if $y \equiv 0$, $p^{\mathrm{h}}_{\mathrm{COM}} = p^{\mathrm{h}}_{\mathrm{COM}}(\xi_1)$ and $l = l(\xi_1)$ so that

$$\kappa_2(\xi_1) = g_0\, M p^{\mathrm{h}}_{\mathrm{COM}}(\xi_1) \tag{3.59}$$

$$= g_0\, M l(\xi_1)\sin(\xi_1). \tag{3.60}$$

Equation (3.47) may be expressed as

$$\xi_2 = I_{\mathrm{zero}}(\xi_1)\dot{\xi}_1 \tag{3.61}$$

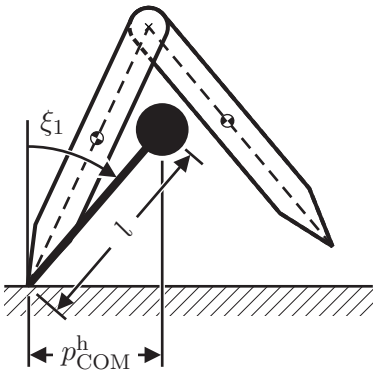

Figure 3.4: A robot with its center of mass labeled. The COM is of mass M with inertia J.

where[3] $I_{\mathrm{zero}}(\xi_1) = 1/\kappa_1(\xi_1)$, is an inertial term. The zero dynamics (3.47) and (3.48) may then be written as a second order system,

$$I_{\mathrm{zero}}(\xi_1)\ddot{\xi}_1 + \frac{\partial I_{\mathrm{zero}}(\xi_1)}{\partial \xi_1}(\dot{\xi}_1)^2 - g_0\, Ml(\xi_1)\sin(\xi_1) = 0. \tag{3.62}$$

From Figure 3.4 it might seem that (3.62) should be the dynamics of a length and inertia varying inverted pendulum, i.e., the length, l, and the inertia about the center of mass (COM), J, vary as function of ξ_1. The equation of motion for such pendulum can be easily derived using the method of Lagrange. The kinetic energy is

$$K(\xi_1) = \frac{1}{2} I(\xi_1)\dot{\xi}_1^2 \tag{3.63}$$

where

$$I(\xi_1) = M\left(\frac{\partial l(\xi_1)}{\partial \xi_1}\right) + M(l(\xi_1))^2 + J(\xi_1). \tag{3.64}$$

The potential energy is

$$V(\xi_1) = Mg_0\, l(\xi_1)\cos(\xi_1), \tag{3.65}$$

and, hence, the equation of motion[4] is,

$$I(\xi_1)\,\ddot{\xi}_1 + \frac{1}{2}\frac{\partial I(\xi_1)}{\partial \xi_1}\,\dot{\xi}_1^2 + Mg_0\left(\frac{\partial l(\xi_1)}{\partial \xi_1}\cos(\xi_1) - l(\xi_1)\sin(\xi_1)\right) = 0. \tag{3.66}$$

Comparing the swing phase zero dynamics (3.62) and the dynamics for the length and inertia varying pendulum (3.66), it is evident that what is suggested by Figure 3.4 does not

[3] Proposition 3.1 on page 43 ensures that $\kappa_1(\xi_1)$ is never zero whenever the robot successfully completes a step.

[4] If l and J do not vary as a function of ξ_1, then $I(\xi_1) = I$, $l(\xi_1) = l$ and (3.66) reduces to the equation of motion for an inverted pendulum, $I\,\ddot{\xi}_1 - Mg_0 l\sin(\xi_1) = 0$.

hold which also implies that the swing phase zero dynamics are not those of an inverted pendulum. It is interesting to note, however, that if the length and inertia varying inverted pendulum had a torque, u, acting between the pendulum and ground, i.e.,

$$I(\xi_1)\,\ddot{\xi}_1 + \frac{1}{2}\frac{\partial I(\xi_1)}{\partial \xi_1}\,\dot{\xi}_1^2 + Mg_0\left(\frac{\partial l(\xi_1)}{\partial \xi_1}\cos(\xi_1) - l(\xi_1)\sin(\xi_1)\right) = u, \tag{3.67}$$

where

$$u = -\frac{1}{2}\frac{\partial I(\xi_1)}{\partial \xi_1}\,\dot{\xi}_1^2 + Mg_0\frac{\partial l(\xi_1)}{\partial \xi_1}\cos(\xi_1), \tag{3.68}$$

then, the forms of (3.62) and (3.67) with u as in (3.68) would be identical.[5] Matching the inertial terms, I and I_{zero}, however, does not yield a positive definite J. That is, supposing I_{zero} has the form of I given in (3.64) implies

$$J(\xi_1) = I_{\text{zero}} - M\left(\frac{\partial l(\xi_1)}{\partial \xi_1}\right) - M(l(\xi_1))^2 \tag{3.69}$$

where l is the distance from the stance leg end to the COM. For every example worked by the author, J is sign indefinite.

3.4 Hybrid zero dynamics

The goal of this section is to incorporate the impact model into the notion of the *maximal internal dynamics compatible with the output being identically zero*, to obtain a zero dynamics of the complete model of the biped walker, (2.23). Towards this goal, let $y = h(q)$ be an output satisfying the hypotheses of Lemma 3.1 and suppose there exists a trajectory, $x(t)$, of the hybrid model (2.23) along which the output is identically zero. If the trajectory contains no impacts with S, then $x(t)$ is a solution of the swing phase dynamics and also of its zero dynamics. If the trajectory does contain impact events, then let (t_0, t_f) be an open interval of time containing exactly one impact at t_e. By definition, on the intervals (t_0, t_e) and (t_e, t_f), $x(t)$ is a solution of the swing phase dynamics and hence also of its zero dynamics, so $x(t) \in Z$; since also by definition of a solution, $x^- := \lim_{t \nearrow t_e} x(t)$ exists, is finite, and lies in S, it follows that $x^- \in S \cap Z$. Moreover, by definition of a solution of (2.23), $x(t_e) := x^+ := \Delta(x^-)$, from which it follows that $\Delta(x^-) \in Z$. On the other hand,

[5] The justification for this input is to account for the energy entering the robot's dynamics via the control u^* given in (3.35).

if $\Delta(S \cap Z) \subset Z$, then from solutions of the swing phase zero dynamics it is clearly possible to construct solutions to the complete model of the biped walker along which the output $y = h(q)$ is identically zero. This leads to the following definition.

Definition 3.1. Let $y = h(q)$ be an output satisfying the hypotheses of Lemma 3.1, and let Z and $\dot{z} = f_{\text{zero}}(z)$ be the associated zero dynamics manifold and zero dynamics of the swing phase model. Suppose that $S \cap Z$ is a smooth, one-dimensional, embedded sub-manifold of $T\mathcal{Q}$. If $\Delta(S \cap Z) \subset Z$, then the nonlinear system with impulse effects,

$$\begin{aligned} \dot{z} &= f_{\text{zero}}(z) \qquad z^- \notin S \cap Z \\ z^+ &= \Delta(z^-) \qquad z^- \in S \cap Z, \end{aligned} \tag{3.70}$$

with $z \in Z$, is the *hybrid zero dynamics* of the model (2.23).

Remark 3.2. *From standard results in [Boo75], $S \cap Z$ will be a smooth one-dimensional embedded sub-manifold if $S \cap Z \neq \emptyset$ and the map $[h' \ (L_f h)' \ p_2^{\text{v}}]'$ has constant rank equal to $2N - 1$ on $S \cap Z$. Since*

$$\frac{\partial}{\partial x} \begin{bmatrix} h \\ L_f h \\ p_2^{\text{v}} \end{bmatrix} = \begin{bmatrix} \dfrac{\partial h}{\partial q} & 0 \\ \dfrac{\partial}{\partial q}\left(\dfrac{\partial h}{\partial q}\,\dot{q}\right) & \dfrac{\partial h}{\partial q} \\ \dfrac{\partial p_2^{\text{v}}}{\partial q} & 0 \end{bmatrix} \tag{3.71}$$

it is clear that this rank condition will be met if the rank of $[h' \ p_2^{\text{v}}]' = N$, and under this rank condition, $S \cap Z \cap \tilde{\mathcal{Q}}$ consists of the isolated zeros of $[h' \ p_2^{\text{v}}]'$. Let q_0^- be a solution of $(h(q), p_2^{\text{v}}(q)) = (0, 0),\ p_2^{\text{h}}(q) > 0$. Then the connected component of $S \cap Z$ containing q_0^- is diffeomorphic to $\mathbb{R}$ per $\sigma : \mathbb{R} \to S \cap Z$, where

$$\sigma(\omega) := \begin{bmatrix} \sigma_q \\ \sigma_{\dot{q}}\,\omega \end{bmatrix} \tag{3.72}$$

$\sigma_q := q_0^-$, *and*

$$\sigma_{\dot{q}} = \begin{bmatrix} \frac{\partial h}{\partial q}(q_0^-) \\ \gamma_0(q_0^-) \end{bmatrix}^{-1} \begin{bmatrix} 0 \\ 1 \end{bmatrix}. \tag{3.73}$$

In view of this, the following additional assumption is made about the output h and the open set $\tilde{\mathcal{Q}}$

HH5) there exists a unique point $q_0^- \in \tilde{\mathcal{Q}}$ *such that* $(h(q_0^-), p_2^{\mathrm{v}}(q_0^-)) = (0,0)$, $p_2^{\mathrm{h}}(q_0^-) > 0$ *and the rank of* $[h' \; p_2^{\mathrm{v}}]'$ *at* q_0^- *equals* N.

The next result characterizes when the swing phase zero dynamics are compatible with the impact model, leading to a non-trivial hybrid zero dynamics.

Theorem 3.2. (Hybrid zero dynamics existence) *Consider the robot model* (2.23) *satisfying RH1)–RH6) and IH1)–IH6) with a smooth function* h *satisfying HH1)–HH5). Then, the following statements are equivalent:*

(a) $\Delta(S \cap Z) \subset Z$;

(b) $h \circ \Delta|_{(S \cap Z)} = 0$ *and* $L_f h \circ \Delta|_{(S \cap Z)} = 0$;

(c) there exists at least one point $(q_0^-, \dot{q}_0^-) \in S \cap Z$ *such that* $\gamma_0(q_0^-)\, \dot{q}_0^- \neq 0$, $h \circ \Delta_q(q_0^-) = 0$, *and* $L_f h \circ \Delta(q_0^-, \dot{q}_0^-) = 0$.

Proof. The equivalence of (a) and (b) is immediate from the definition of Z as the zero set of h and $L_f h$. The equivalence of (b) and (c) follows from Remark 3.2 once it is noted from (2.20) that $L_f h \circ \Delta$ is linear in $\dot{q}$. □

Under the hypotheses of Theorem 3.2, the hybrid zero dynamics are well-defined. Let $z^- \in S \cap Z$, and suppose that $T_I \circ \Delta(z^-) < \infty$. Set $z^+ = \Delta(z^-)$ and let $\varphi : [0, t_f] \to Z$, $t_f = T_I(z^+)$, be a solution of the zero dynamics, (3.41), such that $\varphi(0) = z^+$. Define $\hat{\theta}(t) := \theta \circ \varphi(t)$ and $\dot{\hat{\theta}} := d\hat{\theta}(t)/dt$.

Proposition 3.1. *Assume the hypotheses of Theorem 3.2. Then over any step of the robot,* $\dot{\hat{\theta}} : [0, t_f] \to \mathbb{R}$ *is never zero. In particular,* $\hat{\theta} : [0, t_f] \to \mathbb{R}$ *is strictly monotonic and thus achieves its maximum and minimum values at the end points.*

Proof. Without loss of generality, assume $\hat{\theta}(t_0) < \hat{\theta}(t_f)$. Then $\dot{\hat{\theta}}(t_0) > 0$. To show that $\hat{\theta}(t)$ is monotonic it suffices to show that $\dot{\hat{\theta}}(t) > 0$ for all $t_0 < t < t_f$. Suppose there exists some t_2 (see Figure 3.5) such that $t_0 < t_2 < t_f$ and $\dot{\hat{\theta}}(t_2) = 0$. Let t_2 be the smallest such t. The point $(\hat{\theta}(t_2), 0)$ cannot be an equilibrium point of (3.41) because $\hat{\theta}(t_2) < \hat{\theta}(t_f)$. Hence, there exists some $t_3 > t_2$ such that for all $t_2 < t < t_3$, $\dot{\hat{\theta}}(t) < 0$ and $\hat{\theta}(t) < \hat{\theta}(t_2)$. By the

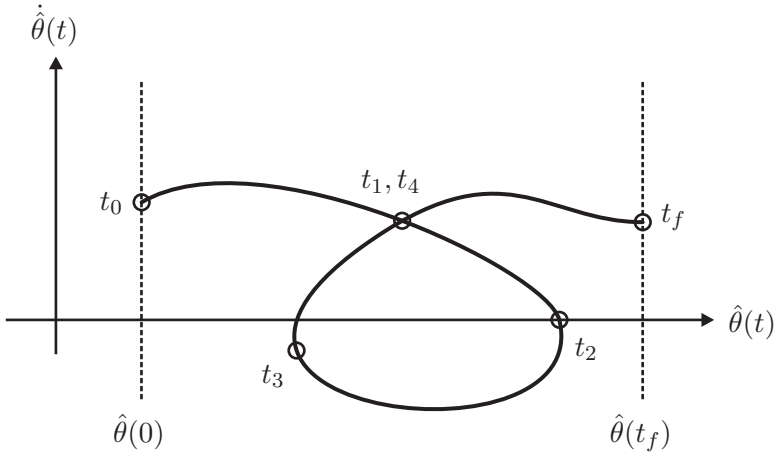

Figure 3.5: Impossible integral curve of the zero dynamics.

assumption that $\hat{\theta}(t) > \hat{\theta}(t_0)$ for all $t > t_0$ and because $\hat{\theta}(t_f) > \hat{\theta}(t_2)$, there must exist a $t_4 > t_3$ such that $\hat{\theta}(t_4) = \hat{\theta}(t_1)$ for some $t_0 < t_1 < t_2$. This contradicts the uniqueness of solutions of (3.41). Hence, there can be no t_2 such that $\dot{\hat{\theta}}(t_2) = 0$ and thus $\dot{\hat{\theta}}(t) > 0$ for all $t_0 < t < t_f$. Therefore, $\hat{\theta} : [t_0, t_f] \to \mathbb{R}$ is strictly monotonic. □

By Remark 3.2, it follows that $\hat{\theta}(0) = \theta \circ \Delta_q(q_0^-)$ and $\hat{\theta}(t_f) = \theta(q_0^-)$, that is, the extrema can be computed *a priori*. Denote these by

$$\theta^- := \theta(q_0^-) \tag{3.74}$$

$$\theta^+ := \theta \circ \Delta_q(q_0^-). \tag{3.75}$$

Without loss of generality, it is assumed that $\theta^+ < \theta^-$; that is, along any step of the hybrid zero dynamics, θ is *monotonically increasing*.

Remark 3.3. *The fact that θ evaluated along a step of the zero dynamics must be monotonic implies that there are restrictions on the walking gaits that can be achieved through computed-torque control based on an output that depends only on the configuration variables.*

3.5 Stability analysis of the zero dynamics

Now, an explicit expression for the Poincaré map of the hybrid zero dynamics will be derived, along with a precise determination of its domain of definition. Fixed points of the Poincaré return map of the hybrid zero dynamics correspond to periodic orbits of the hybrid

zero dynamics. When the hybrid zero dynamics admit an exponentially stable periodic orbit, the general feedback approach developed in [GAP01, PGWA01] can be immediately applied to create a provably, exponentially stable periodic orbit in the full hybrid model.

3.5.1 Poincaré analysis of the zero dynamics

It is shown here that the Poincaré map associated with (3.70) is diffeomorphic to a scalar LTI system, reducing determination of the local stability properties of its fixed point to a simple explicit computation.

Assume the hypotheses of Theorem 3.2. Take the Poincaré section to be $S \cap Z$ so that the Poincaré map is the partial map $\rho : S \cap Z \to S \cap Z$ defined as follows [GAP01]: let $\varphi(t, z_0)$ be a solution of the zero dynamics f_{zero} and consider the time to impact function, (2.25), restricted to Z. Since both $f_{\text{zero}}(z)$ and Z are smooth, a solution of (3.47) and (3.48) from a given initial condition, z_0, is unique and depends smoothly on z_0. Then by [GAP01, Lemma 3], $\tilde{Z} := \{z \in Z \mid 0 < T_I(z) < \infty \text{ and } p_2^{\text{v}}(\varphi(T_I(z), z)) \neq 0\}$ is open. Define the Poincaré return map for the hybrid zero dynamics as

$$\rho(z) := \varphi(T_I \circ \Delta(z), \Delta(z)). \tag{3.76}$$

In a special set of local coordinates, the return map can be explicitly computed. Indeed, express the hybrid zero dynamics in the coordinates of Theorem 3.1, namely, $(\xi_1, \xi_2) = (\theta, \gamma)$. In these coordinates, $S \cap Z$ and $\Delta : (\xi_1^-, \xi_2^-) \to (\xi_1^+, \xi_2^+)$ simplify to

$$\begin{aligned} S \cap Z &= \left\{(\xi_1^-, \xi_2^-) \mid \xi_1^- = \theta^-, \xi_2^- \in \mathbb{R}\right\} && (3.77)\\ \xi_1^+ &= \theta^+ && (3.78)\\ \xi_2^+ &= \delta_{\text{zero}}\, \xi_2^-, && (3.79) \end{aligned}$$

where

$$\delta_{\text{zero}} := \gamma_0(q^+)\, \Delta_{\dot{q}}(q_0^-)\, \sigma_{\dot{q}}(q_0^-), \tag{3.80}$$

a constant that may be computed *a priori*. The hybrid zero dynamics are thus given by (3.47) and (3.48) during the swing phase, and at impact with $S \cap Z$, the re-initialization rules (3.78) and (3.79) are applied. By Proposition 3.1, over any step $\dot{\xi}_1$ is non-zero, and

thus (3.47) and (3.48) are equivalent to

$$\frac{d\xi_2}{d\xi_1} = \frac{\kappa_2(\xi_1)}{\kappa_1(\xi_1)\xi_2}. \tag{3.81}$$

From (3.49), $\dot{\xi}_1 \neq 0$ implies $\xi_2 \neq 0$, and thus $\zeta_2 := \frac{1}{2}(\xi_2)^2$ is a valid change of coordinates on (3.81). In these coordinates, (3.81) becomes

$$\frac{d\zeta_2}{d\xi_1} = \frac{\kappa_2(\xi_1)}{\kappa_1(\xi_1)}. \tag{3.82}$$

For $\theta^+ \leq \xi_1 \leq \theta^-$, define[6]

$$V_{\text{zero}}(\xi_1) := -\int_{\theta^+}^{\xi_1} \frac{\kappa_2(\xi)}{\kappa_1(\xi)}\, d\xi \tag{3.83}$$

$$\zeta_2^- := \frac{1}{2}(\xi_2^-)^2 \tag{3.84}$$

$$\zeta_2^+ := \delta_{\text{zero}}^2\, \zeta_2^-. \tag{3.85}$$

Then (3.82) may be integrated over a step to obtain

$$\zeta_2^- = \zeta_2^+ - V_{\text{zero}}(\theta^-), \tag{3.86}$$

as long as[7] $\zeta_2^+ - V_{\text{zero}}^{\text{MAX}} > 0$, where,

$$V_{\text{zero}}^{\text{MAX}} := \max_{\theta^+ \leq \xi_1 \leq \theta^-} V_{\text{zero}}(\xi_1). \tag{3.87}$$

Theorem 3.3. (Poincaré map for hybrid zero dynamics) *Assume the hypotheses of Theorem 3.2 and let (θ, γ) be as in Theorem 3.1. Then in the coordinates $(\zeta_1, \zeta_2) = (\theta, \frac{1}{2}\gamma^2)$, the Poincaré return map of the hybrid zero dynamics, $\rho : S \cap Z \to S \cap Z$, is given by*

$$\rho(\zeta_2^-) = \delta_{\text{zero}}^2\, \zeta_2^- - V_{\text{zero}}(\theta^-), \tag{3.88}$$

with domain of definition

$$\left\{ \zeta_2^- > 0 \;\middle|\; \delta_{\text{zero}}^2\, \zeta_2^- - V_{\text{zero}}^{\text{MAX}} \geq 0 \right\}. \tag{3.89}$$

If $\delta_{\text{zero}}^2 \neq 1$ and

$$\zeta_2^* := -\frac{V_{\text{zero}}(\theta^-)}{1 - \delta_{\text{zero}}^2} \tag{3.90}$$

[6] In general, V_{zero} must be computed numerically.

[7] By definition, $\zeta_2 := \frac{1}{2}(\xi_2)^2$ must be positive along any solution.

is in the domain of definition of ρ, then it is the fixed point of ρ. Moreover, if ζ_2^* is a fixed point, then ζ_2^* is an exponentially stable equilibrium point of

$$\zeta_2(k+1) = \rho(\zeta_2(k)) \tag{3.91}$$

if, and only if, $0 < \delta_{\text{zero}}^2 < 1$, and in this case, its domain of attraction is (3.89), the entire domain of definition of ρ.

Proof. This follows directly from the above results. □

Remark 3.4. *The domain of definition (3.89) specifies the lower bound on the Poincaré map ρ. That is, if $\zeta_2^- < V_{\text{zero}}^{\text{MAX}}/\delta_{\text{zero}}^2$, then the robot will not successfully complete a step. Viewed another way, $\delta_{\text{zero}}^2\zeta_2^- - V_{\text{zero}}^{\text{MAX}}$ is the amount of energy that may be removed from the system during the step—through perturbations, for example—before the robot will not successfully complete a step.*[8]

These stability results can be reformulated in the following way:

Corollary 3.1. *a) There exists a non-trivial periodic orbit of the hybrid zero dynamics if, and only if, $\delta_{\text{zero}}^2 \neq 1$ and*

$$\frac{\delta_{\text{zero}}^2}{1-\delta_{\text{zero}}^2} V_{\text{zero}}(\theta^-) + V_{\text{zero}}^{\text{MAX}} < 0. \tag{3.92}$$

b) There exists an exponentially stable periodic orbit of the hybrid zero dynamics if, and only if, (3.92) holds and

$$0 < \delta_{\text{zero}}^2 < 1. \tag{3.93}$$

Remark 3.5. *The Lagrangian of the zero dynamics (3.47) and (3.48) can be shown to be $L_{\text{zero}} := K_{\text{zero}} - V_{\text{zero}}$, where V_{zero} is given by (3.83) and*

$$K_{\text{zero}} = \frac{1}{2}\left(\frac{\dot{\xi}_1}{\kappa_1(\xi_1)}\right)^2. \tag{3.94}$$

Remark 3.6. *The time to impact function, $T_I(\xi_2^-)$, may be calculated from (3.47) as*

$$T_I(\xi_2^-) = \int_{\theta^+}^{\theta^-} \frac{1}{\kappa_1(\xi_1)\xi_2(\xi_1, \xi_2^-)}\, d\xi_1 \tag{3.95}$$

where $\xi_2(\xi_1, \xi_2^-)$ is a solution of (3.81) and is monotonic in ξ_2^- which implies that $T_I(\xi_2^-)$ is monotonic in ξ_2^-.

[8] This interpretation is due to Christine Chevallereau.

3.5.2 Imposing modeling hypotheses on the zero dynamics

Although the domain of definition of the Poincaré map is given in (3.89), not all solutions of the zero dynamics satisfy the modeling hypotheses; in particular, walking hypothesis GH2) limits the ratio and sign of the ground reaction forces of the stance leg end during phases of single support. This limit is reflected as an upper bound on the domain of definition of ρ. Let F_1^{T} and F_1^{N} be the tangential and normal forces experienced at the end of the stance leg. The upper bound will be the largest ζ_2^- such that at some point during the associated phase of single support either F_1^{N} becomes negative, or $|F_1^{\mathrm{T}}/F_1^{\mathrm{N}}|$ exceeds the maximum allowed static Coulomb friction coefficient.

Calculation of F_1^{T} and F_1^{N} requires the full $(N+2)$-DOF model. Consider the model (2.5) and apply the feedback u^* from (3.35). Let $\dot{x}_{\mathrm{e}} = f_{\mathrm{e}}(x_{\mathrm{e}}) + g_{\mathrm{e}}(x_{\mathrm{e}})(F_1^{\mathrm{T}}, F_1^{\mathrm{N}})'$ be the resulting closed-loop system written in state space form, where, $x_{\mathrm{e}} := (q_{\mathrm{e}}', \dot{q}_{\mathrm{e}}')'$ and $y_{\mathrm{e}} = h_{\mathrm{e}}(q_{\mathrm{e}}) := (p_1^{\mathrm{h}}(q_{\mathrm{e}}), p_1^{\mathrm{v}}(q_{\mathrm{e}}))'$ is the 2-vector of outputs corresponding to the position of the end of the stance leg. It is easily checked that the decoupling matrix $L_{g_{\mathrm{e}}} L_{f_{\mathrm{e}}} h_{\mathrm{e}}$ is invertible, thus the forces F_1^{T} and F_1^{N} may be calculated as

$$\begin{bmatrix} F_1^{\mathrm{T}} \\ \\ F_1^{\mathrm{N}} \end{bmatrix} = -(L_{g_{\mathrm{e}}} L_{f_{\mathrm{e}}} h_{\mathrm{e}})^{-1} L_{f_{\mathrm{e}}}^2 h_{\mathrm{e}}. \tag{3.96}$$

The above expression is quadratic in $\dot{q}_{\mathrm{e}}$, and, when restricted to Z, is affine in ζ_2. Combining this with (3.82) results in an expression for the forces over a step of the robot that depends only on ξ_1 and ζ_2^-. Express this as

$$\begin{bmatrix} F_1^{\mathrm{N}}(\xi_1, \zeta_2^-) \\ \\ F_1^{\mathrm{T}}(\xi_1, \zeta_2^-) \end{bmatrix} = \Lambda_1(\xi_1)\, \zeta_2^- + \Lambda_0(\xi_1), \tag{3.97}$$

where Λ_0 and Λ_1 are smooth functions of ξ_1. Thus, an upper bound on ζ_2^- so that the pivot assumption holds is given by

$$\zeta_{2,F_1^{\mathrm{N}}}^{\max} := \sup_{\zeta_2^-} \left[\min_{\theta^+ \le \xi_1 \le \theta^-} F_1^{\mathrm{N}}(\xi_1, \zeta_2^-) \right] \ge 0 \tag{3.98}$$

$$\zeta_{2,|F_1^{\mathrm{T}}/F_1^{\mathrm{N}}|}^{\max} := \sup_{\zeta_2^- \le \zeta_{2,F_1^{\mathrm{N}}}^{\max}} \left[\max_{\theta^+ \le \xi_1 \le \theta^-} \left| \frac{F_1^{\mathrm{T}}(\xi_1, \zeta_2^-)}{F_1^{\mathrm{N}}(\xi_1, \zeta_2^-)} \right| \right] \le \mu_s, \tag{3.99}$$

where μ_s is the static Coulomb friction coefficient of the walking surface [HM94], and the domain of definition of the Poincaré return map should thus be restricted to

$$\left\{ \zeta_2^- > 0 \;\middle|\; \delta_{\text{zero}}^2 \, \zeta_2^- - V_{\text{zero}}^{\text{MAX}} \geq 0, \; \zeta_2^- \leq \zeta_{2,|F_1^{\text{T}}/F_1^{\text{N}}|}^{\max} \right\}. \tag{3.100}$$

On a practical note, if the modeling hypotheses included bounds on the maximum actuator torque, these bounds could also be explicitly included in the domain of definition of the Poincaré map in the same manner.

3.6 Creating exponentially stable, periodic orbits in the full model

Fixed points of the Poincaré return map of the hybrid zero dynamics correspond to periodic orbits of the hybrid zero dynamics. By construction of the hybrid zero dynamics, these are also periodic orbits of the full model, (2.23). Moreover, *exponentially stable orbits* of the hybrid zero dynamics correspond to *exponentially stabilizable orbits* of the full model. This is developed next.

Suppose that hypotheses HH1)–HH5) hold and that, in addition, there exists a fixed point, $z^* \in S \cap Z$, of the Poincaré return map for the hybrid zero dynamics. Let $\mathcal{O}$ be the periodic orbit in Z corresponding to z^*; that is,

$$\mathcal{O} := \{ z \in Z \mid z = \varphi(t, \Delta(z^*)), \; 0 \leq t < T_I \circ \Delta(z^*) \}, \tag{3.101}$$

where φ is a solution of the hybrid zero dynamics, (3.70). $\mathcal{O}$ is then a periodic orbit of the full model corresponding to initial condition z^* and control input $u(t) = u^* \circ \varphi(t, \Delta(z^*))$, for $0 \leq t < T_I \circ \Delta(z^*)$, where u^* is given by (3.35).

The application of the pre-feedback

$$u(x) = (L_g L_f h(x))^{-1} (v - L_f^2 h(x)) \tag{3.102}$$

to (2.4) with an output satisfying HH1)–HH4) results in the chain of $N-1$ double integrators,

$$\frac{d^2 y}{dt^2} = v; \tag{3.103}$$

see (3.33). Let $v(y, \dot{y})$ be any feedback controller on (3.103) satisfying conditions CH2)–CH5) of [GAP01], that is,

Controller Hypotheses: for the closed-loop chain of double integrators, $\ddot{y} = v(y, \dot{y})$,

CH2) solutions globally exist on $\mathbb{R}^{2N-2}$, and are unique;

CH3) solutions depend continuously on the initial conditions;

CH4) the origin is globally asymptotically stable, and convergence is achieved in finite time;

CH5) the settling time function[9], $T_{\text{set}} : \mathbb{R}^{2N-2} \to \mathbb{R}$ by

$$\begin{aligned} T_{\text{set}}(y_0, \dot{y}_0) \quad := \quad & \inf\{t > 0 \mid (y(t), \dot{y}(t)) = (0, 0), \\ & (y(0), \dot{y}(0)) = (y_0, \dot{y}_0)\} \end{aligned}$$

depends continuously on the initial condition, $(y_0, \dot{y}_0)$.

Hypotheses CH2)–CH4) correspond to the definition of finite-time stability [Hai86, BB98]; CH5) is also needed, but is not implied by CH2)–CH4) [BB00]. These requirements rule out traditional sliding mode control, with its well-known discontinuous action.

Consider now the full-model (2.23) in closed loop with the feedback

$$u(x) = (L_g L_f h(x))^{-1}(v(h(x), L_f h(x)) - L_f^2 h(x)). \tag{3.104}$$

Take the Poincaré section as S, the walking surface, and let $P : S \to S$ be Poincaré return map. A simple computation shows that the invariance condition, $\Delta(S \cap Z) \subset Z$, implies that P has a well-defined restriction to $S \cap Z$, and that $P|_{S \cap Z} = \rho$, the Poincaré return map of the hybrid zero dynamics. By [GAP01, Theorem 2], it therefore follows that $\mathcal{O}$ is exponentially stable for the full model (2.23) under the feedback (3.104) if, and only if, it is exponentially stable for the hybrid zero dynamics.

Hence, if an output can be selected so that the resulting 1-DOF hybrid zero dynamics admits an exponentially stable orbit, then an exponentially stable walking motion can be achieved under feedback control for the full dynamical model of the robot. Moreover, by

[9] That is, the time it takes for a solution initialized at $(y_0, \dot{y}_0)$ to converge to the origin. The terminology is taken from [BB98].

the results of Section 3.5.2, it can be assured that key modeling assumptions are met for the steady state walking motion. The next chapter looks at a means of systematically selecting the output function.

CHAPTER 4

Control

Chapter 3 provided the conditions for the existence of a zero dynamics for the complete robot model with impacts and established a number of its properties. However, in a concrete manner, the results are not yet practicable for feedback design because the explicit computation of the zero dynamics involves the inversion of a coordinate transformation. This chapter has two principal objectives: to present a class of output functions that leads to computable, closed-form representations of the zero dynamics; and to introduce a finite parameterization of the outputs in a convenient form that will permit the shaping of the zero dynamics by parameter optimization. The output class presented here will be used throughout the rest of the dissertation.

4.1 An almost linear output function structure

Consider the following output function

$$y = h(q) := h_0(q) - h_d \circ \theta(q) \tag{4.1}$$

where $h_0(q)$ specifies $(N-1)$ independent quantities that are to be controlled and $h_d \circ \theta(q)$ specifies the desired evolution of these quantities as a function of the monotonic quantity $\theta(q)$. Driving y to zero will force $h_0(q)$ to track $h_d \circ \theta(q)$, see Figure 1.3. Intuitively, the posture of the robot is being controlled by virtual constraints—here a holonomic constraint parameterized by $\theta(q)$. Note that this is not a trajectory tracking scheme since the desired evolution of $h_0(q)$ is slaved to $\theta(q)$ and not time. Slaving $h_0(q)$ to $\theta(q)$ results in a closed-loop

system which is autonomous.

Choosing

$$h_0(q) := H_0 q \tag{4.2}$$

$$\theta(q) := c\, q \tag{4.3}$$

where $H_0 : \mathbb{R}^N \to \mathbb{R}^{N-1}$ is a linear map, $c : \mathbb{R}^N \to \mathbb{R}$ is a linear functional allows the hypotheses of Lemma 3.1 to be easily satisfied. Concerning those hypotheses, the output function structure of (4.1) with $h_0(q)$ and $\theta(q)$ as in (4.2) and (4.3), respectively, satisfies HH1) (the output only depends on the configuration variables) and will satisfy HH3) (invertibility) if, and only if, $H := [H_0' \; c']'$ is full rank. Hence, if HH2) and HH4) hold, the swing phase zero dynamics can be computed in closed form. Indeed, the coordinate inverse required in (3.45) is given by

$$q = H^{-1} \begin{bmatrix} h_d(\xi_1) \\ \xi_1 \end{bmatrix}. \tag{4.4}$$

In the next section h_d will be specialized to a vector of Bézier polynomials which will make it easy to achieve the invariance condition, $\Delta(S \cap Z) \subset Z$.

Remark 4.1. *Due to the structure of the output (4.1) with h_0 and θ as in (4.2) and (4.3), respectively, HH4) will essentially always hold.*

4.2 Specialization of h_d by Bézier polynomials

A one-dimensional Bézier polynomial [Béz72] of degree M is a polynomial, $b_i : [0, 1] \to \mathbb{R}$, defined by $M + 1$ coefficients, α_k^i, per

$$b_i(s) := \sum_{k=0}^{M} \alpha_k^i \, \frac{M!}{k!(M-k)!} \, s^k (1-s)^{M-k}. \tag{4.5}$$

For later use, note that

$$\frac{\partial b_i(s)}{\partial s} := \sum_{k=0}^{M-1} (\alpha_{k+1}^i - \alpha_k^i) \, \frac{M!}{k!(M-k-1)!} \, s^k (1-s)^{M-k-1}. \tag{4.6}$$

Some particularly useful features of Bézier polynomials are (see [RA90, p. 291])

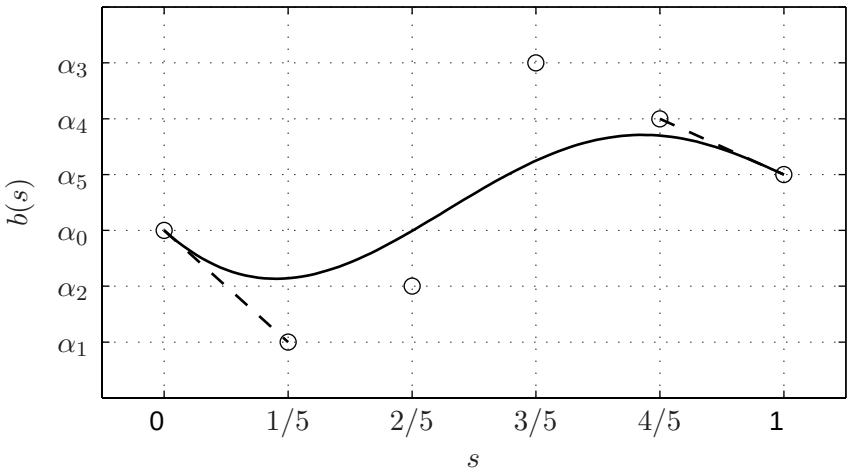

Figure 4.1: An example Bézier fifth-order ($M = 5$) polynomial curve. Note that 1) the curve is contained within the convex hull of the 6 coefficients (as viewed as points in $\mathbb{R}^2$, $\{(0, \alpha_0), (1/5, \alpha_1), \ldots, (1, \alpha_5)\}$), 2) the curve begins at $(0, \alpha_0)$ and ends at $(1, \alpha_5)$, and 3) the curve is tangent to the line segments connecting $(0, \alpha_0)$ and $(1/5, \alpha_1)$, and $(4/5, \alpha_4)$ and $(1, \alpha_5)$ at the start and end points, respectively.

1. the image of the Bézier polynomial is contained in the convex hull of the $M + 1$ coefficients (as viewed as points in $\mathbb{R}^2$, $\{(0, \alpha_0^i)$, $(1/M, \alpha_1^i)$, $(2/M, \alpha_2^i), \ldots,$ $(1, \alpha_M^i)\}$) (the polynomial does not exhibit large oscillations with small parameter variations);

2. $b_i(0) = \alpha_0^i$ and $b_i(1) = \alpha_M^i$; and

3. $(\partial b_i(s)/\partial s)|_{s=0} = M\left(\alpha_1^i - \alpha_0^i\right)$ and $(\partial b_i(s)/\partial s)|_{s=1} = M\left(\alpha_M^i - \alpha_{M-1}^i\right)$.

The first feature will be useful for numerical calculations (such as approximating the gradient of a cost function) where numerical stability is crucial. The second two features are exactly those used to achieve $\Delta(S \cap Z) \subset Z$. See Figure 4.1 for an example Bézier polynomial curve.

A given function $\theta(q)$ of the generalized coordinates will not, in general, take values in the unit interval over a phase of single support. Therefore, to appropriately compose a Bézier polynomial with $\theta(q)$, it is necessary to normalize θ by

$$s(q) := \frac{\theta(q) - \theta^+}{\theta^- - \theta^+}, \tag{4.7}$$

which takes values in $[0, 1]$. Define $h_d \circ \theta(q)$ as

$$h_d \circ \theta(q) := \begin{bmatrix} b_1 \circ s(q) \\ b_2 \circ s(q) \\ \vdots \\ b_{N-1} \circ s(q) \end{bmatrix}. \tag{4.8}$$

Group the parameters α_k^i into an $(N-1) \times (M+1)$ matrix, α, and denote the columns of α by $\alpha_k := (\alpha_k^1, \ldots, \alpha_k^{N-1})'$. For the remainder of the dissertation, the output will be chosen to be of the form (4.1) to (4.3) with h_d chosen as in (4.8). An important class of parameters, α, is now defined.

Definition 4.1. The matrix of parameters α is said to be a *regular parameter* of an output of the form (4.1) to (4.3) with h_d chosen as in (4.8) if the output satisfies HH1)–HH5), which together imply the invertibility of the decoupling matrix and the existence of a two-dimensional, smooth, zero dynamics associated with the single support phase of the robot.

In later chapters it will be important to distinguish between different output functions—and hence walking motions—which differ only in Bézier parameter choice. For this reason, from this point forward quantities related to an output will be labeled with the output's grouped Bézier coefficients label, e.g., θ associated with α will be written θ_α, and the Bézier polynomial order will be written M_α.

Evaluating (4.8) and its derivative with respect to θ_α at the beginning (respectively end) of a phase of single support, that is, where $\theta(q) = \theta_\alpha^+$ (respectively $\theta(q) = \theta_\alpha^-$) will lead to a convenient means of ensuring $\Delta(S \cap Z\alpha) \subset Z_\alpha$. Evaluation of $h_{d,\alpha}$ is particularly trivial,

$$h_{d,\alpha}(\theta_\alpha^+) = \alpha_0 \tag{4.9}$$

$$h_{d,\alpha}(\theta_\alpha^-) = \alpha_M, \tag{4.10}$$

and therefore (4.4) evaluated at θ_α^+ and θ_α^- becomes

$$q_\alpha^+ = H^{-1} \begin{bmatrix} \alpha_0 \\ \theta_\alpha^+ \end{bmatrix} \tag{4.11}$$

$$q_\alpha^- = H^{-1} \begin{bmatrix} \alpha_{M_\alpha} \\ \theta_\alpha^- \end{bmatrix}. \tag{4.12}$$

Differentiation of (4.4) with respect to time yields

$$\dot{q}_\alpha = H^{-1} \begin{bmatrix} \dfrac{\partial h_{d,\alpha}}{\partial \theta} \\ 1 \end{bmatrix} \dot{\theta}_\alpha. \tag{4.13}$$

Taking the partial derivative of (4.8) required by (4.13) yields

$$\begin{aligned} \frac{\partial h_{d,\alpha}}{\partial \theta} &= \frac{\partial b_\alpha}{\partial s_\alpha} \frac{\partial s}{\partial \theta} && (4.14) \\ &= \left(\sum_{k=0}^{M_\alpha} \alpha_k \frac{M_\alpha!}{k!(M_\alpha - k)!} \Big(k s^{k-1} (1-s)^{M_\alpha - k} - \right. \\ &\qquad \left. (M_\alpha - k) s^k (1-s)^{M_\alpha - k - 1} \Big) \right) \frac{1}{\theta_\alpha^- - \theta_\alpha^+} && (4.15) \end{aligned}$$

which when evaluated at θ_α^+ and θ_α^- gives

$$\begin{aligned} \left. \frac{\partial h_{d,\alpha}}{\partial \theta} \right|_{\theta = \theta_\alpha^+} &= \frac{M_\alpha}{\theta_\alpha^- - \theta_\alpha^+} (\alpha_1 - \alpha_0) && (4.16) \\ \left. \frac{\partial h_{d,\alpha}}{\partial \theta} \right|_{\theta = \theta_\alpha^-} &= \frac{M_\alpha}{\theta_\alpha^- - \theta_\alpha^+} (\alpha_{M_\alpha} - \alpha_{M_\alpha - 1}) && (4.17) \end{aligned}$$

therefore (4.13) evaluated at θ_α^+ and θ_α^- becomes

$$\begin{aligned} \dot{q}_\alpha^+ &= H^{-1} \begin{bmatrix} \dfrac{M_\alpha}{\theta_\alpha^- - \theta_\alpha^+} (\alpha_1 - \alpha_0) \\ 1 \end{bmatrix} \dot{\theta}_\alpha^+ && (4.18) \\ \dot{q}_\alpha^- &= H^{-1} \begin{bmatrix} \dfrac{M_\alpha}{\theta_\alpha^- - \theta_\alpha^+} (\alpha_{M_\alpha} - \alpha_{M_\alpha - 1}) \\ 1 \end{bmatrix} \dot{\theta}_\alpha^-. && (4.19) \end{aligned}$$

For two regular parameter sets, α and β, the following theorem gives the conditions under which $\Delta(S \cap Z_\alpha) \subset Z_\beta$. This theorem will be key in the construction of controllers with invariant zero dynamics manifolds and when performing event-based PI control (Section 5.2).

Theorem 4.1. (Achieving $\Delta(S \cap Z_\alpha) \subset Z_\beta$) *Assume the hypotheses of Theorem 3.2 and two outputs h_α and h_β of the form (4.1) with h_0, h_d, and θ as in (4.2), (4.8), and (4.3), respectively. Then, $h_\beta \circ \Delta(S \cap Z_\alpha) = 0$ if, and only if,*

$$\begin{bmatrix} \beta_0 \\ \theta_\beta^+ \end{bmatrix} = H \Delta_q H^{-1} \begin{bmatrix} \alpha_{M_\alpha} \\ \theta_\alpha^- \end{bmatrix}. \tag{4.20}$$

Moreover, if $\delta_{\text{zero},\alpha} \neq 0$*, then* $L_f h_\beta \circ \Delta(S \cap Z_\alpha) = 0$ *if, and only if,*

$$\beta_1 = H_0 \Delta_{\dot{q}} H^{-1} \begin{bmatrix} \dfrac{M_\alpha}{\theta_\alpha^- - \theta_\alpha^+} \left(\alpha_{M_\alpha} - \alpha_{M_\alpha - 1}\right) \\ 1 \end{bmatrix} \frac{\theta_\beta^- - \theta_\beta^+}{M_\beta} \frac{\kappa_{1,\alpha}(\theta_\alpha^-)}{\kappa_{1,\beta}(\theta_\beta^+)} \frac{1}{\delta_{\text{zero},\alpha}} + \beta_0 \tag{4.21}$$

That is, if (4.20) and (4.21) hold, then $\Delta(S \cap Z_\alpha) \subset Z_\beta$*.*

Proof. Using Theorem 3.2 it suffices to show that there exists at least one point $x_\alpha^- = (q_{0,\alpha}^-, \dot{q}_{0,\alpha}^-) \in S \cap Z_\alpha$ such that $\gamma_0(q_{0,\alpha}^-)\, \dot{q}_{0,\alpha}^- \neq 0$, $h_\beta \circ \Delta_q\, q_{0,\alpha}^- = 0$, and $L_f h_\beta \circ \Delta(q_{0,\alpha}^-, \dot{q}_{0,\alpha}^-) = 0$. Evaluating (4.4) on $S \cap Z_\alpha$, $h_\beta \circ \Delta(x_\alpha^-) = 0$ means that $q_\beta^+ = \Delta_q\, q_\alpha^-$. Equating (4.11) and (4.12) with Δ_q yields

$$H^{-1} \begin{bmatrix} \beta_0 \\ \theta_\beta^+ \end{bmatrix} = \Delta_q H^{-1} \begin{bmatrix} \alpha_{M_\alpha} \\ \theta_\alpha^- \end{bmatrix}, \tag{4.22}$$

which may be solved for $(\beta_0', \theta_\beta^+)'$. Achieving $L_f h_\beta \circ \Delta(x_\alpha^-) = 0$ means that $\dot{q}_\beta^+ = \Delta_{\dot{q}}(q_\alpha^-)\, \dot{q}_\alpha^-$. Equating (4.18) and (4.19) with $\Delta_{\dot{q}}$ yields

$$H^{-1} \begin{bmatrix} \dfrac{M_\beta}{\theta_\beta^- - \theta_\beta^+} \left(\beta_1 - \beta_0\right) \\ 1 \end{bmatrix} \dot{\theta}_\beta^+ = \Delta_{\dot{q}} H^{-1} \begin{bmatrix} \dfrac{M_\alpha}{\theta_\alpha^- - \theta_\alpha^+} \left(\alpha_{M_\alpha} - \alpha_{M_\alpha - 1}\right) \\ 1 \end{bmatrix} \dot{\theta}_\alpha^- \tag{4.23}$$

and consequently

$$\frac{M_\beta}{\theta_\beta^- - \theta_\beta^+} \left(\beta_1 - \beta_0\right) \dot{\theta}_\beta^+ = H_0 \Delta_{\dot{q}} H^{-1} \begin{bmatrix} \dfrac{M_\alpha}{\theta_\alpha^- - \theta_\alpha^+} \left(\alpha_{M_\alpha} - \alpha_{M_\alpha - 1}\right) \\ 1 \end{bmatrix} \dot{\theta}_\alpha^- \tag{4.24}$$

which implies

$$\beta_1 = H_0 \Delta_{\dot{q}} H^{-1} \begin{bmatrix} \dfrac{M_\alpha}{\theta^- \alpha - \theta_\alpha^+} \left(\alpha_{M_\alpha} - \alpha_{M_\alpha - 1}\right) \\ 1 \end{bmatrix} \frac{\theta_\beta^- - \theta_\beta^+}{M_\beta} \frac{\dot{\theta}_\alpha^-}{\dot{\theta}_\beta^+} + \beta_0. \tag{4.25}$$

Equation (3.47) implies

$$\dot{\theta}_\alpha^- = \kappa_{1,\alpha}(\theta_\alpha^-) \xi_{2,\alpha}^- \tag{4.26}$$

$$\dot{\theta}_\beta^+ = \kappa_{1,\beta}(\theta_\beta^+) \xi_{2,\beta}^+ \tag{4.27}$$

while (3.79) gives

$$\xi_{2,\beta}^+ = \delta_{\text{zero},\alpha}\, \xi_{2,\alpha}^- \tag{4.28}$$

and, hence, with the assumption that $\delta_{\text{zero},\alpha} \neq 0$,

$$\beta_1 = H_0 \Delta_{\dot{q}} H^{-1} \begin{bmatrix} \dfrac{M_\alpha}{\theta_\alpha^- - \theta_\alpha^+} \left(\alpha_{M_\alpha} - \alpha_{M_\alpha - 1}\right) \\ 1 \end{bmatrix} \frac{\theta_\beta^- - \theta_\beta^+}{M_\beta} \frac{\kappa_{1,\alpha}(\theta_\alpha^-)}{\kappa_{1,\beta}(\theta_\beta^+)} \frac{1}{\delta_{\text{zero},\alpha}} + \beta_0. \tag{4.29}$$

□

Corollary 4.1. (Achieving $\Delta(S \cap Z_\alpha) \subset Z_\alpha$) *Assume the hypotheses of Theorem 3.2 and an output h_α of the form (4.1) with h_0, $h_{d,\alpha}$, and θ_α as in (4.2), (4.8), and (4.3), respectively. Then, $h_\alpha \circ \Delta(S \cap Z_\alpha) = 0$ if, and only if,*

$$\begin{bmatrix} \alpha_0 \\ \theta_\alpha^+ \end{bmatrix} = H \Delta_q H^{-1} \begin{bmatrix} \alpha_{M_\alpha} \\ \theta_\alpha^- \end{bmatrix}. \tag{4.30}$$

Moreover, if $\delta_{\text{zero},\alpha} \neq 0$, then $L_f h_\alpha \circ \Delta(S \cap Z_\alpha) = 0$ if, and only if,

$$\alpha_1 = H_0 \Delta_{\dot{q}} H^{-1} \begin{bmatrix} \left(\alpha_{M_\alpha} - \alpha_{M_\alpha - 1}\right) \\ \dfrac{\theta_\alpha^- - \theta_\alpha^+}{M_\alpha} \end{bmatrix} \frac{\kappa_{1,\alpha}(\theta_\alpha^-)}{\kappa_{1,\alpha}(\theta_\alpha^+)} \frac{1}{\delta_{\text{zero},\alpha}} + \alpha_0 \tag{4.31}$$

That is, if (4.30) and (4.31) hold, then $\Delta(S \cap Z_\alpha) \subset Z_\alpha$.

Remark 4.2. *Corollary 4.1 constrains the coefficients α_0 and α_1 to be functions of α_{M_α} and $\alpha_{M_\alpha - 1}$. Hence, M_α must be chosen to be three or greater to impose configuration and velocity periodicity.*

The following two lemmas give the conditions under which two regular parameter sets, α and β, satisfy $S \cap Z_\beta = S \cap Z_\alpha$ and $\Delta(S \cap Z_\beta) = \Delta(S \cap Z_\alpha)$. These lemmas will be key in transitioning between controllers (Section 5.1).

Lemma 4.1. (Achieving $S \cap Z_\beta = S \cap Z_\alpha$) *Assume two outputs h_α and h_β of the form (4.1) with h_0, h_d, and θ as in (4.2), (4.8), and (4.3), respectively. Then, $S \cap Z_\beta = S \cap Z_\alpha$ if, and only if,*

$$\beta_0 = \alpha_0 \quad \textit{and} \quad \theta_\beta^+ = \theta_\alpha^+ \tag{4.32}$$

and

$$\beta_1 = \frac{M_\alpha}{M_\beta} \frac{\theta_\beta^- - \theta_\beta^+}{\theta_\alpha^- - \theta_\alpha^+} (\alpha_1 - \alpha_0) + \alpha_0 \tag{4.33}$$

Proof. The result follows directly from equating (4.11) for β and α and equating (4.18) for β and α. □

Lemma 4.2. (Achieving $\Delta(S \cap Z_\alpha) = \Delta(S \cap Z_\beta)$) *Assume two outputs h_α and h_β of the form (4.1) with h_0, h_d, and θ as in (4.2), (4.8), and (4.3), respectively. Then, $\Delta(S \cap Z_\alpha) = \Delta(S \cap Z_\beta)$ if, and only if,*

$$\alpha_{M_\alpha} = \beta_{M_\beta} \quad \textit{and} \quad \theta_\alpha^- = \theta_\beta^- \tag{4.34}$$

and

$$\alpha_{M_\alpha - 1} = \frac{M_\beta}{M_\alpha} \frac{\theta_\alpha^- - \theta_\alpha^+}{\theta_\beta^- - \theta_\beta^+} (\beta_{M_\beta - 1} - \beta_{M_\beta}) + \beta_{M_\beta} \tag{4.35}$$

Proof. The result follows directly from equating (4.12) for β and α and equating (4.19) for β and α. □

4.3 Creating exponentially stable fixed points through optimization

The use of optimization in the analysis and design of biped walking motions is not a new concept. Work as early as the 1970s can be found in the biomechanics literature (see [CJ71, Hat76], for example). In more recent years, the design of optimal or approximately optimal trajectories for biped robots has become a popular topic [CA97, CA01, CS00, HAF00, Har99, RB01a, RB01b, RCdWG98]. In each case the approach has been to design time trajectories such that a defined cost is minimized, or approximately minimized, subject to a set of constraints. The optimization technique employed varies. Cabodevila and Abba [CA97] parameterized the robot state as a finite Fourier series and compared the performance of three algorithms: Nelder and Mead, Genetic, and Simulated Annealing. Chevallereau and Aoustin [CA01], and Chevallereau and Sardain [CS00] rewrote the actuated dynamics of the robot as a polynomial function of the unactuated dynamics and used Sequential Quadratic Programming (SQP). Hasegawa, Arakawa, and Fukuda [HAF00] used a modified genetic algorithm to generate reference trajectories parameterized as cubic splines. Hardt [Har99] used an optimization package, DIRCOL [vS99], which implements a sparse SQP algorithm and uses a variable number of cubic splines to approximate the state

and piecewise linear functions to approximate the control signals. Rostami and Bessonnet [RB01b] applied Pontryagin's Maximum Principle. Roussel, Canudas-de-Wit, and Goswami [RCdWG98] approximated the dynamics and used a direct shooting optimization algorithm. Optimization will be used here to design walking motions via the selection output function parameters, the Bézier polynomial coefficients of h_d. The result of optimization is not in an optimal or approximately optimal open-loop trajectory, but rather a *closed-loop system* which creates an exponentially stable orbit, and along this orbit energy consumption has been approximately minimized while satisfying other natural kinematic and dynamic constraints.

Note that in posing the parameter optimization problem (Section 4.3.2), the output function structure, (4.1) to (4.3), is fixed and only the Bézier polynomial coefficients of h_d are allowed to vary. The choice of output function structure, H_0, c, and M, and the use of Bézier polynomials for h_d in this dissertation was based solely upon intuition and experience. Though not explored in this dissertation, it would be interesting to study the effect of varying these choices as well as the effect of choosing altogether different output function structures. For example, in [PGWA01], which addresses the control of the five-link model presented in Chapter 6, a Cartesian approach is taken to output function design. In that work, virtual constraints are posed on the torso angle, horizontal hip position, hip height, and the swing leg end height. These virtual constraints, however, were not chosen so that the corresponding outputs are invariant. So, the stability results of Section 3.5.1 may not be applied. Another example of output function choice is given in [Hür93a]. In that work, a fully actuated model is assumed and the output is chosen to include dependence upon the velocity of the robot. In particular, the horizontal velocity of the center of mass is controlled to be a constant. Although the class of output functions chosen in this dissertation does not allow explicit dependence upon velocity, the effect of velocity dependence used in [Hür93a] may be achieved via the event-based PI control scheme given in Section 5.2.

Before the optimization problem is given, it is worth illustrating how the output function parameters affect gait properties.

4.3.1 How output function parameters affect gait properties: an example

Consider the two-link model presented in Section 2.4 with an output of the form (4.1) to (4.3) with h_d chosen as in (4.8). The goal of this example is to illustrate how selecting the Bézier polynomial coefficients of h_d affect gait properties. The example will proceed by selecting the output details up to, but not including, the Bézier polynomial coefficients and then investigating which parameters give rise to valid walking motions. In the process, the details of hypothesis verification will be illustrated and the need for a systematic approach to parameter selection, optimization, will be motivated.

The first step in output function design is selection of the quantity to be controlled. The controlled quantity is selected to be the hip angle, q_1, since the two-link model has only one actuator at the hip. Hence, $H_0 = [1,\ 0]$. The function $\theta(q)$ is then chosen to be $\theta(q) = q_2$, so $c = [0,\ 1]$, and

$$H = \begin{bmatrix} 1 & 0 \\ 0 & 1 \end{bmatrix} \tag{4.36}$$

As a result, HH3) is clearly satisfied and the decoupling matrix is

$$L_g L_f h(q_1) = \frac{l^2 + \left(2 - \frac{\partial h}{\partial q_2}\right)\left(l_{\mathrm{c}}^2 + l_{\mathrm{c}} l \cos(q_1)\right)}{m l_{\mathrm{c}}^2 \left(l_{\mathrm{c}}^2 + l^2(1 - \cos^2(q_1))\right)}. \tag{4.37}$$

Decoupling matrix invertibility, HH2), will be satisfied if the numerator of (4.37) is different from zero which can be accomplished by appropriately choosing h and $\tilde{\mathcal{Q}} \subset \mathcal{Q}$ for given l and l_{c}. The Bézier polynomial order, M_α, is selected to be four.[1] The first two parameters, α_0 and α_1, are constrained to impose invariance per Corollary 4.1 leaving three free parameters α_2, α_3, and α_4. With only a scalar output and three free parameters, it is feasible to calculate which parameter values give rise to motions that satisfy stability conditions (3.92) and (3.93) and satisfy the remaining unverified hypotheses: GH2), GH4), HH2), HH4), and HH5).[2] This will be accomplished, but to simplify the presentation, fix $\alpha_4 = \pi/5$ which leaves α_2 and α_3 as the only free parameters to be selected. Since HH5) depends only upon

[1] It was found that for choosing $M_\alpha = 3$ did not give rise to any stable motions.

[2] For this two-link model, GH6) will never be satisfied due to the simplicity of the model. See Section 2.4 for a discussion of this issue.

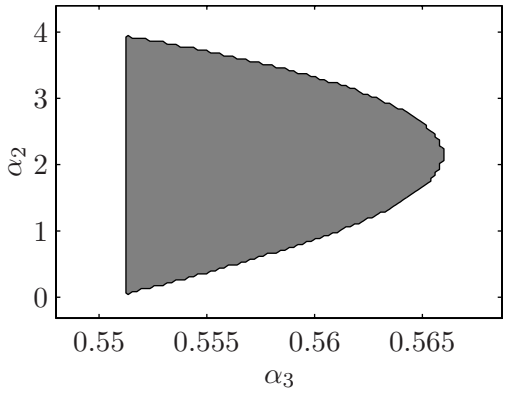

(a) Inside the D-shaped shaded region stability requirements (3.92) and (3.93) are met. Outside one or both are not.

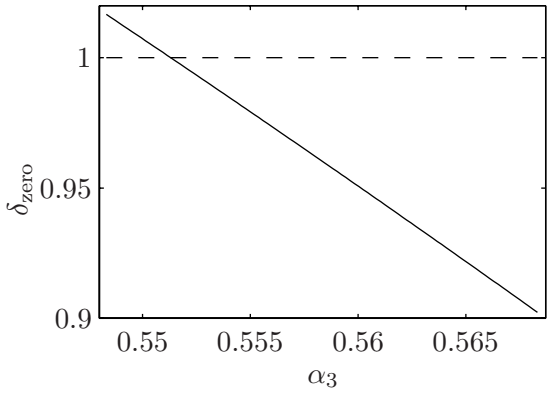

(b) Stability requirement (3.93) is met below the dashed line. Note δ_{zero} depends only on α_3 and α_4.

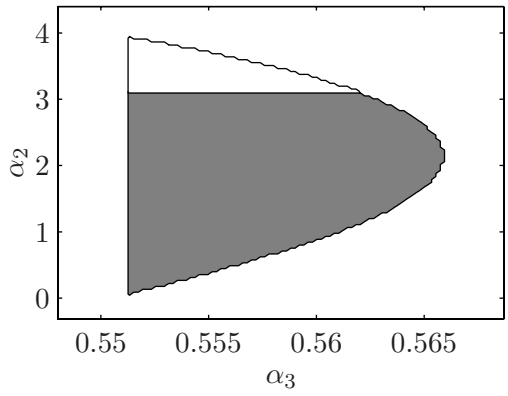

(c) Inside the shaded region HH2), decoupling matrix invertiblity, and HH4) are met. Inside the triangular region above the shaded region, the decoupling matrix is not invertible.

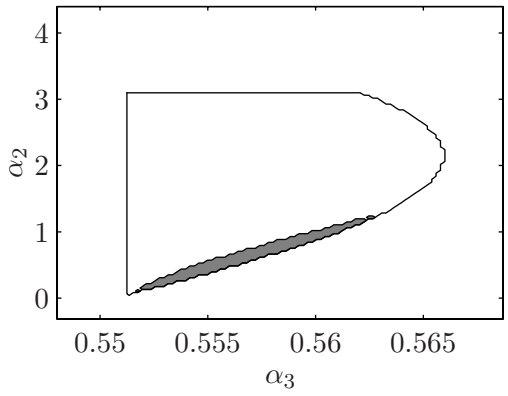

(d) Inside the shaded region the ground contact assumptions given in GH2) and GH4) are met. Outside one or both are not. The coeffiecent of friction is assumed to be 0.6.

Figure 4.2: Determining which parameters give rise to walking for the two-link walker. Note that $\alpha_4 = \pi/5$.

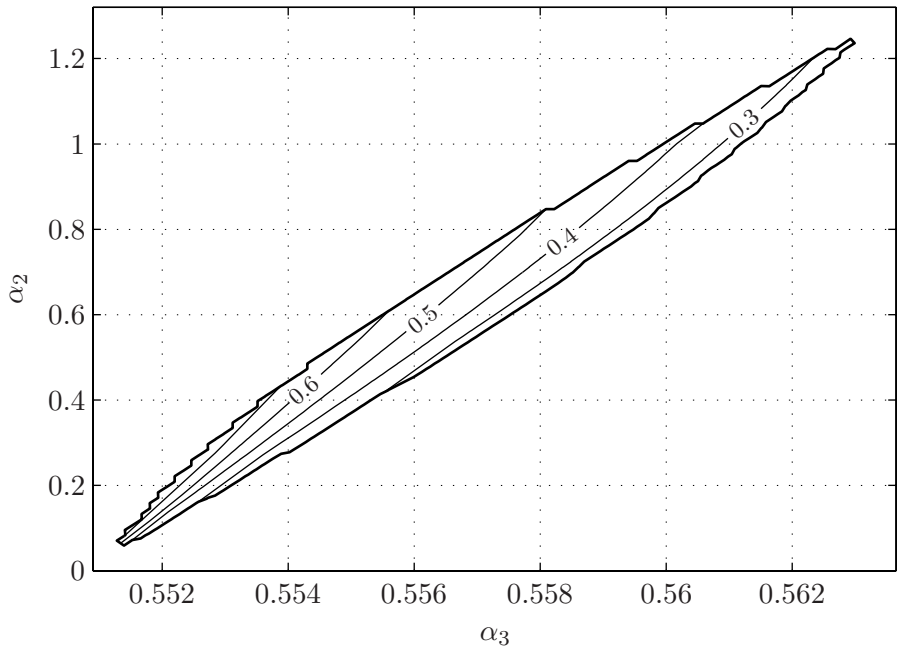

Figure 4.3: Contour plot of average walking rate for parameters which give rise to stable walking. The contour units are meters per second.

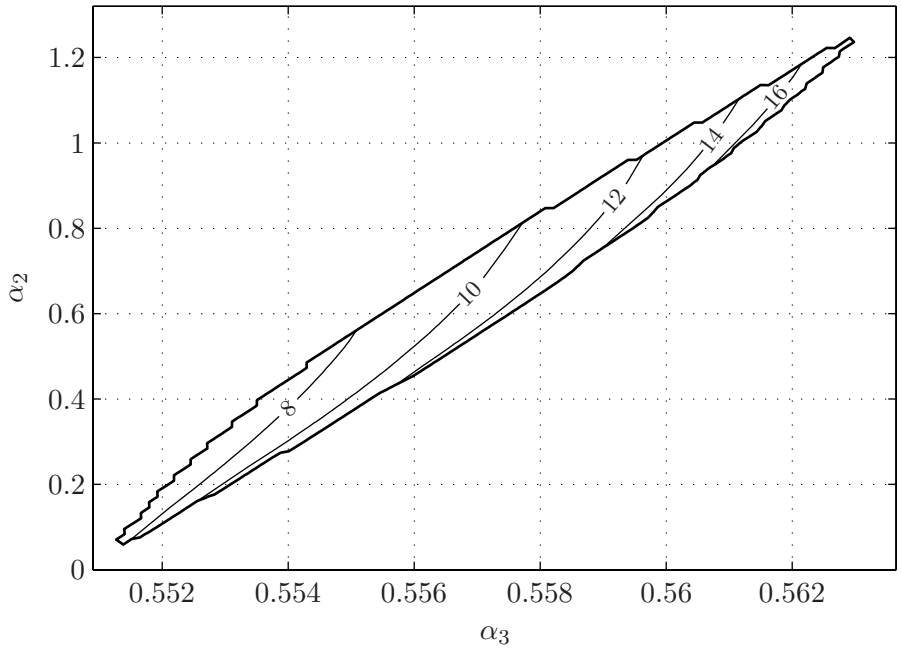

Figure 4.4: Contour plot of the cost for parameters which give rise to stable walking. The cost is $J(\alpha) = \frac{1}{p_2^{\mathrm{h}}(q_0^-)} \int_0^{T_I(\xi_2^-)} (u^*(t))^2 dt$ with units of Joules squared per meter.

q_α^-, given by (4.12), which depends only upon α_4, HH5) is verified since

$$\frac{\partial}{\partial q}\left[\begin{array}{c} h_\alpha \\ p_2^{\mathrm{v}} \end{array}\right]\Bigg|_{q_\alpha^-} = \left[\begin{array}{cc} -0.5093 & 1 \\ -0.6180 & 0.3090 \end{array}\right] \tag{4.38}$$

is full rank. The remaining conditions and hypotheses were checked on a 100 by 100 grid for $-0.7 \leq \alpha_2 \leq 3.7$ and $-0.08 \leq \alpha_3 \leq -0.06$. Figure 4.2(a) gives the region in which the two stability conditions (3.92) and (3.93) are satisfied. The linear shape of the left side of the D-shaped region is a consequence of δ_{zero} being greater than one and δ_{zero} only depending upon α_3 and α_4 (see Figure 4.2(b)). Output assumptions HH2) and HH4) are satisfied for the entire walking motion inside the shaded region of Figure 4.2(c). Inside the triangular region above the shaded region the decoupling matrix becomes singular for at least one point along the walking motion. Inside the shaded region of Figure 4.2(d), the two ground contact assumptions given in GH2) and GH4) are met; namely, the the vertical component of the ground reaction force is positive, the ratio of the horizontal component to the vertical component does not exceed the coefficient of static friction (assumed here to be 0.6), and at impact, the swing leg neither slips nor rebounds. Points inside this region satisfy all gait assumptions, GH1)–GH6), and output assumptions, HH1)–HH5). The grid was refined about this region and the average walking rate, $\bar{\nu}$, and cost,[3]

$$J(\alpha) = \frac{1}{p_2^{\mathrm{h}}(q_0^-)} \int_0^{T_I(\xi_2^-)} ||u^*(t)||_2^2 dt, \tag{4.39}$$

for points inside the region were calculated (see Figure 4.3 and Figure 4.4 for contour plots). It is interesting to note that for this example, the cost associated with walking decreases with increased speed! This is, of course, not the case in general.

For $\alpha_2 = 0.7$ and $\alpha_3 = 0.5575$ the system was simulated for three steps. Table 4.1 and Figure 4.5 give various statistics and plots of interest. Note that the discontinuities in the plots of Figure 4.5 are due to impacts and coordinate relabeling. The swing foot height, Figure 4.5(f), becomes negative due to the foot scuffing that is unavoidable with this simple model (see Section 2.4). Figure 4.6 gives a stick animation of the simulation.

In this simple example it is clear how to choose α_2 and α_3 to achieve walking with certain characteristics. As the Bézier polynomial order, M_α, and the number of links, N,

[3]See the next subsection for a discussion of this cost function.

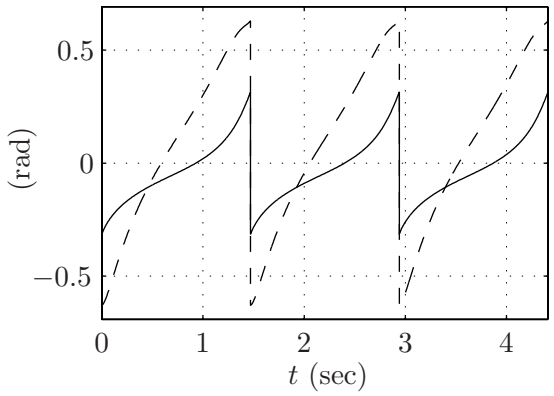

(a) Joint angles, q_1 (solid) and q_2 (dashed), versus time.

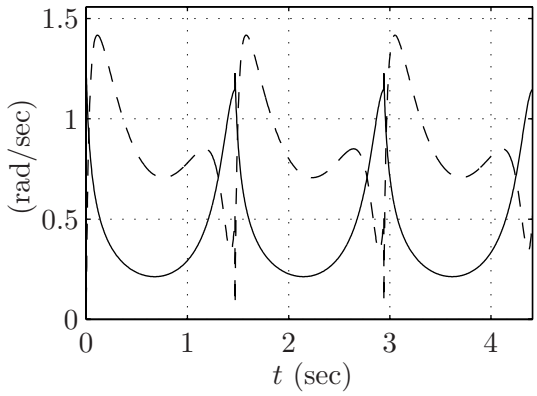

(b) Joint velocities, $\dot{q_1}$ (solid) and $\dot{q_2}$ (dashed), versus time.

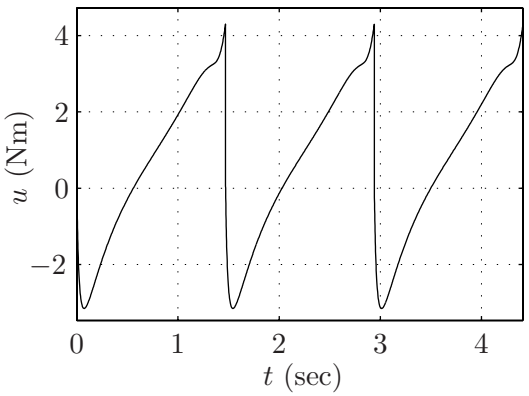

(c) Hip torque, u, versus time.

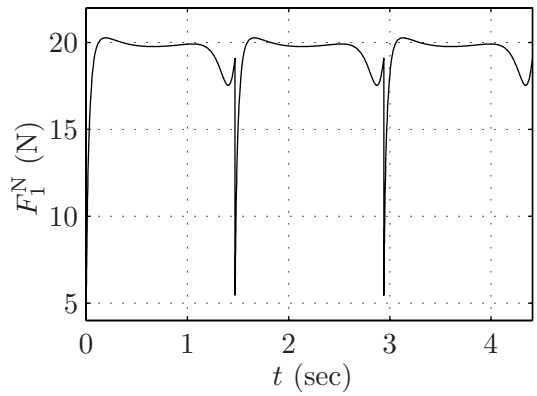

(d) Stance leg end normal force, F_1^{N}, versus time.

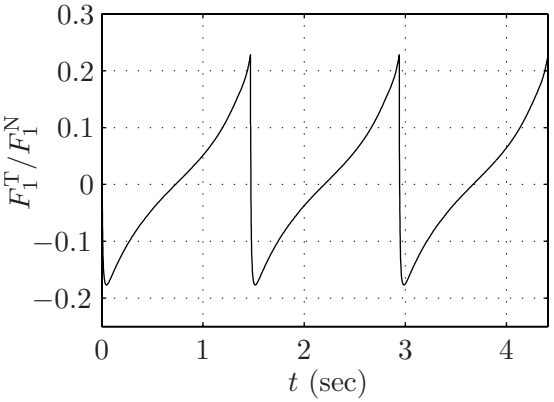

(e) Stance leg end force ratio, $F_1^{\mathrm{T}}/F_1^{\mathrm{N}}$, versus time. The coefficient of static friction is assumed to be 0.6.

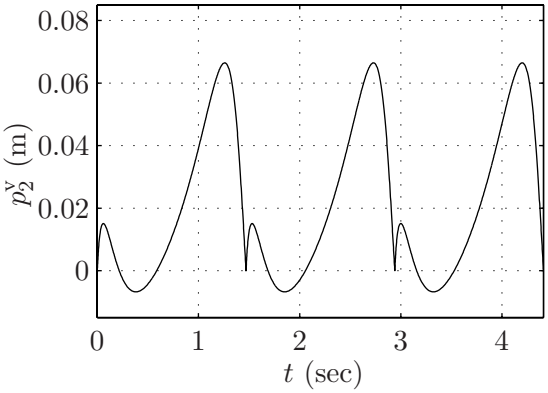

(f) Swing foot height, p_2^{y}, versus time. Note the foot scuffing that is unavoidable with this simple model.

Figure 4.5: Plots corresponding to an example two-link walker gait at 0.42 m/s for three steps. The discontinities are due to impacts and coordinate relabeling.

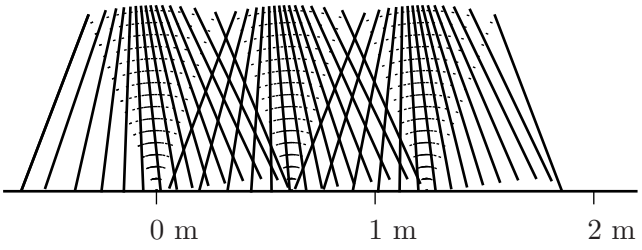

Figure 4.6: Stick animation of two-link walker taking three steps from left to right. The stance leg is dotted.

$J(\alpha)$	ζ_2^*	δ^2_{zero}	$V_{\text{zero}}(\theta^-)$	$V^{\text{MAX}}_{\text{zero}}$	$\bar{\nu}$
(N^2m)	(kgm^2/s)^2	-	(kgm^2/s)^2	(kgm^2/s)^2	(m/s)
10.82	4.45	0.931	-0.306	3.581	0.420

Table 4.1: Example gait statistics for the two-link walker with $\alpha_2 = 0.7$ and $\alpha_3 = 0.5575$.

increase, choosing parameters becomes significantly more difficult. This motivates the use of optimization as an automated means of parameter selection.

4.3.2 The optimization problem

The parameter selection problem will now be cast as a constrained nonlinear optimization problem that may be solved with any number of the numerical optimization tools available. The objective will be to choose the matrix of output function parameters, α, such that (2.23) with output (4.1) with h_0, h_d, and θ as in (4.2), (4.8), and (4.3), respectively, and feedback (3.104) admit an exponentially stable periodic orbit while approximately minimizing some cost function and satisfying a number of constraints. This problem may be solved on the full hybrid model (2.23), but it is computationally expensive, and increasingly

so as the order of the Bézier polynomials of (4.8) and the number of links, N becomes large. Choosing the parameters of (4.2), (4.8), and (4.3) to satisfy the assumptions of Corollary 4.1, however, guarantees that the hybrid zero dynamics (3.70) exist and the unique control associated with the single support phase of model (2.23) is given by (3.35). In this way, the optimization problem may be solved on the (2-dimensional) hybrid zero dynamics (3.70) instead of on the full ($2N$-dimensional) hybrid model (2.23).

Posing the constrained nonlinear optimization problem requires two ingredients: a cost function and a set of constraints. Here, the cost function will be some metric on the hybrid zero dynamics and the constraints will ensure the following: the stability conditions (3.92) and (3.93) are met; that the gait hypothesis GH2), GH4) and GH6) and output function hypotheses HH2), HH4), and HH5) are met; and that the the resultant gait has other desired properties.

In the optimization literature on biped gait design the two most popular cost functions to minimize over a single step are

$$J_1(\alpha) := \frac{1}{p_2^{\mathrm{h}}(q_0^-)} \int_0^{T_I(\xi_2^-)} ||u^*(t)||_2^2 dt \tag{4.40}$$

and

$$J_2(\alpha) := \frac{1}{p_2^{\mathrm{h}}(q_0^-)} \int_0^{T_I(\xi_2^-)} \langle \dot{q}(t), Bu^*(t) \rangle dt \tag{4.41}$$

where $\dot{q}_i$ calculated from (3.46), $T_I(\xi_2^-)$ is the step duration, $p_2^{\mathrm{h}}(q_0^-)$ corresponds to step length, $u^*(t)$ is the result of evaluating (3.35) along a solution of the hybrid zero dynamics, and $\langle a, b \rangle := a'b$. The cost (4.40) has the effect of minimizing the peak torque over a step while (4.41) has the effect of minimizing total power. The total number of parameters for optimization is $(N-1)(M_\alpha - 1)$; $M_\alpha - 1$ free parameters for each output.[4]

Remark 4.3. *The weighting matrix*

$$W(q) := \mathrm{diag}(w_1(\dot{q}_1), \ldots, w_N(\dot{q}_N)), \tag{4.42}$$

with

$$w_i(q_i) := \begin{cases} w_{i,0}, & \mathrm{sgn}(\dot{q}_i) \leq 0 \\ w_{i,1}, & \mathrm{sgn}(\dot{q}_i) > 0, \end{cases} \tag{4.43}$$

[4]By Corollary 4.1 two parameters per output can be calculated from the other $M_\alpha - 1$.

$w_{i,0}, w_{i,1} > 0$ *for* $i = 1, \ldots, N$*, is sometimes included in the inner product of (4.41) so that* $\langle \cdot, \cdot \rangle$ *is replaced with*

$$\langle a, b \rangle_W := a' W b. \tag{4.44}$$

This permits different axes to have different weights associated with their motion as well as different weights to be associated with motions in their positive and negative directions.

The constraints may be divided into two classes: nonlinear inequality constraints (NIC's) and nonlinear equality constraints (NEC's). The following constraints are typically required:

Nonlinear Inequality Constraints

The following three NIC's enforce modeling assumptions per constraints on

NIC1) minimum normal ground reaction force experienced by the stance leg end,

$$F_1^{\mathrm{N}} > 0; \tag{4.45}$$

NIC2) maximum ratio of tangential to normal ground reaction forces experienced by the stance leg end,

$$\left| \frac{F_1^{\mathrm{T}}}{F_1^{\mathrm{N}}} \right| < \mu_s; \tag{4.46}$$

NIC3) swing leg end height to ensure S intersects Z only the end of the step.

Note that other NIC's, such as a constraint on minimum hip height, maximum swing leg deflections, etc., are in general required to achieve a desired walking style.

Nonlinear Equality Constraints

There are five natural NEC's that enforce

NEC1) the average walking rate, $\bar{\nu}$, defined as step length divided by step duration

$$\bar{\nu} := \frac{p_2^{\mathrm{h}}(q_0^-)}{T_I(\xi_2^-)}; \tag{4.47}$$

NEC2) that the post-impact velocity of the swing leg is positive;

NEC3) the validity of the impact of the swing leg end with the walking surface;

NEC4) the existence of a fixed point, $\zeta_2^* > V_{\text{zero}}^{\text{MAX}}/\delta_{\text{zero}}^2$; and

NEC5) the stability of the fixed point, $0 < \delta_{\text{zero}}^2 < 1$.

In this generic form, the parameter optimization problem may be solved with any number of the numerical optimization tools available. For the work reported in this dissertation, the optimization problem was solved with MATLAB's constrained nonlinear optimization tool `fmincon` with the hybrid zero dynamics implemented in C as a MATLAB S-Function (see Appendix B).

It is important to emphasize that the use of the hybrid zero dynamics greatly reduces the computational cost of evaluating the cost function (4.40) or (4.41). Moreover, stability of the closed-loop system may be included as a simple optimization constraint. After optimization, hypothesis HH2), the invertibility of the decoupling matrix, must be checked. This condition is essentially guaranteed whenever $J(\alpha)$ is finite, since singularities in $L_g L_f h$ will normally result in u^* taking on unbounded values; however, a simply connected, open set about the periodic orbit where the decoupling matrix is invertible can be *explicitly* computed by a method developed in Appendix C.

4.3.3 The optimization problem in Mayer form

The optimization problem may also be expressed in Mayer form [Ban86, p. 332] as

$$\dot{x}_1 = \kappa_1(x_1)\, x_2 \tag{4.48}$$

$$\dot{x}_2 = \kappa_2(x_1) \tag{4.49}$$

$$\dot{x}_3 = \dot{J}(x_1, x_2, \alpha). \tag{4.50}$$

where $\dot{J}$ is the time derivative of the cost. Mayer form is used by parameter optimization algorithms that construct an approximate solution to some parameterized set of first order differential equations such that some cost is minimized. Appending the cost as a state enables the cost calculation and solution approximation to be performed with the same algorithm. The cost function (4.40), for example, may be appended as

$$\dot{J}_1(x_1, x_2, \alpha) := \frac{1}{p_2^{\text{h}}(q_0^-)} ||u^*(x_1, x_2, \alpha)||_2^2 \tag{4.51}$$

so that

$$x_3(t_0) = \frac{1}{p_2^{\mathrm{h}}(q_0^-)} \int_0^{t_0} ||u^*(t)||_2^2 dt. \tag{4.52}$$

Posing the problem in Mayer form requires another class of constraints, explicit boundary constraints (EBC's), constraints that give the initial or final state. The following EBC's are required.

Explicit Boundary Constraints

There are five EBC's that give the state at $t = 0$ and $t = T_I(\xi_2^-)$,

EBC1) $x_1(0) = c\,\Delta_q\,\sigma_q$;

EBC2) $x_2(0) = \gamma \circ \Delta \circ \sigma(\zeta_2^*)$;

EBC3) $x_3(0) = 0$;

EBC4) $x_1(T_I(\xi_2^-)) = c\,\sigma_q$; and

EBC5) $x_2(T_I(\xi_2^-)) = \gamma \circ \sigma(\zeta_2^*)$.

Note that $x_3(T_I(\xi_2^-))$ cannot be explicitly given as its calculation requires knowledge of x_1 and x_2 over the entire time interval of optimization. Also note that without use of the hybrid zero dynamics the optimization in Mayer form would have $2N$ states, the derivative of the cost, and $N - 1$ control signals to be included in the problem formulation.

CHAPTER 5

Additional tools

This chapter provides two additional tools that enable the design of controllers that are able to induce walking at more than a single, fixed average walking rate (in steady state). The first is a method for serially composing two controllers so as to transition the robot from walking at a given fixed average walking rate to another, without loss of stability. The controller design is motivated by a switching idea presented in [BAK99]: controllers were first designed to accomplish the individual tasks of juggling, catching, and palming a ping-pong ball by a robot arm; these controllers were then sequentially composed via switching to accomplish the complex task of maneuvering the ping-pong ball in a three-dimensional workspace with an obstacle. The regions of attraction of each controller were first empirically estimated within the full state space of the robot. Switching from one controller to another without loss of stability was then accomplished by comparing the current state of the robot to the region of attraction of the controller for the next desired task. The problem faced in this note is more challenging in that the domains of attraction of any two of the individual controllers may have empty intersection, and hence a transition controller will be required to steer the robot from the region of attraction of one controller into the region of attraction of a second, "nearby" controller.

The second tool is an event-based PI controller that is able to regulate average walking rate to a continuum of values, to reject the effect of moderate disturbances on average walking rate, and to hasten convergence of average walking rate to its steady state value. The controller uses PI control to adjust the parameters in a controller that, for fixed parameter

values, induces an exponentially stable, periodic orbit. Parameter adjustment takes place just after impact (swing leg touching the ground). The analysis of the controller is based on the restricted Poincaré map of the hybrid zero dynamics. This idea is most closely related to the work of [AF99].

5.1 Transitioning

Let α and β be two regular sets of parameters of output (4.1) with $h_0(q)$ and $\theta(q)$ as in (4.2) and (4.3), respectively, with corresponding zero dynamics manifolds, Z_α and Z_β. Suppose that $\Delta(S \cap Z_\alpha) \subset Z_\alpha$ and $\Delta(S \cap Z_\beta) \subset Z_\beta$, and that there exist exponentially stable periodic orbits,[1] $\mathcal{O}_\alpha \subset Z_\alpha$ and $\mathcal{O}_\beta \subset Z_\beta$; denote the corresponding controllers by Γ_α and Γ_β. The goal is to be able to transition from $\mathcal{O}_\alpha$ to $\mathcal{O}_\beta$ without the robot falling (i.e., with stability guaranteed). If it were known that the domains of attraction of the two orbits had a non-empty intersection, then the method of [BAK99] could be applied directly. Numerically evaluating the domains of attraction on the full-order model is unpleasant, so another means of assuring a stable transition is sought that is based on easily computable quantities, the domains of attraction of the restricted Poincaré maps associated with Γ_α and Γ_β.

Since in general $Z_\alpha \cap Z_\beta = \emptyset$, the method for providing a stable transition from Z_α and Z_β will be to introduce a one-step transition controller $\Gamma_{(\alpha\to\beta)}$ whose (swing phase) zero dynamics manifold $Z_{(\alpha\to\beta)}$ connects the zero dynamics manifolds Z_α and Z_β; (see Figure 5.1). More precisely, switching will be synchronized with impact events and the zero dynamics manifold $Z_{(\alpha\to\beta)}$ will be chosen to map exactly from the one-dimensional manifold $\Delta(S \cap Z_\alpha)$ (i.e., the state of the robot just after impact with S under controller Γ_α) to the one-dimensional manifold $S \cap Z_\beta$ (i.e., the state of the robot just before impact with S under controller Γ_β). The one-step transition controller $\Gamma_{(\alpha\to\beta)}$ differs from a deadbeat controller in that $\Gamma_{(\alpha\to\beta)}$ takes *all points* in a subset of manifold $\Delta(S \cap Z_\alpha)$ into a subset of the manifold $S \cap Z_\beta$ as opposed to a deadbeat controller that would map a subset of $\Delta(S \cap Z_\alpha)$ to a *point* in $S \cap Z_\beta$. The design of multi-step transition controllers is also possible but not

[1] Typically, these would correspond to walking at different average walking rates.

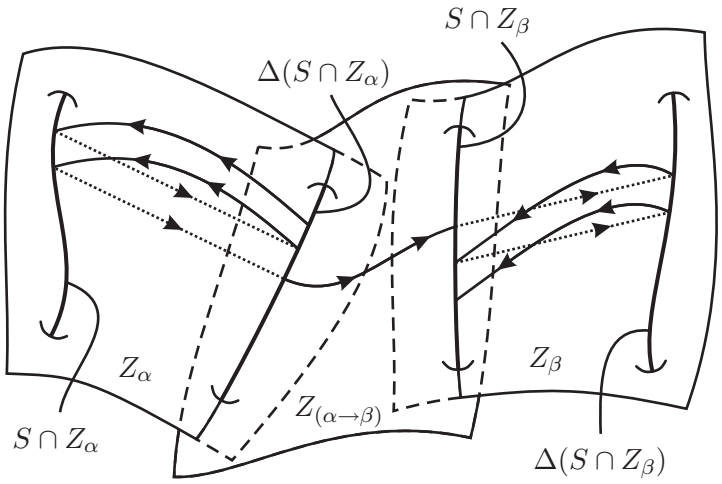

Figure 5.1: Composition of two controllers Γ_α and Γ_β via transition controller $\Gamma_{(\alpha\to\beta)}$. Under the action of Γ_α the dynamics evolve on Z_α. Switching to $\Gamma_{(\alpha\to\beta)}$ when the state enters $\Delta(S \cap Z_\alpha)$ causes the dynamics to evolve along $Z_{(\alpha\to\beta)}$ to $S \cap Z_\beta$. Switching to Γ_β when the state enters $S \cap Z_\beta$ causes the dynamics to evolve on Z_β.

addressed here.

By Lemma 4.1 and Lemma 4.2 any zero dynamics manifold $Z_{(\alpha\to\beta)}$ with parameters

$$\begin{aligned}
(\alpha \to \beta)_0 &= \alpha_0 \\
(\alpha \to \beta)_1 &= \frac{M_\alpha}{M_{(\alpha\to\beta)}} \frac{\theta_\beta^- - \theta_\alpha^+}{\theta_\alpha^- - \theta_\alpha^+} (\alpha_1 - \alpha_0) + \alpha_0 \\
(\alpha \to \beta)_{M_{(\alpha\to\beta)}-1} &= \frac{M_\beta}{M_{(\alpha\to\beta)}} \frac{\theta_\beta^- - \theta_\alpha^+}{\theta_\beta^- - \theta_\beta^+} \left(\beta_{M_\beta - 1} - \beta_{M_\beta}\right) + \beta_{M_\beta} \\
(\alpha \to \beta)_{M_{(\alpha\to\beta)}} &= \beta_{M_\beta} \\
\theta^+_{(\alpha\to\beta)} &= \theta^+_\alpha \\
\theta^-_{(\alpha\to\beta)} &= \theta^-_\beta
\end{aligned} \tag{5.1}$$

satisfies $Z_{(\alpha\to\beta)} \cap \Delta(S \cap Z_\alpha) = \Delta(S \cap Z_\alpha)$ and $\Delta(S \cap Z_{(\alpha\to\beta)}) = \Delta(S \cap Z_\beta)$ (see Figure 5.1). The choice of the intermediate parameter values, $(\alpha \to \beta)_i$, $i = 2$ to $M_{(\alpha\to\beta)} - 2$ affects the walking motion, and one could choose their values through optimization, for example, to minimize the torques required to evolve along the surface $Z_{(\alpha\to\beta)}$. However, the simple choice

$$(\alpha \to \beta)_i = (\alpha_i + \beta_i)/2, \ i = 2 \ \text{ to } \ M_{(\alpha\to\beta)} - 2, \tag{5.2}$$

has proven effective in practice. The reason for this seems to be intimately linked the use of Bézier polynomials (see Section 4.2).

Assume that the parameter matrix given in (5.1) and (5.2) is regular and let $\Gamma_{(\alpha\to\beta)}$ be an associated controller; then $\Gamma_{(\alpha\to\beta)}|_{Z_{(\alpha\to\beta)}}$ is uniquely determined by the matrix of parameters $(\alpha \to \beta)$. The goal now is to determine under what conditions $\Gamma_{(\alpha\to\beta)}$ will effect a transition from the region of attraction (in $S \cap Z_\alpha$) of $\mathcal{O}_\alpha$ to the region of attraction (in $S \cap Z_\beta$) of $\mathcal{O}_\beta$.

Let $P_{(\alpha\to\beta)} : S \to S$ be the Poincaré return map of the model (2.23) in closed loop with $\Gamma_{(\alpha\to\beta)}$ and consider $P_{(\alpha\to\beta)}|_{(S\cap Z_\alpha)}$. By construction of $Z_{(\alpha\to\beta)}$, $\Delta(S \cap Z_\alpha) \subset Z_{(\alpha\to\beta)}$. Since $Z_{(\alpha\to\beta)}$ is invariant under $\Gamma_{(\alpha\to\beta)}$, it follows that $P_{(\alpha\to\beta)}(S \cap Z_\alpha) \subset S \cap Z_{(\alpha\to\beta)}$. But by construction, $S \cap Z_{(\alpha\to\beta)} = S \cap Z_\beta$. Thus, the restriction of the Poincaré return map to $S \cap Z_\alpha$ induces a (partial) map

$$\rho_{(\alpha\to\beta)} : S \cap Z_\alpha \to S \cap Z_\beta. \tag{5.3}$$

In Section 3.5, a closed-form expression for $\rho_{(\alpha\to\beta)}$ is computed on the basis of the two-dimensional zero dynamics associated with $Z_{(\alpha\to\beta)}$.

Let $\mathcal{D}_\alpha \subset S \cap Z_\alpha$ and $\mathcal{D}_\beta \subset S \cap Z_\beta$ be the domains of attraction of the restricted Poincaré maps $\rho_\alpha : S \cap Z_\alpha \to S \cap Z_\alpha$ and $\rho_\beta : S \cap Z_\beta \to S \cap Z_\beta$ associated with the orbits $\mathcal{O}_\alpha$ and $\mathcal{O}_\beta$, respectively. (Since the existence of exponentially stable, periodic orbits has been assumed, these domains are non-empty and open.) It follows that $\rho^{-1}_{(\alpha\to\beta)}(\mathcal{D}_\beta)$ is precisely the set of states in $S \cap Z_\alpha$ that can be steered into the domain of attraction of $\mathcal{O}_\beta$ under the control law $\Gamma_{(\alpha\to\beta)}$. In general, from stability considerations, one is more interested in $\mathcal{D}_\alpha \cap \rho^{-1}_{(\alpha\to\beta)}(\mathcal{D}_\beta)$, the set of states in the domain of attraction of $\mathcal{O}_\alpha$ that can be steered into the domain of attraction of $\mathcal{O}_\beta$ in one step under the control law $\Gamma_{(\alpha\to\beta)}$ (see Figure 5.1).

Theorem 5.1. (Serial composition of stable walking motions) *Assume that α and β are regular parameters of output (4.1) with h_0, h_d, and θ as in (4.2), (4.8), and (4.3), respectively, and that $(\alpha \to \beta)$ defined by (5.1) and (5.2) is also regular. Suppose furthermore that*

1. *$\Delta(S \cap Z_\alpha) \subset Z_\alpha$ and $\Delta(S \cap Z_\beta) \subset Z_\beta$;*

2. *there exist exponentially stable, periodic orbits $\mathcal{O}_\alpha$ and $\mathcal{O}_\beta$ in Z_α and Z_β, respectively, so that the domains of attraction $\mathcal{D}_\alpha \subset S \cap Z_\alpha$ and $\mathcal{D}_\beta \subset S \cap Z_\beta$ of the associated restricted Poincaré maps are non-empty and open.*

Then the set of states in $\mathcal{D}_\alpha$ that can be steered into $\mathcal{D}_\beta$ in one step under any control law $\Gamma_{(\alpha\to\beta)}$ satisfying assumptions CH2)–CH5) of Section 3.6 is equal to $\mathcal{D}_\alpha \cap \rho^{-1}_{(\alpha\to\beta)}(\mathcal{D}_\beta)$.

Proof. This follows directly from the definition of $\rho_{(\alpha\to\beta)}$. □

An example is given in Section 6.5.3.

5.2 Event-based PI control of average walking rate

For a given controller Γ_α satisfying the hypotheses of CH2)–CH5) so that Z_α is invariant under the swing phase zero dynamics in closed loop with Γ_α, the average walking rate is computed from the model (2.23) as follows. Let $P_\alpha : S \to S$ be the Poincaré return map and let $T_{I,\alpha} : TQ \to \mathbb{R}_{\geq 0} \cup \{\infty\}$ be the time to impact function (2.25). Formally, the average walking rate is the (partial) map $\bar{\nu}_\alpha : S \to \mathbb{R}_{\geq 0}$,

$$\bar{\nu}_\alpha := \frac{p_2^{\mathrm{h}} \circ P_\alpha}{T_{I,\alpha} \circ \Delta}, \tag{5.4}$$

where, p_2^{h}, when evaluated on S, computes step length; see Figure 1.4. On the open subset $\tilde{S} \subset S$ where $0 < T_{I,\alpha} \circ \Delta < \infty$ and the associated impacts are transversal to S, both P_α and $T_{I,\alpha} \circ \Delta$ are well-defined and continuous (see [GAP01, Sec. III.B]). It follows that $\bar{\nu}_\alpha$ restricted to $\tilde{S}$ is continuous. Since Γ_α is continuous but not Lipschitz continuous, $\bar{\nu}_\alpha$ is not smooth on any open subset of S. However, if α is a regular parameter value of output (4.1) with h_0, h_d, and θ as in (4.2), (4.8), and (4.3), respectively, giving rise to a hybrid zero dynamics that evolve on the associated zero dynamics manifold Z_α, then $\bar{\nu}_\alpha$ restricted to $\tilde{S} \cap Z_\alpha$ depends smoothly on the states and the parameter values α used to define the outputs, (4.1).

Let $A = \mathbb{R}^{(N-1)\times(M+1)}$ be the set of all Bézier polynomial coefficients, α, for the output (4.1) with h_0, h_d, and θ as in (4.2), (4.8), and (4.3), respectively. For this section, it is

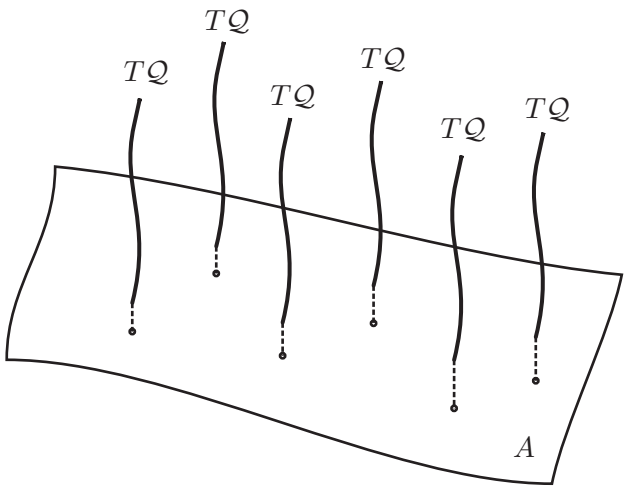

Figure 5.2: Fiber bundle used for event-based PI control. The fiber bundle $\pi : A \times T\mathcal{Q} \to A$. The base, $A = \mathbb{R}^{(N-1)\times(M+1)}$, is the set of all Bézier polynomial coefficients. Above each point in the base are the fibers, copies of the state space, $T\mathcal{Q}$, of the robot.

important to note that the degrees of the Bézier polynomials in h_d are *fixed*. Partition A, and, consequently, each $\alpha = [\alpha_0, \ldots, \alpha_M] \in A$, into two sets:

$$\alpha_{\text{invar}} := [\alpha_0, \alpha_1] \in A_{\text{invar}} := \mathbb{R}^{(N-1)\times 2}, \tag{5.5}$$

the parameters used to render the swing phase zero dynamics invariant under the impact mapping and

$$\alpha_{\text{free}} := [\alpha_2, \ldots, \alpha_M] \in A_{\text{free}} := \mathbb{R}^{(N-1)\times(M-1)}, \tag{5.6}$$

those freely chosen to affect the shape of the walking motion. Note that $A = A_{\text{invar}} \times A_{\text{free}}$ and $\alpha = [\alpha_{\text{invar}},\ \alpha_{\text{free}}]$.

The natural geometric object to use in the analysis of event-based, step-to-step parameter modifications is a fiber bundle. The fiber bundle structure will elucidate the interaction between parameter modifications and the evolution of a Poincaré-like mapping, the flow map. To that end, define the trivial fiber bundle

$$\pi : A \times T\mathcal{Q} \to A \tag{5.7}$$

by $\pi(\alpha, x) \to \alpha$ for $\alpha \in A$ and $x \in T\mathcal{Q}$ (see Figure 5.2). Consider $\mathcal{S} \subset A \times T\mathcal{Q}$ defined by

$$\mathcal{S} := \{(\alpha, x) \in A \times T\mathcal{Q} \mid \alpha \in A,\ p_2^{\text{v}}(x) = 0,\ p_2^{\text{h}}(x) > 0\}. \tag{5.8}$$

which is a fiber bundle with base A and fiber $\pi_{\mathcal{S}}^{-1}(\alpha) = S$ for each $\alpha \in A$ where $\pi_{\mathcal{S}} = \pi|_{\mathcal{S}}$. The fiber bundle $\mathcal{S}$ corresponds to the set of all parameters along with copies of the Poincaré section. Define $\bar{A} \subset A$ to be the set of regular parameters, i.e., for each $\bar{\alpha} \in \bar{A}$ the corresponding output satisfies HH1)–HH5). The set $\bar{A}$ is open since HH2), HH3), and HH5) are rank conditions[2] and since condition HH4) requires a zero of a function that depends continuously on $\bar{\alpha}$ to remain in an open set. With $\bar{A}$, $\mathcal{Z} \subset A \times T\mathcal{Q}$ may be defined as

$$\mathcal{Z} := \{(\alpha, x) \in A \times T\mathcal{Q} \mid \alpha \in \bar{A},\ h_\alpha(x) = 0,\ L_f h_\alpha(x) = 0\} \tag{5.9}$$

which is a fiber bundle with base $\bar{A}$ and fiber $\pi_{\mathcal{Z}}^{-1}(\bar{\alpha}) = Z_{\bar{\alpha}}$, $\bar{\alpha} \in \bar{A}$ and $\pi_{\mathcal{Z}} = \pi|_{\mathcal{Z}}$. The fiber bundle $\mathcal{Z}$ corresponds to the set of parameters giving rise to well-defined swing phase zero dynamics along with the associated zero dynamics manifolds. Since, by assumption, for each $\bar{\alpha} \in \bar{A}$ the output satisfies HH5), the intersection $\mathcal{S} \cap \mathcal{Z}$ is also a fiber bundle with base $\bar{A} \subset A$ and fiber $\pi_{\mathcal{S}\cap\mathcal{Z}}^{-1}(\bar{\alpha}) = S \cap Z_{\bar{\alpha}}$, $\bar{\alpha} \in \bar{A}$ where $\pi_{\mathcal{S}\cap\mathcal{Z}} = \pi|_{\mathcal{S}\cap\mathcal{Z}}$.

In what follows, the fiber bundle structure of $\mathcal{S} \cap \mathcal{Z}$ will permit the creation of event-based PI controllers which modify parameters step-to-step—even those that change $S \cap Z$ step-to-step. Let $\bar{\alpha} \in \bar{A}$ and suppose that $\delta\alpha \in \mathbb{R}^{(N-1)\times(M+1)}$ is such that

$$\delta\alpha \neq 0 \quad \text{and} \quad (\delta\alpha)_0 = (\delta\alpha)_1 = 0. \tag{5.10}$$

Then, for $v, w \in \mathbb{R}$ sufficiently small in magnitude

$$a(\bar{\alpha}, v, w) = [a_{\text{invar}}(\bar{\alpha}, v, w),\ \bar{\alpha}_{\text{free}}] + w\delta\alpha \tag{5.11}$$

is also regular. The function

$$a_{\text{invar}}(\bar{\alpha}, v, w) := [a_{\text{invar},0}(\bar{\alpha}, v),\ a_{\text{invar},1}(\bar{\alpha}, v, w)] \tag{5.12}$$

is defined to ensure invariance of the zero dynamics step-to-step (when $w \neq v$). To ease the cumbersome notation, for the remainder of this section define $\bar{\alpha}_v := \bar{\alpha} + v\delta\alpha$ and, similarly, $\bar{\alpha}_w := \bar{\alpha} + w\delta\alpha$. With this notation, Theorem 4.1 gives $a_{\text{invar},0}$ and θ_a^+

$$\begin{bmatrix} a_{\text{invar},0}(\bar{\alpha}, v) \\ \theta_a^+ \end{bmatrix} := H\Delta_q H^{-1} \begin{bmatrix} (\bar{\alpha}_v)_M \\ \theta^-_{\bar{\alpha}_v} \end{bmatrix} \tag{5.13}$$

[2] An equivalent condition for a square matrix to be full rank is for its determinant to be nonzero. The determinant is a continuous function of matrix entries which, in the case of HH2), HH3), and HH5), are a function of $\bar{\alpha}$.

which ensures that for each $x \in S$ if $h_{\bar{\alpha}}(x) = 0$, then $h_{\bar{\alpha}} \circ \Delta(x) = 0$. If $\delta_{\text{zero},\bar{\alpha}} \neq 0$, then by Theorem 4.1 $a_{\text{invar},1}$ is

$$a_{\text{invar},1}(\bar{\alpha}, v, w) := H_0 \Delta_{\dot{q}} H^{-1} \begin{bmatrix} \frac{M}{\theta^-_{\bar{\alpha}_v} - \theta^+_{\bar{\alpha}_v}} \left((\bar{\alpha}_v)_M - (\bar{\alpha}_v)_{M-1} \right) \\ 1 \end{bmatrix} \cdot \frac{\theta^-_{\bar{\alpha}_w} - \theta^+_{\bar{\alpha}_w}}{M} \frac{\kappa_{1,\bar{\alpha}_v}(\theta^-_{\bar{\alpha}_v})}{\kappa_{1,\bar{\alpha}_w}(\theta^+_{\bar{\alpha}_w})} \frac{1}{\delta_{\text{zero},\bar{\alpha}_v}} + a_{\text{invar},0}(\bar{\alpha}, v) \quad (5.14)$$

which together with $a_{\text{invar},0}$ ensures that for each $x \in S$ if $L_f h_{\bar{\alpha}}(x) = 0$, then $L_f h_{\bar{\alpha}} \circ \Delta(x) = 0$.

Assume that there exists some $\bar{\alpha}^* \in \bar{A}$ such that there exists a corresponding exponentially stable periodic orbit of the restricted Poincaré map, defined in Section 3.5,

$$\rho_{\bar{\alpha}^*} : S \cap Z_{\bar{\alpha}^*} \to S \cap Z_{\bar{\alpha}^*}. \quad (5.15)$$

Let $z^*_{\bar{\alpha}^*} \in \pi^{-1}_{\mathcal{S}\cap\mathcal{Z}}(\bar{\alpha}^*)$ be the corresponding fixed point of $\rho_{\bar{\alpha}^*}$. For $\bar{\alpha}^*$, v, and w fixed, define the induced, restricted flow map

$$\bar{\rho}_{a(\bar{\alpha}^*,v,w)} : \pi^{-1}_{\mathcal{S}\cap\mathcal{Z}} \circ a(\bar{\alpha}^*, \cdot, v) \to \pi^{-1}_{\mathcal{S}\cap\mathcal{Z}} \circ a(\bar{\alpha}^*, v, w) \quad (5.16)$$

by

$$\bar{\rho}(z, a(\bar{\alpha}^*, v, w)) : \varphi_{a(\bar{\alpha}^*,v,w)}(T_{I,a(\bar{\alpha}^*,v,w)}(z), z) \quad (5.17)$$

for $z \in \pi^{-1}_{\mathcal{S}\cap\mathcal{Z}} \circ a(\bar{\alpha}^*, \cdot, v)$. Unlike the restricted Poincaré map, ρ, which maps from a single fiber to itself, the induced, restricted flow map, $\bar{\rho}$, maps from one fiber (parameterized by $v\delta\alpha$) to another (parameterized by $w\delta\alpha$). The parameters $\delta\alpha$, v, and w will now be used to implement event-based PI control on the induced, restricted flow map, (5.16).

Define the single-input, single-output dynamic system on $\mathcal{S} \cap \mathcal{Z} \times \mathbb{R}^2$,

$$\begin{aligned} z(k+1) &= \bar{\rho}(z(k), \alpha(k)) \\ \alpha(k) &= a(\bar{\alpha}^*, v(k), w(k)) \\ v(k+1) &= w(k) \\ \eta(k+1) &= \bar{\nu}(z(k), \alpha(k)) \\ y(k) &= \eta(k) \end{aligned} \quad (5.18)$$

with input $w \in \mathbb{R}$ and output $y \in \mathbb{R}$ equal to the average walking rate. It's linearization is

$$\begin{aligned}
\delta z(k+1) &= a_{11}\delta z(k) + a_{12}\delta v(k) + b_1 \delta w(k) \\
\delta \alpha(k) &= \delta a(\bar{\alpha}^*, v(k), w(k)) \\
\delta v(k+1) &= \delta w(k) \\
\delta \eta(k+1) &= a_{31}\delta z(k) + a_{32}\delta v(k) + b_3 \delta w(k) \\
\delta y(k) &= \delta \eta(k)
\end{aligned} \tag{5.19}$$

where

$$\begin{aligned}
a_{11} &:= \frac{\partial \bar{\rho}}{\partial z}(z(k), a(\bar{\alpha}^*, v(k), w(k)))\Big|_{\substack{z=z^*_{\bar{\alpha}^*} \\ v=0 \\ w=0}} \\
a_{12} &:= \frac{\partial \bar{\rho}}{\partial v}(z(k), a(\bar{\alpha}^*, v(k), w(k)))\Big|_{\substack{z=z^*_{\bar{\alpha}^*} \\ v=0 \\ w=0}} \\
b_1 &:= \frac{\partial \bar{\rho}}{\partial w}(z(k), a(\bar{\alpha}^*, v(k), w(k)))\Big|_{\substack{z=z^*_{\bar{\alpha}^*} \\ v=0 \\ w=0}} \\
a_{31} &:= \frac{\partial \bar{\nu}}{\partial z}(z(k), a(\bar{\alpha}^*, v(k), w(k)))\Big|_{\substack{z=z^*_{\bar{\alpha}^*} \\ v=0 \\ w=0}} \\
a_{32} &:= \frac{\partial \bar{\nu}}{\partial v}(z(k), a(\bar{\alpha}^*, v(k), w(k)))\Big|_{\substack{z=z^*_{\bar{\alpha}^*} \\ v=0 \\ w=0}} \\
b_3 &:= \frac{\partial \bar{\nu}}{\partial w}(z(k), a(\bar{\alpha}^*, v(k), w(k)))\Big|_{\substack{z=z^*_{\bar{\alpha}^*} \\ v=0 \\ w=0}}
\end{aligned} \tag{5.20}$$

The linearized system (5.19) is exponentially stable if, and only if, $|a_{11}| < 1$. The DC-gain is non-zero if, and only if,

$$a_{31}(b_1 + a_{12}) + (a_{32} + b_3)(1 - a_{11}) \neq 0 \tag{5.21}$$

Theorem 5.2. *Let $\bar{\alpha}^* \in \bar{A}$ be a regular parameter value for which there exists an exponentially stable periodic orbit in $Z_{\bar{\alpha}^*}$. Denote the corresponding fixed point of the Poincaré return map by $z^*_{\bar{\alpha}^*}$. Assume there exists $\delta\alpha$ satisfying (5.10) and such that the non-zero DC-gain condition, (5.21), holds. Then average walking rate can be regulated via PI control. In particular, there exist $\epsilon > 0$, and scalars K_P and K_I such that for all η^* such that*

$|\eta^* - \bar{\nu}(z^*_{\bar{\alpha}^*}, \bar{\alpha}^*)| < \epsilon$, *the system consisting of (5.18) in closed-loop with the proportional plus integral controller*

$$\begin{aligned} e(k+1) &= e(k) + (\eta^* - \eta(k)) \\ w(k) &= K_P(\eta^* - \eta(k)) + K_I e(k) \end{aligned} \tag{5.22}$$

has an exponentially stable equilibrium, and thus, when initialized sufficiently near the equilibrium, $\lim_{k\to\infty}(\eta^* - \eta(k)) = 0$.

Proof. The linear system (5.19) is exponentially stable because the exponential stability of the fixed-point $z^*_{\bar{\alpha}^*}$ implies that $|a_{11}| < 1$. This, combined with the DC-gain being non-zero, implies the existence of a PI controller of the form

$$\begin{aligned} \delta e(k+1) &= \delta e(k) + (\delta\eta^* - \delta\eta(k)) \\ \delta w(k) &= K_p(\delta\eta^* - \delta\eta(k)) + K_I \delta e(k) \end{aligned} \tag{5.23}$$

such that the closed-loop system (5.19) with (5.23) is exponentially stable and satisfies $\lim_{k\to\infty}(\delta\eta^* - \delta\eta(k)) = 0$, where $\delta\eta^* - \bar{\nu}(z_{\bar{\alpha}^*}, \bar{\alpha}^*)$. Since the closed-loop of (5.19) with (5.23) is the linearization of (5.18) in closed-loop with (5.22), the result follows. □

CHAPTER 6

Experimental verification

This chapter describes the experimental verification of the theoretical framework developed in Chapters 2–5 on the prototype biped RABBIT. The framework's ability to systematically generate controllers with desired kinematic and dynamic properties enabled the direct implementation of controllers that induced stable walking. To have the dynamic design specifications more closely match the experimental result, three implementation issues had to be addressed: the inertia added by the boom system used to constrain RABBIT to be planar, friction in the gear reducers, and the discrepancy between the energy dissipated by RABBIT's swing leg end ground contact and the energy dissipation as predicted by the rigid impact model. The chapter begins with a description of the prototype, continues with a controller design example, then discusses several implementation issues, and concludes with a presentation of six experiments.

6.1 The prototype RABBIT

The five-link, planar prototype RABBIT (see Figure 6.1(a)) is located at the Laboratoire D'Automatique de Grenoble in Grenoble, France. It was constructed jointly by several French research laboratories, spanning Mechanical Engineering, Automatic Control, and Robotics [Che03a, CAA+02]. The RABBIT project was initiated in 1997 and is funded by the French CNRS and the French National Research Council. Its central mission is to build a prototype for studying truly dynamic motion control. In particular, the mechanism was designed to allow for high speed walking and running.

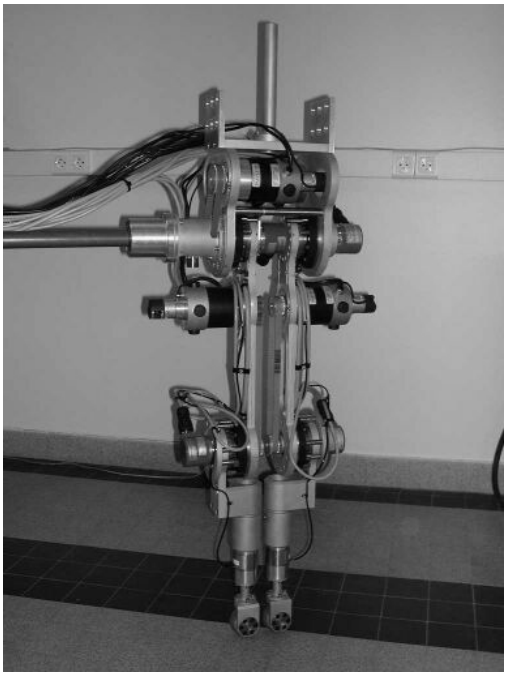

(a) A front view.

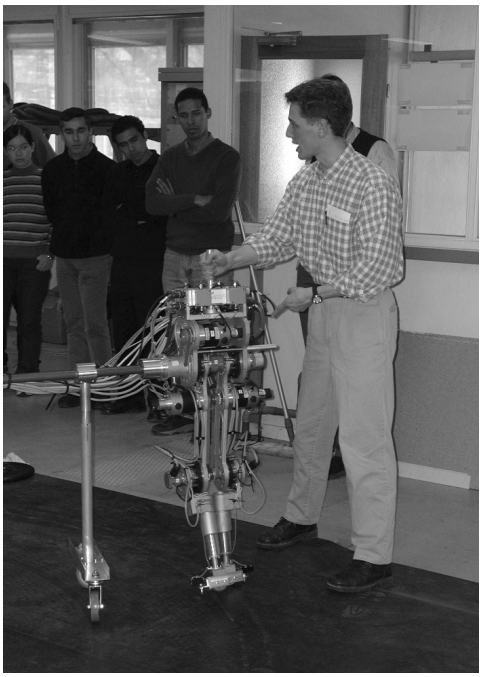

(b) The author guides RABBIT through a step. Note the "training wheels" connected to boom.

Figure 6.1: Photos of the biped prototype RABBIT.

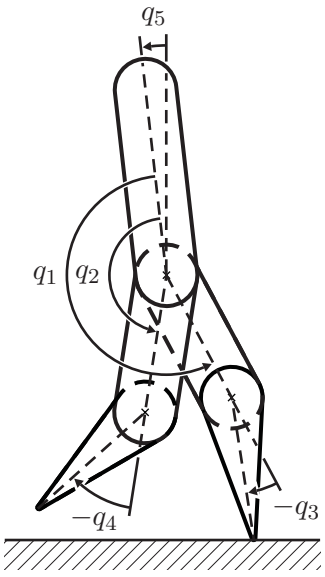

Figure 6.2: Schematic of the prototype RABBIT with measurement conventions.

RABBIT's five links are connected by revolute joints that form two symmetric legs and a torso (see Figure 6.2). An actuator supplies torque between each of the four internal joints: one at each knee and one between the torso and each femur. All actuators are identical and capable of producing a peak torque of 150 Nm. To prevent motions in the frontal plane, RABBIT was constructed with a boom attached at the hip; see Figure 6.3. RABBIT's symmetry about the frontal plane enables it to walk in either direction: clockwise or counterclockwise. RABBIT has no feet and no means of supplying actuation between the stance leg end and the ground. The model of RABBIT therefore satisfies RH1)–RH5), and, with the coordinate choice indicated in Figure 6.2, satisfies RH6). The equations of motion during the swing phase are (2.4) with D, E, G, and B given in Appendix D. These equations correspond to an underactuated, planar five-link inverted pendulum. The linear transformation matrix, R, required by the rigid impact map (2.20) is also given in Appendix D. The extended model (2.5) required by the impact map is not given, but may be readily derived using the methodology given in Appendix E. The link parameter values were identified by a group associated with the project and are given in Table 6.1 with the measurement conventions given in Figure 6.4. To obtain configuration information, encoders are located at each internal joint giving the robot's shape, and between the boom and hip giving the robot's absolute orientation. Binary contact switches located at the leg ends are used to detect whether or not a leg is in contact with the walking surface (see Figure 6.5). Initially, RABBIT had force sensors incorporated as structural components of its tibias to measure ground reaction forces. The force sensors were too fragile and failed after only several days of experiments. They were replaced with metal blanks and the contact switches. The binary contact switches provide less information than did the force sensors but are more mechanically robust.

For a real-time control platform RABBIT uses a dSPACE DS1103 system. With the DS1103 system, run-time software is created by automatic translation and cross-compiling of Simulink diagrams for the system's 400 MHz PowerPC 604e DSP, allowing the real-time controller software to be developed in a high-level language. This obviates the need for low-level I/O programming and facilitates debugging. In addition, the system provides low-level computation, digital-to-analog and analog-to-digital conversion, as well as a user

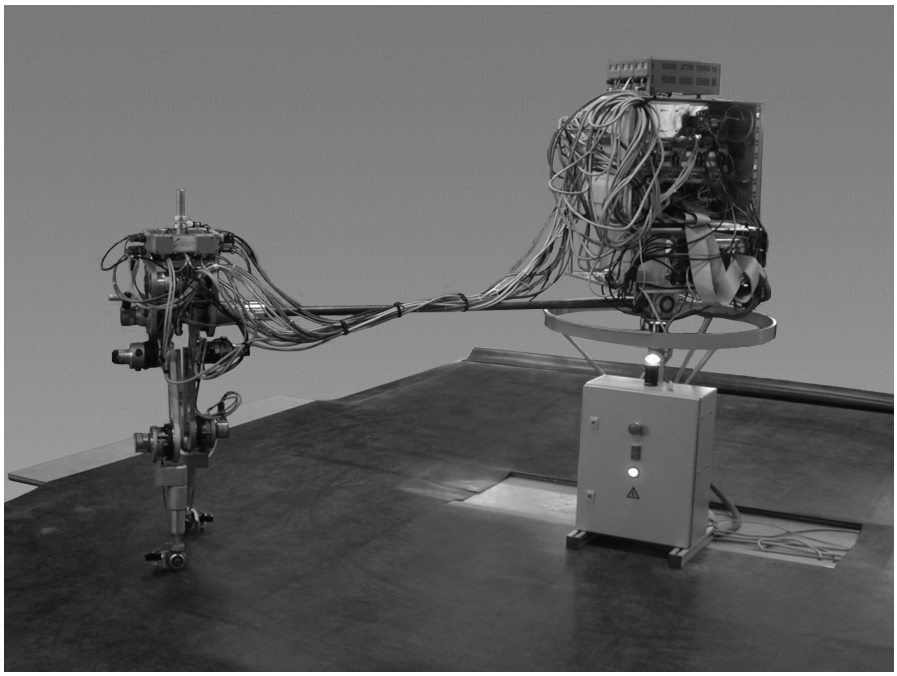

Figure 6.3: The biped prototype RABBIT's experimental setup.

Model parameter	Units	Label	Value
Mass	kg	M_T	12
		M_f	6.8
		M_t	3.2
Length	m	l_T	0.63
		l_f	0.4
		l_t	0.4
Inertia	m^2kg	I_T	1.33
		I_f	0.47
		I_t	0.20
Mass center	m	p_T^M	0.24
		p_f^M	1.11
		p_t^M	0.24

Table 6.1: Identified link parameters for RABBIT.

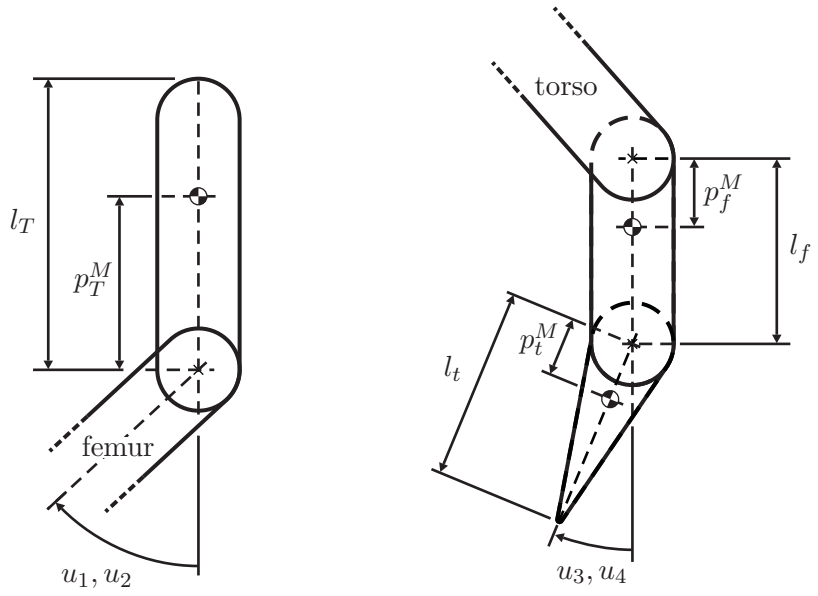

(a) Schematic of torso.

(b) Schematic of leg.

Figure 6.4: Schematic of RABBIT's link parameter measurement conventions.

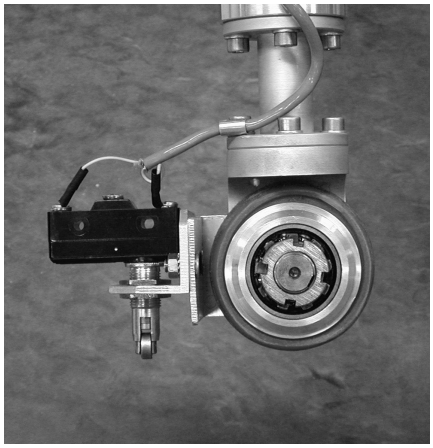

Figure 6.5: RABBIT's frontal plane leg end wheel with contact switch.

interface—all in a single package.

6.2 Example controller design

This section illustrates the application of the theoretical framework for stability analysis and performance enhancement on the model of RABBIT. A controller based upon the results of Chapters 3 and 4 that induces walking at 0.8 m/s will be designed and simulated.

Using the Bézier polynomial almost linear output function structure of (4.1) with $h_0(q)$ and $\theta(q)$ as in (4.2) and (4.3), controller design is equivalent to choice of 1) the quantities to be controlled, H_0, 2) the function $\theta(q)$, c, 3) the Bézier polynomial order, M, and 4) the Bézier polynomial coefficients, α. Choosing

$$H_0 = \begin{bmatrix} I & 0 \end{bmatrix} \tag{6.1}$$

$$c = \begin{bmatrix} -1 & 0 & -1/2 & 0 & -1 \end{bmatrix} \tag{6.2}$$

clearly guarantees that $H = [H_0' \; c']'$ is invertible, satisfying HH3), and results in the output

$$y = h_0(q) - h_d \circ \theta(q) \tag{6.3}$$

$$= \begin{bmatrix} q_1 \\ q_2 \\ q_3 \\ q_4 \end{bmatrix} - h_d \circ \theta(q). \tag{6.4}$$

Figure 6.6 gives $\theta(q)$ corresponding to this choice of c. In light of Remark 4.2, M is chosen to be 6 which leaves five free parameters to be chosen for each output. This implies a total of 20 output function parameters to be chosen via optimization. For a particular choice of α, HH5) must be checked to ensure smoothness of $S \cap Z$. This entails evaluating the rank[1] of

$$\frac{\partial}{\partial q} \begin{bmatrix} h(q) \\ p_2^{\mathrm{v}}(q) \end{bmatrix} \Bigg|_{x \in S \cap Z} = \begin{bmatrix} H_0 - \dfrac{M}{\theta^- - \theta^+} (\alpha_M - \alpha_{M-1})\, c \\ \dfrac{\partial p_2^{\mathrm{v}}(q)}{\partial q} \Big|_{q=q_0^-} \end{bmatrix}. \tag{6.5}$$

where $p_2^{\mathrm{v}}(q)$ is the height of the swing end. Hypothesis HH2), the invertibility of the decoupling matrix, is checked for choice of α by using the technique presented in [PGWA01].

[1] See Remark 3.2 on page 42.

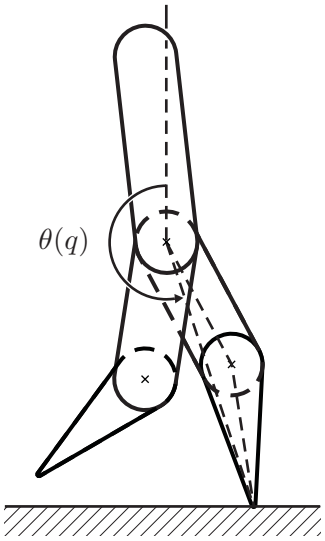

Figure 6.6: The measurement convention for the scalar function $\theta(q)$. This $\theta(q)$ was used for the example and exerpiments.

If the optimization constraints are satisfied, as detailed in Section 4.3, so will the remaining gait, impact model, and output function hypotheses.

The optimization problem is posed as described in Section 4.3.2 to choose the 20 free parameters of α. Three additional nonlinear inequality constraints are imposed to obtain a human-like gait. The first two, when satisfied, prevent the stance and swing leg knees from hyper-extending,

NIC4)

$$q_3 < 0, \tag{6.6}$$

NIC5)

$$q_4 < 0, \tag{6.7}$$

and the third, when satisfied, prevents the hip from dropping too low,

NIC6)

$$p^{\mathrm{v}}_{\mathrm{H}} - p^{\mathrm{v}}_{\mathrm{H,min}} > 0, \tag{6.8}$$

where $p^{\mathrm{v}}_{\mathrm{H,min}}$ is the minimum hip height. MATLAB's constrained nonlinear optimization tool `fmincon` was used to approximately minimize the cost $J_1(\alpha)$, (4.40), subject to NIC1)–NIC6) and NEC1)–NEC5).

$J(\alpha)$	ζ_2^*	δ^2_{zero}	$V_{\text{zero}}(\theta^-)$	$V^{\text{MAX}}_{\text{zero}}$	$\bar{\nu}$
(N^2m)	$(\text{kgm}^2/\text{s})^2$	-	$(\text{kgm}^2/\text{s})^2$	$(\text{kgm}^2/\text{s})^2$	(m/s)
91.0	549	0.741	-142	182	0.800

Table 6.2: Example gait statistics for RABBIT.

Table 6.2 summarizes the result of optimizing for a desired average walking rate of 0.8 m/s. From a reasonable initial condition, the optimization took approximately 1 min on a PC based computer with a 2 GHz Pentium IV processor. The walking motion is exponentially stable since $\delta^2_{\text{zero}}/(1-\delta^2_{\text{zero}})V_{\text{zero}}(\theta^-) + V^{\text{MAX}}_{\text{zero}} = -224 < 0$ and $0 < \delta^2_{\text{zero}} < 1$ per Corollary 3.1. This controller was initialized on $S \cap Z$ at the fixed point and simulated for three steps using MATLAB with `m`-files generated via the method described in Appendix F. Figure 6.7 is a stick figure animation of the result. Note that the walking motion appears to be natural. Figure 6.8 gives the joint trajectories. Figures 6.9(a) and 6.9(b) are the motor torques for the hip and knees. Of the four associated torques, the peak torque occurs at the stance leg hip and is approximately 64 Nm. Figures 6.9(c) and 6.9(d) are plots of the motor speed versus torque requirements for one step of the walking motions. Note that the requirements for this motion are well below the manufacturer's limits indicated by the shaded region. Figures 6.10(a) and 6.10(b) are normal and tangential ground reaction forces. Figure 6.10(c) is a plot of their ratio. Note that the ratio $F_1^{\text{T}}/F_1^{\text{N}}$ is substantially below the static friction limit, $\mu_s = 0.6$. The trajectory of the swing leg end height is given in Figure 6.10(d).

6.3 Implementation issues

This section presents three important aspects of RABBIT's implementation whose effects are not addressed by the theoretical framework. They are the boom used to constrain RABBIT's motions to be planar, RABBIT's gear reducers, and RABBIT's irregular, non-rigid walking surface. To have the dynamic design specifications more closely match the experimental result, these effects were accommodated in the design of controllers for the

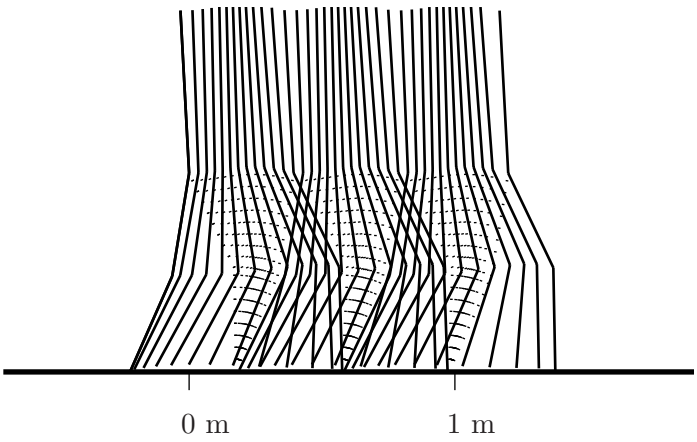

Figure 6.7: Stick animation of a simulation of RABBIT taking three steps. Note that walking is from left to right and that the stance leg is dotted.

experiments presented in Section 6.5.

6.3.1 Constraining RABBIT to be planar

The boom attached to RABBIT's hip constrains RABBIT's motions to the sagittal plane and constrains the sagittal plane to be tangent to a sphere centered at the universal joint that connects the boom to the center stand (see Figure 6.3). RABBIT therefore walks in a circle whose radius is determined by the length of the boom. The boom system consists of the boom, center stand, counterweight, and cabling (see Figure 6.11). "Training wheels," shown in Figure 6.1 but not drawn in Figure 6.11, were attached to the boom to provide a measure of safety. The training wheel's post has a prismatic joint with a stop to prevent the robot's hip from dropping too low. The boom system also includes two encoders at the universal joint on center stand to measure horizontal and vertical angular displacement of the boom about the stand. A boom system of this sort was also used for MIT Leg Lab's Spring Flamingo [PCT+01] as well as several of their other robots. The other typical means of constraining a biped robot's motion to be planar is through the the use of wide feet. This idea was used in the design of Kenkyaku [FM86] and Meltran II [KT96], among others. The advantage of a boom system over wide feet is that a boom is able to constrain the robot's motion even when none of the feet are on the ground. This is important in

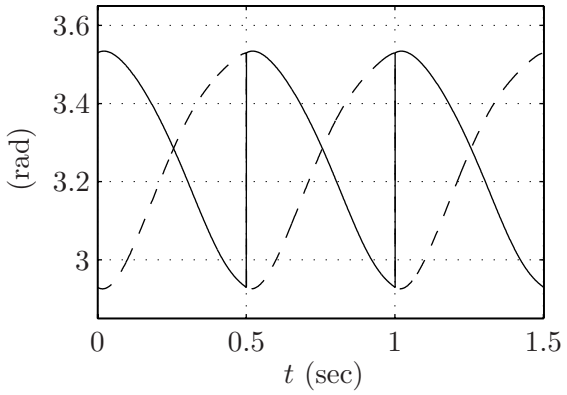

(a) q_1 (solid) and q_2 (dashed) versus time.

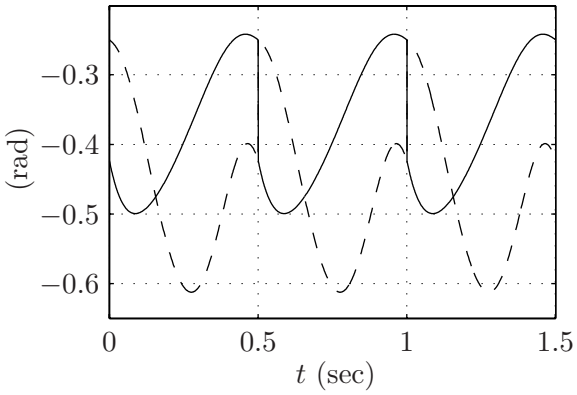

(b) q_3 (solid) and q_4 (dashed) versus time.

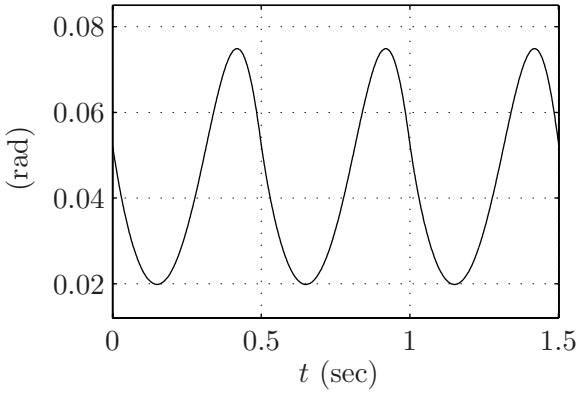

(c) q_5 versus time.

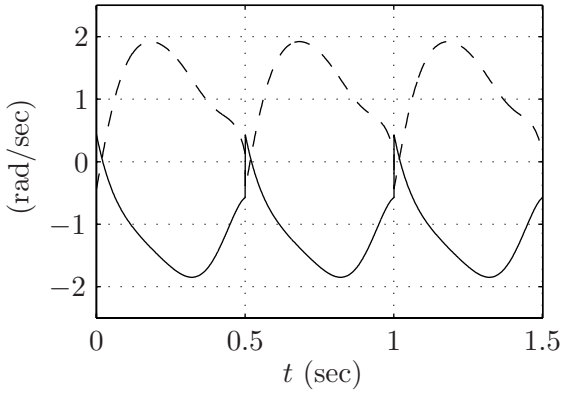

(d) $\dot{q}_1$ (solid) and $\dot{q}_2$ (dashed) versus time.

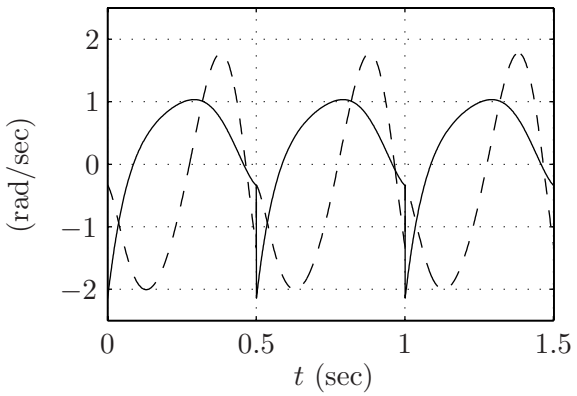

(e) $\dot{q}_3$ (solid) and $\dot{q}_4$ (dashed) versus time.

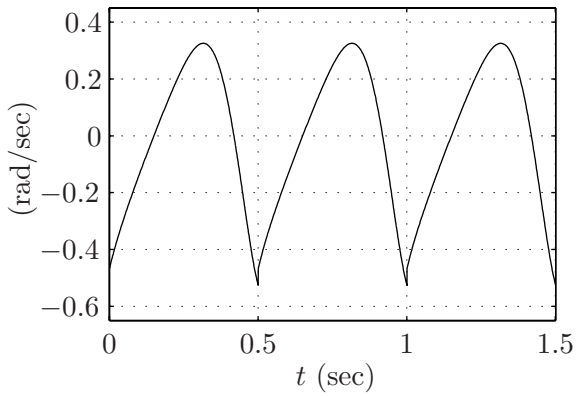

(f) $\dot{q}_5$ versus time.

Figure 6.8: State trajectory plots corresponding to a simulated gait of RABBIT. Three steps are taken at an average walking rate of 0.8 m/s each step. The discontinuities are due to impacts and coordinate relabeling.

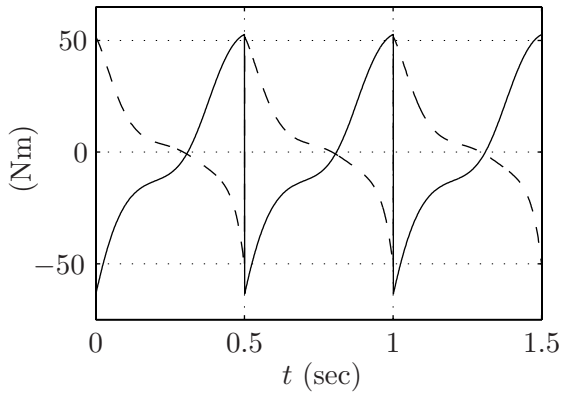

(a) u_1 (solid) and u_2 (dashed) versus time.

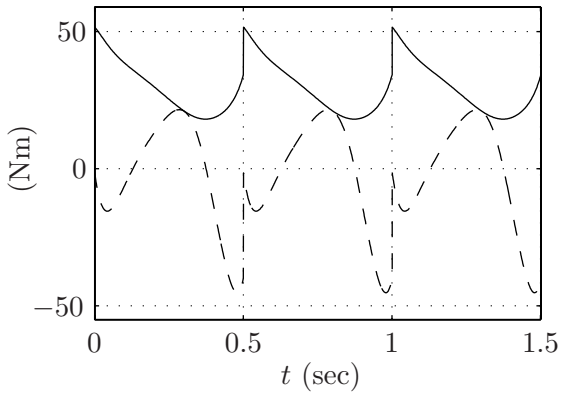

(b) u_3 (solid) and u_4 (dashed) versus time.

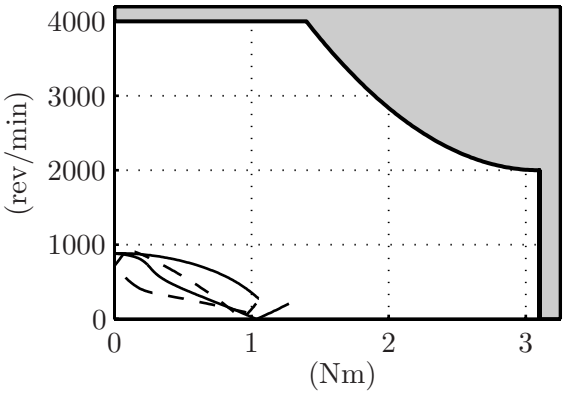

(c) Hip motor rotor speed versus torque output at motor shaft. The stance leg curve is solid and the swing leg curve is dashed.

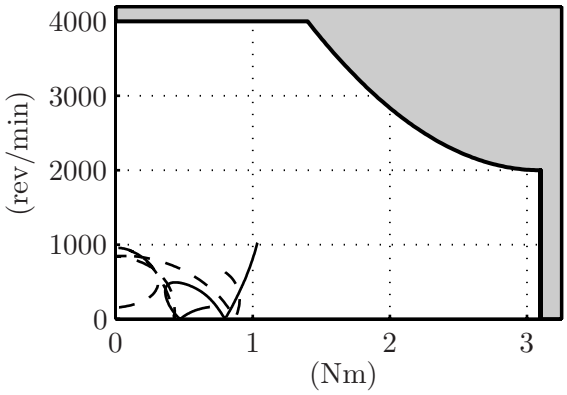

(d) Knee motor rotor speed versus torque output at motor shaft. The stance leg curve is solid and the swing leg curve is dashed.

Figure 6.9: Commanded control signals corresponding to a simulated gait of RABBIT. Three steps are taken at an average walking rate of 0.8 m/s each step. The discontinities are due to impacts and coordinate relabeling.

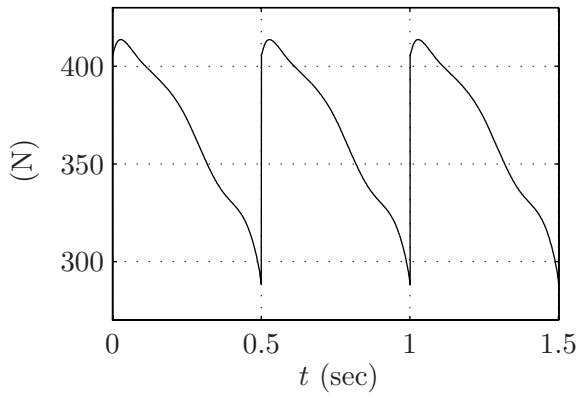

(a) F_1^{N} versus time.

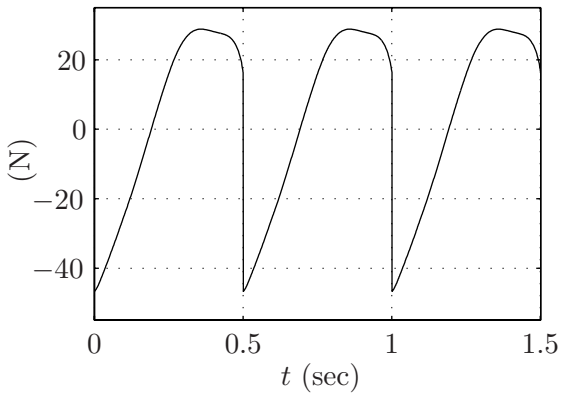

(b) F_1^{T} versus time.

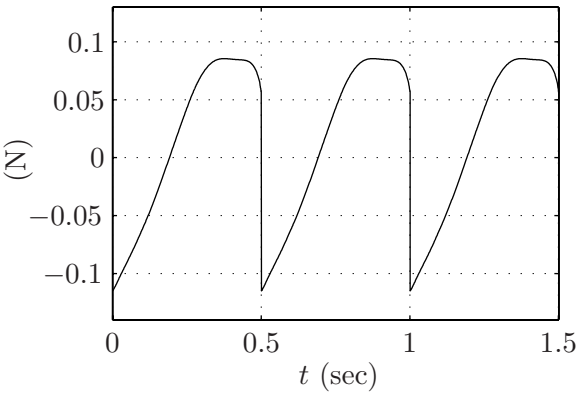

(c) $F_1^{\mathrm{T}}/F_1^{\mathrm{N}}$ versus time.

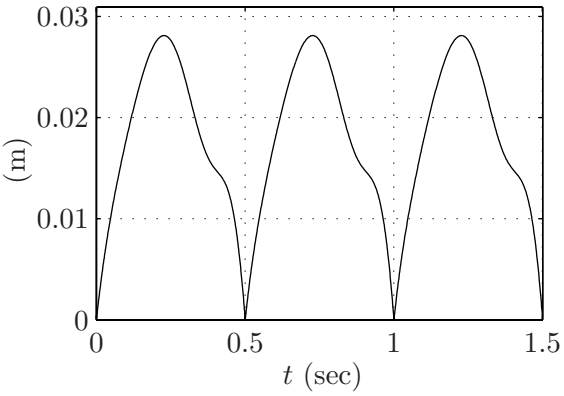

(d) p_2^{y} versus time.

Figure 6.10: Other plots corresponding to a simulated gait of RABBIT. Three steps are taken at an average walking rate of 0.8 m/s each step. The discontinities are due to impacts and coordinate relabeling.

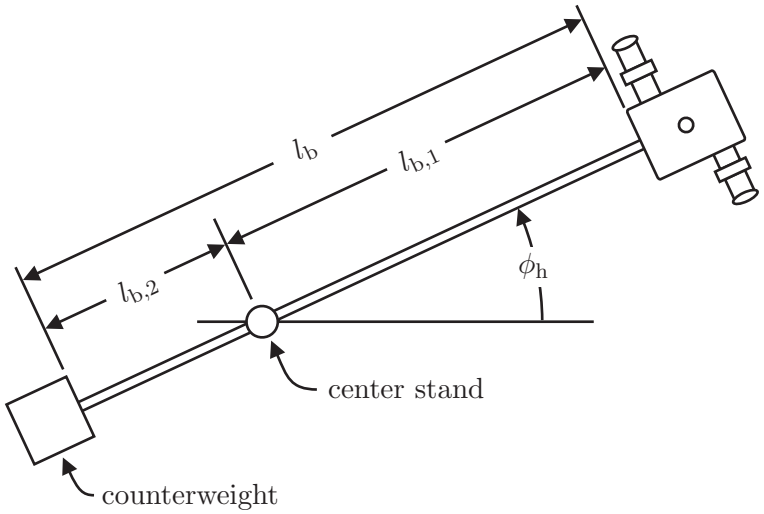

(a) Overhead view of RABBIT'S experimental setup. For clarity, the electronics are not drawn.

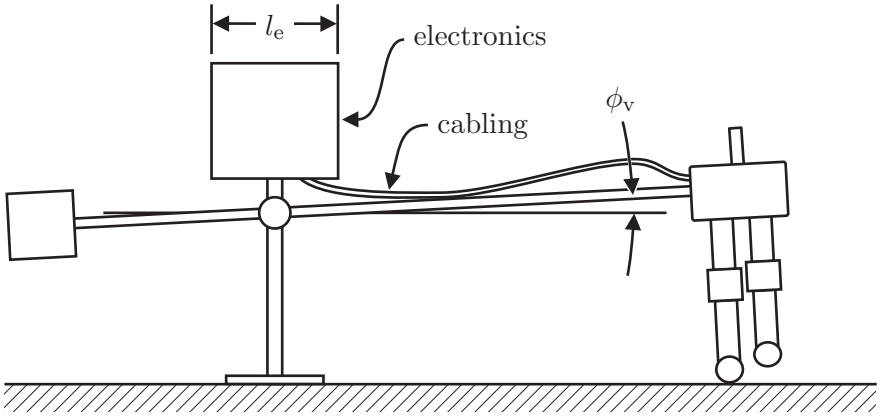

(b) Side view of RABBIT's experimental setup.

Figure 6.11: Various dimensions of RABBIT's experimental setup.

the case of RABBIT, as one of its stated purposes is to study running, which necessarily has a flight phase, i.e., a phase when no feet are in contact with the ground. The use of a boom, however, requires some means of allowing the legs move radially when in contact with the ground. To accomplish this in RABBIT, wheels aligned with the frontal plane were attached at the leg ends (see Figure 6.5). Another consideration with a boom system is how to connect power and communications cabling to the experimental setup. Unless a slip ring is used, cabling connected to the experimental setup will become twisted or wound as the robot makes laps. Unfortunately, a slip ring was not installed at the time when the experiments reported in this chapter were performed, and RABBIT had to be "unwound" after each experiment.

The inertia of the boom system used to constrain RABBIT's motion to be planar results in additional inertia that is significant enough to require incorporation into RABBIT's model. The inertia has four components due to 1) the boom connecting RABBIT, the center stand, and the counterbalance, 2) the counterbalance, 3) the cabling connecting RABBIT to the support electronics, and 4) the support electronics (see Figure 6.3 and Figure 6.11). Since the training wheels are not always used, and since they are relatively light, their inertia is not included. The inertia may be approximated as

$$I_{\text{support}} = \underbrace{\frac{1}{3}\frac{m_{\text{b}}}{l_{\text{b}}}\left(l_{\text{b},1}^3 + l_{\text{b},2}^3\right)}_{\text{boom}} + \underbrace{m_{\text{w}}\, l_{\text{b},2}^2}_{\text{counterbalance}} + \underbrace{\frac{1}{3} m_{\text{c}}\, l_{\text{b},1}^2}_{\text{cabling}} \tag{6.9}$$

$$I_{\text{electronics}} = \frac{1}{12} m_{\text{e}}\, l_{\text{e}}^2 \tag{6.10}$$

This results in additional kinetic energy,

$$K_{\text{support}} = \frac{1}{2} I_{\text{support}} \left(\dot{\phi}_{\text{h}}^2 + \dot{\phi}_{\text{v}}^2\right) + \frac{1}{2} I_{\text{electronics}} \dot{\phi}_{\text{h}}^2 \tag{6.11}$$

where ϕ_{h} and ϕ_{v} are the horizontal and vertical angular displacement of RABBIT about the center stand (see Figure 6.11). The angles ϕ_{h} and ϕ_{v} and may be approximated by

$$\phi_{\text{h}} \approx \frac{p_{\text{H}}^{\text{h}}(q) - p_{\text{H}}^{\text{h}}(q_0)}{l_{\text{b},1}} \tag{6.12}$$

$$\phi_{\text{v}} \approx \frac{p_{\text{H}}^{\text{v}}(q) - p_{\text{H}}^{\text{v}}(q_0)}{l_{\text{b},1}} \tag{6.13}$$

where q_0 is RABBIT's configuration at the beginning of a step and p_{H}^{h} and p_{H}^{v} are the horizontal and vertical positions of the hip.

Model parameter	Units	Label	Value
Constraint boom length	m	l_{b}	1.5
Hip to stand distance	m	$l_{\mathrm{b},1}$	1.4
Stand height	m	l_{s}	1.4
Constraint boom mass	kg	m_{b}	5.0
Cable mass	kg	m_{c}	2.0
Counterbalance mass	kg	m_{w}	0.0
Support electronics mass	kg	m_{e}	20.0

Table 6.3: RABBIT's experimental platform parameters.

There is also additional potential energy due to the boom, the counterbalance, and the cabling,

$$V_{\mathrm{support}} = \underbrace{\frac{1}{2} g_0 \frac{m_{\mathrm{b}}}{l_{\mathrm{b}}} \sin(\phi_{\mathrm{v}}) \left(l_{\mathrm{b},1}^2 - l_{\mathrm{b},2}^2 \right)}_{\text{boom}} - \underbrace{g_0 m_{\mathrm{w}} \, l_{\mathrm{b},2} \sin(\phi_{\mathrm{v}})}_{\text{counterbalance}} + \underbrace{\frac{1}{2} g_0 m_{\mathrm{c}} \sin(\phi_{\mathrm{v}}) l_{\mathrm{b},1}}_{\text{cabling}} . \tag{6.14}$$

Note that the counterbalance mass may be chosen to be,

$$m_{\mathrm{w}} = \frac{1}{l_{\mathrm{b},2}} \left(\frac{1}{2} \frac{m_{\mathrm{b}}}{l_{\mathrm{b}}} \left(l_{\mathrm{b},1}^2 - l_{\mathrm{b},2}^2 \right) + \frac{1}{2} m_{\mathrm{c}} l_{\mathrm{b},1} \right) \tag{6.15}$$

to negate the potential energy due to the boom and cabling. In the experiments described in Section 6.5, no counterbalance was used due to the small value of $l_{\mathrm{b},2}$; the required counterbalance of 52 kg could not be securely fasted to the boom because of the short length of $l_{\mathrm{b},2}$.

The controllers used for the experiments reported in Section 6.5 were designed using equations of motion which included the boom system's effects. These equations of motion were calculated by first forming an updated Lagrangian—the planar model's Lagrangian with the kinetic energy K_{support} added and the potential energy V_{support} subtracted—and then using the method of Lagrange given in Appendix E. Table 6.3 gives the parameter values for the boom system setup used for the experiments.

Aside from the ability to counterbalance the boom, the choice of boom length has other important considerations. The longer the boom, the better the approximation of

RABBIT as a planar mechanical system; however, the longer the boom, the greater the undesirable dynamic effects of the additional kinetic (6.11) and potential (6.14) energies, and the greater the flexibility of the boom. Boom flexibility was found to be of great significance experimentally. The boom was initially chosen to be 3 m in length. Flexing of the tubular steel boom affected forces on RABBIT's hip large enough to cause foot slippage. In response, the boom was swapped for a 1.5 m one, and the foot slippage problem subsided.

6.3.2 Gear reducers and joint friction

To allow smaller, lighter weight motors to be used, RABBIT has gear reducers between its motors and links. The gear reducers have two important effects on RABBIT's dynamics. The first effect is to add significant joint friction, which effectively eliminates all passive motions of the joints. The second effect is to approximately decouple the robot's dynamics leaving the motor's rotor inertia as the only significant inertial load on the motor. Both effects were taken into consideration in the control implementation described in Section 6.4.

The joint friction was modeled by viscous and static friction terms,

$$F(q, \dot{q}) := F'_{\mathrm{v}} \dot{q} + F'_{\mathrm{s}} \operatorname{sgn}(\dot{q}) \tag{6.16}$$

where[2] $F_{\mathrm{v}} = (F_{\mathrm{v,H}}, F_{\mathrm{v,H}}, F_{\mathrm{v,K}}, F_{\mathrm{v,K}})$ and $F_{\mathrm{s}} = (F_{\mathrm{s,H}}, F_{\mathrm{s,H}}, F_{\mathrm{s,K}}, F_{\mathrm{s,K}})$. The identified values of RABBIT's frictional parameters are given in Table 6.4. Note that both the viscous and static friction values are substantial. At the hip, the static friction is approximately ten percent of the motor/gear reducer system's peak available torque of 150 Nm.

Another, in some ways desirable, effect of gear reducers is to scale the inertial load seen by the motors. This scaling has the effect of approximately decoupling the robot's actuated dynamics so that the only significant dynamic terms are the inertia of the motors' rotors and the unactuated dynamics (see Appendix G). Writing the model in motor coordinates makes this evident.

[2] As is commonly done to circumvent the difficulties associated with the discontinuity of the signum function, in implementation, a scaled arctangent function was used in its place, i.e., for large τ,

$$\operatorname{sgn}(x) \approx \frac{2}{\pi} \tan^{-1}(\tau x) \tag{6.17}$$

.

Model parameter	Units	Label	Value
Gear ratio	-	n_{g}	50
Motor rotor inertia	$\mathrm{m}^2\mathrm{kg}$	I_{a}	0.83
Viscous friction	Ns	$F_{\mathrm{v,H}}$	16.5
		$F_{\mathrm{v,K}}$	5.48
Static friction	Nm	$F_{\mathrm{s,H}}$	15.0
		$F_{\mathrm{s,K}}$	8.84

Table 6.4: Addition dynamic parameters for RABBIT.

Define the motor shaft coordinates

$$\bar{q} := N_{\mathrm{g}} q \tag{6.18}$$

where

$$N_{\mathrm{g}} = \mathrm{diag}(n_{\mathrm{g}}, n_{\mathrm{g}}, n_{\mathrm{g}}, n_{\mathrm{g}}, 1) \tag{6.19}$$

and n_{g} are the gear reducers' gear ratio (the four gear reducers are identical). Since the torso, q_5, is unactuated, $(N_{\mathrm{g}})_{55} = 1$. Using Proposition G.1, when the motors' rotor inertias and the gear ratios are included in RABBIT's swing phase model, (2.2), and the model is written in the motor shaft coordinates, the equations of motion become

$$\begin{bmatrix} \frac{1}{n_{\mathrm{g}}^2} D_{1,1} + I_{\mathrm{a}} I & \frac{1}{n_{\mathrm{g}}} D_{1,2} \\ \frac{1}{n_{\mathrm{g}}} D'_{1,2} & (D)_{5,5} \end{bmatrix} \ddot{\bar{q}} + \begin{bmatrix} \frac{1}{n_{\mathrm{g}}^2} C_{1,1} & \frac{1}{n_{\mathrm{g}}} C_{1,2} \\ \frac{1}{n_{\mathrm{g}}} C'_{1,2} & (C)_{5,5} \end{bmatrix} \dot{\bar{q}} + N_{\mathrm{g}}^{-1} G - N_{\mathrm{g}}^{-1} F = B \bar{u} \tag{6.20}$$

where $\bar{u} := (\bar{u}_1, \bar{u}_2, \bar{u}_3, \bar{u}_4)$ are the torques supplied at the output shafts of the motors and I_{a} is the inertia of the motors' rotors (the four motors are identical). Notice that the actuated dynamics are approximately decoupled and the motors' rotor inertias and the unactuated dynamics as the only significant dynamics. RABBIT's motors' rotor inertia and gear ratio are given in Table 6.4.

6.3.3 The walking surface

The tradeoff between the dissipation due to impacts and the energy gained through shape change (cf. Theorem 3.3 and Corollary 3.1) determine closed-loop system's Poincaré

map's fixed point, i.e., the resultant average walking rate and stability. Imperfections in the model parameters and unmodeled dynamics during the swing phase affect the energy gained through shape change. Imperfections in the impact model affect the amount of energy dissipated. To study the later, RABBIT was simulated using a compliant ground contact model described in [PGWA01]. It was found that stability was preserved, but the steady-state average walking rate differed from the average walking rate designed assuming rigid impacts. This was also found experimentally.

The floor on which RABBIT walks is concrete with 30 cm wide cabling access trenches covered with 4 mm steel plates. In preliminary experiments it was found that after stepping on one of the four plates crossing RABBIT's path, RABBIT would slow significantly. Since the gait—change in the shape over a step—was the same, this indicated that the energy dissipated due to impacting the concrete surface is less than the energy dissipated due to impacting the steel plates. To help make the walking surface uniform, the floor was covered with 1.5 cm particle board which was then covered with a layer of 3 mm rubber (see Figure 6.3). Aside from helping to make the walking surface uniform, the rubber layer was added in hopes of extending the life of RABBIT by providing a modest amount of damping.

For the wood and rubber walking surface, it was found that the in the design of walking motions, the amount of energy dissipated at impact had to be scaled to be less than the rigid model predicted at low walking speeds and more at higher walking speeds. This was accomplished through trial and error by scaling δ_{zero}, (3.80), by some constant a. A series of controllers over a range of values of a were generated and then evaluated using the experiment procedure described in Section 6.5 to determine their steady-state average walking rates. The value of a resulting in a controller that induced the desired average walking rate was recorded. Figure 6.12 gives a plot of these values of a verses the corresponding average walking rate. Surprisingly, the relationship is approximately linear; the least squares fit is $a(\bar{\nu}) = 1.2957 - 0.4250\bar{\nu}$. This apparently linear relationship between average walking rate and impact scaling is reminiscent of the classical coefficient of restitution relation, $e = 1 - av_0$, where e is the coefficient of restitution, a is some material-dependent constant, and v_0 is the impacting velocity [Gol60, p. 258]. It is hypothesized that this approximately linear relation will hold for other walking surfaces, suggesting it as a means of identifying

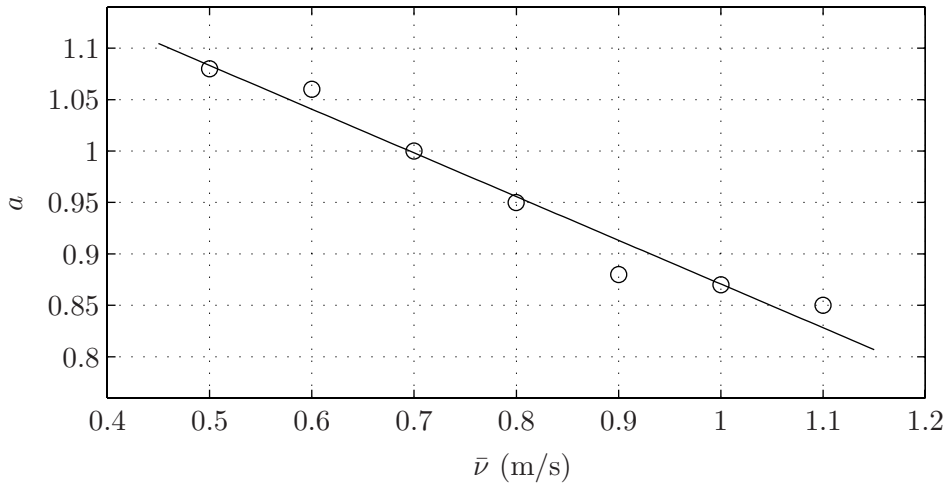

Figure 6.12: Average walking rate verses impact map scaling constant a. The solid line is a least squares fit to empirically determined impact scalings (indicated by circles).

the surface to determine how the rigid impact model, i.e., δ_{zero}, should be modulated as a function of $\bar{\nu}$.

6.4 The control algorithm implementation: imposing the virtual constraints

The swing phase zero dynamics (3.47) and (3.48) are independent of the feedback used to zero the output that gives rise to them. Section 3.6 introduced one possible feedback, (3.104), a computed torque pre-feedback plus finite time converging controllers. The input-output linearization of the computed torque pre-feedback decoupled the dynamics resulting in a chain of four double integrators. The finite-time converging controllers stabilized the origin of the double integrators in finite time enabling the stability of the robot's walking motion to be assessed via the hybrid zero dynamics' scalar return map. In light of the decoupling effect of the reducers (see Section 6.3.2 and Appendix G), and the likely inaccuracy of the parameter identification, high-gain decoupled PD controllers were used in place of the feedback (3.104) to impose the virtual constraints on RABBIT. It was found that this control was able to zero the outputs sufficiently well to induce walking with dynamic characteristics similar to the theoretical design.

Control parameter	Units	Label	Value
Proportional gains	N	$K_{P,\mathrm{H}}$	2000
		$K_{P,\mathrm{K}}$	1500
Derivative gains	Ns	$K_{D,\mathrm{H}}$	10
		$K_{D,\mathrm{K}}$	10
Single support delay	ms	T_{SS}	200
Double stance delay	ms	T_{DS}	100

Table 6.5: Experiment control parameter values.

For the experiments described in the next section, outputs of the form (4.1) with $h_0(q)$ and $\theta(q)$ as in (4.2) and (4.3) were used with H_0, c, and M as in Section 6.2. Also as in Section 6.2, to design the gait (select α) an optimization problem was posed to approximately minimize $J_1(\alpha)$ with the additional nonlinear inequality constraints, NIC4)–NIC6). To accommodate the implementation issues described in Section 6.3, the hybrid zero dynamics used in the optimization process were updated to include the additional kinetic energy, potential energy, joint friction, and δ_{zero} was scaled. To zero the output resulting from optimization, the decoupled, PD controller with friction compensation

$$u = -K_P e - K_D \dot{e} + F_{\mathrm{v}} h_d \circ \hat{\theta}(\hat{q}) + F_{\mathrm{s}} \operatorname{sgn}(e) \tag{6.21}$$

was used where the terms $F_{\mathrm{v}} h_d \circ \hat{\theta}(q)$ and $F_{\mathrm{s}} \operatorname{sgn}(e)$ correspond to feed-forward viscous and static friction compensation terms and $K_P = (K_{P,\mathrm{H}}, K_{P,\mathrm{H}}, K_{P,\mathrm{K}}, K_{P,\mathrm{K}})$ and $K_D = (K_{D,\mathrm{H}}, K_{D,\mathrm{H}}, K_{D,\mathrm{K}}, K_{D,\mathrm{K}})$ are the proportional and derivative gains given in Table 6.5. The error signals are defined as

$$e := H_0 \hat{q} - h_d \circ \hat{\theta}(\hat{q}) \tag{6.22}$$

$$\dot{e} := H_0 \dot{\hat{q}} - \frac{\partial h_d}{\partial \theta} \dot{\hat{\theta}}(\dot{\hat{q}}) \tag{6.23}$$

where $(\hat{q}, \dot{\hat{q}})$ is RABBIT's state with relabeling,

$$(\hat{q}, \dot{\hat{q}}) := \begin{cases} (q, \dot{q}) & \text{if stance leg is right leg} \\ (Rq, R\dot{q}) & \text{if stance leg is left leg.} \end{cases} \tag{6.24}$$

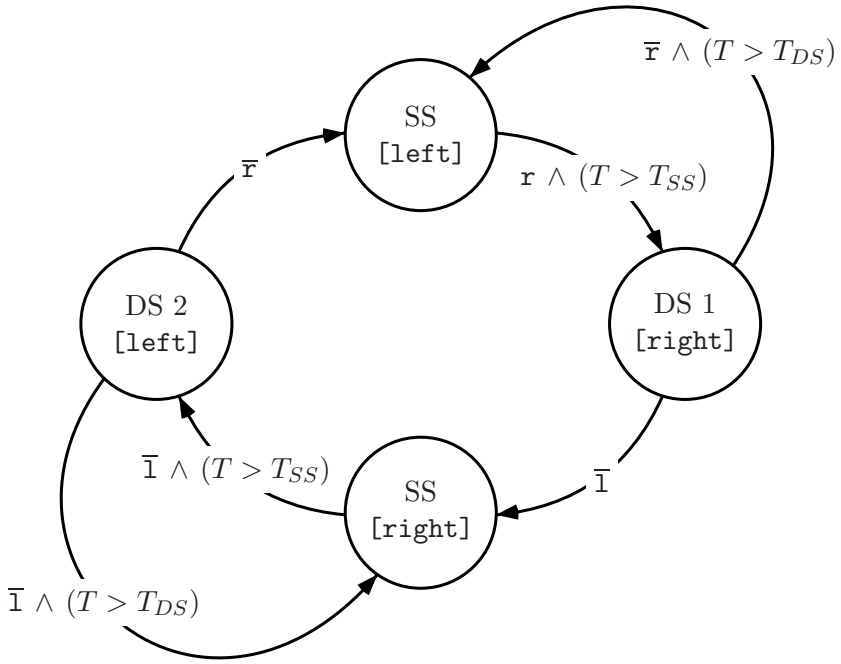

Figure 6.13: State diagram of RABBIT's leg configuration logic. The states are labeled with "SS" and "DS" for "single support" and "double support," respectively, and with the declared, current stance leg indicated by `[left]` and `[right]`. Contact switches signals on the left, `l`, and right, `r`, legs with a delay timer, T, drive state transitions. Delay threshold T_{DS} must be exceeded to transition back from a double support state to a previous single support state. Delay threshold T_{SS} must be exceeded to transition from a single support state to a double support state. The delay time is reset at each transition.

The state machine Figure 6.13 gives the logic for determining the current stance leg as required by (6.24). The delay thresholds, T_{SS} and T_{DS} given in Table 6.5, prevent chatter in the stance leg declaration. Since h_d is only designed for $0 < (\theta(q) - \theta^+)/(\theta^- - \theta^+) < 1$, the scalar function of the robot's states $\theta(q)$ was saturated,

$$(\hat{\theta}(q), \dot{\hat{\theta}}(q)) := \begin{cases} (\theta(q), \dot{\theta}(\dot{q})) & 0 < \frac{\theta(q)-\theta^+}{\theta^- - \theta^+} < 1 \\ (\theta^-, 0) & \frac{\theta(q)-\theta^+}{\theta^- - \theta^+} > 1 \\ (\theta^+, 0) & \frac{\theta(q)-\theta^+}{\theta^- - \theta^+} < 0. \end{cases} \tag{6.25}$$

The velocities were estimated using a five-point numerical differentiator described in [DGMS94] applied to the encoder outputs.

The PD based feedback (6.21) was chosen over a sliding mode, or finite-time converging controller because of its robustness to noise and uncertainty. The feedback (6.21) provided

surprisingly good joint-level tracking (see, for example, Figures H.1 and H.2).

The feedback (6.21)–(6.25) was implemented on the dSPACE DS1103 system running with a sample period of 1.5 ms (667 Hz) using the Simulink diagram given in Figure 6.14. The diagram is comprised of a combination of standard Simulink blocks and custom C S-Functions. To facilitate debugging, a companion Simulink diagram for simulation of RABBIT was created (see Figure 6.15). The companion diagram uses the same control block—the shaded block of Figures 6.14 and 6.15 with the block's contents given in Figure 6.16—as the one used on the dSPACE system. In the simulation diagram, the control block's inputs and outputs are connected to a model of RABBIT walking on a compliant surface. See [PGWA01, Rou98] for discussions of this simulator. To provide high-level control, the feedback implementation has a state machine which provides an interface between the user and the lower-level, continuous control. The implementation also has safety mechanisms which set the commanded control signals to zero in the event of an anomalous condition, such as a joint exceeding a position limit, or upon user request. One of the advantages of dSPACE's systems is that they provide the ability to interactively communicate with the real-time program running on the hardware's DSP. In the case of RABBIT, a PC running Windows NT and ControlDesk, dSPACE's windows-based interface software, was connected with the DS1103 system using a dedicated TCP/IP over Ethernet network. A user interface to the controller's state machine was designed in ControlDesk. Figure 6.17 gives the two main ControlDesk interface diagrams of this interface.

6.5 The experiments

This section describes six experiments which highlight the capabilities and robustness of controllers designed via the theoretical framework presented in Chapters 2–5. To perform the experiments, two research visits were made to the Laboratoire D'Automatique de Grenoble where RABBIT is located. The first visit lasted two weeks, from August 15th until August 26th 2002, and the second visit lasted three weeks, from February 24th until March 14th 2003.

During the first visit, RABBIT had not yet been installed into its permanent location. It

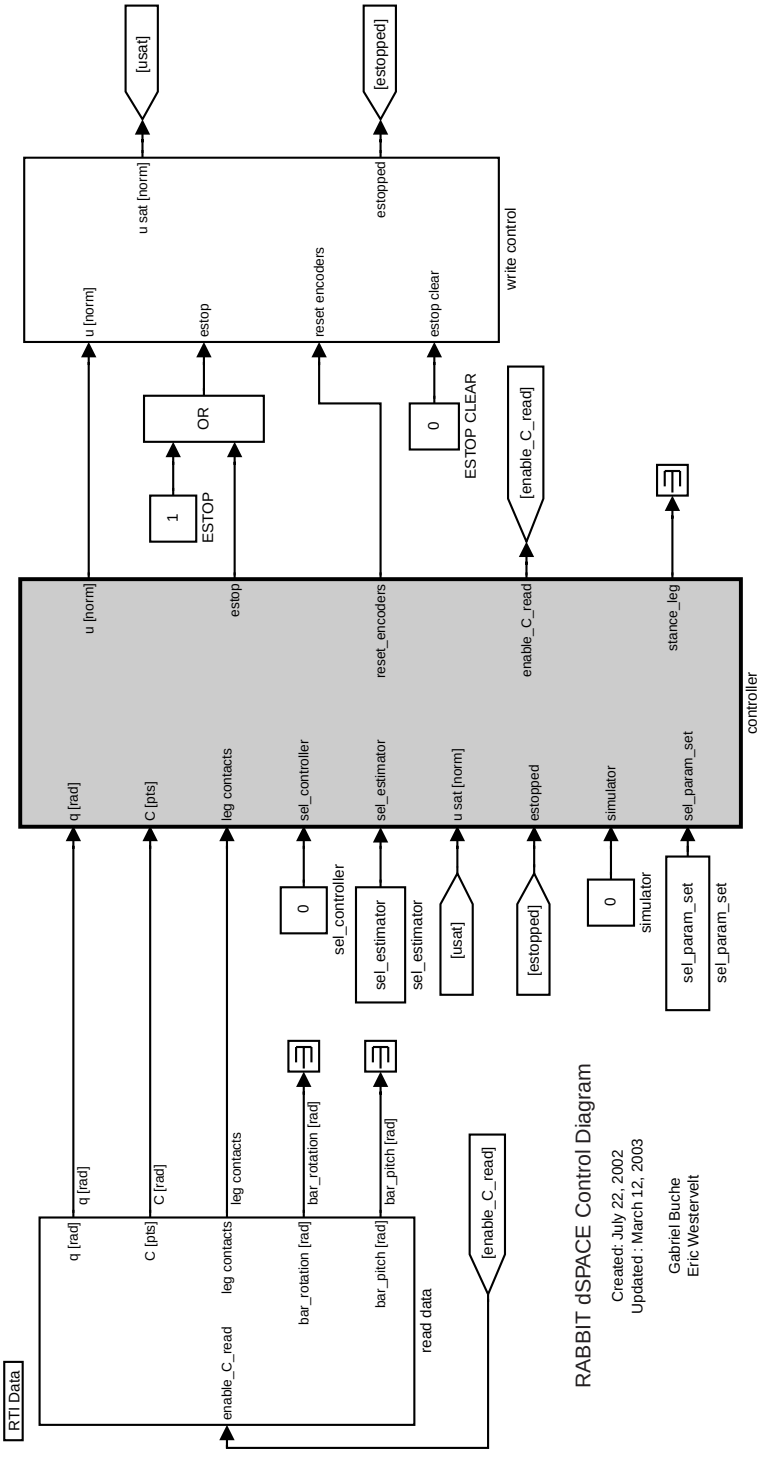

Figure 6.14: RABBIT's controller Simulink diagram.

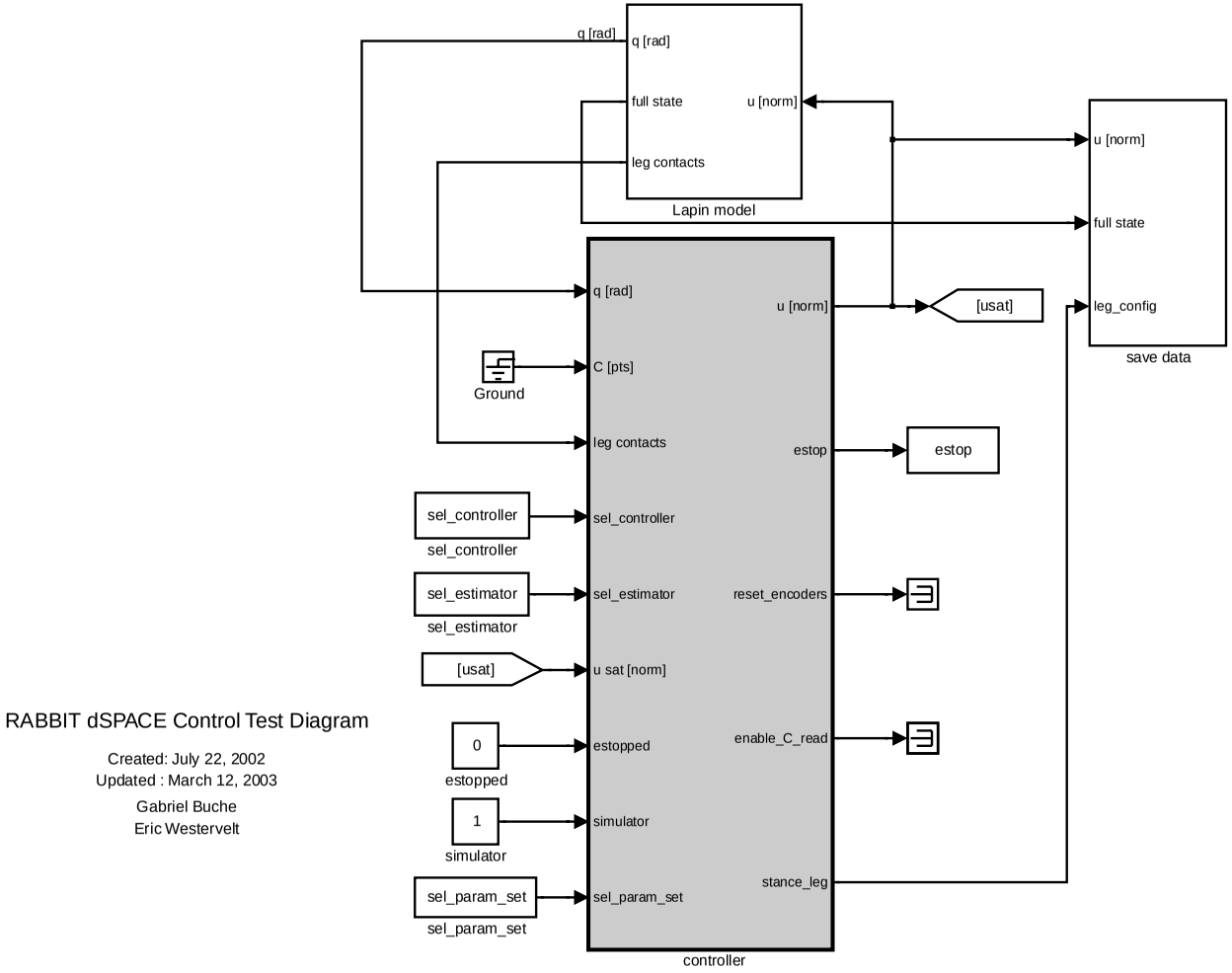

Figure 6.15: RABBIT's controller test Simulink diagram.

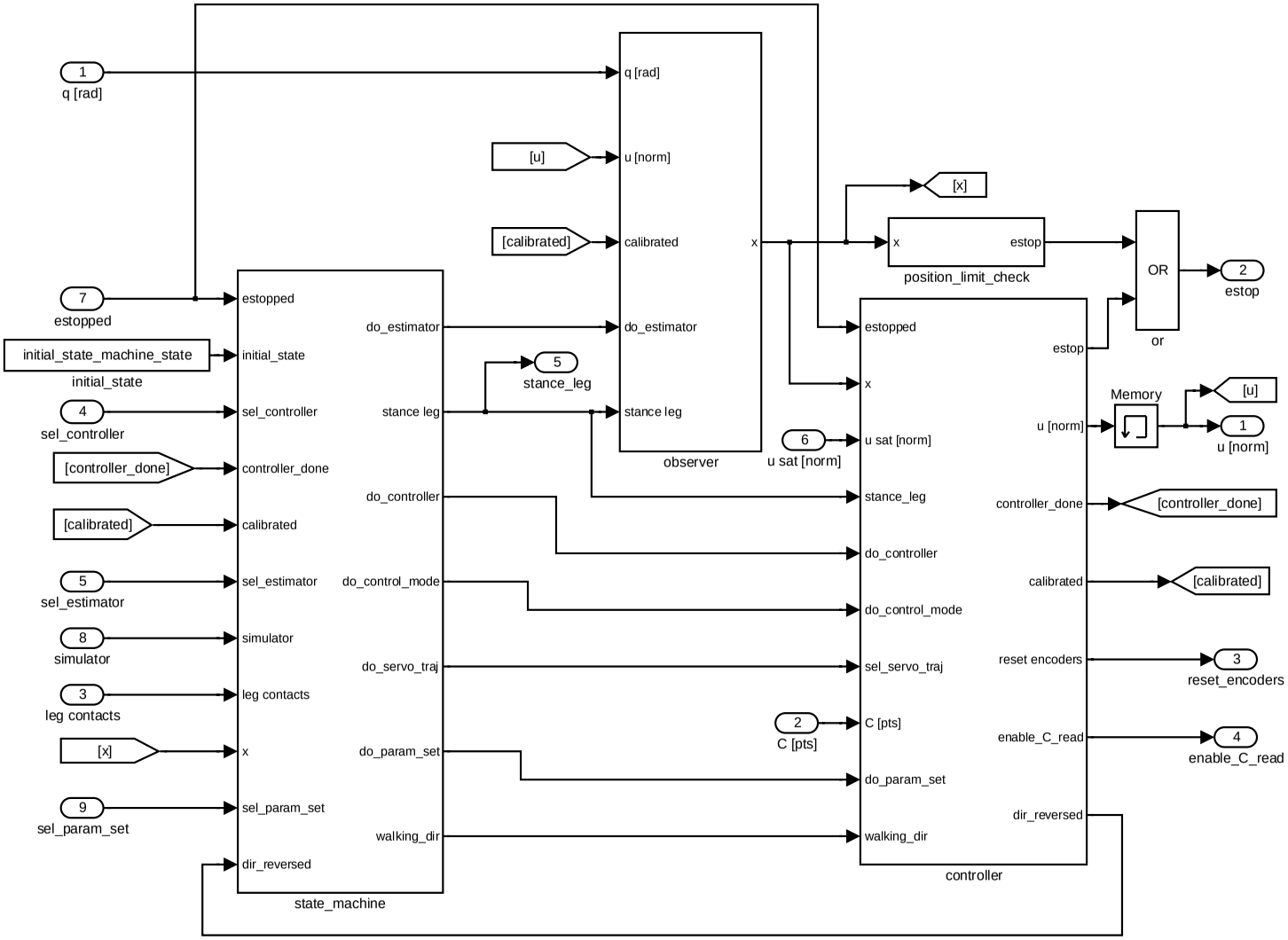

Figure 6.16: RABBIT's controller Simulink diagram observer and controller block.

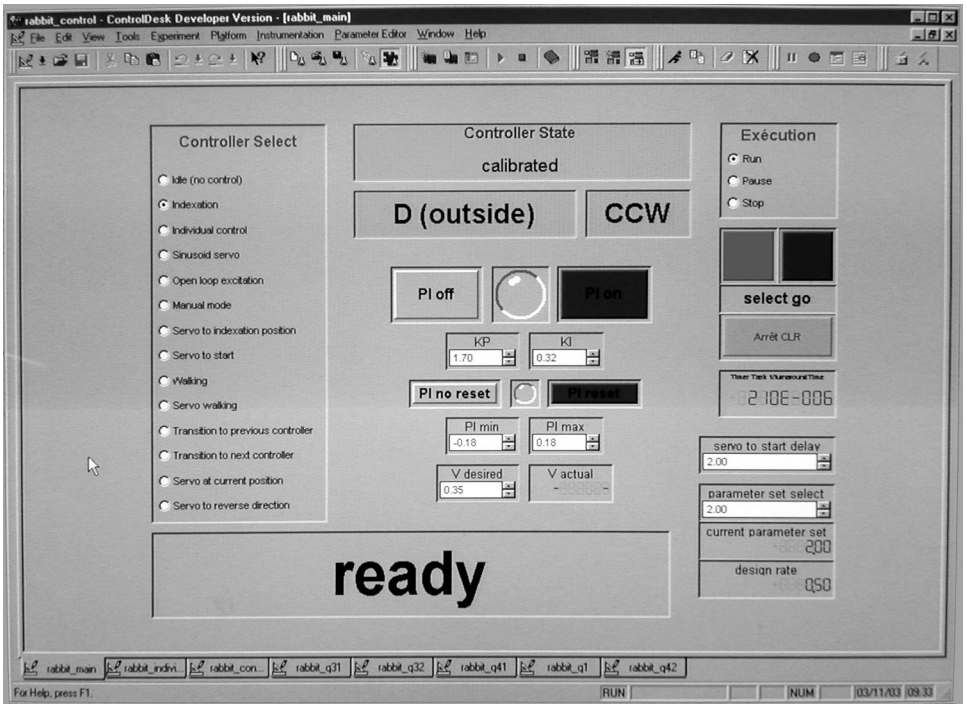

(a) Main controller interface.

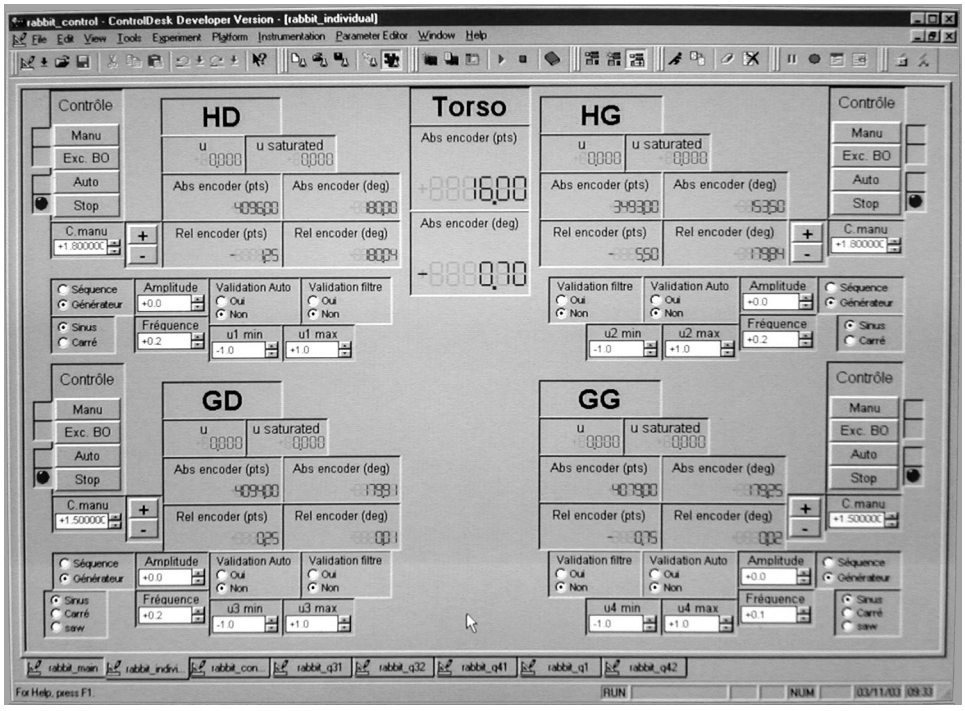

(b) Individual link control interface.

Figure 6.17: dSPACE control interface screen shots.

was located in a lab where the workspace was limited, only allowing about nine consecutive steps to be taken. Hence, testing if a controller induced a stable gait was impossible. That limitation notwithstanding, three important tasks where accomplished: 1) familiarization with RABBIT's experimental setup, 2) creation of the Simulink and C S-Function software for control implementation, and, most importantly, 3) controlling RABBIT to walk for its first time ever, on the first try. The last accomplishment was achieved using a controller designed via the method described in Section 6.4. Aside from the tuning of the PD gains, no tweaking or tuning of the robot's gait, i.e., the output function parameters α, was necessary to successfully walk. This is a testament to the utility of the theoretical framework.

At the start of the second visit, RABBIT had just been installed into its permanent location, pictured in Figure 6.3, where about 200 consecutive steps (6 to 7 laps about the center stand) were possible. The limit on the total number of steps was due to the winding of the power and Ethernet cabling about the center stand. During the visit, many small details had to be addressed to improve the experimental platform. Some of these included changing the mounting hardware of the contact switchings, installing the wood and rubber walking surface, shortening the boom, fixing a broken encoder, and modifying the training wheels. All six experiments reported were performed during this second visit using the shortened bar on the wood and rubber walking surface. The experiments were conducted as follows: the experiment began with the robot suspended in the air, lifted by an experimenter. After an encoder calibration phase, the robot was servoed to a configuration $(q, \dot{q}) = (q_0, 0) \in \Delta(S \cap Z_\alpha)$ and then placed on the ground. Once on the ground, data collection was initiated and the control was switched to the zero dynamics based feedback controller (6.21)–(6.25). Switching with $(q, \dot{q}) = (q_0, 0) \in \Delta(S \cap Z_\alpha)$ is possible since the zero dynamics are asymptotically stable in double support. To initiate walking, an experimenter pushed the robot's torso—temporarily fully actuating the robot's underactuated dynamics—supplying the energy required to land the robot's state in the basin of attraction of the Poincaré return map. Once in motion, the robot reached steady state walking within ten to twenty steps. To stop the robot, an experimenter grabbed the torso—again, fully actuating the robot's dynamics—slowing the robot to a stop in double support. This ability to interact with the robot's dynamics by pushing on the robot is a consequence of

the zero dynamics' parameterization by $\theta(q)$. Through mechanical coupling, forces on the robot drive $\theta(q)$ which, in turn, determines the evolution of the robot's actuated DOF. Figure 6.18 gives video frames of RABBIT taking two consecutive steps for a typical walking motion.

6.5.1 Walking at 0.7 m/s

In this first experiment,[3] RABBIT was controlled with a feedback designed to induce walking at 0.7 m/s. The experiment lasted approximately 93 seconds during which RABBIT took 170 steps. Figures H.1–H.6 are plots of various quantities of interest over a representative time interval containing approximately nine steps. Figures H.1–H.4 give the tracking performance along with the associated errors, (6.22) and (6.23). Note that the peak error in configuration tracking is less than 0.043 rad (2.5 degrees) while the peak error in velocity tracking is much as 1.4 rad/s. Figure H.5 gives the commanded control signals. The peak commanded torque is less than 100 Nm, two thirds of the actuators' 150 Nm maximum. Figure H.6 gives the trace of the torso angle. Note that the torso angle is not a directly controlled quantity. Figure H.7 gives the traces of the horizontal and vertical angular displacements of the boom, ϕ_{h} and ϕ_{v}, for the experiment. As indicated by Figure H.7(a), the robot took approximately six laps about the center stand to complete the 170 steps. Note the constant slope and monotonicity of the trace of ϕ_{h} indicating smooth, horizontal motion of the hip. The trace of Figure H.7(b) gives ϕ_{v} over the representative time interval. Note that the DC offset varies step-to-step (which corresponds to peak-to-peak in this case). Inspection of the trace of ϕ_{v} for the entire experiment, plotted in Figure H.7(c), reveals that the envelope of ϕ_{v} is periodic. This periodicity has an amplitude of 0.009 rad (0.5 degrees) and is due to the nonuniformity in the walking surface height. Figure H.8 gives the step length, step duration, and the ratio of step length to step duration, step rate. The data points of Figure H.8 were calculated upon swing foot touchdown declaration as determined by the state machine given in Figure 6.13. The step lengths given in Figure H.8(a) were calculated using the measured joint angles and the robot's identified link lengths Table 6.1. In each plot of Figure H.8, squares indicate data points corresponding to the inner leg—the

[3] The data file for this experiment is `3_13_03_exp_004.mat`.

Figure 6.18: Video frames of RABBIT taking two consecutive steps.

leg closer to the center stand—and circles indicate data points corresponding to the outer leg—the leg further from the center stand. Labeling the data points in this way reveals differences between the inner and outer legs in step length, step duration, and step rate. Since the two legs are, to within close approximation, identical, the difference is likely due to the non-sagittal plane dynamics created by the boom system. Aside from the differences between the inner and outer legs, the variances in step length and step duration have several contributing factors. The ones believed to be most significant are nonuniformity in the walking surface, variance in the declaration of leg touchdown, and flexibility in the robot's joints. Careful comparison of Figures H.8(b) and H.8(c) with Figure H.7(a) reveals that the step rate is periodic in ϕ_{h}. This periodicity is due to nonuniformity in the walking surface: one section of the wood and rubber walking surface was not firmly lying on the ground because of unevenness in the underlying concrete floor.

6.5.2 Demonstration of robustness to perturbations

This second experiment[4] demonstrates the robustness of controllers designed via the theoretical framework. Two types of perturbations were applied to RABBIT controlled by a feedback designed to induce walking at 0.9 m/s. The first was a 10 kg mass added to the torso, which resulted in a shift of the average walking rate from 0.9 m/s to 1.0 m/s (see Figure H.16(c)). In the fifth experiment, described in Section 6.5.5, it will be demonstrated that the designed fixed average walking rate may be recovered through the use of event-based integral control. In addition to the sizable perturbation to the robot's model (recall the robot weighs 32 kg), the second perturbation was short duration forces applied to the RABBIT's torso by an experimenter in both the forward and reverse directions. Despite both these significant perturbations, RABBIT did not fall during the experiment which lasted approximately 74 seconds where RABBIT took 164 steps.

Figures H.9–H.14 are plots of various quantities of interest over a representative time interval in which the robot was pushed in the forward direction (at approximately 20.5 seconds) and in the reverse direction (at approximately 29 seconds). Note the increases in tracking errors during the application of these forces (see Figures H.9–H.12) and the change

[4]The data file for this experiment is `3_13_03_exp_012.mat`.

in the reference motion, h_d and $(\partial h_d/\partial\hat{\theta})\dot{\hat{\theta}}$. The commanded control signals are within the actuators' limits, except during the force perturbations when they saturate (see Figures H.13(a) and H.13(b)). The slope of ϕ_{h} is less constant than in the previous experiment (cf. Figures H.7(a) and H.15(a)). The change in slope is due to RABBIT's average walking rate changing in response to the force perturbations. As in the last experiment, ϕ_{v} is periodic due to the nonuniformity in the walking surface height (see Figure H.15(b)). Both the step length (see Figure H.16(a)) and the step duration (see Figure H.16(b)) vary greatly during the application of the perturbation forces.

6.5.3 Transitioning between controllers

This third experiment[5] demonstrates the use of the transition controllers presented in Section 5.1. For the experiment, the controller applied to RABBIT was transitioned between controllers at 0.1 m/s intervals from 0.5 m/s to 0.8 m/s and then back from 0.8 m/s to 0.5 m/s twice (see Figure H.24(c)). The transitioning controllers were designed according to (5.1) and (5.2). The experiment lasted approximately 86 seconds during which RABBIT took 139 steps.

Figures H.17–H.22 are plots of various quantities of interest over a representative time interval of approximately twenty-six steps where the control was transitioned from 0.6 m/s to 0.8 m/s. Note the change in the reference motion, h_d and $(\partial h_d/\partial\hat{\theta})\dot{\hat{\theta}}$, with no visible difference in the tracking error (see Figures H.17–H.20), or in commanded control signal (see Figure H.21). Also note the changes in slope of ϕ_{h} due to the changes in average walking rate (see Figure H.23(a)). As should be expected, both the step length and the step duration vary with the applied controller (see Figures H.24(a) and H.24(b)).

6.5.4 Using event-based integral control to modify the fixed point

In this fourth experiment,[6] the same feedback used in the first experiment to induce walking at 0.7 m/s was applied with the addition of an event-based PI control, described in Section 5.2, used to modify the steady state average walking rate from 0.7 m/s to 0.6 m/s.

[5]The data file for this experiment is `3_11_03_exp_006.mat`.
[6]The data file for this experiment is `3_14_03_exp_003.mat`.

The event-based control acts through step-to-step modifications of the Bézier polynomial coefficients, α, synchronized with double support.

The event-based control was performed on the stance and swing leg relative angles, q_1 and q_2, which results in a change of the torso angle (see Figure 6.2). This was accomplished by setting $\delta\alpha$ to zero except for

$$\delta\alpha_j^i = 1, \text{ for } i = 1, 2 \text{ and } j = 2, \ldots, M. \tag{6.26}$$

The controller (5.22) with set-point $\eta^* = 0.6$ and control gains $K_I = 0.06$ and $K_P = 0$ was applied on the 15th step (at approximately 11 seconds). The proportional gain, K_P, was set to zero because of the noise introduced by the variance in step rate. The experiment lasted approximately 110 seconds during which RABBIT took 181 steps. Figure H.31 gives the value of w of (5.22) versus time. Note that the ringing in w and, consequently, in average walking rate is likely due to the integral gain being set too large (see Figure H.33). Yet, if that is, indeed, the case, it still took over 50 steps for the average walking rate to converge to 0.6 m/s (see Figure H.33(c)).

Figures H.25–H.30 are plots of various quantities of interest for the entire experiment. Note the change in the reference motion, h_d and $(\partial h_d/\partial\hat{\theta})\dot{\hat{\theta}}$, for q_1 and q_2 with no visible difference in the tracking error (see Figures H.25–H.28) or in commanded control signal (see Figure H.29). Figure H.30 gives the torso angle change resulting from the changing of q_1 and q_2. Figure H.32 gives the effect on ϕ_{h} and ϕ_{v}.

6.5.5 Using event-based integral control to reject a perturbation

In this fifth experiment,[7] the same feedback used in the first experiment to induce walking at 0.7 m/s was applied but with a 10 kg mass attached to the torso. This perturbation resulted in a shift of the average walking rate from 0.7 m/s to approximately 0.85 m/s (the change in average walking rate was determined in a separate experiment not reported in this dissertation). The average walking rate of 0.7 m/s was recovered using the event-based integral control described in the previous experiment but with $K_I = 0.04$ and $\eta^* = 0.7$ applied on the 14th step (at approximately 11 seconds). The experiment lasted approximately

[7] The data file for this experiment is `3_14_03_exp_004.mat`.

95 seconds during which RABBIT took 164 steps.

Figure H.40 gives the value of w of (5.22) versus time. Again, note that the ringing in w and, consequently, in average walking rate (see Figure H.42) is likely due to the integral gain being too large. Figures H.34–H.39 are plots of various quantities of interest for the entire experiment. As before, note the change in the reference motion, h_d and $(\partial h_d/\partial\hat{\theta})\dot{\hat{\theta}}$, for q_1 and q_2 with no visible difference in the tracking error (see Figures H.34–H.37) or in commanded control signal (see Figure H.38). The torso angle trace reflecting the action of the event-based integral control is given in Figure H.39. This regulation of the torso angle by integral control was able to recover the 0.7 m/s average walking rate (see Figure H.42(c)). Figure H.41 gives the effect on ϕ_{h} and ϕ_{v}.

6.5.6 Using event-based integral control to stop the robot

In this sixth and final experiment,[8] event-based integral control was used to stop RABBIT from a steady state average walking rate of 0.5 m/s. This was achieved by slowing the average walking rate of RABBIT to where it did not have enough energy to successfully complete a step. The integral control described in the fourth experiment (Section 6.5.4) with $K_I = 0.04$ and $\eta^* = 0$ was applied on the 34th step (at approximately 29 seconds) and RABBIT was stopped by the 39th step (at approximately 34 seconds). After stopping, RABBIT rocked back and forth until all kinetic energy from walking was dissipated.

Figures H.43–H.48 are plots of various quantities of interest for a time interval including a portion of the steady state walking cycle and the stopping of RABBIT. Note the changes in the reference motion, h_d and $(\partial h_d/\partial\hat{\theta})\dot{\hat{\theta}}$, for q_1 and q_2 as the integral control is applied (see Figures H.43–H.46) and the decrease in the commanded control signals (see Figure H.47). The increase in the torso angle (see Figure H.48) reflects the action of the integral control (see Figure H.49). The oscillation in ϕ_{h} (see Figure H.50(a)) and the sign reversal of step length (see Figure H.51(a)) at approximately 33 seconds reflect the rocking of RABBIT back and forth after stopping. The final five data points of Figure H.51(c) that seem to indicate apparently large sign-changing average walking rates are a consequence of the way in which the average walking rate was calculated (the ratio between step length and step

[8] The data file for this experiment is `3_14_03_exp_009.mat`.

duration).

CHAPTER 7

Conclusion and future work

7.1 Conclusion

This dissertation presents the beginnings of a coherent framework for the control of biped locomotion. The framework builds on previous work by formalizing an approach common to most schemes for the control of biped walking. That approach is to structure the control in such a way as to simplify the controller design process. The approach can be found, for example, in the regulation of angular momentum by Sano and Furusho [SF90], of total energy by Goswami, Espiau, and Keramane [GEK96], of the robot's center of mass trajectory by Kajita and Tani [KT96], via virtual model control by Pratt et al. [PCT+01, PP98], and of the Zero Moment Point by many [VBSS90, LYT00, YSIT99, HHHT98]. This framework is an attempt to give a rigorous formulation to this common approach in hopes of providing a foundation for the further development of control design techniques that are systematically able to induce walking or running with known kinematic and dynamic properties. Development of the theoretical framework involved a sequence of key steps.

The first step was the right choice of modeling complexity. The class of models treated by this dissertation, given in Chapter 2, was chosen to be only as complex as required to capture the primary difficulties inherent to the control of biped walking. Those difficulties are limb coordination, effective underactuation, hybrid dynamics, static instability, and the designing of limit cycles. Addressing these difficulties in a manner conducive to control design was a result of the remaining steps.

The second step, described in Chapter 3, was the casting of the gait coordination problem as an output function design problem. This was accomplished by choosing the output to encode the robot's posture—thus coordinating the limbs—over a step parameterized by a scalar function of the robot's configuration. Encoding of the posture in this way is thought of as imposing virtual constraints—holonomic constraints parameterized by the robot's state. Since the system is underactuated, zeroing the output results in zero dynamics: the largest internal dynamics compatible with the output being identically zero. Under certain assumptions on the output (HH1)–HH4)) and on the coordinate labeling (RH6)) the form of the zero dynamics becomes apparent. The notion of virtual constraints is likely to be useful in the control of other mechanical systems where coordination of the system's motion is more naturally parameterized by state than by time.

The third step, also described in Chapter 3, was to incorporate the impacts, which occur as a consequence of swing leg touchdown, into the notion of zero dynamics by specializing the output to one whose zero set—the associated zero dynamics manifold—is invariant under the impact mapping. This lead to the definition of a new notion of zero dynamics, the hybrid zero dynamics. The hybrid zero dynamics were defined analogously to the zero dynamics. The key to the hybrid zero dynamics is invariance of the zero dynamics manifold under the impact map not just at a point, but on an entire subset of the zero dynamics manifold (at the intersection with the chosen Poincaré section). Choosing the output such that the hybrid zero dynamics exists results in the Poincaré return map restricted to the zero dynamics manifold being diffeomorphic to a scalar, linear time invariant system, rendering transparent the existence (or nonexistence) of a dynamically stable walking motion. Moreover, in Section 3.5.2 it was shown that then the modeling hypotheses may be incorporated into the stability analysis by exactly calculating the upper bound on the domain of definition of the hybrid zero dynamics' Poincaré return map.

The fourth step, described in Chapter 4, makes the results of Chapter 3 practicable. The output functions were further specialized to an almost linear structure utilizing carefully chosen functions, Bézier polynomials. Though any number of other functions could have been chosen, Bézier polynomials were selected because of their convenient properties which, in particular, makes achieving invariance of the zero dynamics manifold simple. The almost

linear structure enabled trivial inversion of certain coordinate transformations so that zero dynamics could be written down in closed form. The use of polynomials finitely parameterized the outputs which enabled them—and therefore walking motions—to be automatically designed using standard parameter optimization techniques on the hybrid zero dynamics. Appropriate choice of constraints in the optimization process permitted desired kinematic and dynamic properties to be achieved. Moreover, for the class of models treated in this dissertation, regardless of the number of links, the dimension of the hybrid zero dynamics is always two. Thus, in the design of walking motions via parameter optimization, the dimension of the underlying system's dynamics being tuned is fixed with respect to the number of links of the robot. The only increase in complexity that results from the addition of links is an increase in the number of output parameters.

The fifth step, described in Section 5.1, was the development of a means to compose two controllers, Γ_α and Γ_β, that induce walking at fixed average walking rates. The key to composition is the introduction of a transition controller, $\Gamma_{(\alpha\to\beta)}$, whose zero dynamics manifold is chosen such that it matches the zero dynamics manifolds associated with Γ_α and Γ_β in such a way as to enable transition from a subset of the domain of definition of the Poincaré return map associated with Γ_α to the domain of definition of the Poincaré return map associated with Γ_β. Properties of the Bézier polynomials used in the output makes transition controller design particularly simple.

The sixth step, described in Section 5.2, was the development of an outer-loop event-based PI control for the online regulation of average walking rate. This outer-loop control acts step-to-step, synchronized with impact events, just after double support, by modifying the Bézier polynomial coefficients, α. By supplying feedback on the robot's average walking rate, event-based control is able to regulate average walking rate to a continuum of values, to reject the effect of moderate disturbances on average walking rate, and to hasten convergence of average walking rate to its steady state value.

Chapter 6 described the experimental verification of the theoretical framework developed in Chapters 2–5 on a prototype biped, RABBIT. A main highlight was that the control of dynamic walking was achieved without the tweaking or tuning of the gait. The only tuning required was on the gains of the control used to impose the virtual constraints (zero

the outputs) and scaling of the impact map as encapsulated in the hybrid zero dynamics. To have the dynamic design specifications of walking motions designed via the theoretical frame work more closely match the experimental results, several effects were accommodated in the controllers' design. These effects were the inertia added by the boom system used to constrain RABBIT to be planar, the friction and decoupling effect of the gear reducers, and the non-rigidity of the walking surface. The decoupling effect of the gear reducers enabled the virtual constraints to be imposed through the use of high-gain, decoupled PD controllers. It was found that controllers designed via the theoretical framework and implemented in this way have a surprising amount of robustness to exogenous, modeling, and parameter perturbations. The reason for this is, in part, the inherent robustness afforded by exponential stability of the Poincaré map's fixed point; see [CAA+02].

7.2 Future work

Research into the control of biped locomotion, and, more generally legged locomotion, is still in its infancy. There are many, interesting questions to be answered and ideas to be explored. Some research topics that follow as more direct extensions to the framework begun in this dissertation are now listed.

Addition of feet. To require that the effective underactuation inherent to biped robots be addressed, bipeds in the class models treated in this dissertation do not have feet and are therefore underactuated. Though the introduction of feet adds additional phases to the walking cycle, the additional torque available during the stance phase results in full actuation which can be used to improve the robustness. Moreover, any practicable biped will, almost surely, need feet to perform the statically stable maneuvers necessary for walking on surfaces with low coefficients of friction, for climbing, for negotiating obstacles, etc.

Building in reflexes. Though controllers developed via this framework are robust to modest perturbations, it is necessary to design controllers for recovery from more significant perturbations, i.e., to build in reflexes [BH95, BT86]. Understanding how to

recover from large perturbations seems especially important for bipeds because of their typically high center of mass and relatively small support polygons that makes them susceptible to overturning by exogenous perturbation forces.

Walking on uneven terrain. The ability to climb and descend stairs, walk on uneven surfaces and inclines, and step over support discontinuities are some of the main benefits of legged locomotion. As it stands, the presented framework has not addressed these important abilities. Incorporating these abilities into this dissertation's framework is possible and will likely require the use of the additional tools presented in Chapter 5.

Walking in three-dimensions. Since the sagittal plane dynamics are almost decoupled from those in the frontal plane [FS90, Kuo99, BK00], it is conjectured that the controllers developed in this dissertation can be directly implemented with controllers for the stabilization of motions in the frontal plane to produce stable, dynamic three-dimensional walking.

Online gait learning. An intuitively appealing approach used for the control of biped walking is the tracking of walking trajectories generated online via learning [Jua00, MM94, Mil94]. The idea is to track trajectories that are modified online using some technique of approximate optimization. Unfortunately, the performance of such schemes has been rather poor since the learning algorithms employed are not informed of the biped's stability. With the framework this dissertation, however, such learning could be applied for the online modification of the robot's gait as specified by the coefficients of Bézier polynomials while ensuring gait stability.

Running. The primary difference between running and walking is the presence of a flight phase, when no part of the biped is in contact with the ground. During the flight phase, the addition of a nonholonomic constraint—the conservation of angular momentum of the biped about its center of mass—makes significantly more difficult the design of a feedback law which restricts the robot's dynamics to an easily characterized submanifold of its state space. Controlling the robot to land in a desired configuration is

equivalent to the falling cat problem (reorientation of a falling body using only shape change). Currently, only feed-forward solutions to this problem exist [CS93, FGL94, SKI99], but work toward understanding the geometry of this type of nonholonomic constraint is ongoing [Kri90, BRM92]. Appendix I presents some preliminary work on understanding the stability of running gaits.

7.3 Final thoughts

Since control is often unseen, hidden inside computer code, it is too often overlooked [Åst03]. Such is the case, in general, with the control of biped locomotion. The control of the biped appears as an afterthought to the mechanism's design. The reality is, however, that requirements on performance, energy efficiency, and stability necessitate control which is able to treat the difficulties inherent to biped locomotion. For this reason, the efforts placed in the development of control and mechanism development ought to be, at least, equalized. This is not to diminish the need for well designed mechanisms and the development of novel actuators and sensors, all of which are of great importance. The ideal setting would be one in which the development of control for locomotion informs the mechanism design and vice versa.

It seems inevitable that legged robots, in particular bipeds, will eventually make their way into the market place and the work environment. Endowing these machines with the capability of navigating even structured environments will involve the development of controllers composed of many sub-controllers each designed to accomplish a specific task. For example, the framework developed in this dissertation would be just one of those sub-controllers. Other controllers would enable stair climbing and descending, recovery from large perturbations, etc. It will be interesting to see how this development occurs and how the issues of stability and energy efficiency impact that development.

APPENDICES

APPENDIX A

Equations of motion for the 4-DOF model of the 2-link walker

This appendix gives the details of the 4-DOF equations of motion for the two-link model. Definition of the constants can be found in Section 2.4. Values of the model parameters can be found in Table 2.1.

The equations have the general matrix form

$$D(q)\ddot{q} + C(q,\dot{q})\dot{q} + G(q) = Bu \tag{A.1}$$

where $q := (q_1, q_2, p_{\mathrm{H}}^{\mathrm{h}}, p_{\mathrm{H}}^{\mathrm{v}})$ and

$$\begin{aligned}
(D(q))_{1,1} &= l_{\mathrm{c}}^2 m + 2I + m(l - l_{\mathrm{c}})^2 \\
(D(q))_{1,2} &= m(l - l_{\mathrm{c}})^2 + I \\
(D(q))_{1,3} &= (l - l_{\mathrm{c}}) m \cos(q_1 - q_2) \\
(D(q))_{1,4} &= -(l - l_{\mathrm{c}}) m \sin(q_1 - q_2) \\
(D(q))_{2,1} &= m(l - l_{\mathrm{c}})^2 + I \\
(D(q))_{2,2} &= m(l - l_{\mathrm{c}})^2 + I \\
(D(q))_{2,3} &= (l - l_{\mathrm{c}}) m \cos(q_1 - q_2) \\
(D(q))_{2,4} &= -(l - l_{\mathrm{c}}) m \sin(q_1 - q_2) \\
(D(q))_{3,1} &= (l - l_{\mathrm{c}}) m \cos(q_1 - q_2) \\
(D(q))_{3,2} &= (l - l_{\mathrm{c}}) m \cos(q_1 - q_2) \\
(D(q))_{3,3} &= m
\end{aligned}$$

$$
\begin{aligned}
(D(q))_{3,4} &= 0 \\
(D(q))_{4,1} &= -(l - l_{\mathrm{c}})m\sin(q_1 - q_2) \\
(D(q))_{4,2} &= -(l - l_{\mathrm{c}})m\sin(q_1 - q_2) \\
(D(q))_{4,3} &= 0 \\
(D(q))_{4,4} &= m
\end{aligned}
$$

$$
\begin{aligned}
(C(q,\dot{q}))_{1,1} &= 0 \\
(C(q,\dot{q}))_{1,2} &= (l - l_{\mathrm{c}})m(\sin(q_1 - q_2)\dot{p}_{\mathrm{H}}^{\mathrm{h}} + \cos(q_1 - q_2)\dot{p}_{\mathrm{H}}^{\mathrm{v}}) \\
(C(q,\dot{q}))_{1,3} &= (l - l_{\mathrm{c}})m\sin(q_1 - q_2)\dot{q}_2 \\
(C(q,\dot{q}))_{1,4} &= (l - l_{\mathrm{c}})m\cos(q_1 - q_2)\dot{q}_2 \\
(C(q,\dot{q}))_{2,1} &= -(l - l_{\mathrm{c}})m(\sin(q_1 - q_2)\dot{p}_{\mathrm{H}}^{\mathrm{h}} + \cos(q_1 - q_2)\dot{p}_{\mathrm{H}}^{\mathrm{v}}) \\
(C(q,\dot{q}))_{2,2} &= 0 \\
(C(q,\dot{q}))_{2,3} &= -(l - l_{\mathrm{c}})m\sin(q_1 - q_2)\dot{q}_1 \\
(C(q,\dot{q}))_{2,4} &= -(l - l_{\mathrm{c}})m\cos(q_1 - q_2)\dot{q}_1 \\
(C(q,\dot{q}))_{3,1} &= -(l - l_{\mathrm{c}})m\sin(q_1 - q_2)\dot{q}_1 \\
(C(q,\dot{q}))_{3,2} &= (l - l_{\mathrm{c}})m\sin(q_1 - q_2)\dot{q}_2 \\
(C(q,\dot{q}))_{3,3} &= 0 \\
(C(q,\dot{q}))_{3,4} &= 0 \\
(C(q,\dot{q}))_{4,1} &= -(l - l_{\mathrm{c}})m\cos(q_1 - q_2)\dot{q}_1 \\
(C(q,\dot{q}))_{4,2} &= (l - l_{\mathrm{c}})m\cos(q_1 - q_2)\dot{q}_2 \\
(C(q,\dot{q}))_{4,3} &= 0 \\
(C(q,\dot{q}))_{4,4} &= 0
\end{aligned}
$$

$$
\begin{aligned}
(G(q))_{1,1} &= g_0(ml_{\mathrm{c}}\sin(q_1) + (l - l_{\mathrm{c}})m\sin(q_1 - q_2)) \\
(G(q))_{2,1} &= -g_0m(l - l_{\mathrm{c}})\sin(q_1 - q_2) \\
(G(q))_{3,1} &= 0 \\
(G(q))_{4,1} &= 2g_0m
\end{aligned}
$$

$$B = \begin{bmatrix} 0 \\ 1 \\ 0 \\ 0 \end{bmatrix}$$

The linear transformation matrix required by (2.20) is

$$R = \begin{bmatrix} 1 & -1 \\ 0 & -1 \end{bmatrix}. \tag{A.2}$$

APPENDIX B

Optimization algorithm implementation

This appendix gives the pseudocode for the S-Function called by MATLAB's constrained nonlinear optimization tool `fmincon` which is used for walking motion design as described in Section 4.3.2. Use of an S-Function (which is compiled) in place of a MATLAB script (which is interpreted) increases optimization speed by decreasing the iteration time interval. The S-Function computes both the cost and the constraints required by the `fmincon` algorithm.

The pseudocode below is implemented entirely in C (without call to MATLAB), including the integration of the zero dynamics. Communication between the S-Function and the `fmincon` routine is accomplished by copying global variables to and from the MATLAB workspace. Continuity of the cost function, (4.40) or (4.41), with respect to the output function parameters along with use of a small optimization step size makes use of the gradient-based `fmincon` algorithm feasible. In the event the algorithm lands in a regime where no feasible periodic orbit exists (there is no fixed point of the Poincaré return map), the values for the cost and the constraints of the previous optimization step are used. If the algorithm persists in such a regime, the optimization process is terminated manually. The pseudocode is as follows.

1: copy variables from MATLAB workspace
2: per Corollary 4.1, compute output function parameters from reduced set of parameters
3: per (3.90), calculate the Poincaré return map fixed point
4: **if** fixed point exists (per inequality (3.89)) **then**
5: integrate the hybrid zero dynamics

```
    evaluate constraints
    save cost and constraints (in case fixed point does not exist on next optimization step)
else
    if first optimization step call then
        optimization failure
    else
        use previously computed cost and constraint values
    end if
end if
write variables to MATLAB workspace
```

APPENDIX C

Proving decoupling matrix invertibility

Existence of the zero dynamics depends upon the invertibility of the decoupling matrix. Since the decoupling matrix can have singularities even at points where the Jacobian of the output, $\partial h/\partial q$, has full row rank[1], proof of the invertibility of the decoupling matrix must be local in q. If the decoupling matrix is sufficiently simple, as in the case of the three-link biped of [GAP01], it may be possible to analytically find regions in q where the matrix is non-singular by examination of the determinant, or linear dependence of the columns or rows. When the decoupling matrix is more complex, as in the five-link biped of [PGWA01], direct proof of invertibility is highly non-trivial. In this case, there is a need to resort to an automated methodology.

One such methodology is to demonstrate sign definiteness of the decoupling matrix's determinant in an open set about the robot's trajectories. Sign definiteness implies the determinate never equals zero in that set and, hence, in that set, the decoupling matrix is invertible. This is the method used here. The proof is carried out in two steps. In the first step, the decoupling matrix is simplified by the application of an invertible feedback [RvdSMK99] to the model[2]. In the second step, elementary bounds on the individual terms appearing in the determinant of the decoupling matrix are determined and used to compute upper and lower bounds on the determinant of the decoupling matrix.

[1]First note that $L_g L_f h = \partial h/\partial q\, D^{-1} B$. Although $D^{-1}B$ has full column rank (since $D(q)$ is positive definite and B is a constant, full column rank matrix), application of Sylvester's inequality [Che84, p. 31] shows that the rank of $L_g L_f h$ is strictly greater than $N-2$, *not* $N-1$.

[2]By standard results in [Isi95], the invertibility of the decoupling matrix is invariant under the application of invertible feedbacks.

To apply the technique of [RvdSMK99], first note that in the coordinates of RH6) B has the form

$$B = \begin{bmatrix} I \\ 0 \end{bmatrix}. \tag{C.1}$$

so that the q may be partitioned as

$$q_a = (q_q, \ldots, q_{N-1})' \quad \text{and} \quad q_u = q_N, \tag{C.2}$$

the "actuated" coordinates and "un-actuated" coordinate, respectively. Write (2.2) as

$$D_{11}(q)\ddot{q}_a + D_{12}(q)\ddot{q}_u + C_1(q,\dot{q})\dot{q} + G_1(q) = u \tag{C.3}$$

$$D_{21}(q)\ddot{q}_a + D_{22}(q)\ddot{q}_u + C_2(q,\dot{q})\dot{q} + G_2(q) = 0, \tag{C.4}$$

and solve[3] (C.4) for $\ddot{q}_u$ as

$$\ddot{q}_u = -D_{22}(q)^{-1}\left(D_{21}(q)\ddot{q}_a + C_2(q,\dot{q})\dot{q} + G_2(q)\right). \tag{C.5}$$

Substituting (C.5) into (C.3) yields

$$\hat{D}(q)\ddot{q}_a + \hat{C}(q,\dot{q})\dot{q} + \hat{G}(q) = u \tag{C.6}$$

where

$$\hat{D}(q) = D_{11}(q) - D_{12}(q)D_{22}^{-1}(q)D_{21}(q) \tag{C.7}$$

$$\hat{C}(q,\dot{q}) = C_1(q,\dot{q}) - D_{12}(q)D_{22}^{-1}(q)C_2(q,\dot{q}) \tag{C.8}$$

$$\hat{G}(q) = G_1(q) - D_{12}(q)D_{22}^{-1}(q)G_2(q). \tag{C.9}$$

Applying the partial linearizing feedback

$$u = \hat{D}(q)v + \hat{C}(q,\dot{q})\dot{q} + \hat{G}(q) \tag{C.10}$$

to (C.3) with (C.5) results in

$$\ddot{q}_a = v \tag{C.11}$$

The model (C.11) and (C.5) is feedback equivalent to the original system. It can be expressed in state space form with the same choice of x as before to obtain

$$\dot{x} = \hat{f}(x) + \hat{g}(x)v. \tag{C.12}$$

[3]The invertibility of D_{22} is assured by the positive definiteness of D.

Since the rank of the decoupling matrix is invariant under invertible feedback, the decoupling matrices for systems (2.4) and (C.12) have the same rank. The determinant of the decoupling matrix for (C.12) can be directly computed and shown to be of the form[4]

$$\det L_{\hat{g}} L_{\hat{f}} h(q) = \frac{\mathrm{Num}(q)}{\mathrm{Den}(q)} \tag{C.13}$$

with

$$\mathrm{Num}(q) = \sum_{i=1}^{n_{num}} k_{i,num}\, g_{i,num}\left(c_{i,num}\, q\right) \quad \text{and} \quad \mathrm{Den}(q) = \sum_{i=1}^{n_{den}} k_{i,den}\, g_{i,den}\left(c_{i,den}\, q\right) \tag{C.14}$$

where the $k_{i,*}$'s are constants, $g_{i,*}$'s are sine and cosine functions, and $c_{i,*}$'s are row vectors in $\mathbb{R}^N$. For a given subset $\mathcal{O} \subset \mathcal{Q}$ (recall that $\mathcal{Q}$ is the allowed set for the configuration variables), upper and lower bounds on the determinant of the decoupling matrix can be found via calculation of the minimum and maximum of each of the $n_{num} + n_{den}$ terms of the numerator and denominator over $\mathcal{O}$. For example, if the denominator in (C.13) is positive, then

$$\max_{q\in\mathcal{O}} \det L_{\hat{g}} L_{\hat{f}} h(q) \leq \frac{\max_{q\in\mathcal{O}} \mathrm{Num}(q)}{\min_{q\in\mathcal{O}} \mathrm{Den}(q)} \leq \frac{\max_{i\in I} \max_{q\in\mathcal{O}_i} \mathrm{Num}(q)}{\min_{i\in I} \min_{q\in\mathcal{O}_i} \mathrm{Den}(q)}, \tag{C.15}$$

where, $\mathcal{O} \subset \bigcup_{i\in I} \mathcal{O}_i$, and the $\mathcal{O}_i$ are closed and bounded. The max and min operations in (C.15) are especially trivial to evaluate if the sets $\mathcal{O}_i$ are selected to be of the form

$$\mathcal{O}_i := \left\{ x \;\middle|\; q_{1,i}^{min} \leq q_1 \leq q_{1,i}^{max},\ q_{2,i}^{min} \leq q_2 \leq q_{2,i}^{max},\ \cdots,\ q_{N,i}^{min} \leq q_N \leq q_{N,i}^{max} \right\}. \tag{C.16}$$

Determination of the individual closed sets $\mathcal{O}_i$ is accomplished by dividing the time trajectory into disjoint pieces and over bounding the configuration variables in each time interval to guarantee that the trajectory of the configuration variables lies strictly in the interior of $\mathcal{O}_i$. It should be noted that: 1) this process could be iterated to prove the decoupling matrix's invertibility over a larger subset of the robots's state space, and, 2) the fact that this method works is not an accident. Results from real analysis can be used to show that the decoupling matrix is invertible on an open set about the configuration variable trajectories if, and only if, a there exists a set $\mathcal{O}$ which is the interior of a union of a *finite* number of closed sets $\mathcal{O}_i$ as described above.

For an example of this technique applied see [PGWA01].

[4]It is straightforward to check that the decoupling matrix depends only upon the configuration variables, q, and not on the angular velocities.

APPENDIX D

Equations of motion for 5-DOF model of RABBIT

This appendix gives the details of the equations of motion for RABBIT during the swing phase. The intention is to impress upon the reader the complexity of the robot's dynamics. It is clear that little understanding of the model's dynamic behavior can be understood from direct inspection of its equations of motion in this form. Chapter 3 demonstrates that despite this apparent complexity, the structure of dynamics may be leveraged for controller design. Definition of the constants can be found in Section 6.1. Values of the constants used in the design of the controllers tested in the experiments can be found in Table 6.1.

The equations have the general matrix form

$$D(q)\ddot{q} + C(q,\dot{q})\dot{q} + G(q) = Bu \tag{D.1}$$

where $q := (q_1, q_2, q_3, q_4, q_5)$ and

$$\begin{aligned}
(D(q))_{1,1} &= I_t + I_f + 4M_f l_f l_t \cos(q_3) + 2M_f l_t^2 + 2M_t l_f l_t \cos(q_3) + 2M_T l_f l_t \cos(q_3) + \\
&\quad I_{a,\mathrm{H}} - 2p_f^M l_t \cos(q_3) + 2M_f l_f^2 - 2p_t^M l_t + M_t l_f^2 + M_T l_f^2 + M_T l_t^2 - 2p_f^M l_f + 2M_t l_t^2 \\
(D(q))_{1,2} &= -p_t^M l_f \cos(-q_2 - q_4 + q_1) - M_t l_t l_f \cos(q_1 + q_3 - q_2) - M_t l_f^2 \cos(q_1 - q_2) - \\
&\quad p_f^M l_f \cos(q_1 - q_2) - p_f^M l_t \cos(q_1 + q_3 - q_2) - p_t^M l_t \cos(-q_2 - q_4 + q_1 + q_3) \\
(D(q))_{1,3} &= -2p_t^M l_t + 2M_f l_t^2 + 2M_f l_f l_t \cos(q_3) + M_t l_f l_t \cos(q_3) + 2M_t l_t^2 + \\
&\quad M_T l_f l_t \cos(q_3) - p_f^M l_t \cos(q_3) + I_t + M_T l_t^2 \\
(D(q))_{1,4} &= -p_t^M l_t \cos(-q_2 - q_4 + q_1 + q_3) - p_t^M l_f \cos(-q_2 - q_4 + q_1)
\end{aligned}$$

$$
\begin{aligned}
(D(q))_{1,5} &= 2M_f l_t^2 - p_t^M l_f \cos(-q_2 - q_4 + q_1) - M_t l_t l_f \cos(q_1 + q_3 - q_2) - \\
&\quad M_t l_f^2 \cos(q_1 - q_2) - p_f^M l_f \cos(q_1 - q_2) - p_f^M l_t \cos(q_1 + q_3 - q_2) + \\
&\quad 2M_t l_f l_t \cos(q_3) + 2M_T l_f l_t \cos(q_3) + 2M_f l_f^2 - 2p_t^M l_t + M_t l_f^2 + M_T l_f^2 + \\
&\quad M_T l_t^2 + 4M_f l_f l_t \cos(q_3) - 2p_f^M l_f + 2M_t l_t^2 - p_T^M l_t \cos(q_1 + q_3) - \\
&\quad p_T^M l_f \cos(q_1) - 2p_f^M l_t \cos(q_3) - p_t^M l_t \cos(-q_2 - q_4 + q_1 + q_3) + I_f + I_t \\
(D(q))_{2,1} &= -p_t^M l_f \cos(-q_2 - q_4 + q_1) - M_t l_t l_f \cos(q_1 + q_3 - q_2) - M_t l_f^2 \cos(q_1 - q_2) - \\
&\quad p_f^M l_f \cos(q_1 - q_2) - p_f^M l_t \cos(q_1 + q_3 - q_2) - p_t^M l_t \cos(-q_2 - q_4 + q_1 + q_3) \\
(D(q))_{2,2} &= M_t l_f^2 + I_f + 2p_t^M l_f \cos(q_4) + I_{a,\mathrm{H}} + I_t \\
(D(q))_{2,3} &= -l_t(p_f^M \cos(q_1 + q_3 - q_2) + M_t l_f \cos(q_1 + q_3 - q_2) + \\
&\quad p_t^M \cos(-q_2 - q_4 + q_1 + q_3)) \\
(D(q))_{2,4} &= I_t + p_t^M l_f \cos(q_4) \\
(D(q))_{2,5} &= M_t l_f^2 - p_f^M l_f \cos(q_1 - q_2) - M_t l_f^2 \cos(q_1 - q_2) + 2p_t^M l_f \cos(q_4) - \\
&\quad p_t^M l_t \cos(-q_2 - q_4 + q_1 + q_3) - p_t^M l_f \cos(-q_2 - q_4 + q_1) + I_t + I_f - \\
&\quad p_f^M l_t \cos(q_1 + q_3 - q_2) - M_t l_t l_f \cos(q_1 + q_3 - q_2) \\
(D(q))_{3,1} &= -2p_t^M l_t + 2M_f l_t^2 + 2M_f l_f l_t \cos(q_3) + M_t l_f l_t \cos(q_3) + 2M_t l_t^2 + \\
&\quad M_T l_f l_t \cos(q_3) - p_f^M l_t \cos(q_3) + I_t + M_T l_t^2 \\
(D(q))_{3,2} &= -l_t(p_f^M \cos(q_1 + q_3 - q_2) + M_t l_f \cos(q_1 + q_3 - q_2) + \\
&\quad p_t^M \cos(-q_2 - q_4 + q_1 + q_3)) \\
(D(q))_{3,3} &= -2p_t^M l_t + 2M_f l_t^2 + I_{a,\mathrm{K}} + 2M_t l_t^2 + I_t + M_T l_t^2 \\
(D(q))_{3,4} &= -p_t^M l_t \cos(-q_2 - q_4 + q_1 + q_3) \\
(D(q))_{3,5} &= -2p_t^M l_t + 2M_f l_t^2 + 2M_t l_t^2 + M_T l_t^2 + M_T l_f l_t \cos(q_3) + M_t l_f l_t \cos(q_3) + \\
&\quad 2M_f l_f l_t \cos(q_3) - p_T^M l_t \cos(q_1 + q_3) - p_t^M l_t \cos(-q_2 - q_4 + q_1 + q_3) - \\
&\quad p_f^M l_t \cos(q_3) + I_t - p_f^M l_t \cos(q_1 + q_3 - q_2) - M_t l_t l_f \cos(q_1 + q_3 - q_2) \\
(D(q))_{4,1} &= -p_t^M l_t \cos(-q_2 - q_4 + q_1 + q_3) - p_t^M l_f \cos(-q_2 - q_4 + q_1) \\
(D(q))_{4,2} &= I_t + p_t^M l_f \cos(q_4) \\
(D(q))_{4,3} &= -p_t^M l_t \cos(-q_2 - q_4 + q_1 + q_3) \\
(D(q))_{4,4} &= I_t + I_{a,\mathrm{K}} \\
(D(q))_{4,5} &= p_t^M l_f \cos(q_4) - p_t^M l_t \cos(-q_2 - q_4 + q_1 + q_3) + I_t - p_t^M l_f \cos(-q_2 - q_4 + q_1)
\end{aligned}
$$

$$
\begin{aligned}
(D(q))_{5,1} &= 2M_f l_t^2 - p_t^M l_f \cos(-q_2 - q_4 + q_1) - M_t l_t l_f \cos(q_1 + q_3 - q_2) - \\
&\quad M_t l_f^2 \cos(q_1 - q_2) - p_f^M l_f \cos(q_1 - q_2) - p_f^M l_t \cos(q_1 + q_3 - q_2) + \\
&\quad 2M_t l_f l_t \cos(q_3) + 2M_T l_f l_t \cos(q_3) + 2M_f l_f^2 - 2p_t^M l_t + M_t l_f^2 + M_T l_f^2 + \\
&\quad M_T l_t^2 + 4M_f l_f l_t \cos(q_3) - 2p_f^M l_f + 2M_t l_t^2 - p_T^M l_t \cos(q_1 + q_3) - \\
&\quad p_T^M l_f \cos(q_1) - 2p_f^M l_t \cos(q_3) - p_t^M l_t \cos(-q_2 - q_4 + q_1 + q_3) + I_f + I_t \\
(D(q))_{5,2} &= M_t l_f^2 - p_f^M l_f \cos(q_1 - q_2) - M_t l_f^2 \cos(q_1 - q_2) + 2p_t^M l_f \cos(q_4) - \\
&\quad p_t^M l_t \cos(-q_2 - q_4 + q_1 + q_3) - p_t^M l_f \cos(-q_2 - q_4 + q_1) + I_t + I_f - \\
&\quad p_f^M l_t \cos(q_1 + q_3 - q_2) - M_t l_t l_f \cos(q_1 + q_3 - q_2) \\
(D(q))_{5,3} &= -2p_t^M l_t + 2M_f l_t^2 + 2M_t l_t^2 + M_T l_t^2 + M_T l_f l_t \cos(q_3) + M_t l_f l_t \cos(q_3) + \\
&\quad 2M_f l_f l_t \cos(q_3) - p_T^M l_t \cos(q_1 + q_3) - p_t^M l_t \cos(-q_2 - q_4 + q_1 + q_3) - \\
&\quad p_f^M l_t \cos(q_3) + I_t - p_f^M l_t \cos(q_1 + q_3 - q_2) - M_t l_t l_f \cos(q_1 + q_3 - q_2) \\
(D(q))_{5,4} &= p_t^M l_f \cos(q_4) - p_t^M l_t \cos(-q_2 - q_4 + q_1 + q_3) + I_t - p_t^M l_f \cos(-q_2 - q_4 + q_1) \\
(D(q))_{5,5} &= 2p_t^M l_f \cos(q_4) + 2M_f l_t^2 - 2p_t^M l_f \cos(-q_2 - q_4 + q_1) - \\
&\quad 2M_t l_t l_f \cos(q_1 + q_3 - q_2) - 2M_t l_f^2 \cos(q_1 - q_2) - 2p_f^M l_f \cos(q_1 - q_2) - \\
&\quad 2p_f^M l_t \cos(q_1 + q_3 - q_2) + 2M_t l_f l_t \cos(q_3) + 2M_T l_f l_t \cos(q_3) + 2M_f l_f^2 - \\
&\quad 2p_t^M l_t + 2M_t l_f^2 + M_T l_f^2 + M_T l_t^2 + 4M_f l_f l_t \cos(q_3) - 2p_f^M l_f + 2M_t l_t^2 - \\
&\quad 2p_T^M l_t \cos(q_1 + q_3) - 2p_T^M l_f \cos(q_1) - 2p_f^M l_t \cos(q_3) - \\
&\quad 2p_t^M l_t \cos(-q_2 - q_4 + q_1 + q_3) + I_T + 2I_f + 2I_t
\end{aligned}
$$

$$
\begin{aligned}
(C(q,\dot{q}))_{1,1} &= -l_t(2M_f l_f \sin(q_3) + M_t l_f \sin(q_3) + M_T l_f \sin(q_3) - p_f^M \sin(q_3))\dot{q}_3 \\
(C(q,\dot{q}))_{1,2} &= -\dot{q}_4 p_t^M l_f \sin(-q_2 - q_4 + q_1) - \dot{q}_2 M_t l_f^2 \sin(q_1 - q_2) - \\
&\quad \dot{q}_2 p_t^M l_f \sin(-q_2 - q_4 + q_1) - \dot{q}_2 p_f^M l_f \sin(q_1 - q_2) - \\
&\quad \dot{q}_5 p_t^M l_f \sin(-q_2 - q_4 + q_1) - \dot{q}_5 p_f^M l_f \sin(q_1 - q_2) - \dot{q}_5 M_t l_f^2 \sin(q_1 - q_2) - \\
&\quad \dot{q}_5 M_t l_t l_f \sin(q_1 + q_3 - q_2) - \dot{q}_5 p_t^M l_t \sin(-q_2 - q_4 + q_1 + q_3) - \\
&\quad \dot{q}_5 p_f^M l_t \sin(q_1 + q_3 - q_2) - \dot{q}_2 M_t l_t l_f \sin(q_1 + q_3 - q_2) - \\
&\quad \dot{q}_2 p_t^M l_t \sin(-q_2 - q_4 + q_1 + q_3) - \dot{q}_2 p_f^M l_t \sin(q_1 + q_3 - q_2) - \\
&\quad \dot{q}_4 p_t^M l_t \sin(-q_2 - q_4 + q_1 + q_3) \\
(C(q,\dot{q}))_{1,3} &= -l_t(\dot{q}_5 + \dot{q}_3 + \dot{q}_1)(2M_f l_f \sin(q_3) + M_t l_f \sin(q_3) + M_T l_f \sin(q_3) - p_f^M \sin(q_3)) \\
(C(q,\dot{q}))_{1,4} &= (-\dot{q}_2 - \dot{q}_4 - \dot{q}_5)(p_t^M l_t \sin(-q_2 - q_4 + q_1 + q_3) + p_t^M l_f \sin(-q_2 - q_4 + q_1))
\end{aligned}
$$

$$
\begin{aligned}
(C(q,\dot{q}))_{1,5} &= -2\dot{q}_3 M_f l_f l_t \sin(q_3) - \dot{q}_3 M_t l_f l_t \sin(q_3) - \dot{q}_3 M_T l_f l_t \sin(q_3) + \\
&\quad \dot{q}_3 p_f^M l_t \sin(q_3) - \dot{q}_2 p_f^M l_f \sin(q_1 - q_2) - \dot{q}_2 M_t l_f^2 \sin(q_1 - q_2) - \\
&\quad \dot{q}_2 p_t^M l_f \sin(-q_2 - q_4 + q_1) - \dot{q}_4 p_t^M l_f \sin(-q_2 - q_4 + q_1) - \\
&\quad \dot{q}_5 p_T^M l_f \sin(q_1) - \dot{q}_5 p_f^M l_f \sin(q_1 - q_2) - \dot{q}_5 p_t^M l_f \sin(-q_2 - q_4 + q_1) - \\
&\quad \dot{q}_5 M_t l_f^2 \sin(q_1 - q_2) - \dot{q}_5 M_t l_t l_f \sin(q_1 + q_3 - q_2) - \dot{q}_5 p_T^M l_t \sin(q_1 + q_3) - \\
&\quad \dot{q}_5 p_t^M l_t \sin(-q_2 - q_4 + q_1 + q_3) - \dot{q}_5 p_f^M l_t \sin(q_1 + q_3 - q_2) - \\
&\quad \dot{q}_4 p_t^M l_t \sin(-q_2 - q_4 + q_1 + q_3) - \dot{q}_2 M_t l_t l_f \sin(q_1 + q_3 - q_2) - \\
&\quad \dot{q}_2 p_t^M l_t \sin(-q_2 - q_4 + q_1 + q_3) - \dot{q}_2 p_f^M l_t \sin(q_1 + q_3 - q_2) \\
(C(q,\dot{q}))_{2,1} &= \dot{q}_1 p_f^M l_f \sin(q_1 - q_2) + \dot{q}_3 M_t l_t l_f \sin(q_1 + q_3 - q_2) + \\
&\quad \dot{q}_1 M_t l_t l_f \sin(q_1 + q_3 - q_2) + \dot{q}_3 p_t^M l_t \sin(-q_2 - q_4 + q_1 + q_3) + \\
&\quad \dot{q}_1 p_t^M l_f \sin(-q_2 - q_4 + q_1) + \dot{q}_1 M_t l_f^2 \sin(q_1 - q_2) + \\
&\quad \dot{q}_1 p_f^M l_t \sin(q_1 + q_3 - q_2) + \dot{q}_1 p_t^M l_t \sin(-q_2 - q_4 + q_1 + q_3) + \\
&\quad \dot{q}_3 p_f^M l_t \sin(q_1 + q_3 - q_2) + \dot{q}_5 p_f^M l_f \sin(q_1 - q_2) + \\
&\quad \dot{q}_5 p_t^M l_f \sin(-q_2 - q_4 + q_1) + \dot{q}_5 M_t l_f^2 \sin(q_1 - q_2) + \\
&\quad \dot{q}_5 M_t l_t l_f \sin(q_1 + q_3 - q_2) + \dot{q}_5 p_t^M l_t \sin(-q_2 - q_4 + q_1 + q_3) + \\
&\quad \dot{q}_5 p_f^M l_t \sin(q_1 + q_3 - q_2) \\
(C(q,\dot{q}))_{2,2} &= -l_f \dot{q}_4 p_t^M \sin(q_4) \\
(C(q,\dot{q}))_{2,3} &= l_t(\dot{q}_5 + \dot{q}_3 + \dot{q}_1)(p_f^M \sin(q_1 + q_3 - q_2) + M_t l_f \sin(q_1 + q_3 - q_2) + \\
&\quad p_t^M \sin(-q_2 - q_4 + q_1 + q_3)) \\
(C(q,\dot{q}))_{2,4} &= -l_f(\dot{q}_2 + \dot{q}_4 + \dot{q}_5) p_t^M \sin(q_4) \\
(C(q,\dot{q}))_{2,5} &= \dot{q}_1 p_f^M l_f \sin(q_1 - q_2) + \dot{q}_3 M_t l_t l_f \sin(q_1 + q_3 - q_2) + \\
&\quad \dot{q}_1 M_t l_t l_f \sin(q_1 + q_3 - q_2) - l_f \dot{q}_4 p_t^M \sin(q_4) + \\
&\quad \dot{q}_3 p_t^M l_t \sin(-q_2 - q_4 + q_1 + q_3) + \dot{q}_1 p_t^M l_f \sin(-q_2 - q_4 + q_1) + \\
&\quad \dot{q}_1 M_t l_f^2 \sin(q_1 - q_2) + \dot{q}_1 p_f^M l_t \sin(q_1 + q_3 - q_2) + \\
&\quad \dot{q}_1 p_t^M l_t \sin(-q_2 - q_4 + q_1 + q_3) + \dot{q}_3 p_f^M l_t \sin(q_1 + q_3 - q_2) + \\
&\quad \dot{q}_5 p_f^M l_f \sin(q_1 - q_2) + \dot{q}_5 p_t^M l_f \sin(-q_2 - q_4 + q_1) + \dot{q}_5 M_t l_f^2 \sin(q_1 - q_2) + \\
&\quad \dot{q}_5 M_t l_t l_f \sin(q_1 + q_3 - q_2) + \dot{q}_5 p_t^M l_t \sin(-q_2 - q_4 + q_1 + q_3) + \\
&\quad \dot{q}_5 p_f^M l_t \sin(q_1 + q_3 - q_2) \\
(C(q,\dot{q}))_{3,1} &= l_t(\dot{q}_1 + \dot{q}_5)(2M_f l_f \sin(q_3) + M_t l_f \sin(q_3) + M_T l_f \sin(q_3) - p_f^M \sin(q_3))
\end{aligned}
$$

$$
\begin{aligned}
(C(q,\dot{q}))_{3,2} &= -l_t(\sin(q_1+q_3-q_2)l_f M_t\dot{q}_2 + \sin(-q_2-q_4+q_1+q_3)p_t^M\dot{q}_2 + \\
&\quad \sin(q_1+q_3-q_2)p_f^M\dot{q}_2 + \sin(-q_2-q_4+q_1+q_3)p_t^M\dot{q}_4 + \\
&\quad \dot{q}_5 p_t^M \sin(-q_2-q_4+q_1+q_3) + \dot{q}_5 p_f^M \sin(q_1+q_3-q_2) + \\
&\quad \dot{q}_5 M_t l_f \sin(q_1+q_3-q_2)) \\
(C(q,\dot{q}))_{3,3} &= 0 \\
(C(q,\dot{q}))_{3,4} &= -l_t(\dot{q}_2+\dot{q}_4+\dot{q}_5)p_t^M \sin(-q_2-q_4+q_1+q_3) \\
(C(q,\dot{q}))_{3,5} &= -l_t(-2\sin(q_3)l_f M_f\dot{q}_1 - \sin(q_3)l_f M_t\dot{q}_1 - \sin(q_3)l_f M_T\dot{q}_1 + \sin(q_3)p_f^M\dot{q}_1 + \\
&\quad \sin(-q_2-q_4+q_1+q_3)p_t^M\dot{q}_2 + \sin(q_1+q_3-q_2)p_f^M\dot{q}_2 + \\
&\quad \sin(q_1+q_3-q_2)l_f M_t\dot{q}_2 + \sin(-q_2-q_4+q_1+q_3)p_t^M\dot{q}_4 + \dot{q}_5 p_f^M \sin(q_3) + \\
&\quad \dot{q}_5 p_T^M \sin(q_1+q_3) - 2\dot{q}_5 M_f l_f \sin(q_3) - \dot{q}_5 M_t l_f \sin(q_3) - \dot{q}_5 M_T l_f \sin(q_3) + \\
&\quad \dot{q}_5 p_t^M \sin(-q_2-q_4+q_1+q_3) + \dot{q}_5 M_t l_f \sin(q_1+q_3-q_2) + \\
&\quad \dot{q}_5 p_f^M \sin(q_1+q_3-q_2)) \\
(C(q,\dot{q}))_{4,1} &= \dot{q}_1 p_t^M l_t \sin(-q_2-q_4+q_1+q_3) + \dot{q}_1 p_t^M l_f \sin(-q_2-q_4+q_1) + \\
&\quad \dot{q}_3 p_t^M l_t \sin(-q_2-q_4+q_1+q_3) + \dot{q}_5 p_t^M l_t \sin(-q_2-q_4+q_1+q_3) + \\
&\quad \dot{q}_5 p_t^M l_f \sin(-q_2-q_4+q_1) \\
(C(q,\dot{q}))_{4,2} &= l_f(\dot{q}_2+\dot{q}_5)p_t^M \sin(q_4) \\
(C(q,\dot{q}))_{4,3} &= l_t(\dot{q}_5+\dot{q}_3+\dot{q}_1)p_t^M \sin(-q_2-q_4+q_1+q_3) \\
(C(q,\dot{q}))_{4,4} &= 0 \\
(C(q,\dot{q}))_{4,5} &= \dot{q}_1 p_t^M l_t \sin(-q_2-q_4+q_1+q_3) + \dot{q}_1 p_t^M l_f \sin(-q_2-q_4+q_1) + \\
&\quad \dot{q}_2 p_t^M l_f \sin(q_4) + \dot{q}_3 p_t^M l_t \sin(-q_2-q_4+q_1+q_3) + \dot{q}_5 p_t^M l_f \sin(q_4) + \\
&\quad \dot{q}_5 p_t^M l_t \sin(-q_2-q_4+q_1+q_3) + \dot{q}_5 p_t^M l_f \sin(-q_2-q_4+q_1)
\end{aligned}
$$

$$
\begin{aligned}
(C(q,\dot{q}))_{5,1} &= \dot{q}_1 p_f^M l_f \sin(q_1 - q_2) + \dot{q}_3 M_t l_t l_f \sin(q_1 + q_3 - q_2) + \\
&\quad \dot{q}_1 M_t l_t l_f \sin(q_1 + q_3 - q_2) - 2\dot{q}_3 M_f l_f l_t \sin(q_3) - \dot{q}_3 M_t l_f l_t \sin(q_3) + \\
&\quad \dot{q}_1 p_T^M l_t \sin(q_1 + q_3) - \dot{q}_3 M_T l_f l_t \sin(q_3) + \dot{q}_3 p_f^M l_t \sin(q_3) + \\
&\quad \dot{q}_3 p_T^M l_t \sin(q_1 + q_3) + \dot{q}_5 p_T^M l_f \sin(q_1) + \dot{q}_1 p_T^M l_f \sin(q_1) + \\
&\quad \dot{q}_3 p_t^M l_t \sin(-q_2 - q_4 + q_1 + q_3) + \dot{q}_1 p_t^M l_f \sin(-q_2 - q_4 + q_1) + \\
&\quad \dot{q}_1 M_t l_f^2 \sin(q_1 - q_2) + \dot{q}_1 p_f^M l_t \sin(q_1 + q_3 - q_2) + \\
&\quad \dot{q}_1 p_t^M l_t \sin(-q_2 - q_4 + q_1 + q_3) + \dot{q}_3 p_f^M l_t \sin(q_1 + q_3 - q_2) + \\
&\quad \dot{q}_5 p_f^M l_f \sin(q_1 - q_2) + \dot{q}_5 p_t^M l_f \sin(-q_2 - q_4 + q_1) + \dot{q}_5 M_t l_f^2 \sin(q_1 - q_2) + \\
&\quad \dot{q}_5 M_t l_t l_f \sin(q_1 + q_3 - q_2) + \dot{q}_5 p_T^M l_t \sin(q_1 + q_3) + \\
&\quad \dot{q}_5 p_t^M l_t \sin(-q_2 - q_4 + q_1 + q_3) + \dot{q}_5 p_f^M l_t \sin(q_1 + q_3 - q_2) \\
(C(q,\dot{q}))_{5,2} &= -l_f \dot{q}_4 p_t^M \sin(q_4) - \dot{q}_2 p_f^M l_f \sin(q_1 - q_2) - \dot{q}_2 M_t l_f^2 \sin(q_1 - q_2) - \\
&\quad \dot{q}_2 p_t^M l_f \sin(-q_2 - q_4 + q_1) - l_f \dot{q}_4 p_t^M \sin(-q_2 - q_4 + q_1) - \\
&\quad \dot{q}_5 p_f^M l_f \sin(q_1 - q_2) - \dot{q}_5 p_t^M l_f \sin(-q_2 - q_4 + q_1) - \dot{q}_5 M_t l_f^2 \sin(q_1 - q_2) - \\
&\quad \dot{q}_5 M_t l_t l_f \sin(q_1 + q_3 - q_2) - \dot{q}_5 p_t^M l_t \sin(-q_2 - q_4 + q_1 + q_3) - \\
&\quad \dot{q}_5 p_f^M l_t \sin(q_1 + q_3 - q_2) - \dot{q}_4 p_t^M l_t \sin(-q_2 - q_4 + q_1 + q_3) - \\
&\quad \dot{q}_2 M_t l_t l_f \sin(q_1 + q_3 - q_2) - \dot{q}_2 p_t^M l_t \sin(-q_2 - q_4 + q_1 + q_3) - \\
&\quad \dot{q}_2 p_f^M l_t \sin(q_1 + q_3 - q_2) \\
(C(q,\dot{q}))_{5,3} &= l_t(\dot{q}_5 + \dot{q}_3 + \dot{q}_1)(M_t l_f \sin(q_1 + q_3 - q_2) - 2M_f l_f \sin(q_3) + \\
&\quad p_f^M \sin(q_1 + q_3 - q_2) - M_T l_f \sin(q_3) + \sin(q_1 + q_3) p_T^M + p_f^M \sin(q_3) + \\
&\quad p_t^M \sin(-q_2 - q_4 + q_1 + q_3) - M_t l_f \sin(q_3)) \\
(C(q,\dot{q}))_{5,4} &= (-\dot{q}_2 - \dot{q}_4 - \dot{q}_5)(p_t^M l_f \sin(q_4) + p_t^M l_t \sin(-q_2 - q_4 + q_1 + q_3) + \\
&\quad p_t^M l_f \sin(-q_2 - q_4 + q_1))
\end{aligned}
$$

$$
\begin{aligned}
(C(q,\dot{q}))_{5,5} &= \dot{q}_3 p_t^M l_t \sin(-q_2-q_4+q_1+q_3) + \dot{q}_1 p_f^M l_f \sin(q_1-q_2) + \\
&\quad \dot{q}_1 p_t^M l_f \sin(-q_2-q_4+q_1) + \dot{q}_1 M_t l_f^2 \sin(q_1-q_2) + \\
&\quad \dot{q}_1 p_f^M l_t \sin(q_1+q_3-q_2) - l_f \dot{q}_4 p_t^M \sin(q_4) + \\
&\quad \dot{q}_1 p_t^M l_t \sin(-q_2-q_4+q_1+q_3) - \dot{q}_2 p_t^M l_f \sin(-q_2-q_4+q_1) - \\
&\quad \dot{q}_2 M_t l_f^2 \sin(q_1-q_2) - \dot{q}_2 p_f^M l_f \sin(q_1-q_2) - l_f \dot{q}_4 p_t^M \sin(-q_2-q_4+q_1) - \\
&\quad \dot{q}_4 p_t^M l_t \sin(-q_2-q_4+q_1+q_3) - \dot{q}_2 M_t l_t l_f \sin(q_1+q_3-q_2) - \\
&\quad \dot{q}_2 p_f^M l_t \sin(q_1+q_3-q_2) - \dot{q}_2 p_t^M l_t \sin(-q_2-q_4+q_1+q_3) + \\
&\quad \dot{q}_3 p_f^M l_t \sin(q_1+q_3-q_2) + \dot{q}_1 p_T^M l_f \sin(q_1) + \dot{q}_3 M_t l_t l_f \sin(q_1+q_3-q_2) + \\
&\quad \dot{q}_1 M_t l_t l_f \sin(q_1+q_3-q_2) - \dot{q}_3 M_T l_f l_t \sin(q_3) - \dot{q}_3 M_t l_f l_t \sin(q_3) + \\
&\quad \dot{q}_1 p_T^M l_t \sin(q_1+q_3) + \dot{q}_3 p_T^M l_t \sin(q_1+q_3) + \dot{q}_3 p_f^M l_t \sin(q_3) - \\
&\quad 2\dot{q}_3 M_f l_f l_t \sin(q_3)
\end{aligned}
$$

$$
\begin{aligned}
(G(q))_{1,1} &= g_0(l_f \sin(q_1+q_5) M_T + l_t \sin(q_1+q_3+q_5) M_T + 2 l_f \sin(q_1+q_5) M_f + \\
&\quad 2 l_t \sin(q_1+q_3+q_5) M_f - \sin(q_1+q_5) p_f^M + 2 l_t \sin(q_1+q_3+q_5) M_t - \\
&\quad \sin(q_1+q_3+q_5) p_t^M + l_f \sin(q_1+q_5) M_t) \\
(G(q))_{2,1} &= g_0(-\sin(q_2+q_5) p_f^M - l_f \sin(q_2+q_5) M_t - \sin(q_2+q_4+q_5) p_t^M) \\
(G(q))_{3,1} &= g_0(l_t \sin(q_1+q_3+q_5) M_T + 2 l_t \sin(q_1+q_3+q_5) M_f + \\
&\quad 2 l_t \sin(q_1+q_3+q_5) M_t - \sin(q_1+q_3+q_5) p_t^M) \\
(G(q))_{4,1} &= -g_0 \sin(q_2+q_4+q_5) p_t^M \\
(G(q))_{5,1} &= g_0(l_f \sin(q_1+q_5) M_T + l_t \sin(q_1+q_3+q_5) M_T - \sin(q_5) p_T^M + \\
&\quad 2 l_f \sin(q_1+q_5) M_f + 2 l_t \sin(q_1+q_3+q_5) M_f - \sin(q_1+q_5) p_f^M - \\
&\quad \sin(q_2+q_5) p_f^M + 2 l_t \sin(q_1+q_3+q_5) M_t - \sin(q_1+q_3+q_5) p_t^M + \\
&\quad l_f \sin(q_1+q_5) M_t - l_f \sin(q_2+q_5) M_t - \sin(q_2+q_4+q_5) p_t^M)
\end{aligned}
$$

$$
B = \begin{bmatrix} I \\ 0 \end{bmatrix}.
$$

The linear transformation matrix required by (2.20) is

$$R = \begin{bmatrix} 0 & 1 & 0 & 0 & 0 \\ 1 & 0 & 0 & 0 & 0 \\ 0 & 0 & 0 & 1 & 0 \\ 0 & 0 & 1 & 0 & 0 \\ 0 & 0 & 0 & 0 & 1 \end{bmatrix}.$$

APPENDIX E

Rigid body model derivation via the method of Lagrange

This appendix derives the equations of motion for N-link, rigid body open-chain robots with N one-DOF revolute joints moving in three-dimensions using the method of Lagrange. The planar biped models of this dissertation are a subclass of the class of models treated in this appendix. With one exception these calculations parallel and, at points, duplicate the calculations performed in [MLS93, pp. 161–171] and [SV89, pp. 136–141]. The exception is that each center of mass (COM) of the individual links is not assumed to be coincident with the origin of its body coordinate frame (i.e., $\bar{r} \neq 0$ in Figure E.1). This is interesting because while the origin of the link body coordinate frames may be designed to be collocated with the their respective centers of mass, upon robot construction and parameter identification collocation is unlikely to hold.

E.1 The Lagrangian

The Lagrangian for an N-link, rigid body open-chain robot with N one-DOF revolute joints is a functional acting on points in the state space, $x = (q, \dot{q}) \in \mathcal{X} = T\mathcal{Q}$, where $\mathcal{Q}$ is a is a simply connected, open subset of $[0, 2\pi)^{N+3} \times \mathbb{R}^3$. The generalized coordinates $q \in \mathcal{Q}$ give the robot's shape, orientation, and position in three-dimensional space. The Lagrangian is defined to be the difference between the kinetic and potential energies

$$L(q, \dot{q}) := K(q, \dot{q}) - V(q). \tag{E.1}$$

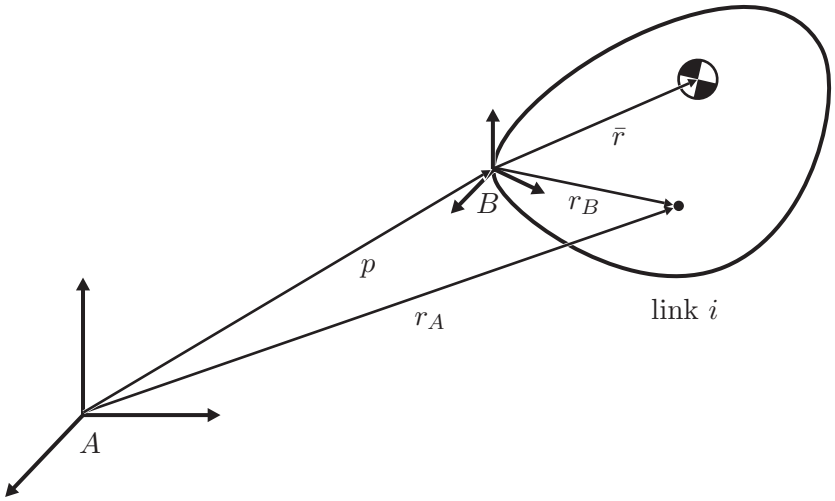

Figure E.1: A single link of an open-chain robot used to explain the method of Lagrange. A is an inertial coordinate frame and B is a body coordinate frame, i.e., it is affixed to the link. The vector $\bar{r}$ is from the origin of B to the center of mass of the link. The vector r_A (resp. r_B) is from the origin of A (resp. B) to an arbitrary point in the link. The vector p is from the origin of A to the origin of B.

From Hamilton's principle, the equations of motion can be calculated directly from the Lagrangian as

$$\frac{d}{dt}\frac{\partial L}{\partial \dot{q}_i} - \frac{\partial L}{\partial q_i} = f_i \tag{E.2}$$

where f_i are joint torques and other nonconservative forces affecting the i^{th} generalized coordinate [GPS02, pp. 34–45].

The calculation of the equations of motion using the method of Lagrange will proceed by calculation the robot kinetic energy, calculation of the robot potential energy, and calculation of the particular form the equations of motion used in this dissertation.

E.2 The kinetic energy

The first ingredient required to calculate the Lagrangian is the total kinetic energy of the robot. The kinetic energy of a single link will be calculated first and then the kinetic energy of the entire robot will be calculated.

The kinetic energy of an individual link (rigid body) is given by

$$K = \frac{1}{2}\int_V \rho(r_B)||\dot{r}_A||^2 dV \tag{E.3}$$

where $V \subset \mathbb{R}^3$ is the region of three-dimensional space occupied by the link, $\rho(r_B)$, $r_B \in V$ is the density of the link at point r_B, and $||\cdot||$ is the two-norm. The total mass of the link is

$$m = \int_V \rho(r) dV \tag{E.4}$$

and the center of mass is then

$$\bar{r} = \frac{1}{m}\int_V \rho(r) r dV. \tag{E.5}$$

Note that $\bar{r}$ in (E.5) is in whatever coordinate frame the integral is performed. To prevent clutter, the subscripts indicating the link will will be dropped until the end of the section.

Using the coordinate frames A and B as given in Figure E.1, let $R_{AB} \in SO(3)$, i.e., R_{AB} is a rotation matrix, which takes vectors expressed in the coordinates of the body frame B into vectors expressed in the coordinates of the inertial frame A. Hence, r_A and $\dot{r}_A$ may be expressed

$$r_A = p + R_{AB} r_B \tag{E.6}$$

$$\dot{r}_A = \dot{p} + \dot{R}_{AB} r_B. \tag{E.7}$$

Let $\omega_B \in \mathbb{R}^3$ be the angular velocity vector of the link expressed in the body coordinate frame and note that $\dot{R}_{AB}$ may be expressed in terms of ω_B:

$$\dot{R}_{AB} = R_{AB} R_{AB}^{-1} \dot{R}_{AB} \tag{E.8}$$

$$\dot{R}_{AB} = R_{AB} \widehat{\omega}_B \tag{E.9}$$

where

$$\widehat{\omega}_B := R_{AB}^{-1} \dot{R}_{AB} \tag{E.10}$$

and $\widehat{\omega} \in so(3)$, i.e., $\widehat{\omega}$ is an element of the Lie algebra of $SO(3)$, is a skew-symmetric matrix and may be expressed as

$$\widehat{\omega} = \begin{bmatrix} 0 & -\omega_3 & \omega_2 \\ \omega_3 & 0 & -\omega_1 \\ -\omega_2 & \omega_1 & 0 \end{bmatrix}. \tag{E.11}$$

Hence, the total kinetic energy (E.3) may be expanded as

$$K = \frac{1}{2}\int_V \rho(r_B)||\dot{p} + \dot{R}_{AB} r_B||^2 dV \tag{E.12}$$

$$= \frac{1}{2}\int_V \rho(r_B)\left(||\dot{p}||^2 + ||\dot{R}_{AB} r_B||^2 + 2\dot{p}'\dot{R}_{AB} r_B\right) dV \tag{E.13}$$

$$= \frac{1}{2}\int_V \rho(r_B)\left(||\dot{p}||^2 + ||R_{AB}\widehat{\omega}_B r_B||^2 + 2\dot{p}' R_{AB}\widehat{\omega}_B r_B\right) dV. \tag{E.14}$$

The first term of (E.14) is due to translation of the link with respect to A

$$K_{\text{translation}} = \frac{1}{2}\int_V \rho(r_B)||\dot{p}||^2 dV \tag{E.15}$$

$$= \frac{1}{2}\, m||\dot{p}||^2. \tag{E.16}$$

The second term of (E.14) is due to rotation of the link about the origin of B

$$K_{\text{rotation}} = \frac{1}{2}\int_V \rho(r_B)(R_{AB}\widehat{\omega}_B r_B)'(R_{AB}\widehat{\omega}_B r_B) dV \tag{E.17}$$

$$= \frac{1}{2}\int_V \rho(r_B) r_B'\widehat{\omega}_B'\dot{R}_{AB}'\dot{R}_{AB}\widehat{\omega}_B r_B dV \tag{E.18}$$

$$= \frac{1}{2}\int_V \rho(r_B) r_B'\widehat{\omega}_B'\widehat{\omega}_B r_B dV \tag{E.19}$$

$$= \frac{1}{2}\int_V \rho(r_B)(-\omega_B'\widehat{r}_B')(-\widehat{r}_B\omega_B) dV \tag{E.20}$$

$$= \frac{1}{2}\,\omega_B'\left(\int_V \rho(r_B)\widehat{r}_B'\widehat{r}_B dV\right)\omega_B \tag{E.21}$$

$$= \frac{1}{2}\,\omega_B' I_{\text{rotation}}\omega_B \tag{E.22}$$

where I_{rotation} is the inertia tensor of link expressed in the body frame. The third term of (E.14)—and the one of interest here since it is normally zero—is due to non-collocation of the origin of B and the COM of the link

$$K_{\text{non-collocation}} = \int_V \rho(r_B)\dot{p}' R_{AB}\widehat{\omega}_B r_B dV \tag{E.23}$$

$$= m\dot{p}' R_{AB}\widehat{\omega}_B\,\bar{r}_B. \tag{E.24}$$

Hence, the total kinetic energy for the link may be expressed as

$$K = \frac{1}{2}\, m||\dot{p}||^2 + \frac{1}{2}\omega_B' I_{\text{rotation}}\omega_B + m\dot{p}' R_{AB}\widehat{\omega}_B\,\bar{r}_B \tag{E.25}$$

The dependence of $\dot{p}$, ω_B, R_{AB} and I_{rotation} upon q and $\dot{q}$ has been suppressed up until this point. Each of these terms will be expressed in such a way that (E.25) may be written in quadratic form. It will be assumed that q and $\dot{q}$ are with respect to the inertial frame A.

The translational velocity of the origin of B with respect to A is

$$\begin{aligned} \dot{p}(q,\dot{q}) &= \frac{\partial p}{\partial q}\,\dot{q} && \text{(E.26)} \\ &=: J_p(q)\dot{q}. && \text{(E.27)} \end{aligned}$$

Expanding (E.10) yields

$$\widehat{\omega}_B(q,\dot{q}) = \sum_{i=1}^{N+6} R_{AB}^{-1}(q)\frac{\partial R_{AB}(q)}{\partial q_i}\,\dot{q}_i \tag{E.28}$$

which may be rewritten as

$$\omega_B = J_{AB}(q)\dot{q} \tag{E.29}$$

where

$$J_{AB}(q) := \left[\left(R_{AB}^{-1}(q)\frac{\partial R_{AB}(q)}{\partial q_1}\right)^{\vee} \ldots \left(R_{AB}^{-1}(q)\frac{\partial R_{AB}(q)}{\partial q_{N+6}}\right)^{\vee}\right] \tag{E.30}$$

and $(\widehat{\omega})^{\vee}$ extracts the three parameters of the skew-symmetric matrix $\widehat{\omega}$ (i.e., $(\widehat{\omega})^{\vee} = \omega$). Now, the kinetic energy of an individual link (E.25) may be expressed as

$$\begin{aligned} K(q,\dot{q}) &= \frac{1}{2}\,m\dot{q}' J_p'(q)J_p(q)\dot{q} + \frac{1}{2}\dot{q}' J_{AB}'(q)I_{\text{rotation}}(q)J_{AB}(q)\dot{q} \\ &\quad -m\dot{q}' J_p'(q)R_{AB}(q)\widehat{\bar{r}}_B J_{AB}(q)\dot{q} && \text{(E.31)} \\ &= \frac{1}{2}\dot{q}' D(q)\dot{q} && \text{(E.32)} \end{aligned}$$

where

$$\begin{aligned} D(q) &= mJ_p(q)'J_p(q) + J_{AB}'(q)I_{\text{rotation}}(q)J_{AB}(q) \\ &\quad -2mJ_p'(q)R_{AB}(q)\widehat{\bar{r}}_B J_{AB}(q). \end{aligned} \tag{E.33}$$

The total kinetic energy of the robot is the sum of the individual link inertia

$$K(q,\dot{q}) = \sum_{i=1}^{N+6} K_i(q,\dot{q}) \tag{E.34}$$

where K_i is the kinetic energy of link i.

E.3 The potential energy

The second ingredient required to calculate the Lagrangian is the total potential energy of the robot. Calculation of the potential energy is considerably less complicated than calculation of the kinetic energy.

Let $p_i^{\mathrm{y}}(q)$ be the height of the center of mass of link i. The potential energy for link i is simply

$$V_i(q) = g_0 m_i p_i^{\mathrm{y}}(q) \tag{E.35}$$

where g_0 is the acceleration due to gravity. The total potential energy of the robot is then

$$V(q) = \sum_{i=1}^{N+6} V_i(q). \tag{E.36}$$

E.4 Equations of motion

The equations of motion may now be directly calculated using (E.2). The two primary structural properties of the Lagrangian that will be exploited are the form of (E.32) and the independence of the potential energy of $\dot{q}$. First, expand (E.2) as

$$\frac{d}{dt}\frac{\partial K(q,\dot{q})}{\partial \dot{q}_i} - \frac{\partial K(q,\dot{q})}{\partial q_i} + \frac{\partial V(q)}{\partial q_i} = f_i \tag{E.37}$$

where f_i are nonconservative forces affecting the i^{th} generalized coordinate. Expanding the first term of (E.37) yields

$$\frac{d}{dt}\frac{\partial K(q,\dot{q})}{\partial \dot{q}_i} = \frac{d}{dt}\left(\sum_{j=1}^{N+6} D_{ij}(q)\dot{q}_j\right) \tag{E.38}$$

$$= \sum_{j=1}^{N+6} D_{ij}(q)\ddot{q}_j + \sum_{j,k=1}^{N+6} \frac{\partial D_{ij}(q)}{\partial q_k}\dot{q}_j\dot{q}_k. \tag{E.39}$$

Expanding the second term of (E.37) yields

$$\frac{\partial K(q,\dot{q})}{\partial q_i} = \frac{1}{2}\sum_{j,k=1}^{N+6} \frac{\partial D_{kj}(q)}{\partial q_i}\dot{q}_j\dot{q}_k. \tag{E.40}$$

Hence, (E.37) may be written as

$$\sum_{j=1}^{N+6} D_{ij}(q)\ddot{q}_j + \sum_{j,k=1}^{N+6}\left(\frac{\partial D_{ij}(q)}{\partial q_k}\dot{q}_j\dot{q}_k - \frac{1}{2}\frac{\partial D_{kj}(q)}{\partial q_i}\dot{q}_j\dot{q}_k\right) + \frac{\partial V(q)}{\partial q_i} = f_i. \tag{E.41}$$

To write (E.41) vector form define the Christoffel symbol to be

$$\Gamma_{ijk} := \frac{1}{2}\left(\frac{\partial D_{ij}(q)}{\partial q_k} + \frac{\partial D_{ik}(q)}{\partial q_j} - \frac{\partial D_{kj}(q)}{\partial q_i}\right) \tag{E.42}$$

so that the matrix Coriolis matrix $C(q,\dot{q}) \in \mathbb{R}^{(N+6)\times(N+6)}$ may be defined as

$$C_{ij}(q,\dot{q}) := \sum_{k=1}^{N+6} \Gamma_{ijk}(q)\dot{q}_k. \tag{E.43}$$

The effect of the potential energy is represented by $G \in \mathbb{R}^{N+6}$ defined as

$$G_i(q) := \frac{\partial V(q)}{\partial q_i}. \tag{E.44}$$

The torques and other nonconservative forces affecting the i^{th} generalized coordinate can often be decomposed as

$$f_i(q, \dot{q}, u) = F_i(q, \dot{q}) + E_i(q)F_{\text{ext}} + B_i(q)\tau. \tag{E.45}$$

where F is a vector of frictional forces and $E_i(q)$ and B_i are the i^{th} rows of the matrices E and B which are defined as follows. Decompose $u \in \mathbb{R}^P$ into the torques and nonconservative forces, $u = (F_{\text{ext}}, \tau)$, where $F_{\text{ext}} \in \mathbb{R}^{(P-P_\tau)}$ and $\tau \in \mathbb{R}^{P_\tau}$. Let the nonconservative forces act at $p_j(q)$, $j = 1, \ldots, (P - P_\tau)$ so that

$$E(q) = \left(\frac{\partial p(q)}{\partial q} \right)'. \tag{E.46}$$

Similarly, let $\tilde{q}_j(q)$, $j = 1, \ldots, P_\tau$, be the points of application of torques so that

$$B(q) = \left(\frac{\partial \tilde{q}(q)}{\partial q} \right)'. \tag{E.47}$$

Finally, assuming the decomposition of f_i given in (E.45), the equations of motion may be written in vector form as

$$D(q)\ddot{q} + C(q, \dot{q})\dot{q} + G(q) - F(q, \dot{q}) = E(q)F_{\text{ext}} + B(q)\tau \tag{E.48}$$

APPENDIX F

Auto-generation of MATLAB m-files

By means of a simple example, this appendix gives a convenient scheme for the automatic generation of m-files from symbolic MATLAB code which expedites m-file generation and helps to minimize the introduction of typographical errors. The primary tool exploited is the MATLAB function `char` which converts matrix or scalar symbolic expressions to strings. In this dissertation, all simulation routines containing the result of symbolic computations use this scheme.

In this example, a MATLAB function, `generate_myfcn_maclaurin5`, is used to generate a second MATLAB function, `myfcn_maclaurin5.m`, that computes the fifth order Maclaurin expansion of $\ln(1+x)$. The function `generate_myfcn_maclaurin5` is

```
function generate_myfcn_maclaurin5
syms x
f = taylor(log(1+x),5);
fid = fopen('myfcn_maclaurin5.m','w');
fprintf(fid,'function f = myfcn_maclaurin5(x)\n');
fprintf(fid,'%% MYFCN_MACLAURIN5\n\n');
fprintf(fid,'%%Eric Westervelt\n');
fprintf(fid,'%%%s\n\n',datestr(now));
fprintf(fid,['f = ',char(f),';\n']);
fclose(fid);
```

Running this function at the MATLAB command line generates `myfcn_maclaurin5.m`,

```
>> generate_myfcn_maclaurin5
>> type myfcn_maclaurin5
function f = myfcn_maclaurin5(x)
% MYFCN_MACLAURIN5

%Eric Westervelt
%23-Jun-2003 18:22:35

f = x-1/2*x^2+1/3*x^3-1/4*x^4;
>> myfcn_maclaurin5(0.2)-log(1+0.2)
ans =
 -5.4890e-005
```

Though not used to great advantage, this example illustrates the general idea of auto-generation of MATLAB `m`-files: perform symbolic computations and then create (an) `m`-file(s) from the symbolic computation result using the `char` function. This scheme becomes more useful as the size of the symbolic expression to be written in the `m`-file increases.

APPENDIX G

Adding motor and gear reducer dynamics

This appendix treats the additional dynamic effects of the motors used to actuate the links of the general N-link robot of Appendix E. Two motor characteristics of interest will be incorporated into the equations of motion: the motor inertias and the gear ratios. It will be shown that for sufficiently large gear ratios, the motor inertias and the unactuated dynamics become the dominate terms of (E.48).

The presentation begins with an assumption that is not technically needed, but will simplify the subsequent development.

Assumption G.1. *For each actuated joint i, located on link i, assume that q_i corresponds to the relative angle between the links that comprise the joint (see Figure G.1). For each unactuated joint, q_i may be a relative or absolute angle.*

Define the motor shaft angle of joint i

$$\bar{q}_i := n_{\mathrm{g},i}\, q_i \tag{G.1}$$

where $n_{\mathrm{g},i}$ is the gear ratio for joint i and is typically much larger than 1 (for joints without gear reducers or for unactuated joints set $n_{\mathrm{g},i}$ to be 1). Then,

$$\bar{q} = N_{\mathrm{g}}\, q, \tag{G.2}$$

where $N_{\mathrm{g}} = \mathrm{diag}(n_{\mathrm{g},1}, \ldots, n_{\mathrm{g},N})$. Let $I_{\mathrm{a},i}$ be the inertia of the motor used to actuate joint q_i (for unactuated joints set $I_{\mathrm{a},i} = 0$). The additional kinetic energy for link i due to the

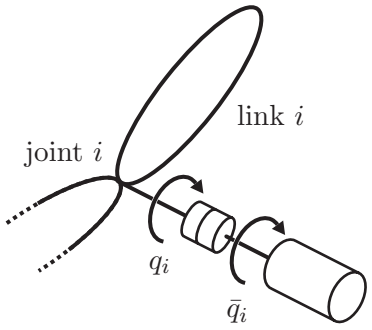

Figure G.1: Joint i on link i of an open-chain robot actuated by a motor through a gear reducer. The angle between link i and the previous link is q_i. The angle of the motor shaft is $\bar{q}_i = n_{\mathrm{g},i}\, q_i$ where $n_{\mathrm{g},i}$ is the gear ratio for joint i.

rotor is added to (E.31) and may be expressed as

$$K_{i,\mathrm{rotor}}(\bar{q}) = \frac{1}{2} I_{\mathrm{a},i} \dot{\bar{q}}_i^2. \tag{G.3}$$

For the entire robot, the additional kinetic energy may be expressed

$$K_{\mathrm{rotor}}(\bar{q}) = \frac{1}{2} \dot{\bar{q}}' I_{\mathrm{a}} \dot{\bar{q}}. \tag{G.4}$$

where $I_{\mathrm{a}} := (I_{\mathrm{a},1}, \ldots, I_{\mathrm{a},N})'$. In q coordinates

$$K_{\mathrm{rotor}}(q) = \frac{1}{2} \dot{q}' N_{\mathrm{g}}' I_{\mathrm{a}} N_{\mathrm{g}} \dot{q}. \tag{G.5}$$

When K_{rotor} is added to (E.34), the constant, diagonal term $N_{\mathrm{g}}' I_{\mathrm{a}} N_{\mathrm{g}}$ appears in the equations of motion (E.48) as being added to $D(q)$.

Proposition G.1. *Assume an N-link, rigid body open-chain robot model satisfying Assumption G.1 with motors and gear reducers with gear ratios $N_{\mathrm{g}} = \mathrm{diag}(n_{\mathrm{g},1}, \ldots, n_{\mathrm{g},N})$ and rotor inertias $I_{\mathrm{a}} := (I_{\mathrm{a},1}, \ldots, I_{\mathrm{a},N})'$. Then, in coordinates $\bar{q}$ given in (G.2), the model equations of motion are*

$$\bar{D}(\bar{q})\ddot{\bar{q}} + \bar{C}(\bar{q}, \dot{\bar{q}})\dot{\bar{q}} + \bar{G}(\bar{q}) - \bar{F}(\bar{q}, \dot{\bar{q}}) = \bar{E}(\bar{q}) F_{\mathrm{ext}} + \bar{B}\bar{u} \tag{G.6}$$

where $\bar{u} = N_{\mathrm{g}}^{-1} u$ are the motor torques, and

$$\bar{D}(\bar{q}) := N_{\mathrm{g}}^{-1} D(\bar{q}) N_{\mathrm{g}}^{-1} + I_{\mathrm{a}} \tag{G.7}$$

$$\bar{C}(\bar{q}, \dot{\bar{q}}) := N_{\mathrm{g}}^{-1} C(\bar{q}, \dot{\bar{q}}) N_{\mathrm{g}}^{-1} \tag{G.8}$$

$$\bar{G}(\bar{q}) := N_{\mathrm{g}}^{-1} G(\bar{q}) \tag{G.9}$$

$$\bar{F}(\bar{q}, \dot{\bar{q}}) := N_{\mathrm{g}}^{-1} F(\bar{q}, \dot{\bar{q}}) \tag{G.10}$$

$$\bar{E}(\bar{q}) := N_{\mathrm{g}}^{-1} \bar{E}(\bar{q}) \tag{G.11}$$

$$\bar{B} := B \tag{G.12}$$

with D, C, G, F, E, and B as in (E.48).

Proof. Assumption G.1 ensures that $B(q) = B = \bar{B}$. The remainder of the result follows by substitution. □

Remark G.1. *When the robot's dynamics (E.48) is expressed in motor coordinates the following hold. The entries $(D)_{ij}$ and $(C)_{ij}$ are scaled by $1/(n_{\mathrm{g},i} n_{\mathrm{g},j})$, and the entries $(G)_i$, $(F)_i$, and $(E)_i$ are scaled by $1/n_{\mathrm{g},i}$.*

Remark G.2. *The rotor inertias of the motor used to actuate link i, $I_{\mathrm{a},i}$, only appears in the i^{th} diagonal entry of $\bar{D}$ and is unscaled by any of the gear ratios.*

Remark G.3. *If joint i is unactuated, then $(D)_{ii}$ and $(C)_{ii}$ will be unscaled and the other entries of the ith column and row of D and C will be only partially scaled.*

Remark G.4. *In light of Remarks G.1–G.3, the actuated dynamics will be dominated by the rotor inertia I_{a} and be coupled with the unactuated dynamics.*

APPENDIX H

Experimental Verification Plots

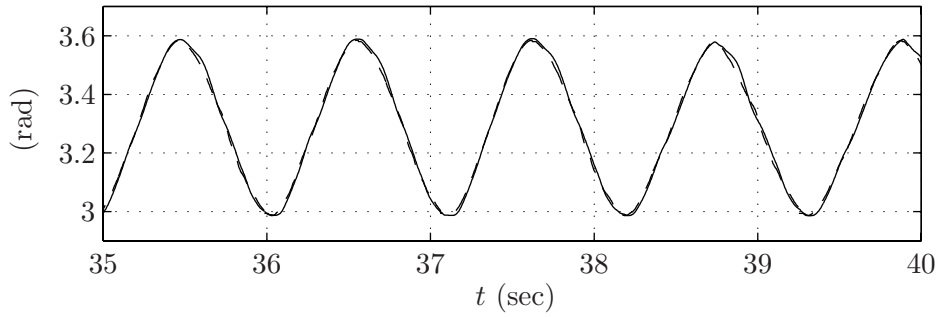

(a) q_1 (solid) and $h_{d,1}$ (dashed) versus time.

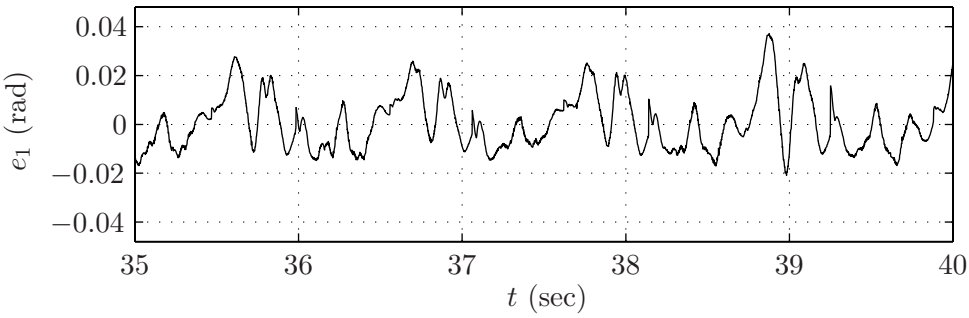

(b) $e_1 = q_1 - h_{d,1}$ versus time.

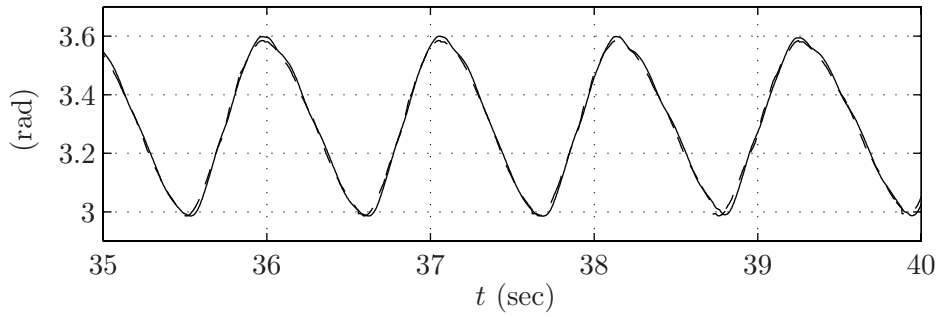

(c) q_2 (solid) and $h_{d,2}$ (dashed) versus time.

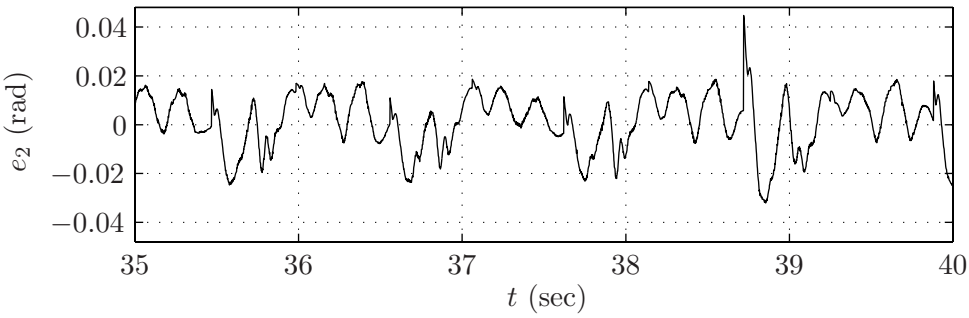

(d) $e_2 = q_2 - h_{d,2}$ versus time.

Figure H.1: Walking at 0.7 m/s: q_1, e_1, q_2, and e_2 versus time.

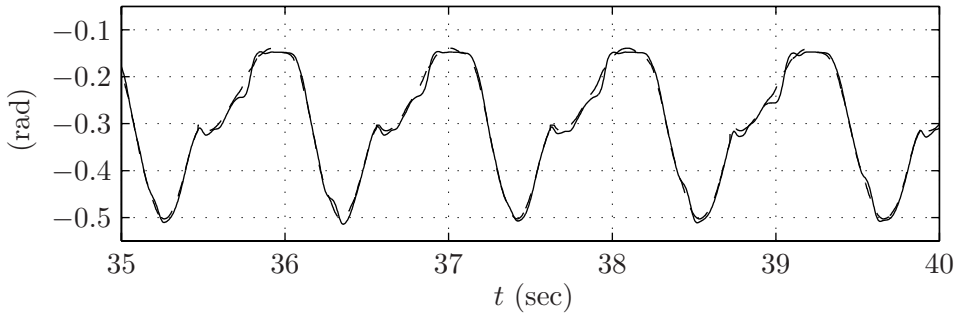

(a) q_3 (solid) and $h_{d,3}$ (dashed) versus time.

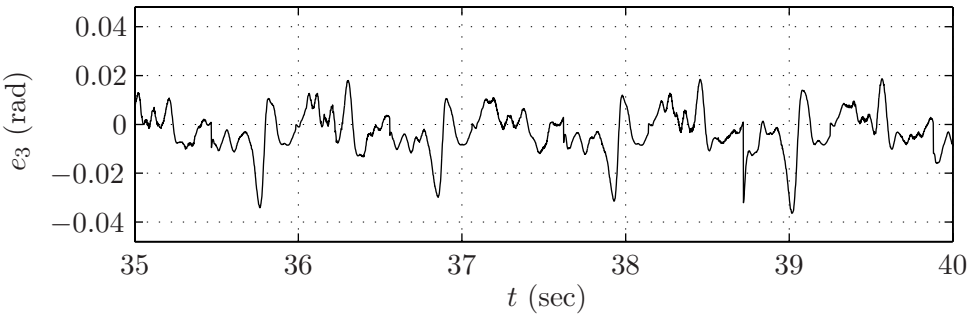

(b) $e_3 = q_3 - h_{d,3}$ versus time.

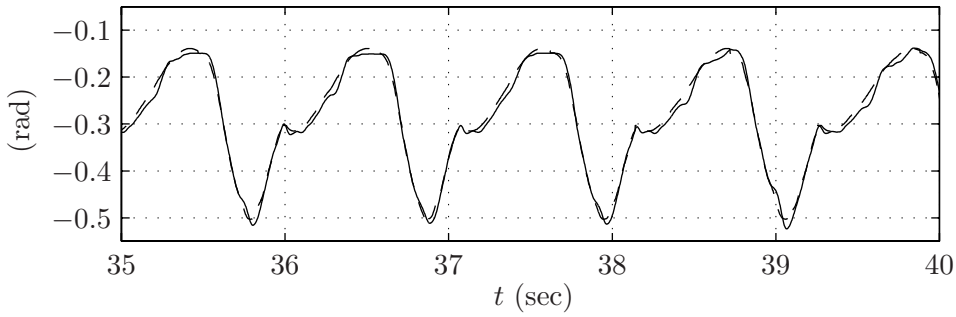

(c) q_4 (solid) and $h_{d,4}$ (dashed) versus time.

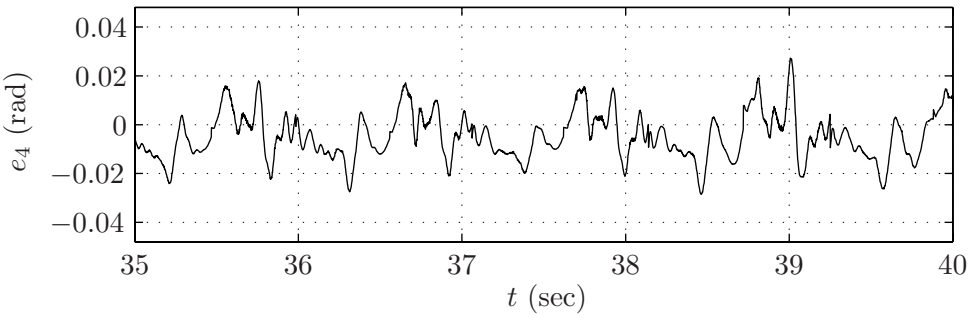

(d) $e_4 = q_4 - h_{d,4}$ versus time.

Figure H.2: Walking at 0.7 m/s: q_3, e_3, q_4, and e_4 versus time.

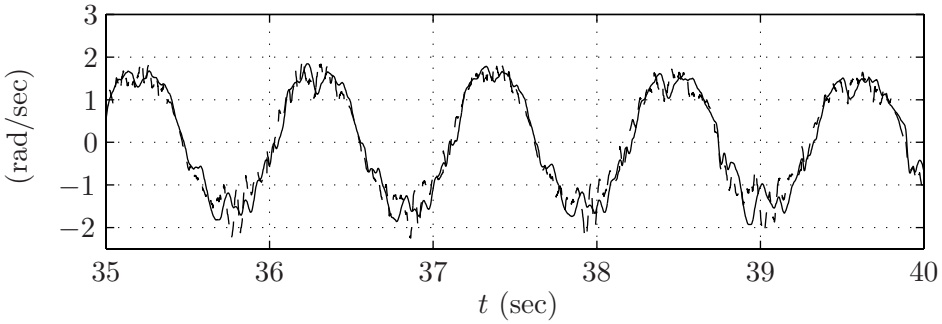

(a) $\dot{q}_1$ (solid) and $(\partial h_{d,1}/\partial\hat{\theta})\dot{\hat{\theta}}$ (dashed) versus time.

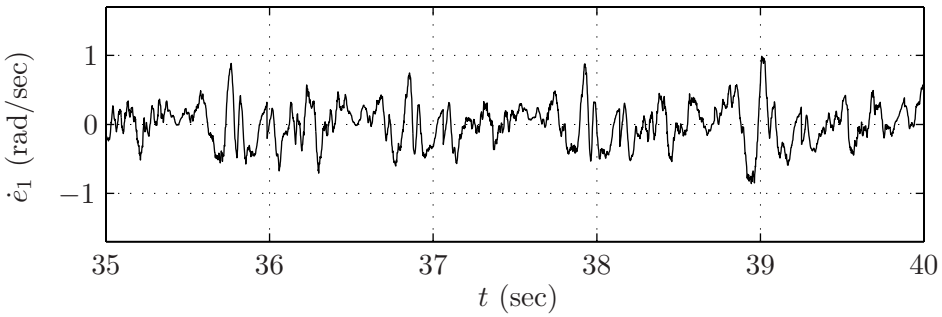

(b) $\dot{e}_1 = \dot{q}_1 - (\partial h_{d,1}/\partial\hat{\theta})\dot{\hat{\theta}}$ versus time.

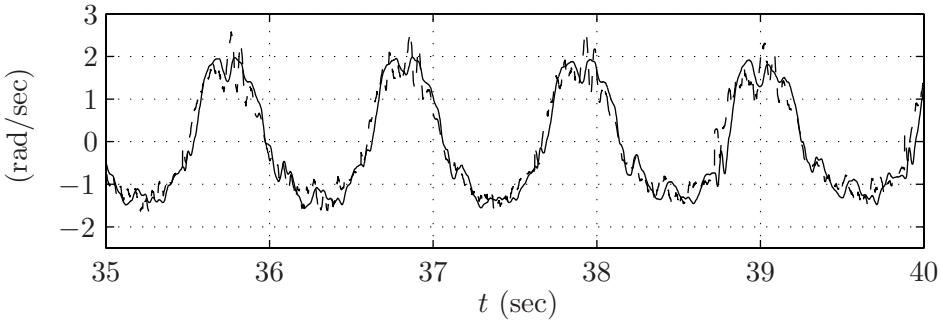

(c) $\dot{q}_2$ (solid) and $(\partial h_{d,2}/\partial\hat{\theta})\dot{\hat{\theta}}$ (dashed) versus time.

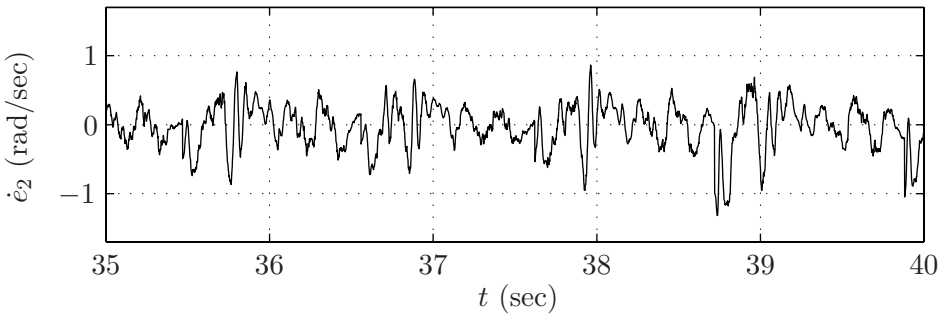

(d) $\dot{e}_2 = \dot{q}_2 - (\partial h_{d,2}/\partial\hat{\theta})\dot{\hat{\theta}}$ versus time.

Figure H.3: Walking at 0.7 m/s: $\dot{q}_1$, $\dot{e}_1$, $\dot{q}_2$, and $\dot{e}_2$ versus time.

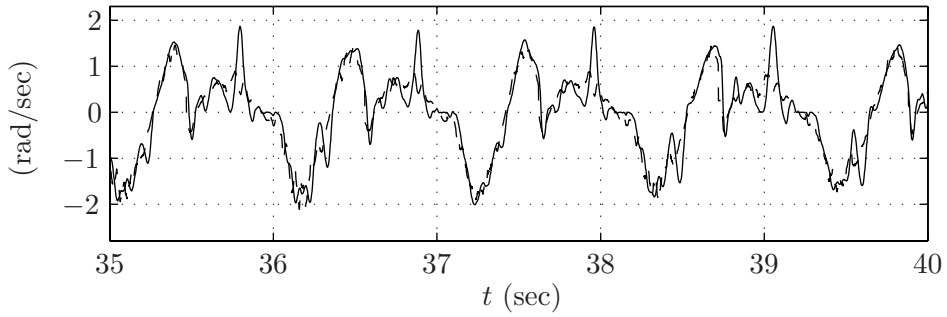

(a) $\dot{q}_3$ (solid) and $(\partial h_{d,3}/\partial\hat{\theta})\dot{\hat{\theta}}$ (dashed) versus time.

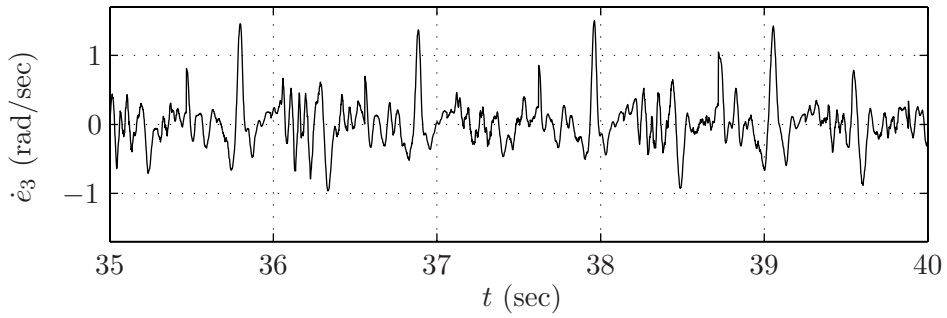

(b) $\dot{e}_3 = \dot{q}_3 - (\partial h_{d,3}/\partial\hat{\theta})\dot{\hat{\theta}}$ versus time.

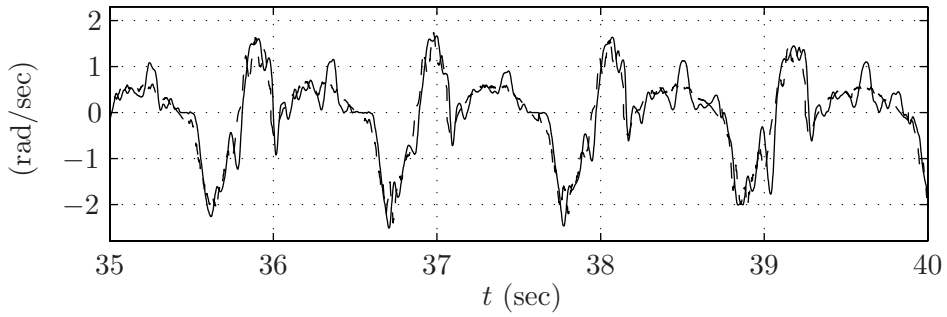

(c) $\dot{q}_4$ (solid) and $(\partial h_{d,4}/\partial\hat{\theta})\dot{\hat{\theta}}$ (dashed) versus time.

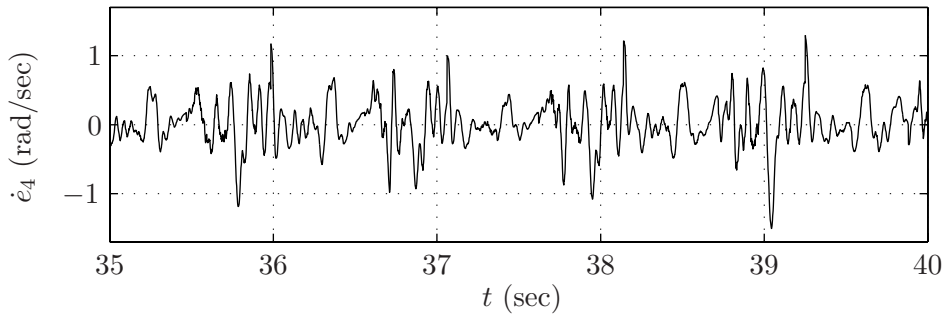

(d) $\dot{e}_4 = \dot{q}_4 - (\partial h_{d,4}/\partial\hat{\theta})\dot{\hat{\theta}}$ versus time.

Figure H.4: Walking at 0.7 m/s: $\dot{q}_3$, $\dot{e}_3$, $\dot{q}_4$, and $\dot{e}_4$ versus time.

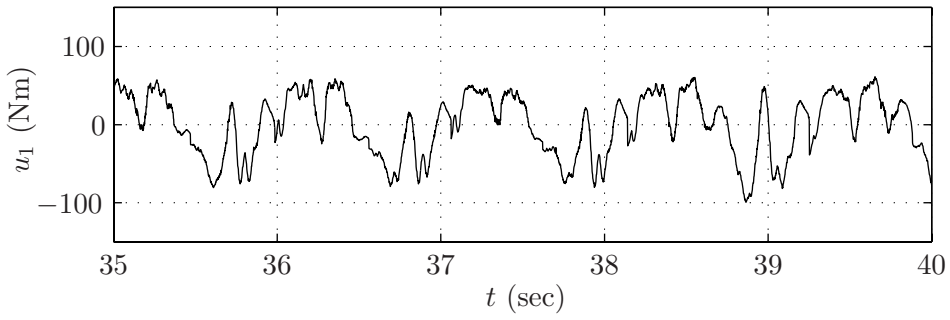

(a) u_1 versus time.

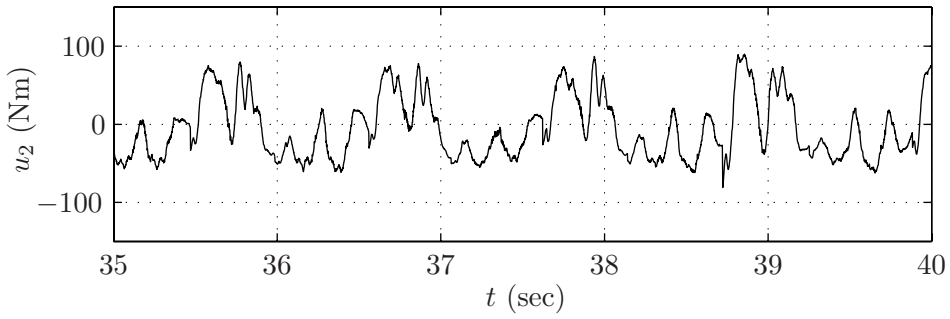

(b) u_2 versus time.

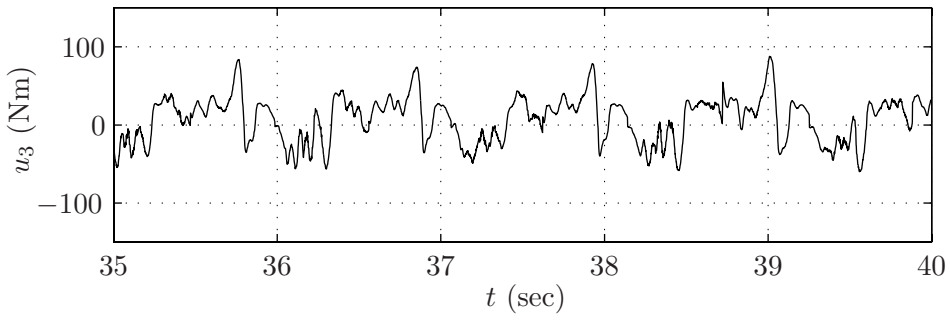

(c) u_3 versus time.

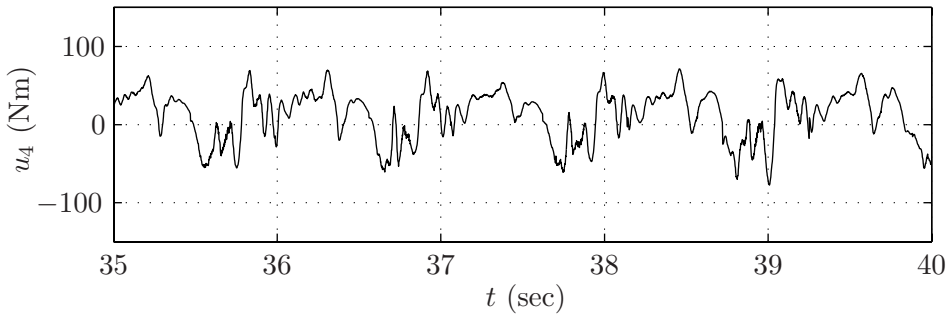

(d) u_4 versus time.

Figure H.5: Walking at 0.7 m/s: u_1, u_2, u_3, and u_4 versus time.

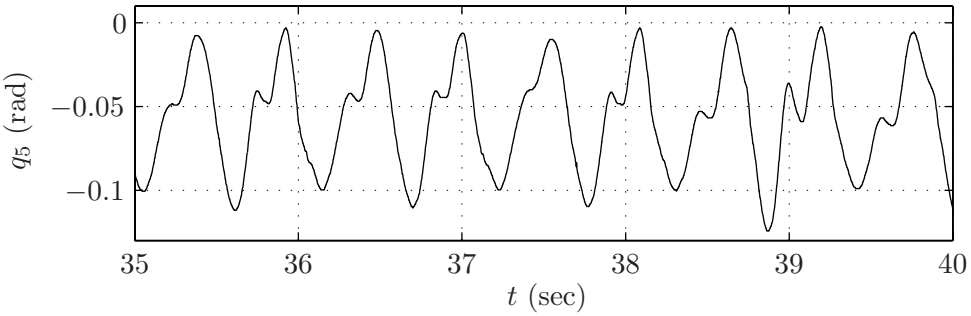

(a) q_5 versus time.

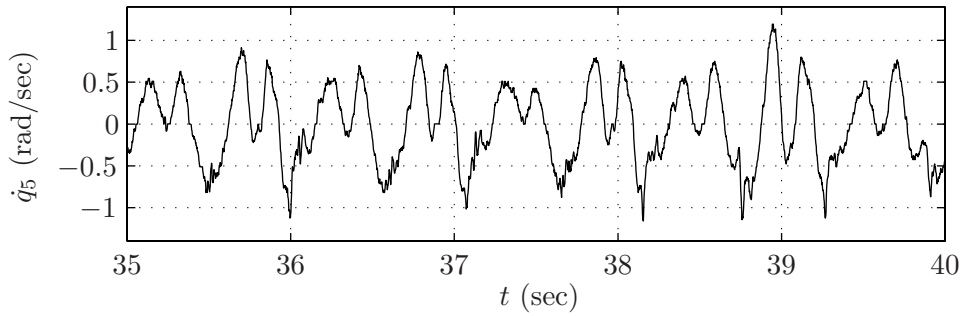

(b) $\dot{q}_5$ versus time.

Figure H.6: Walking at 0.7 m/s: q_5, $\dot{q}_5$ versus time.

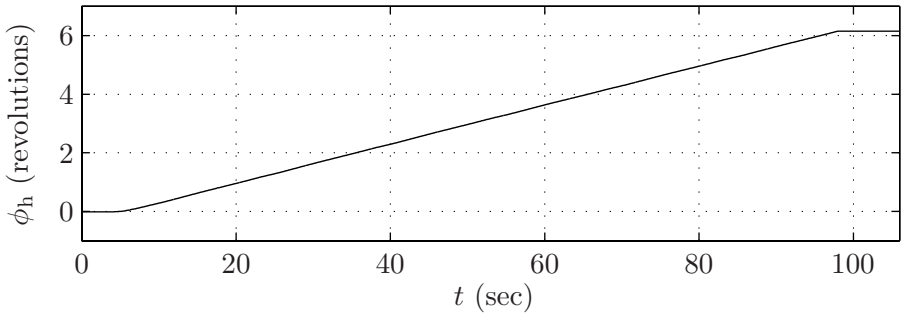

(a) ϕ_h versus time.

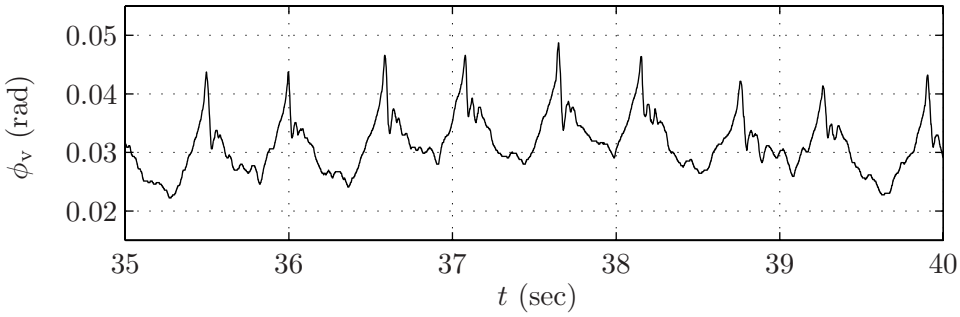

(b) ϕ_v versus time (portion of trace).

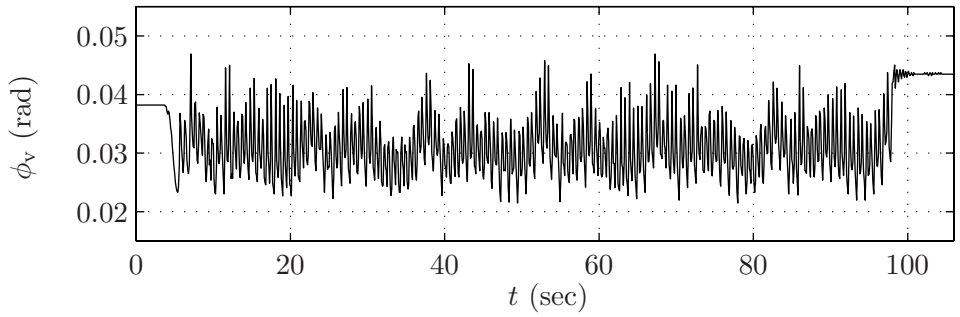

(c) ϕ_v versus time (entire trace).

Figure H.7: Walking at 0.7 m/s: ϕ_h and ϕ_v versus time.

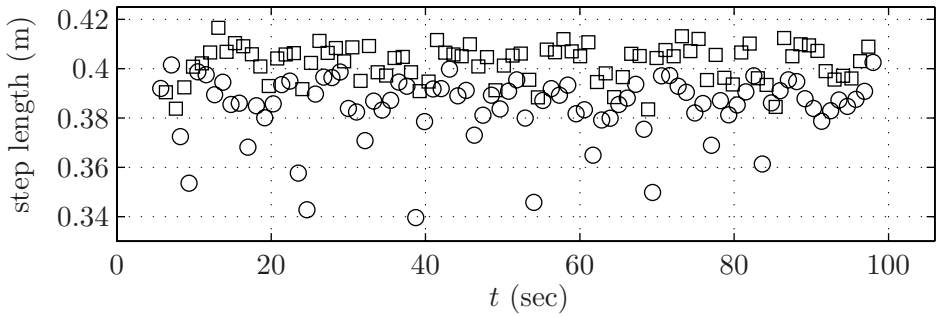

(a) step length versus time.

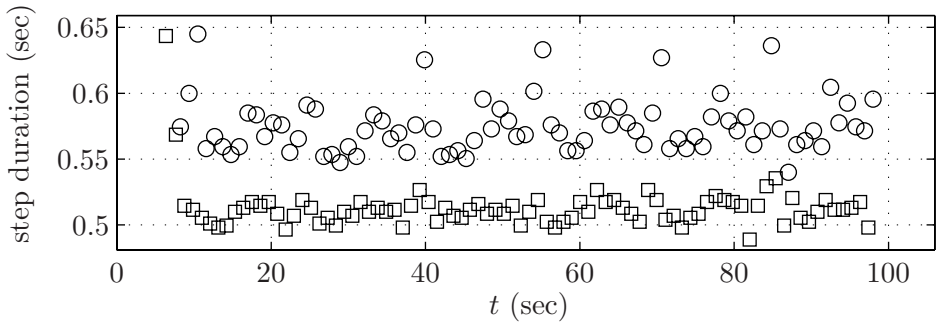

(b) step duration versus time.

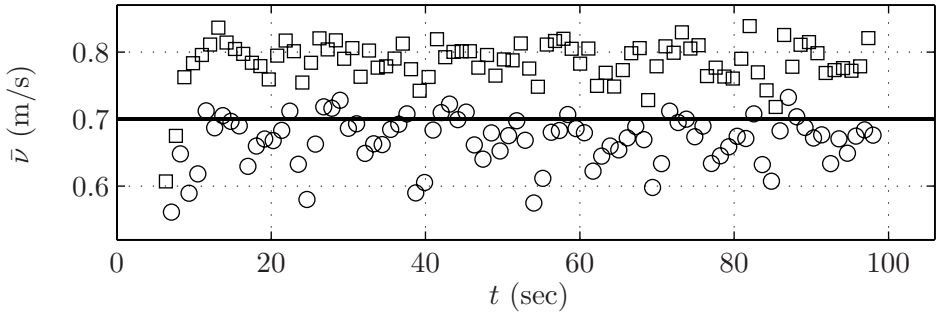

(c) $\bar{\nu}$ = (step length)/(step duration) (circles and squares) and designed $\bar{\nu}$ (solid line) versus time.

Figure H.8: Walking at 0.7 m/s: step length, step duration, and average walking rate versus time. Circles represent steps taken by the outer leg, squares represent steps taken by the inner leg.

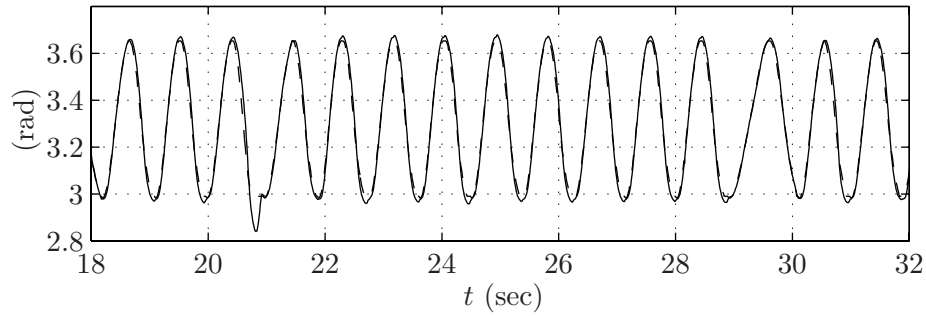

(a) q_1 (solid) and $h_{d,1}$ (dashed) versus time.

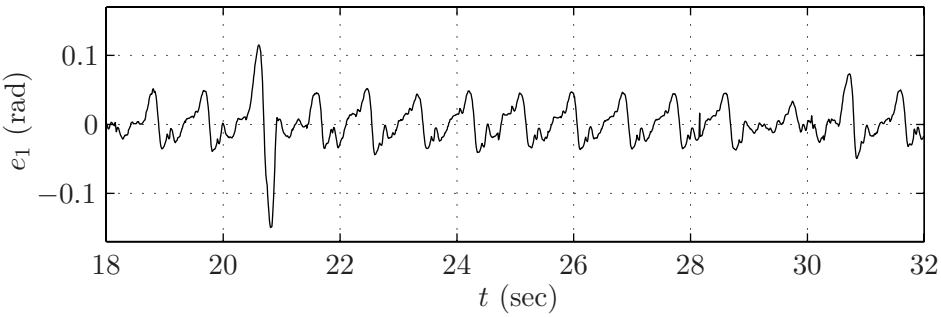

(b) $e_1 = q_1 - h_{d,1}$ versus time.

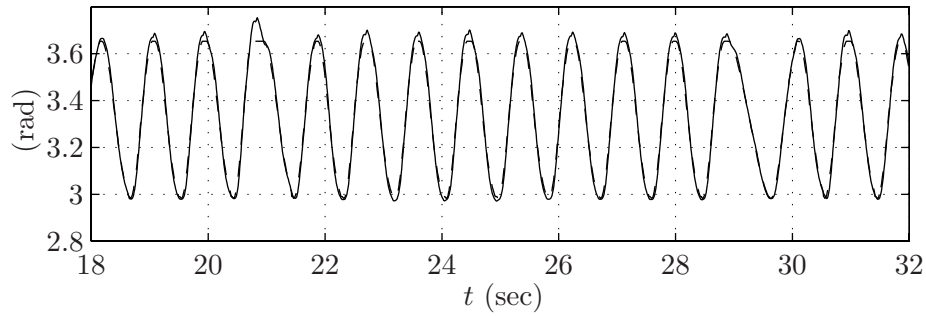

(c) q_2 (solid) and $h_{d,2}$ (dashed) versus time.

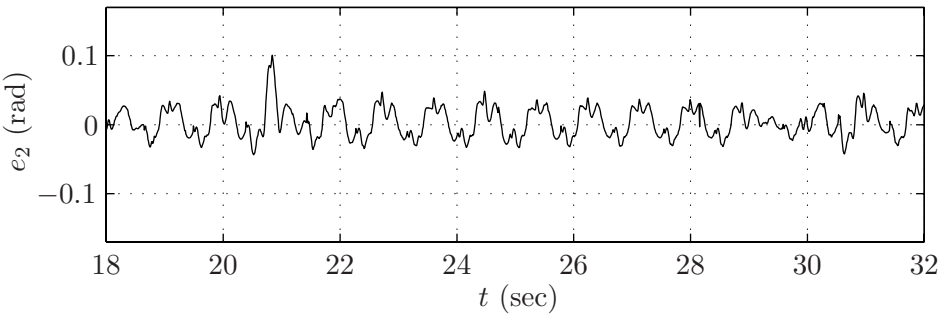

(d) $e_2 = q_2 - h_{d,2}$ versus time.

Figure H.9: Robustness demonstration: q_1, e_1, q_2, and e_2 versus time.

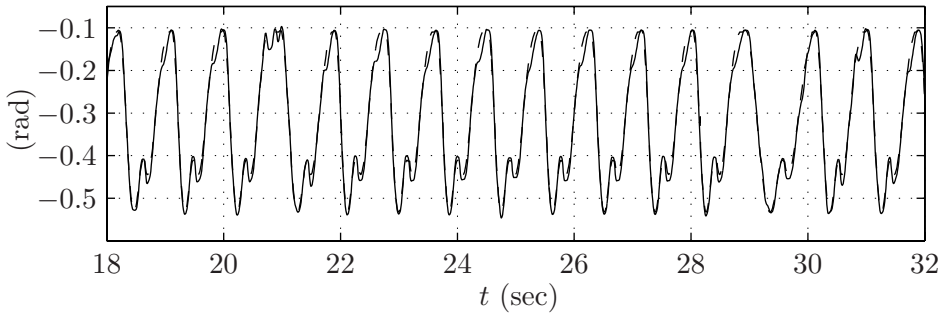

(a) q_3 (solid) and $h_{d,3}$ (dashed) versus time.

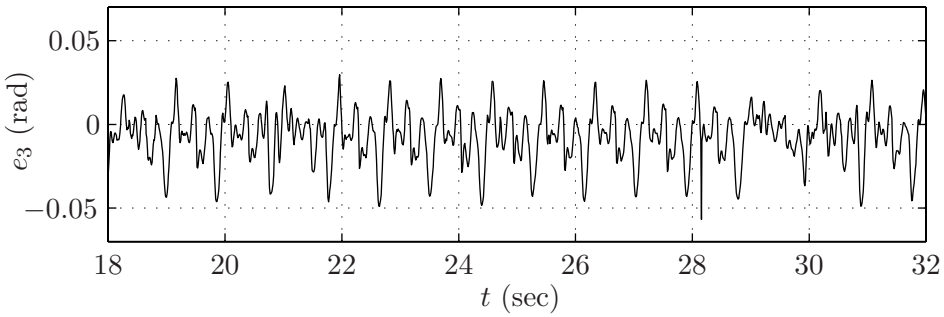

(b) $e_3 = q_3 - h_{d,3}$ versus time.

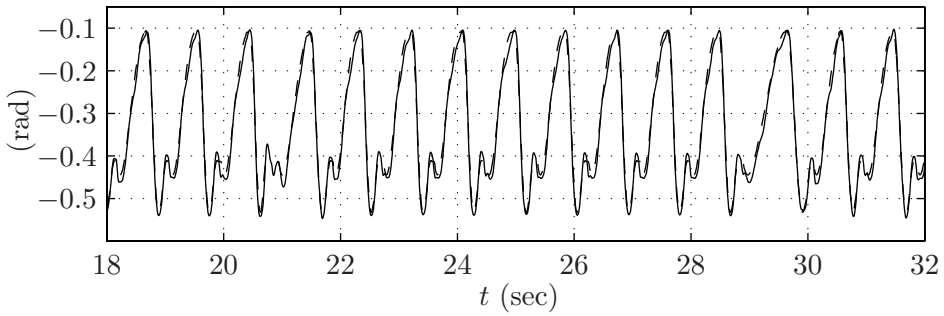

(c) q_4 (solid) and $h_{d,4}$ (dashed) versus time.

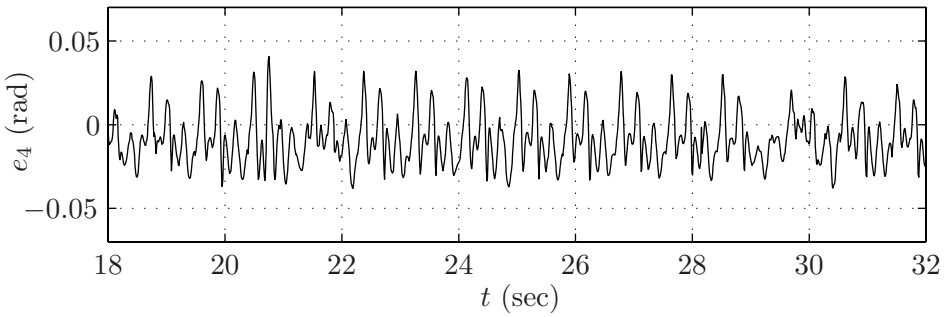

(d) $e_4 = q_4 - h_{d,4}$ versus time.

Figure H.10: Robustness demonstration: q_3, e_3, q_4, and e_4 versus time.

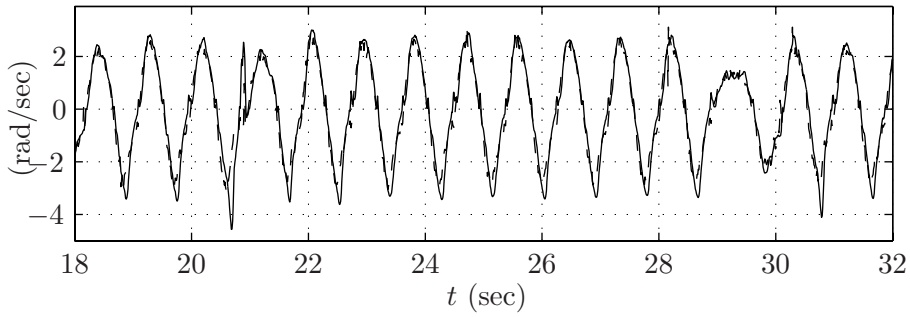

(a) $\dot{q}_1$ (solid) and $(\partial h_{d,1}/\partial\hat{\theta})\dot{\hat{\theta}}$ (dashed) versus time.

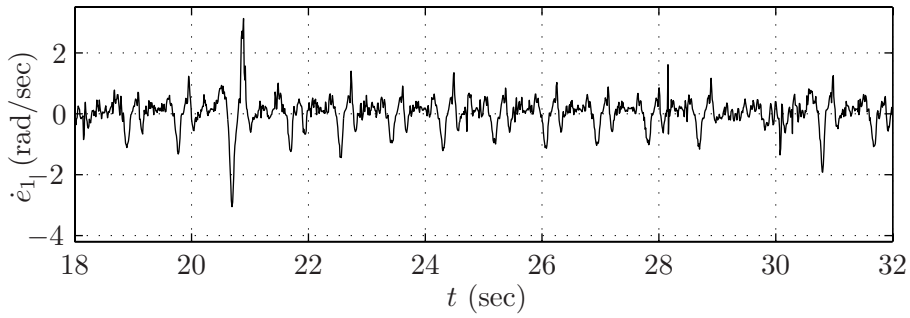

(b) $\dot{e}_1 = \dot{q}_1 - (\partial h_{d,1}/\partial\hat{\theta})\dot{\hat{\theta}}$ versus time.

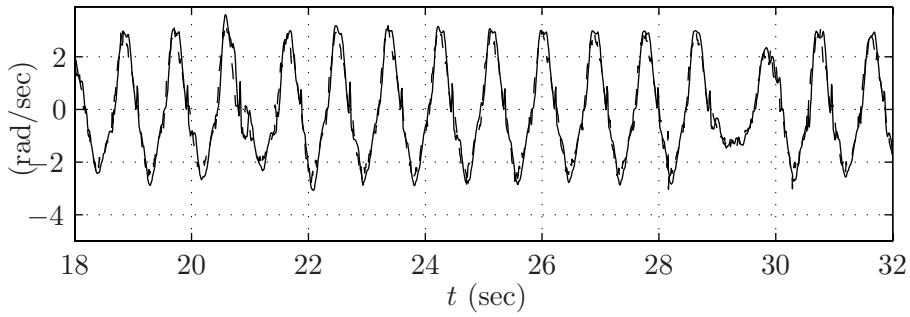

(c) $\dot{q}_2$ (solid) and $(\partial h_{d,2}/\partial\hat{\theta})\dot{\hat{\theta}}$ (dashed) versus time.

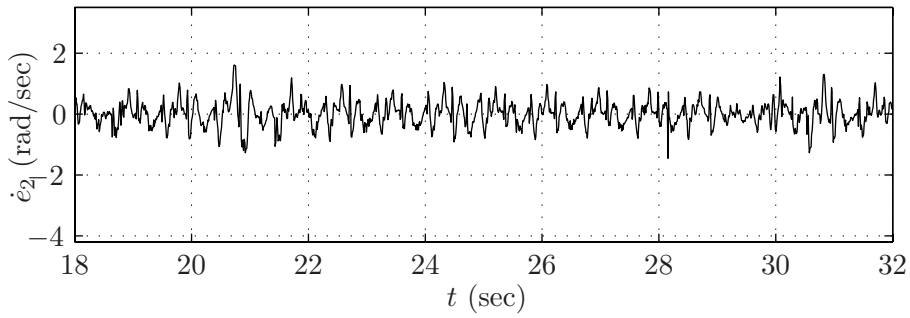

(d) $\dot{e}_2 = \dot{q}_2 - (\partial h_{d,2}/\partial\hat{\theta})\dot{\hat{\theta}}$ versus time.

Figure H.11: Robustness demonstration: $\dot{q}_1$, $\dot{e}_1$, $\dot{q}_2$, and $\dot{e}_2$ versus time.

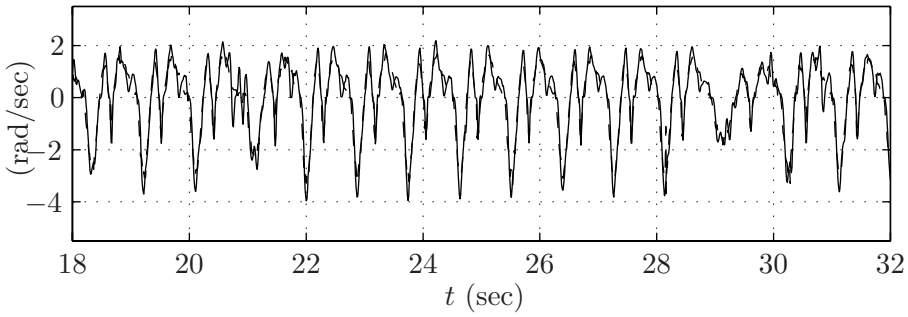

(a) $\dot{q}_3$ (solid) and $(\partial h_{d,3}/\partial\hat{\theta})\dot{\hat{\theta}}$ (dashed) versus time.

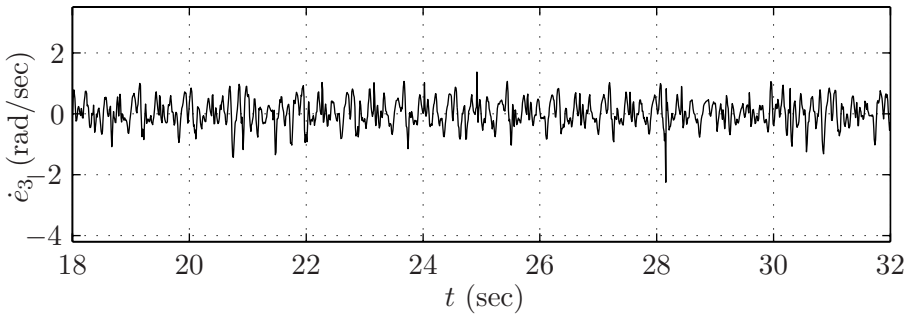

(b) $\dot{e}_3 = \dot{q}_3 - (\partial h_{d,3}/\partial\hat{\theta})\dot{\hat{\theta}}$ versus time.

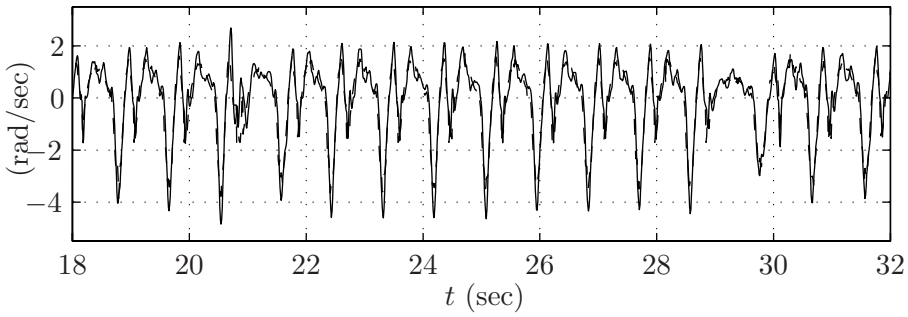

(c) $\dot{q}_4$ (solid) and $(\partial h_{d,4}/\partial\hat{\theta})\dot{\hat{\theta}}$ (dashed) versus time.

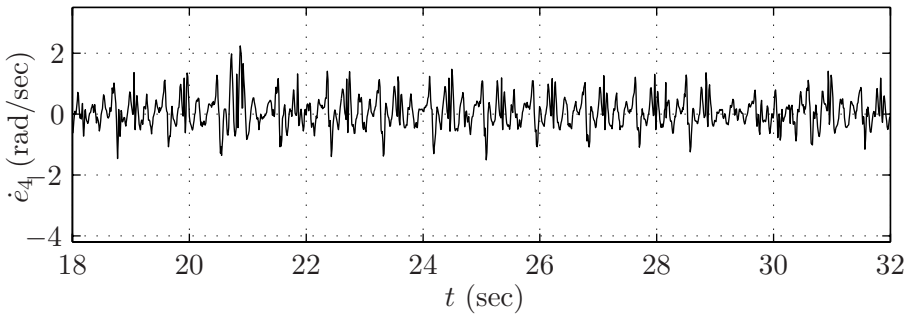

(d) $\dot{e}_4 = \dot{q}_4 - (\partial h_{d,4}/\partial\hat{\theta})\dot{\hat{\theta}}$ versus time.

Figure H.12: Robustness demonstration: $\dot{q}_3$, $\dot{e}_3$, $\dot{q}_4$, and $\dot{e}_4$ versus time.

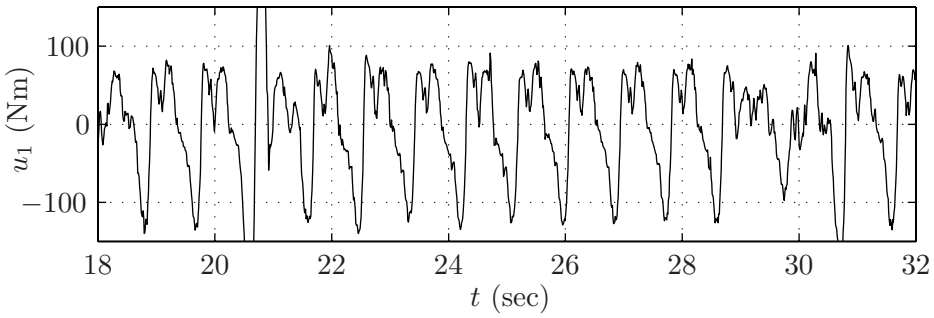

(a) u_1 versus time.

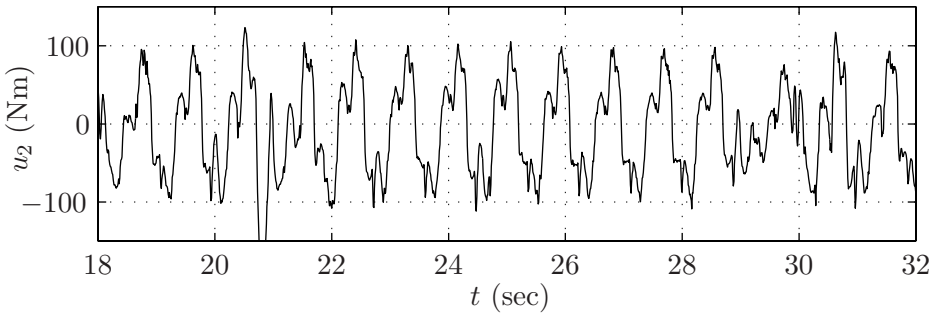

(b) u_2 versus time.

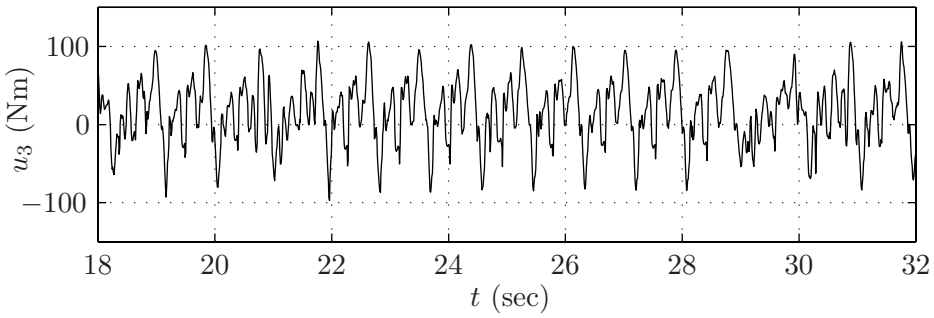

(c) u_3 versus time.

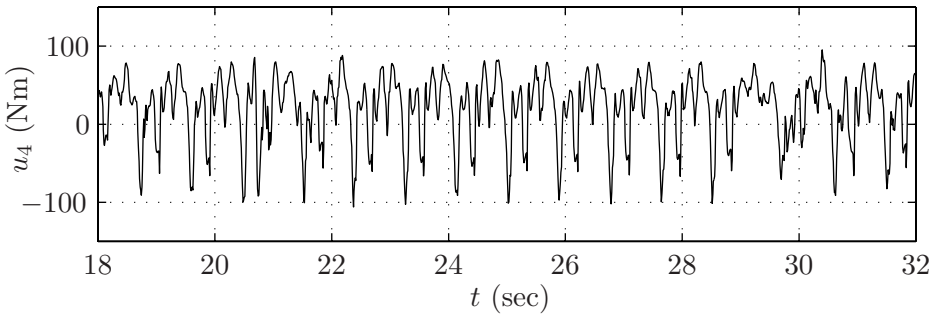

(d) u_4 versus time.

Figure H.13: Robustness demonstration: u_1, u_2, u_3, and u_4 versus time.

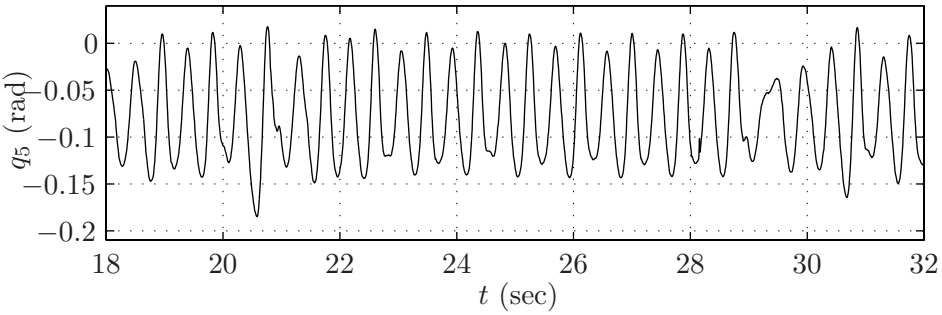

(a) q_5 versus time.

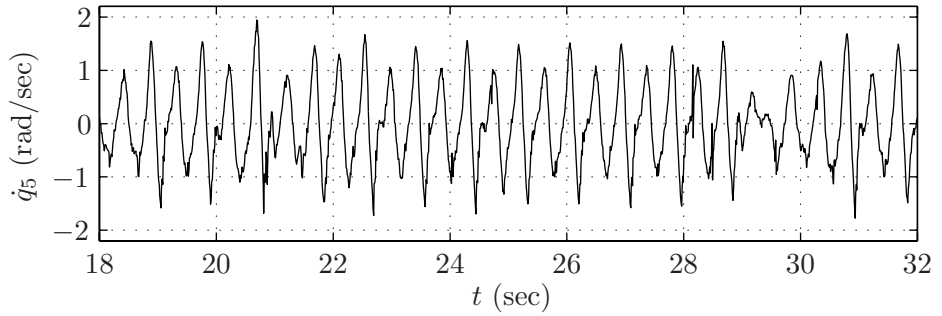

(b) $\dot{q}_5$ versus time.

Figure H.14: Robustness demonstration: q_5, $\dot{q}_5$ versus time.

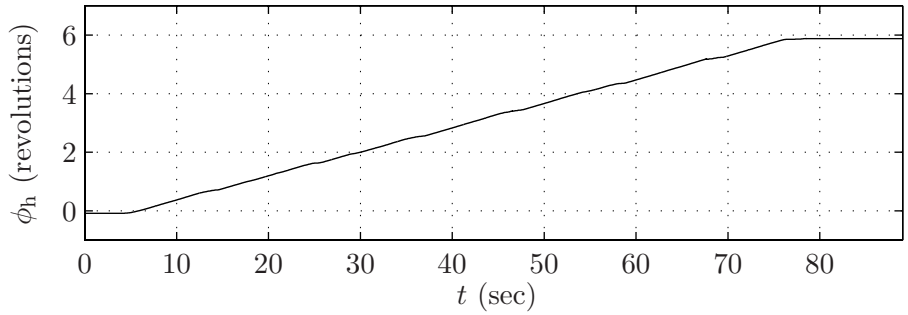

(a) ϕ_{h} versus time.

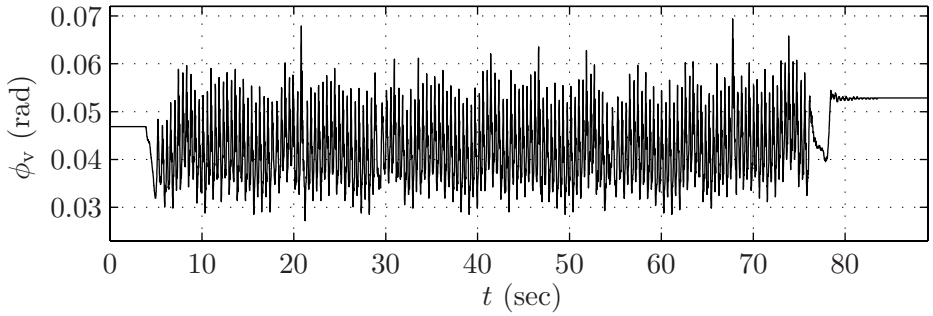

(b) ϕ_{v} versus time (portion of trace).

Figure H.15: Robustness demonstration: ϕ_{h} and ϕ_{v} versus time.

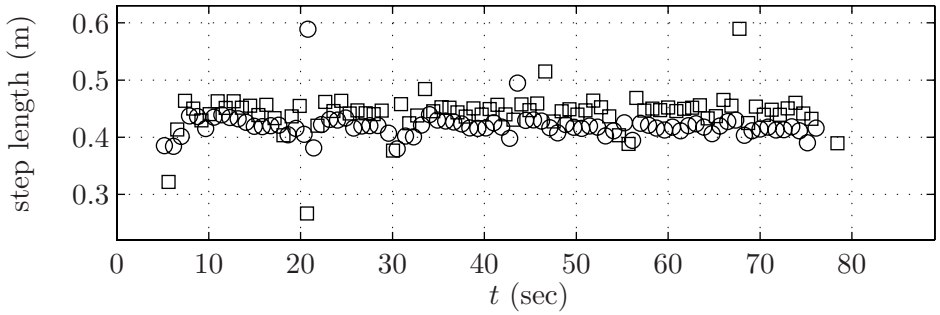

(a) step length versus time.

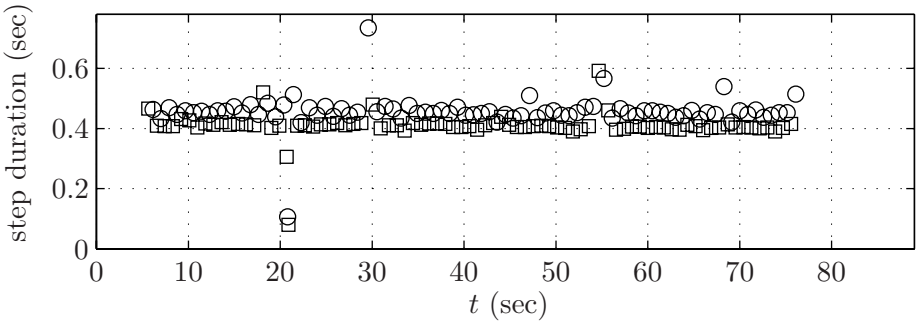

(b) step duration versus time.

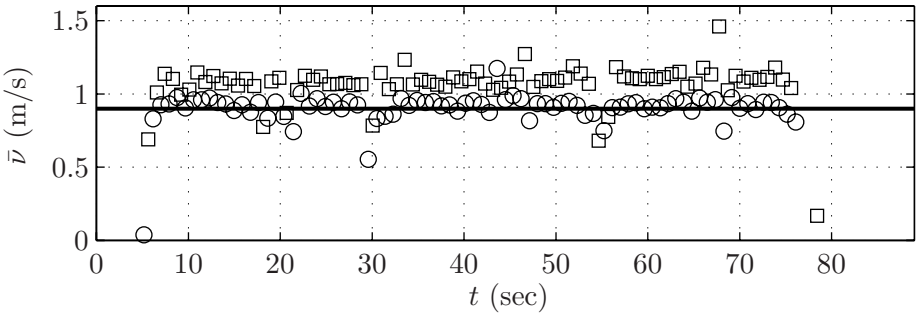

(c) $\bar{\nu}$ = (step length)/(step duration) (circles and squares) and designed $\bar{\nu}$ (solid line) versus time.

Figure H.16: Robustness demonstration: step length, step duration, and average walking rate versus time. Circles represent steps taken by the outer leg, squares represent steps taken by the inner leg.

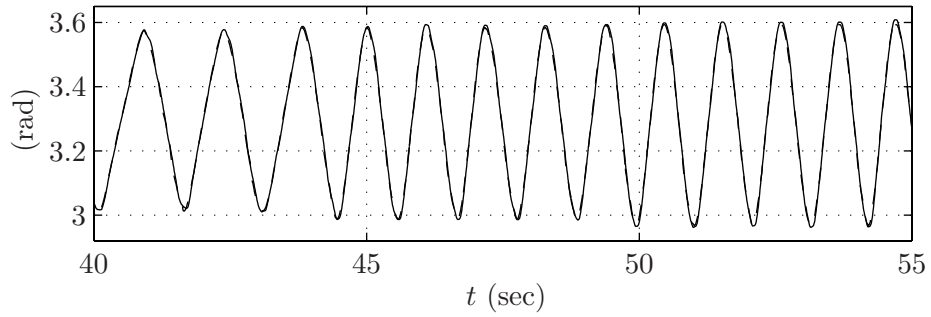

(a) q_1 (solid) and $h_{d,1}$ (dashed) versus time.

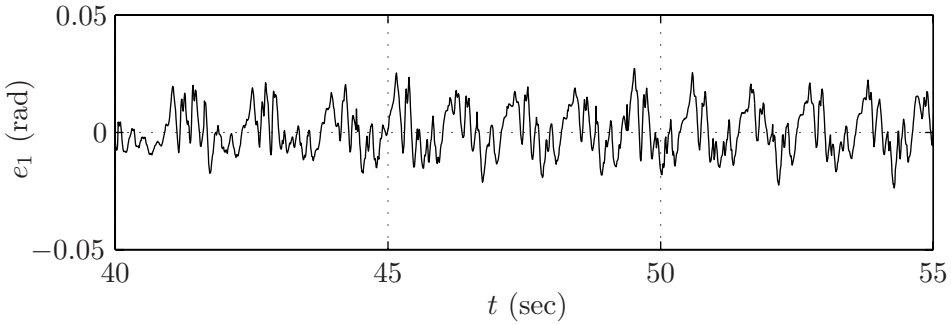

(b) $e_1 = q_1 - h_{d,1}$ versus time.

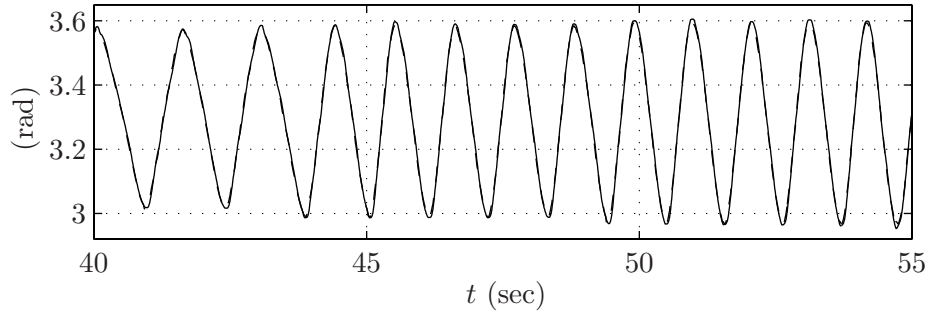

(c) q_2 (solid) and $h_{d,2}$ (dashed) versus time.

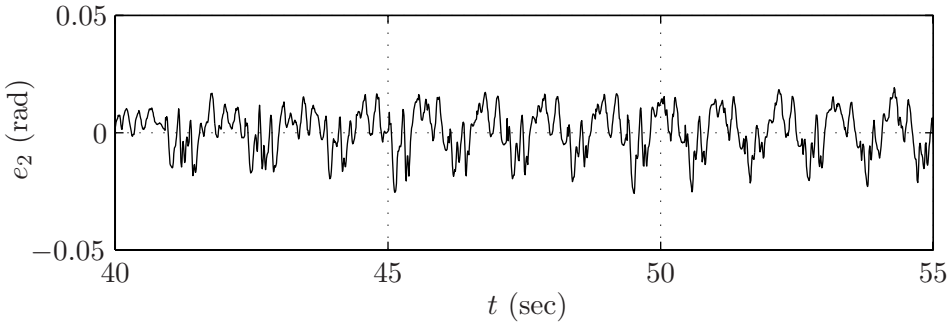

(d) $e_2 = q_2 - h_{d,2}$ versus time.

Figure H.17: Transitioning: q_1, e_1, q_2, and e_2 versus time.

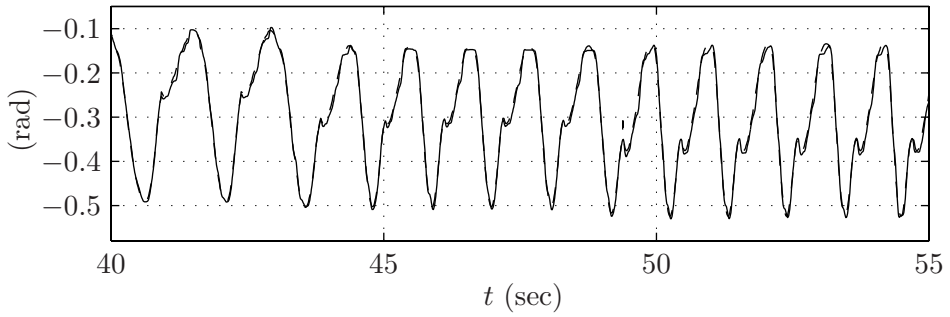

(a) q_3 (solid) and $h_{d,3}$ (dashed) versus time.

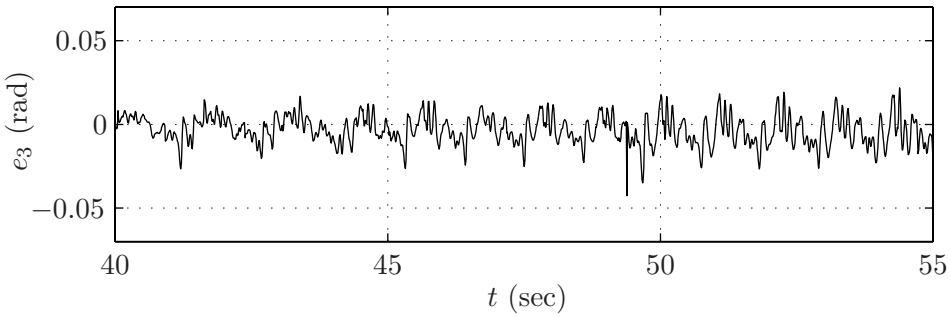

(b) $e_3 = q_3 - h_{d,3}$ versus time.

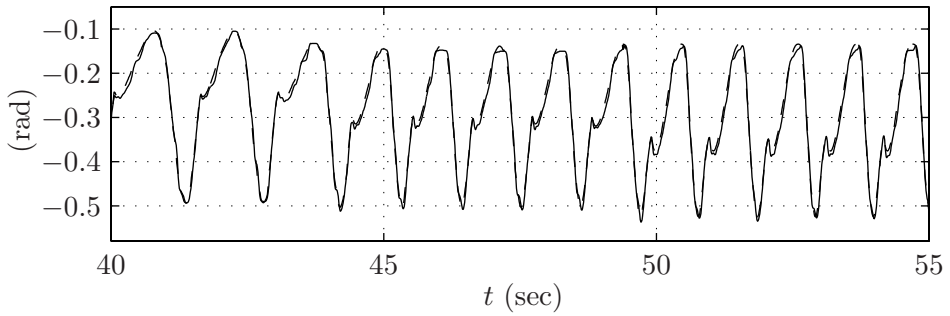

(c) q_4 (solid) and $h_{d,4}$ (dashed) versus time.

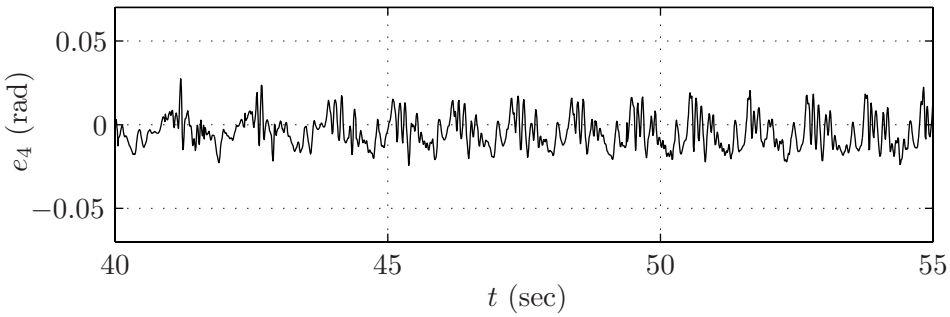

(d) $e_4 = q_4 - h_{d,4}$ versus time.

Figure H.18: Transitioning: q_3, e_3, q_4, and e_4 versus time.

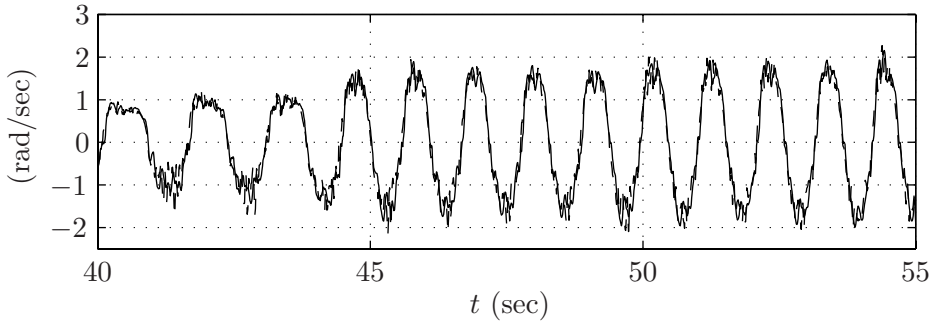

(a) $\dot{q}_1$ (solid) and $(\partial h_{d,1}/\partial\hat{\theta})\dot{\hat{\theta}}$ (dashed) versus time.

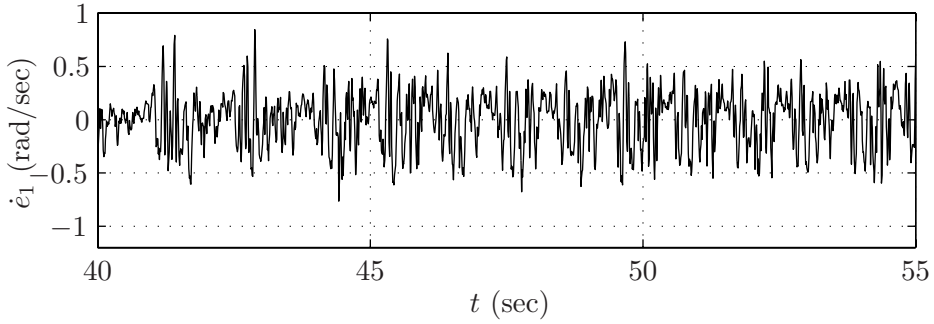

(b) $\dot{e}_1 = \dot{q}_1 - (\partial h_{d,1}/\partial\hat{\theta})\dot{\hat{\theta}}$ versus time.

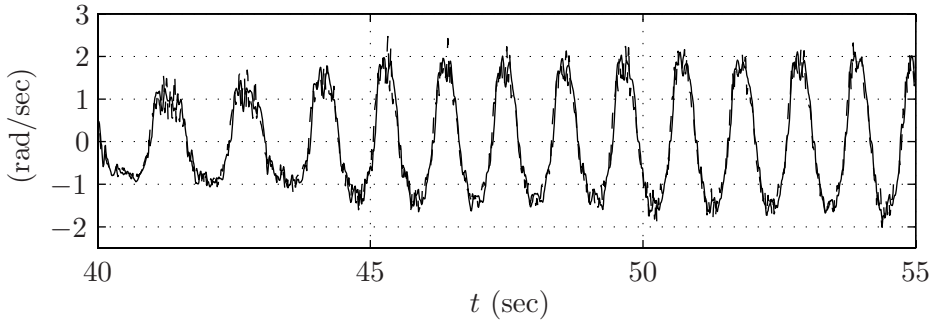

(c) $\dot{q}_2$ (solid) and $(\partial h_{d,2}/\partial\hat{\theta})\dot{\hat{\theta}}$ (dashed) versus time.

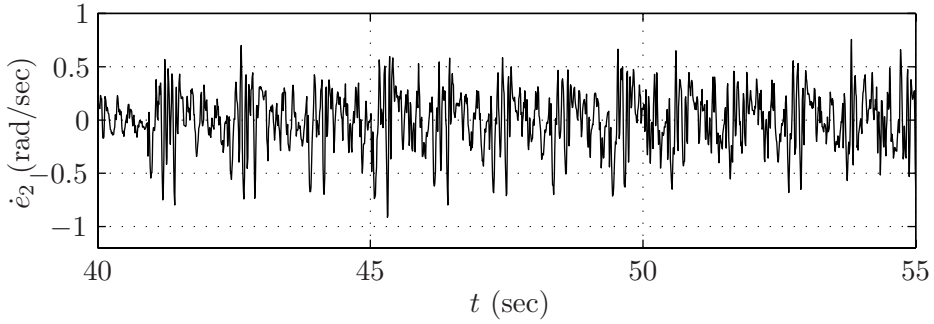

(d) $\dot{e}_2 = \dot{q}_2 - (\partial h_{d,2}/\partial\hat{\theta})\dot{\hat{\theta}}$ versus time.

Figure H.19: Transitioning: $\dot{q}_1$, $\dot{e}_1$, $\dot{q}_2$, and $\dot{e}_2$ versus time.

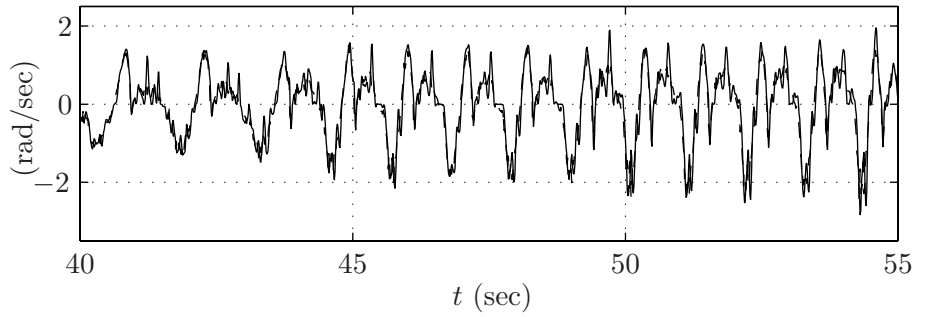

(a) $\dot{q}_3$ (solid) and $(\partial h_{d,3}/\partial\hat{\theta})\dot{\hat{\theta}}$ (dashed) versus time.

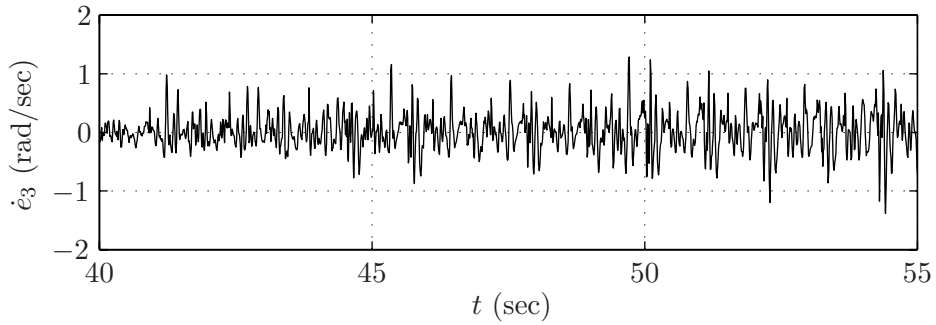

(b) $\dot{e}_3 = \dot{q}_3 - (\partial h_{d,3}/\partial\hat{\theta})\dot{\hat{\theta}}$ versus time.

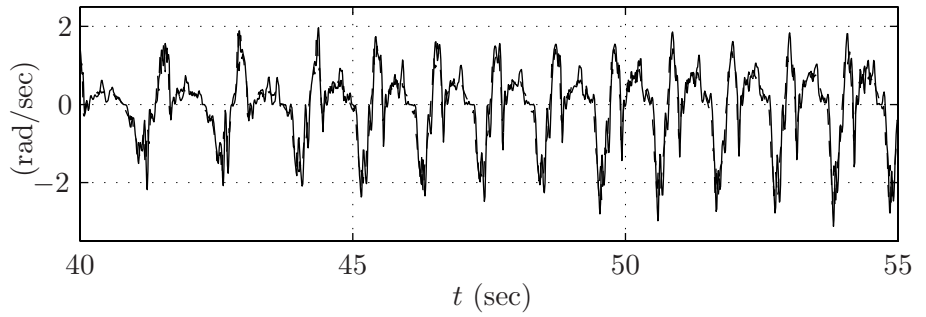

(c) $\dot{q}_4$ (solid) and $(\partial h_{d,4}/\partial\hat{\theta})\dot{\hat{\theta}}$ (dashed) versus time.

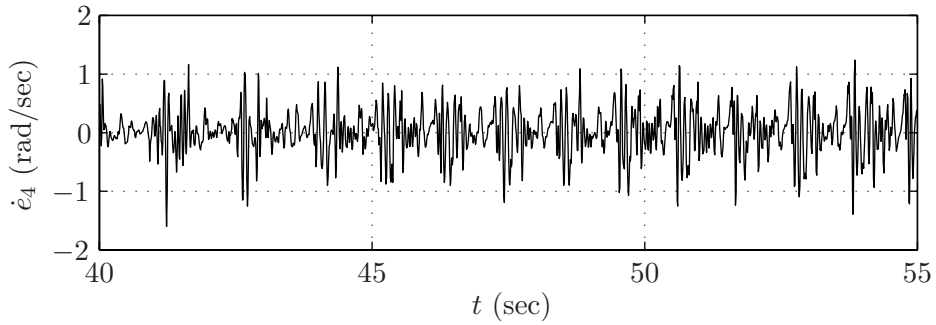

(d) $\dot{e}_4 = \dot{q}_4 - (\partial h_{d,4}/\partial\hat{\theta})\dot{\hat{\theta}}$ versus time.

Figure H.20: Transitioning: $\dot{q}_3$, $\dot{e}_3$, $\dot{q}_4$, and $\dot{e}_4$ versus time.

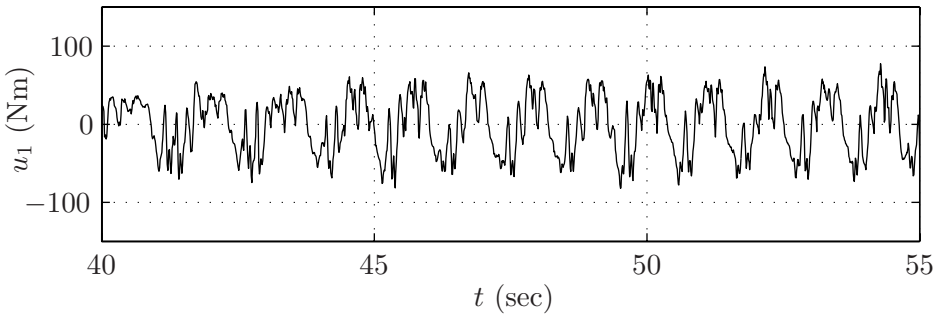

(a) u_1 versus time.

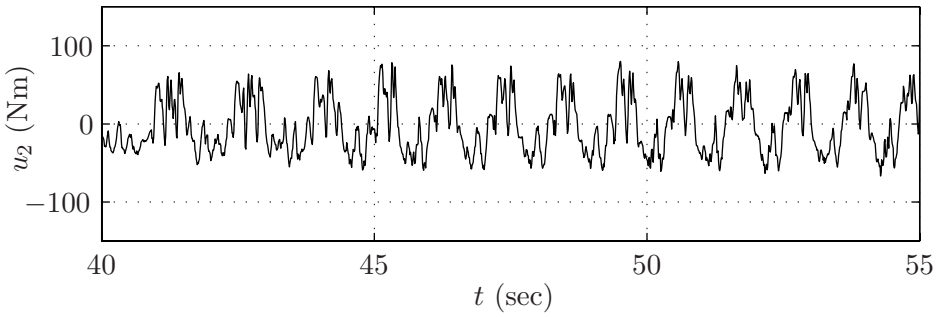

(b) u_2 versus time.

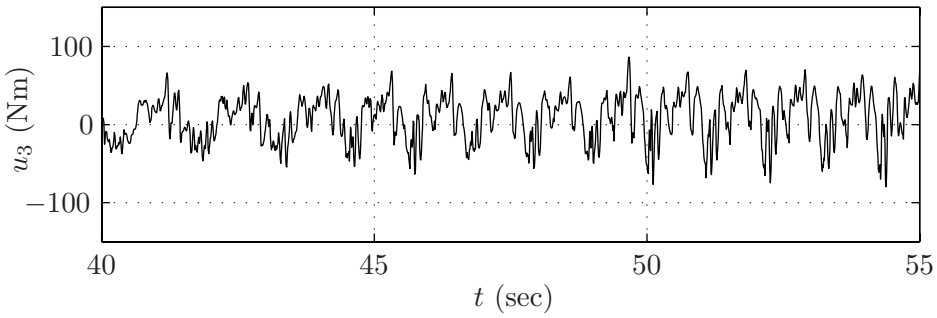

(c) u_3 versus time.

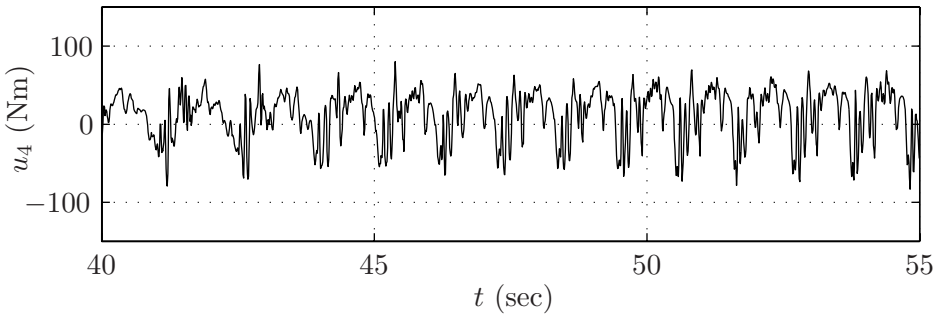

(d) u_4 versus time.

Figure H.21: Transitioning: u_1, u_2, u_3, and u_4 versus time.

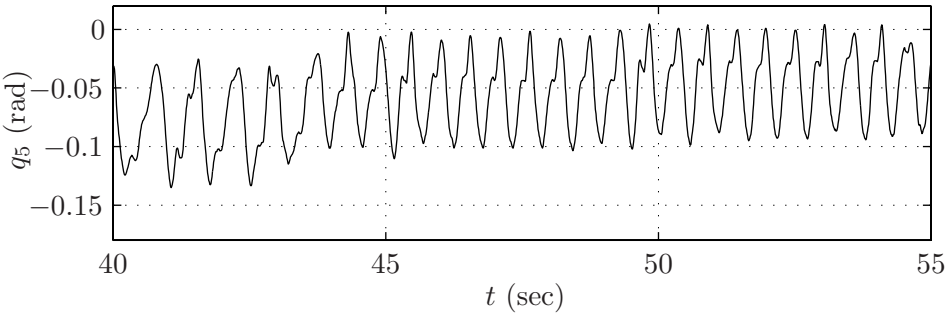

(a) q_5 versus time.

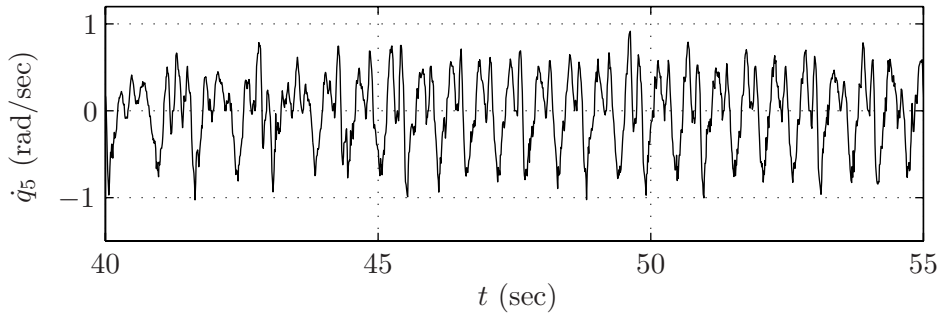

(b) $\dot{q}_5$ versus time.

Figure H.22: Transitioning: q_5, $\dot{q}_5$ versus time.

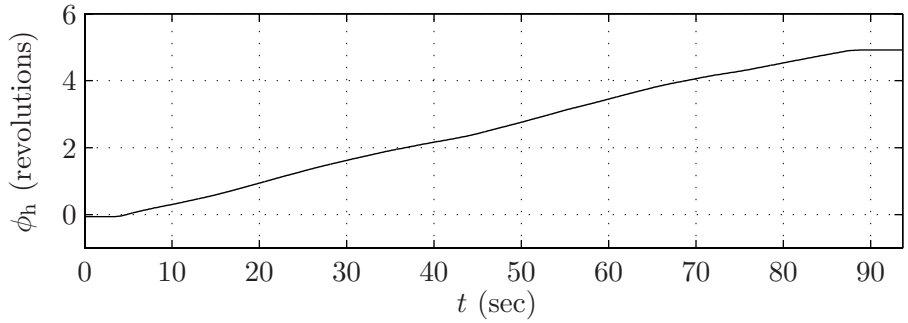

(a) ϕ_{h} versus time.

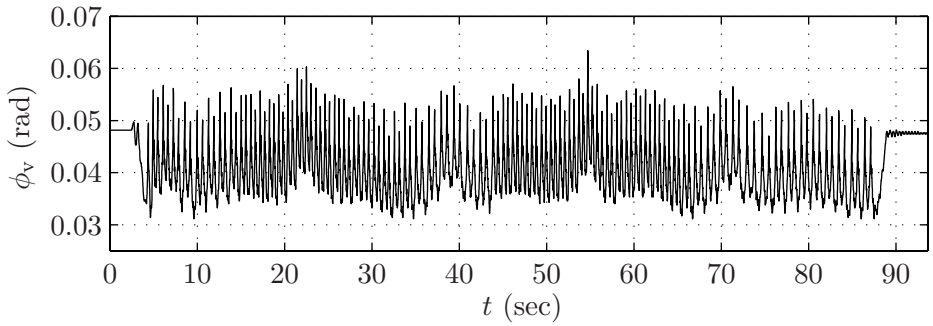

(b) ϕ_{v} versus time (portion of trace).

Figure H.23: Transitioning: ϕ_{h} and ϕ_{v} versus time.

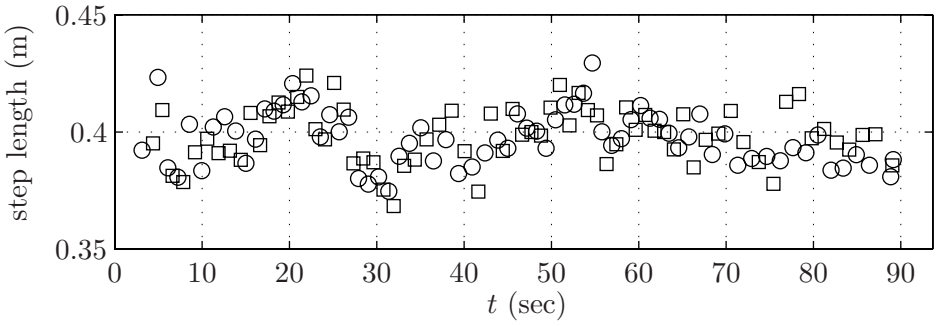

(a) step length versus time.

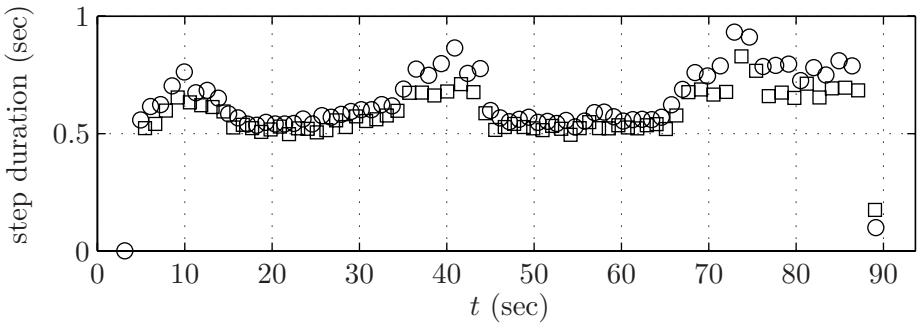

(b) step duration versus time.

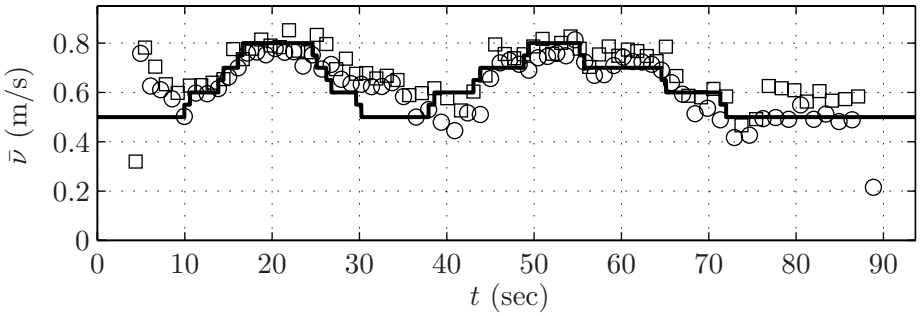

(c) $\bar{\nu}$ = (step length)/(step duration) (circles and squares) and designed $\bar{\nu}$ (solid line) versus time.

Figure H.24: Transitioning: step length, step duration, and average walking rate versus time. Circles represent steps taken by the outer leg, squares represent steps taken by the inner leg.

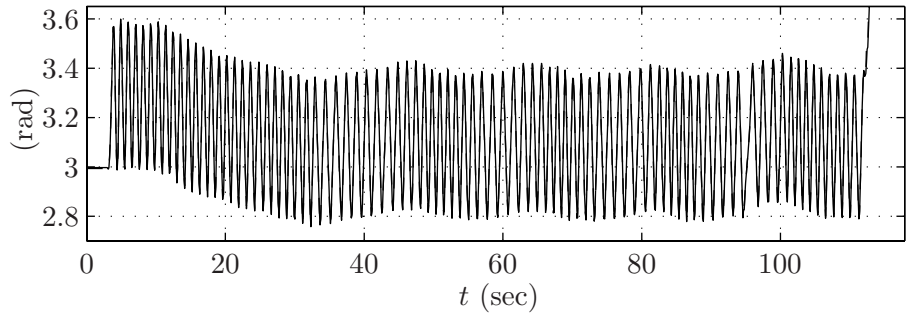

(a) q_1 (solid) and $h_{d,1}$ (dashed) versus time.

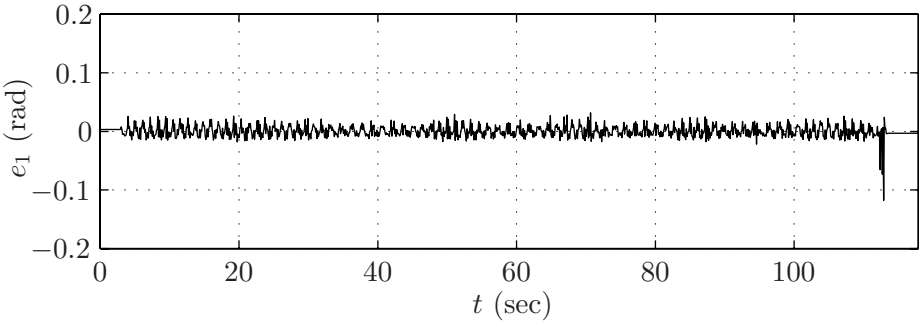

(b) $e_1 = q_1 - h_{d,1}$ versus time.

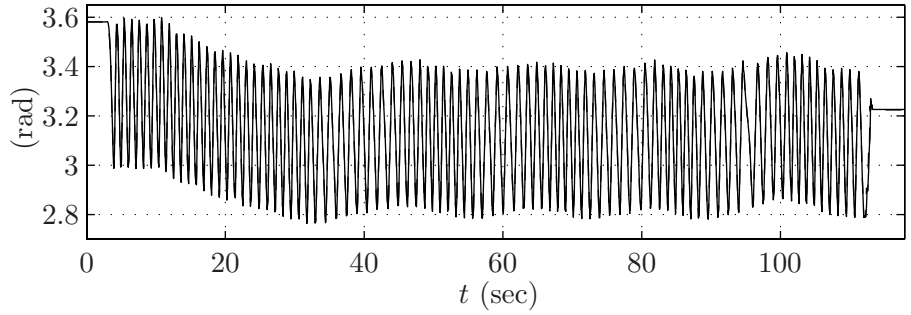

(c) q_2 (solid) and $h_{d,2}$ (dashed) versus time.

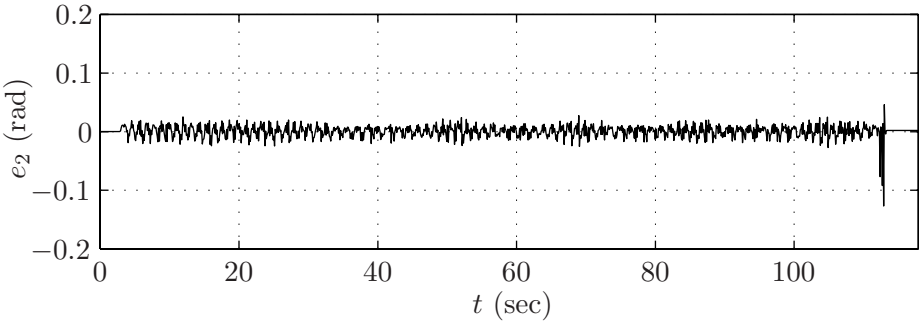

(d) $e_2 = q_2 - h_{d,2}$ versus time.

Figure H.25: I-control to change fixed point: q_1, e_1, q_2, and e_2 versus time.

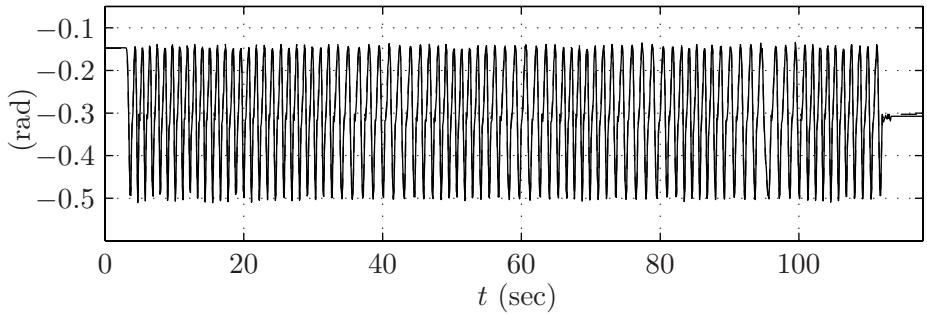

(a) q_3 (solid) and $h_{d,3}$ (dashed) versus time.

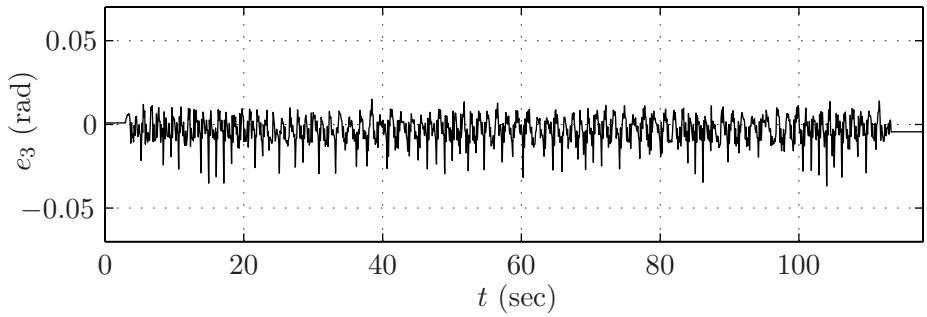

(b) $e_3 = q_3 - h_{d,3}$ versus time.

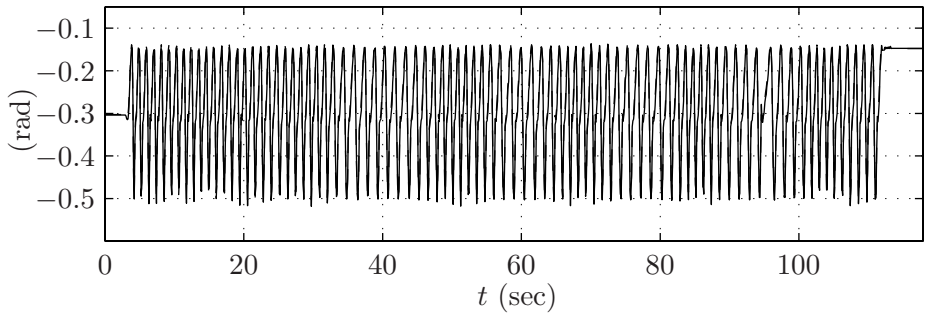

(c) q_4 (solid) and $h_{d,4}$ (dashed) versus time.

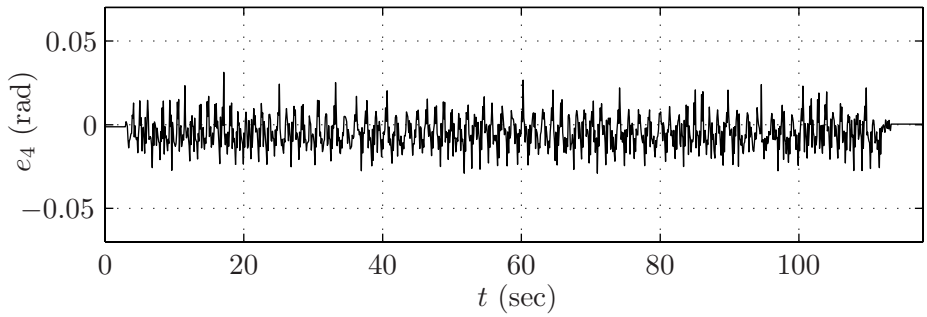

(d) $e_4 = q_4 - h_{d,4}$ versus time.

Figure H.26: I-control to change fixed point: q_3, e_3, q_4, and e_4 versus time.

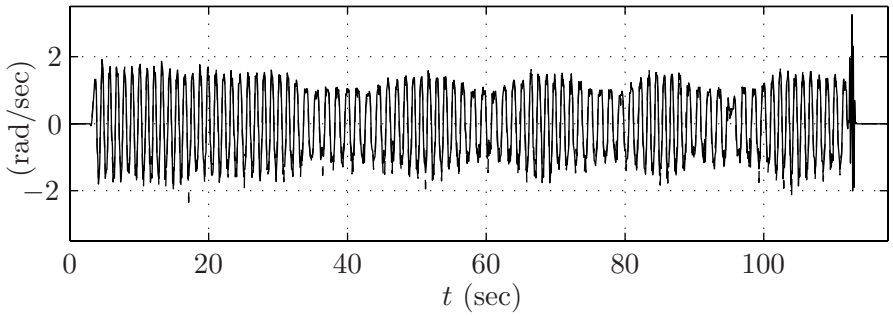

(a) $\dot{q}_1$ (solid) and $(\partial h_{d,1}/\partial\hat{\theta})\dot{\hat{\theta}}$ (dashed) versus time.

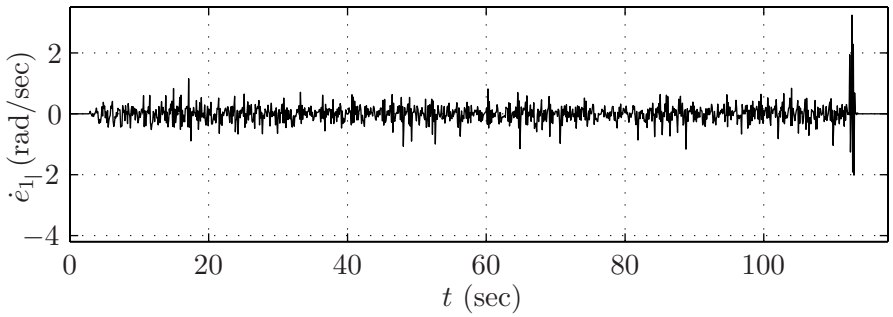

(b) $\dot{e}_1 = \dot{q}_1 - (\partial h_{d,1}/\partial\hat{\theta})\dot{\hat{\theta}}$ versus time.

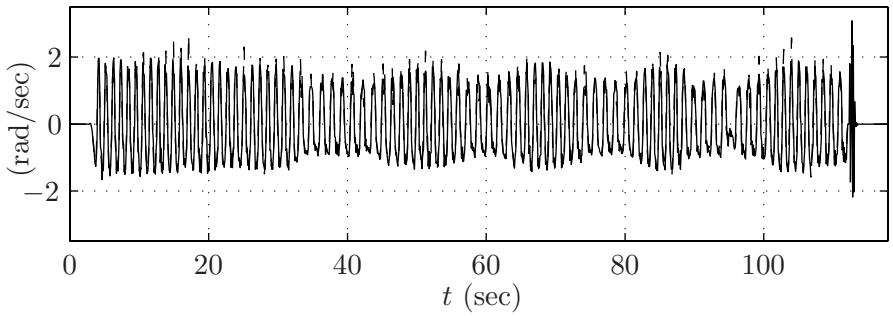

(c) $\dot{q}_2$ (solid) and $(\partial h_{d,2}/\partial\hat{\theta})\dot{\hat{\theta}}$ (dashed) versus time.

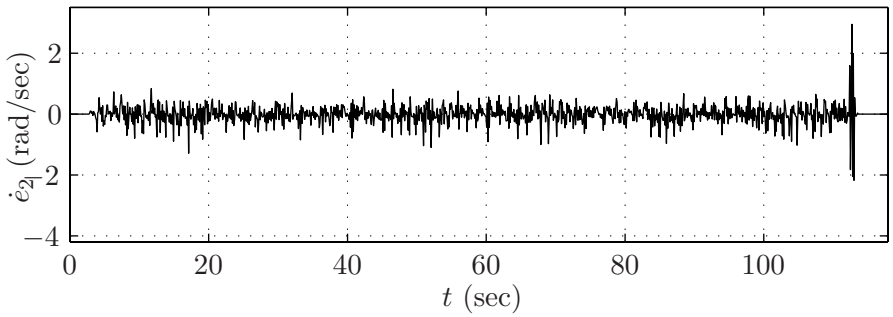

(d) $\dot{e}_2 = \dot{q}_2 - (\partial h_{d,2}/\partial\hat{\theta})\dot{\hat{\theta}}$ versus time.

Figure H.27: I-control to change fixed point: $\dot{q}_1$, $\dot{e}_1$, $\dot{q}_2$, and $\dot{e}_2$ versus time.

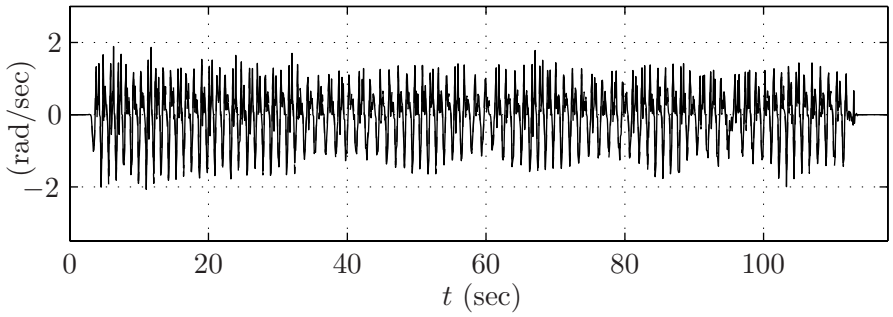

(a) $\dot{q}_3$ (solid) and $(\partial h_{d,3}/\partial\hat{\theta})\dot{\hat{\theta}}$ (dashed) versus time.

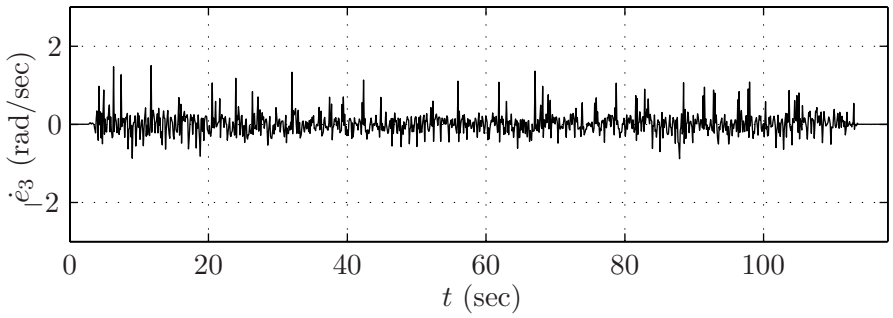

(b) $\dot{e}_3 = \dot{q}_3 - (\partial h_{d,3}/\partial\hat{\theta})\dot{\hat{\theta}}$ versus time.

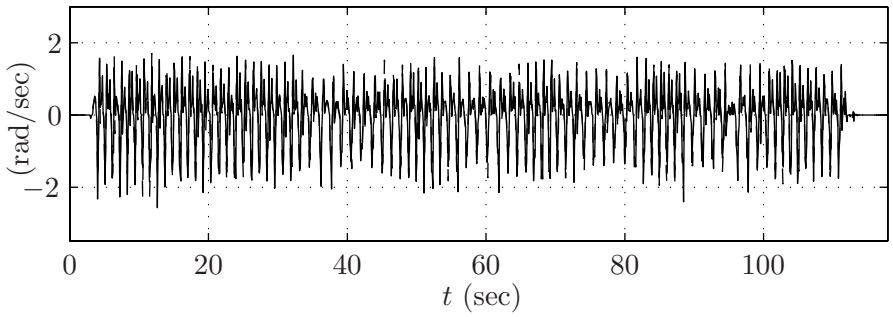

(c) $\dot{q}_4$ (solid) and $(\partial h_{d,4}/\partial\hat{\theta})\dot{\hat{\theta}}$ (dashed) versus time.

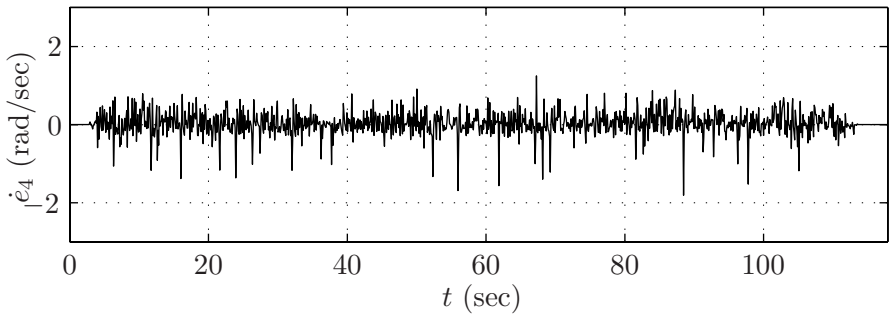

(d) $\dot{e}_4 = \dot{q}_4 - (\partial h_{d,4}/\partial\hat{\theta})\dot{\hat{\theta}}$ versus time.

Figure H.28: I-control to change fixed point: $\dot{q}_3$, $\dot{e}_3$, $\dot{q}_4$, and $\dot{e}_4$ versus time.

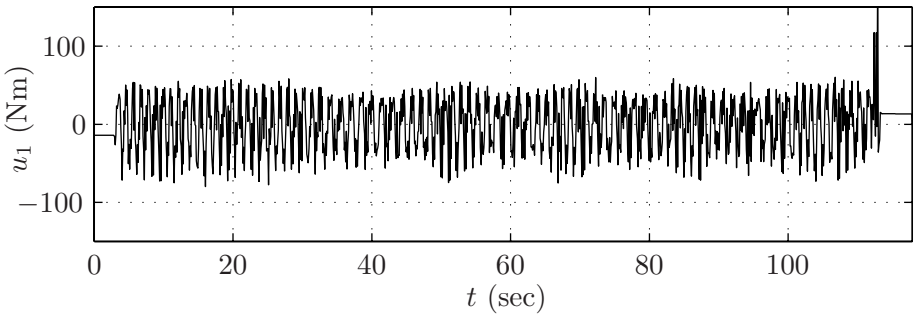

(a) u_1 versus time.

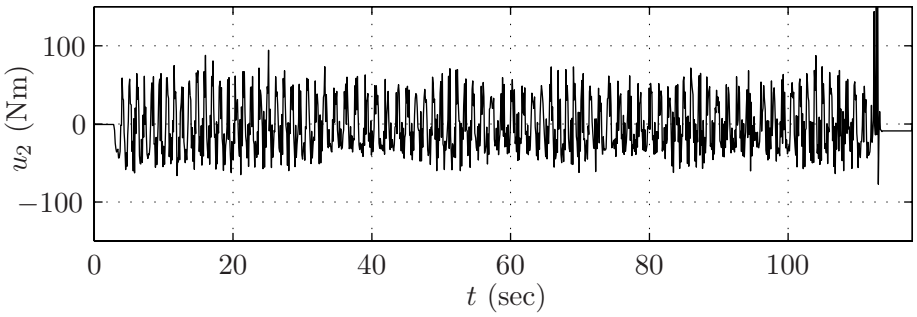

(b) u_2 versus time.

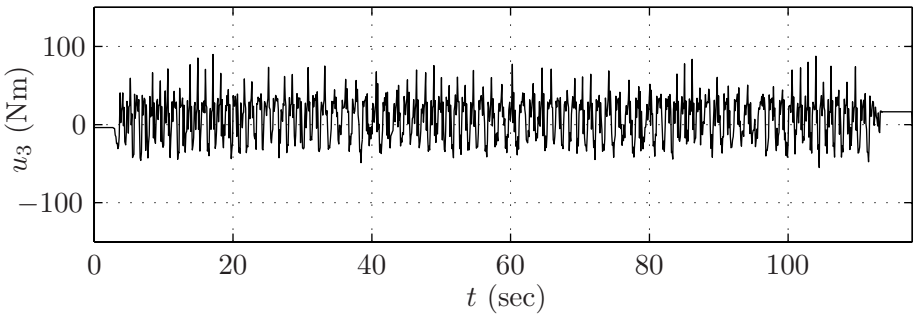

(c) u_3 versus time.

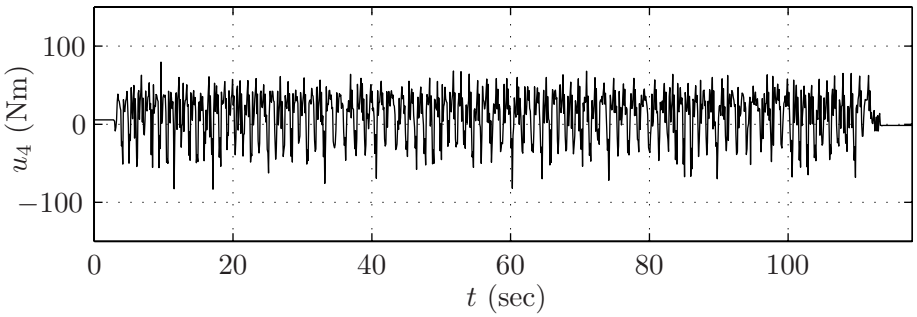

(d) u_4 versus time.

Figure H.29: I-control to change fixed point: u_1, u_2, u_3, and u_4 versus time.

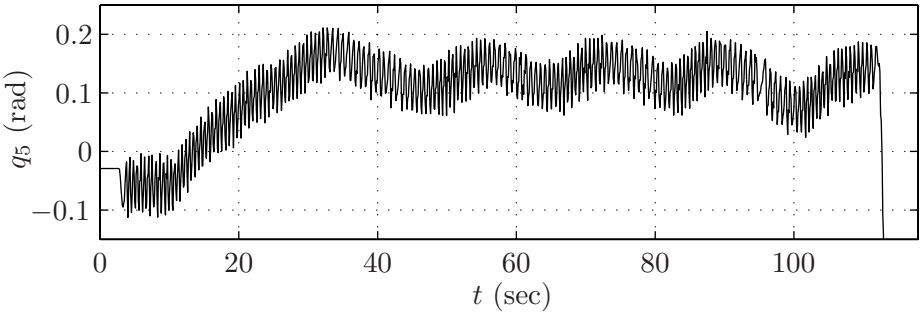

(a) q_5 versus time.

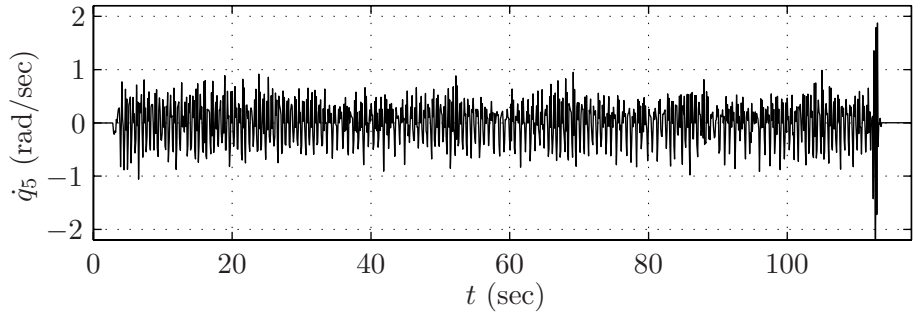

(b) $\dot{q}_5$ versus time.

Figure H.30: I-control to change fixed point: q_5, $\dot{q}_5$ versus time.

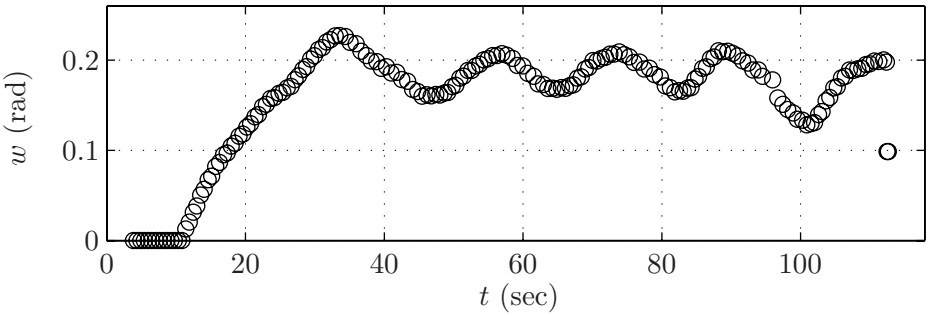

Figure H.31: I-control to change fixed point: w versus time.

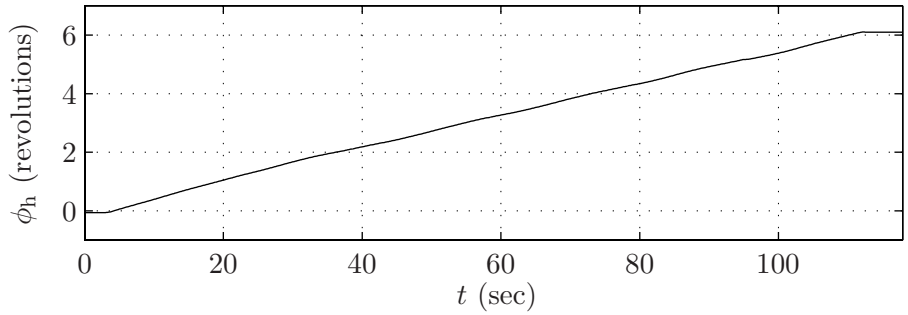

(a) ϕ_{h} versus time.

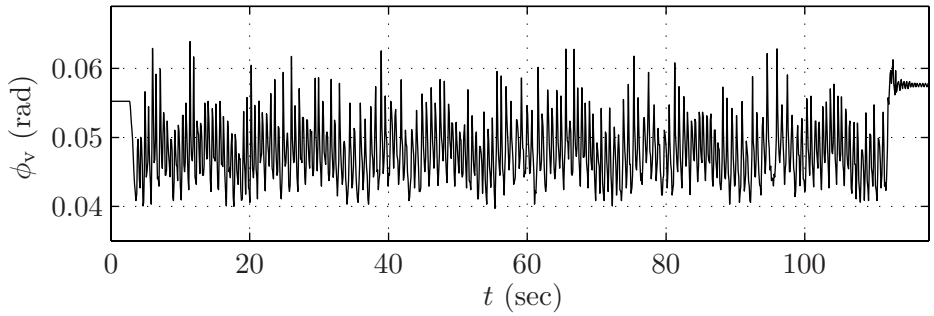

(b) ϕ_{v} versus time (portion of trace).

Figure H.32: I-control to change fixed point: ϕ_{h} and ϕ_{v} versus time.

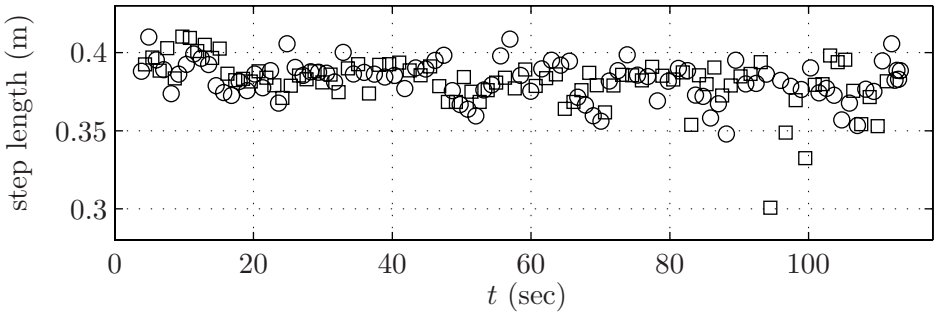

(a) step length versus time.

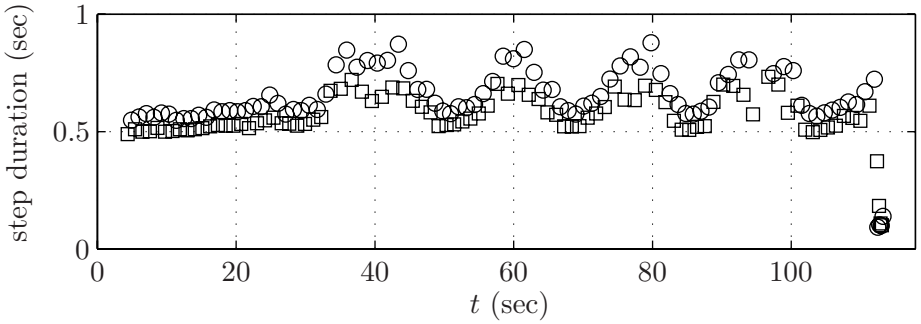

(b) step duration versus time.

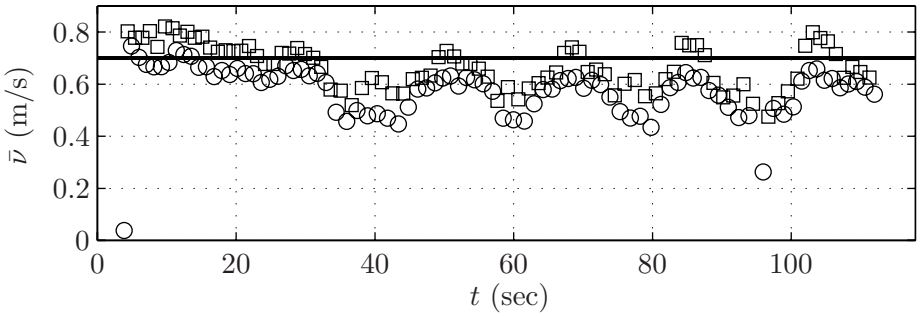

(c) $\bar{\nu}$ = (step length)/(step duration) (circles and squares) and designed $\bar{\nu}$ (solid line) versus time.

Figure H.33: I-control to change fixed point: step length, step duration, and average walking rate versus time. Circles represent steps taken by the outer leg, squares represent steps taken by the inner leg.

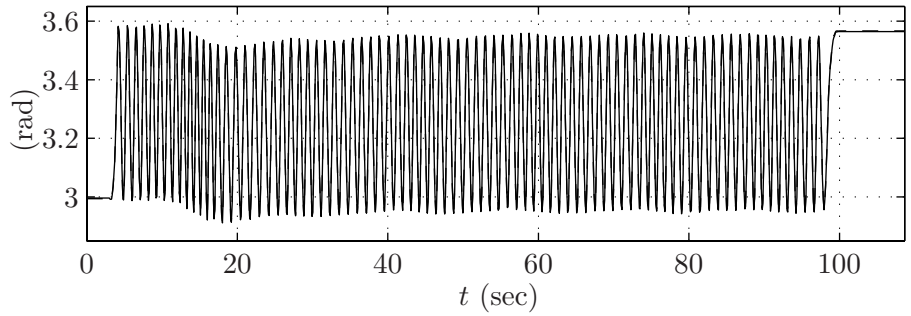

(a) q_1 (solid) and $h_{d,1}$ (dashed) versus time.

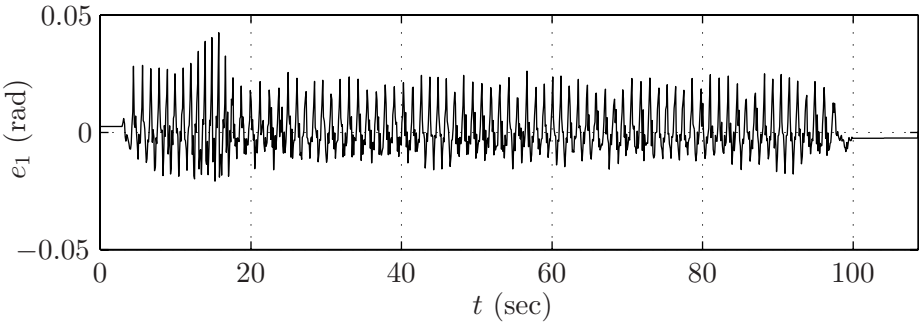

(b) $e_1 = q_1 - h_{d,1}$ versus time.

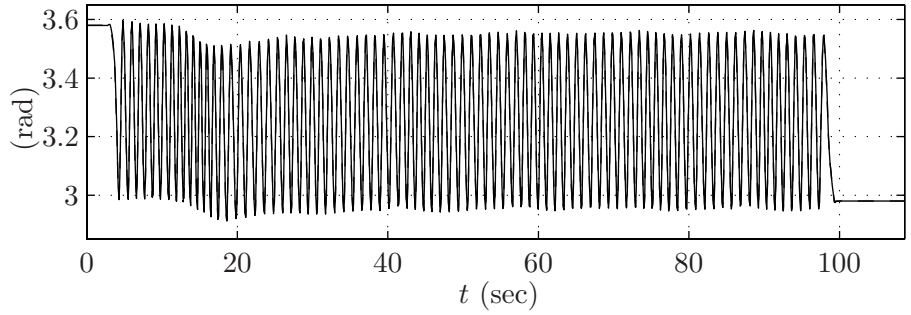

(c) q_2 (solid) and $h_{d,2}$ (dashed) versus time.

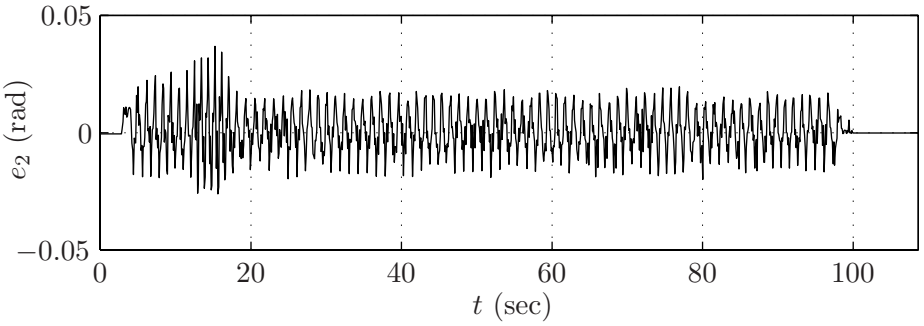

(d) $e_2 = q_2 - h_{d,2}$ versus time.

Figure H.34: I-control to reject a perturbation: q_1, e_1, q_2, and e_2 versus time.

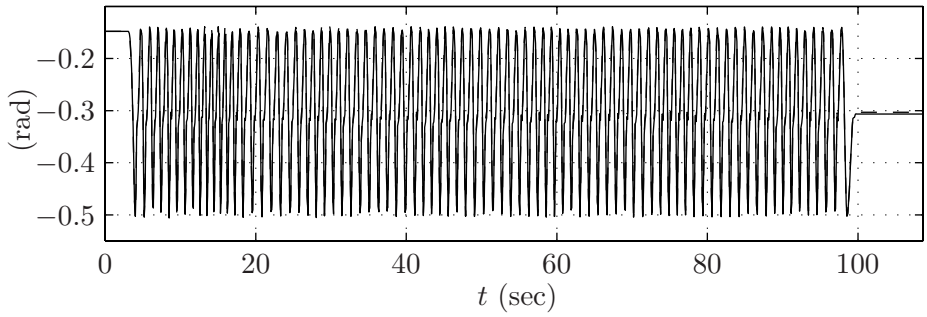

(a) q_3 (solid) and $h_{d,3}$ (dashed) versus time.

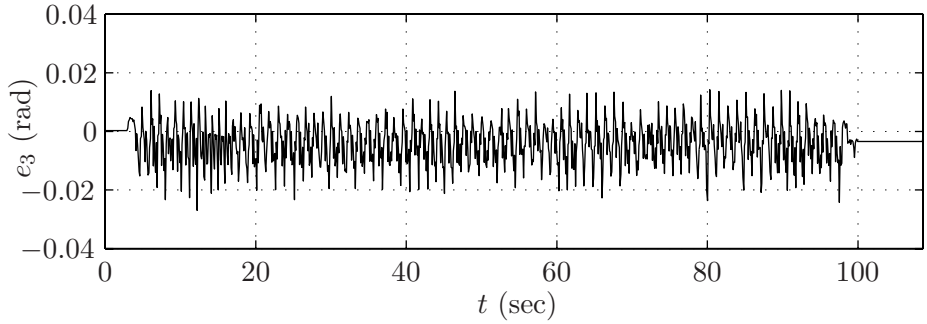

(b) $e_3 = q_3 - h_{d,3}$ versus time.

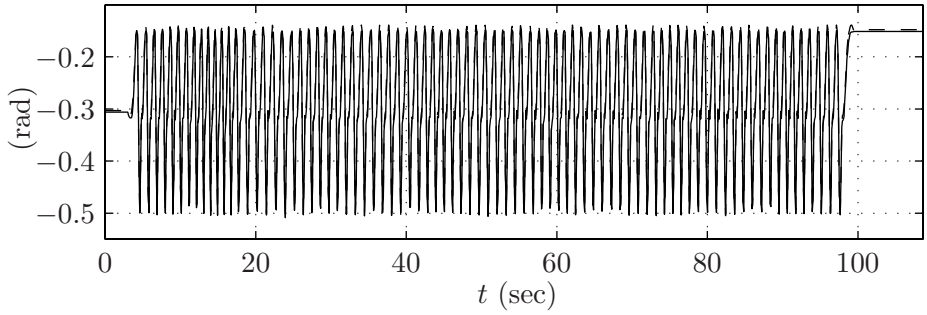

(c) q_4 (solid) and $h_{d,4}$ (dashed) versus time.

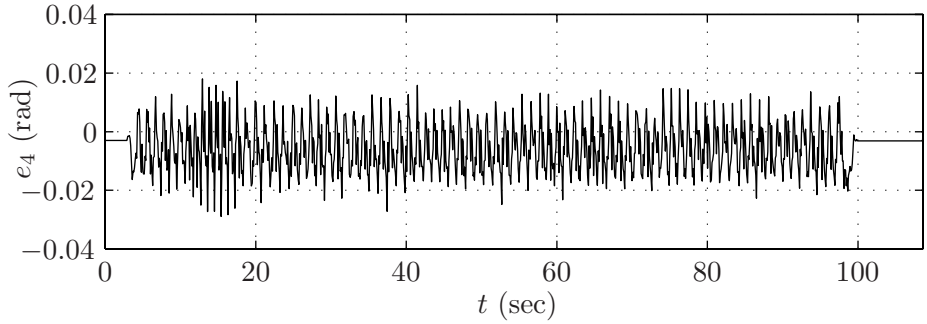

(d) $e_4 = q_4 - h_{d,4}$ versus time.

Figure H.35: I-control to reject a perturbation: q_3, e_3, q_4, and e_4 versus time.

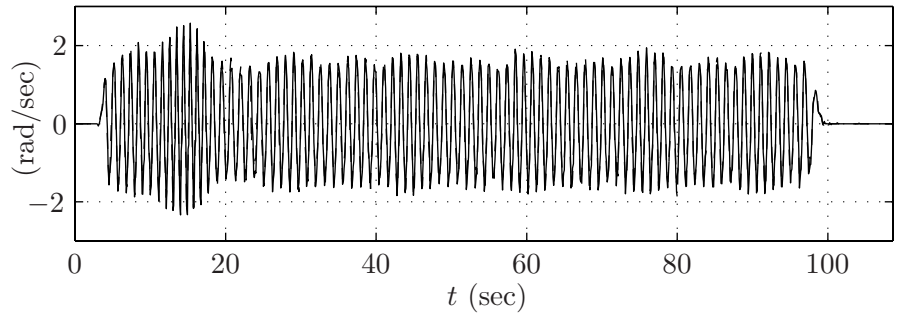

(a) $\dot{q}_1$ (solid) and $(\partial h_{d,1}/\partial\hat{\theta})\dot{\hat{\theta}}$ (dashed) versus time.

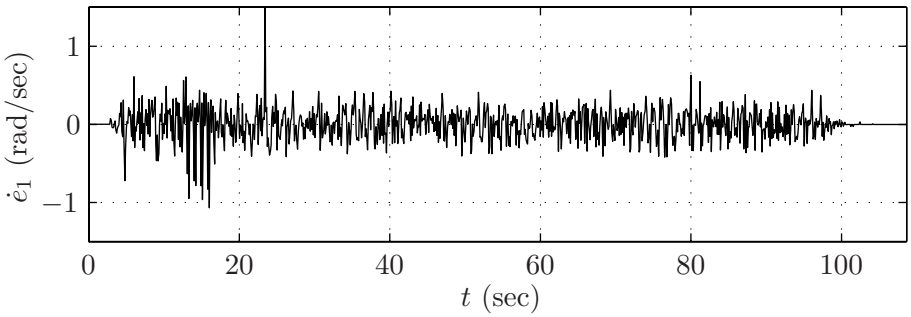

(b) $\dot{e}_1 = \dot{q}_1 - (\partial h_{d,1}/\partial\hat{\theta})\dot{\hat{\theta}}$ versus time.

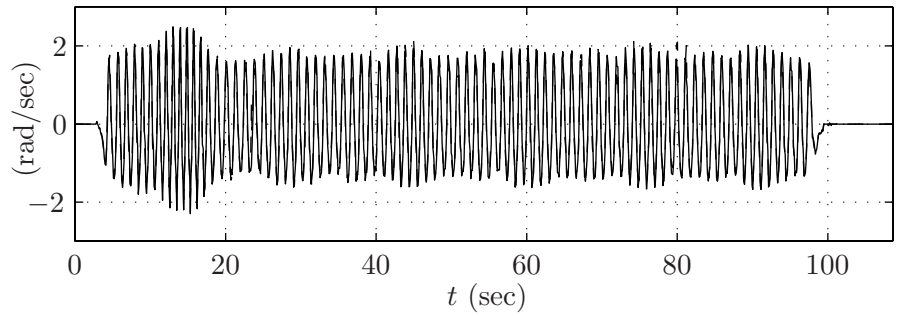

(c) $\dot{q}_2$ (solid) and $(\partial h_{d,2}/\partial\hat{\theta})\dot{\hat{\theta}}$ (dashed) versus time.

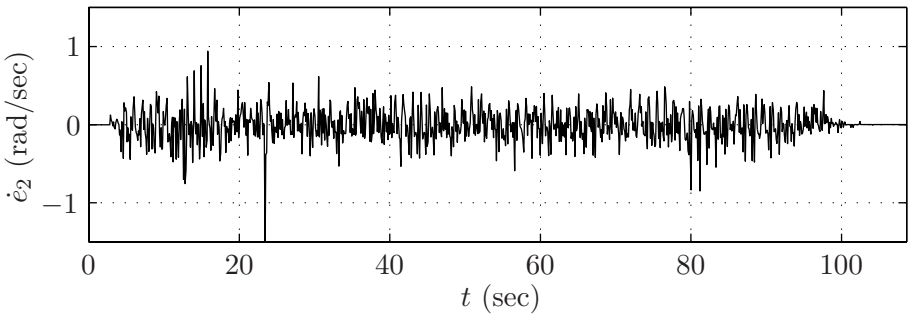

(d) $\dot{e}_2 = \dot{q}_2 - (\partial h_{d,2}/\partial\hat{\theta})\dot{\hat{\theta}}$ versus time.

Figure H.36: I-control to reject a perturbation: $\dot{q}_1$, $\dot{e}_1$, $\dot{q}_2$, and $\dot{e}_2$ versus time.

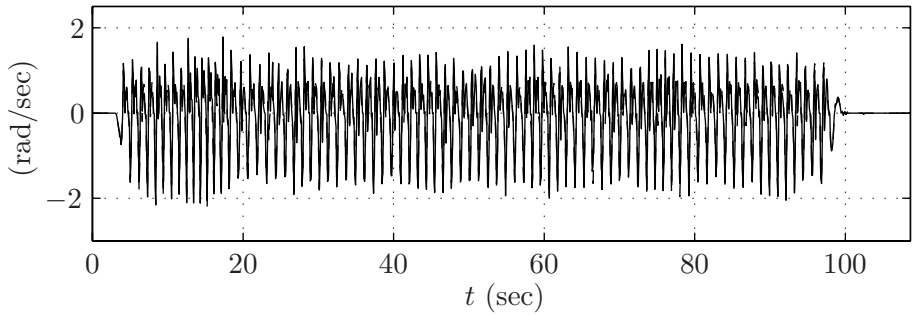

(a) $\dot{q}_3$ (solid) and $(\partial h_{d,3}/\partial\hat{\theta})\dot{\hat{\theta}}$ (dashed) versus time.

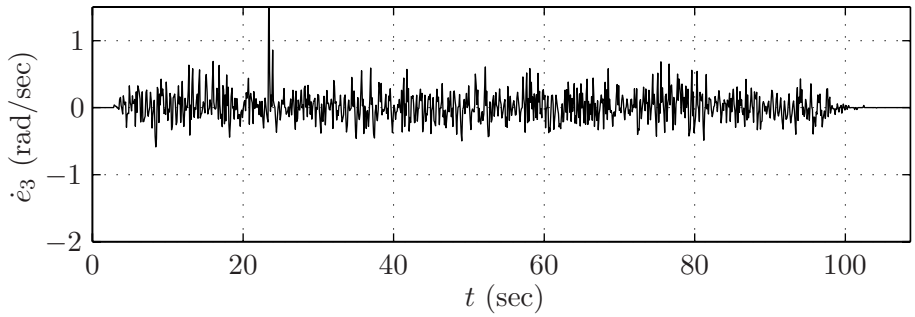

(b) $\dot{e}_3 = \dot{q}_3 - (\partial h_{d,3}/\partial\hat{\theta})\dot{\hat{\theta}}$ versus time.

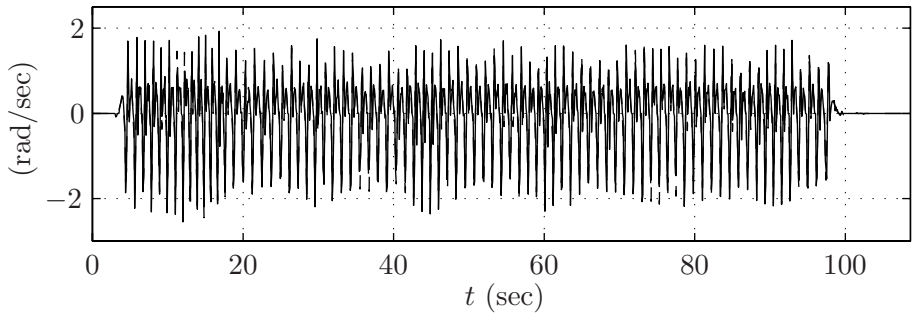

(c) $\dot{q}_4$ (solid) and $(\partial h_{d,4}/\partial\hat{\theta})\dot{\hat{\theta}}$ (dashed) versus time.

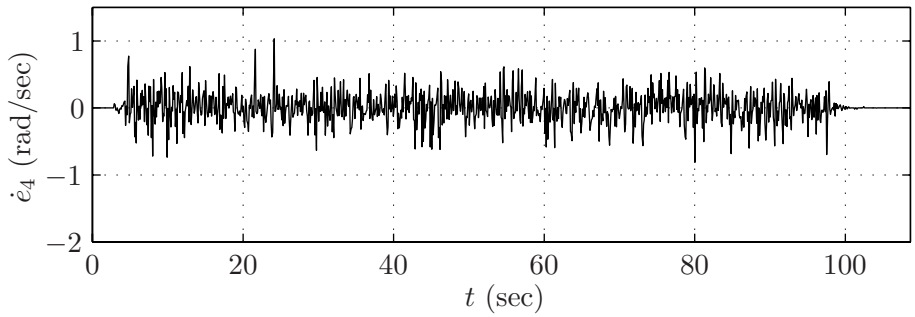

(d) $\dot{e}_4 = \dot{q}_4 - (\partial h_{d,4}/\partial\hat{\theta})\dot{\hat{\theta}}$ versus time.

Figure H.37: I-control to reject a perturbation: $\dot{q}_3$, $\dot{e}_3$, $\dot{q}_4$, and $\dot{e}_4$ versus time.

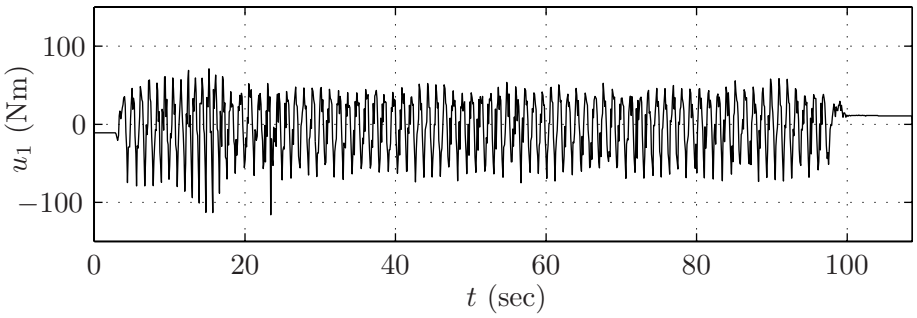

(a) u_1 versus time.

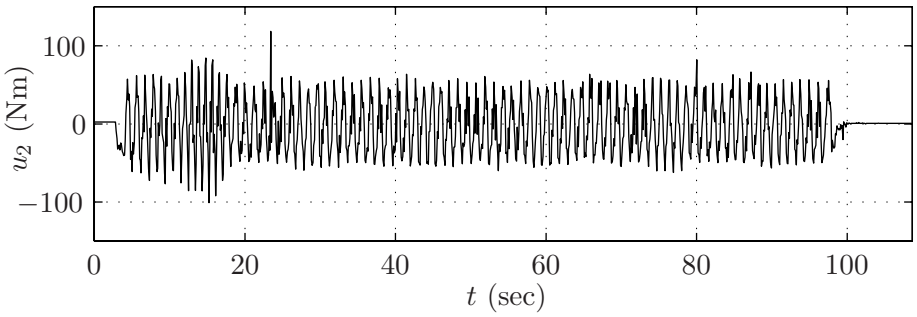

(b) u_2 versus time.

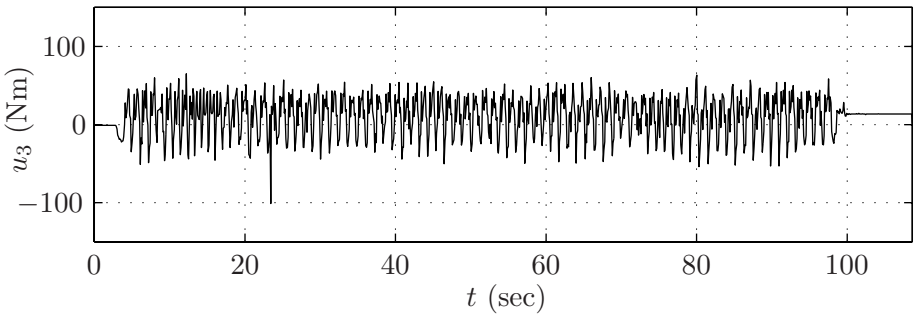

(c) u_3 versus time.

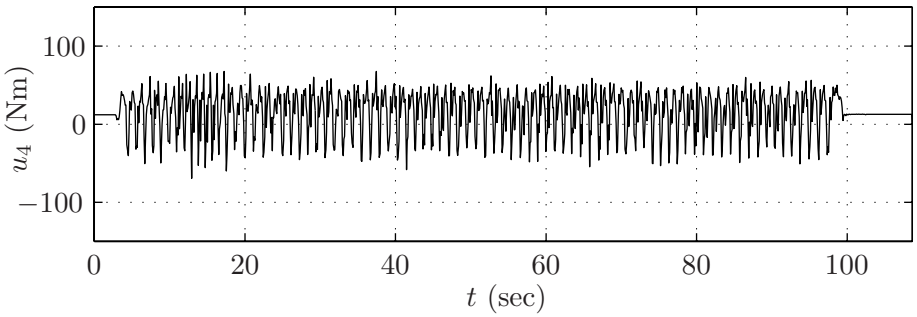

(d) u_4 versus time.

Figure H.38: I-control to reject a perturbation: u_1, u_2, u_3, and u_4 versus time.

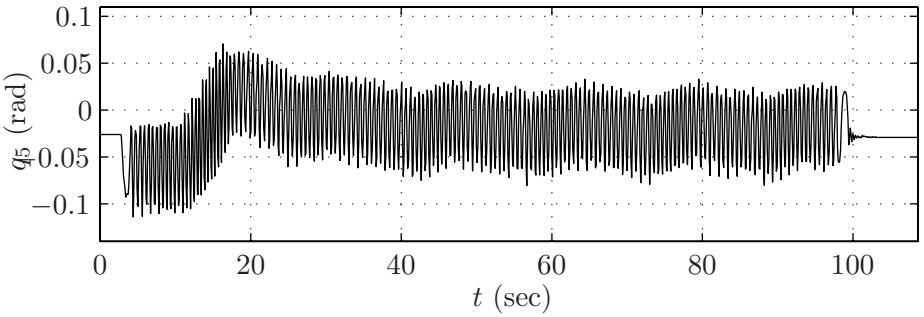

(a) q_5 versus time.

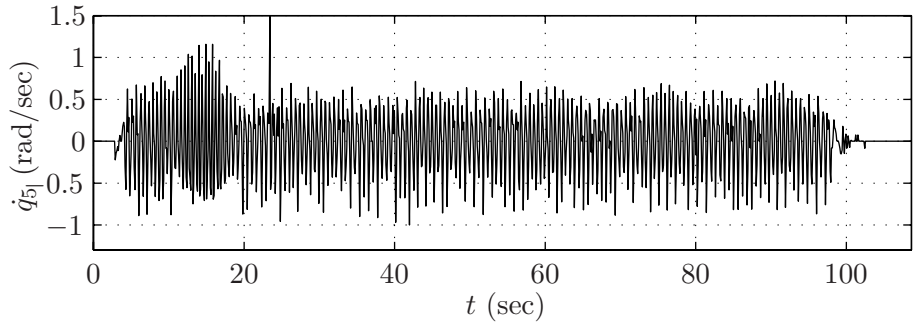

(b) $\dot{q}_5$ versus time.

Figure H.39: I-control to reject a perturbation: q_5, $\dot{q}_5$ versus time.

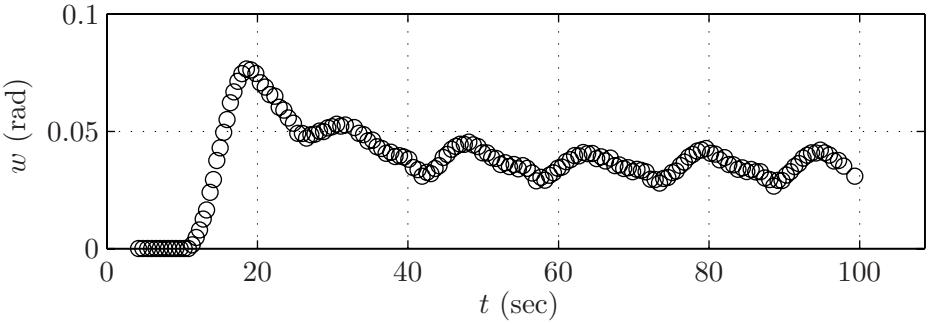

Figure H.40: I-control to reject a perturbation: w versus time.

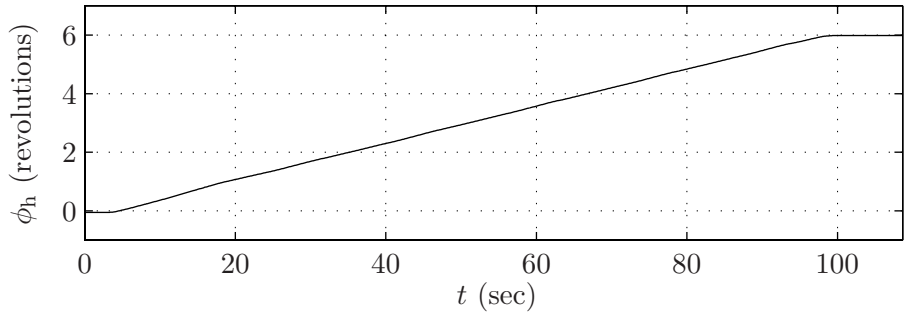

(a) ϕ_{h} versus time.

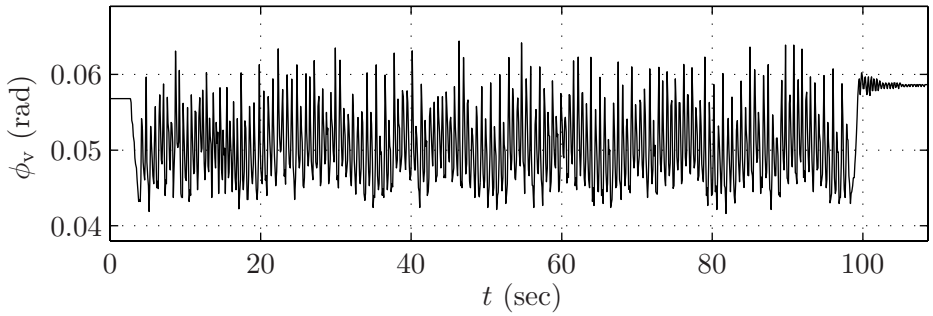

(b) ϕ_{v} versus time (portion of trace).

Figure H.41: I-control to reject a perturbation: ϕ_{h} and ϕ_{v} versus time.

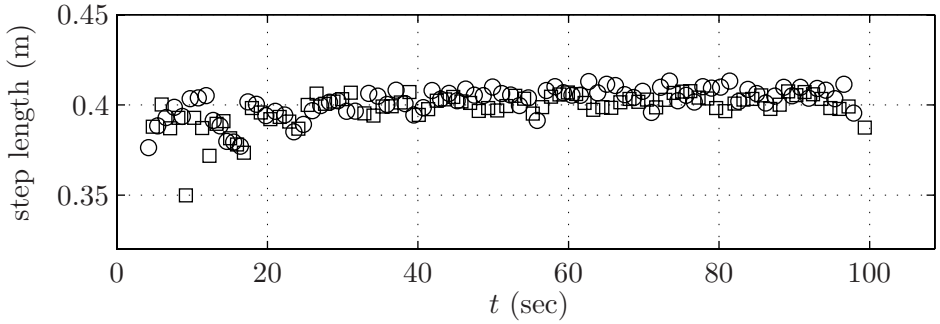

(a) step length versus time.

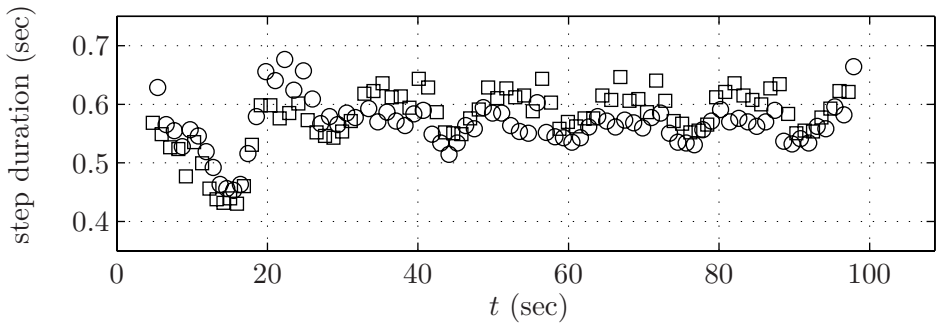

(b) step duration versus time.

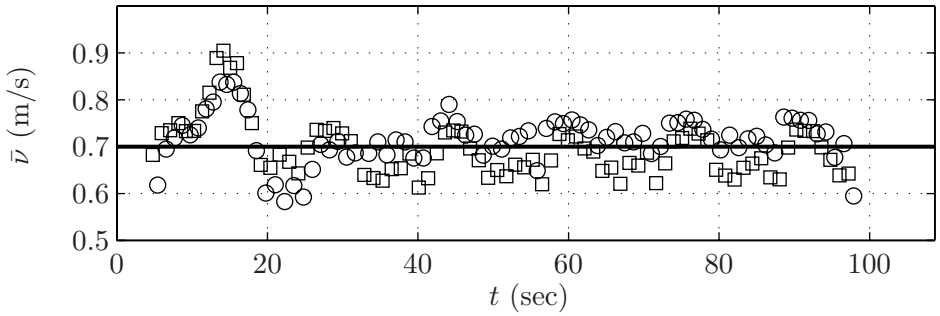

(c) $\bar{\nu}$ = (step length)/(step duration) (circles and squares) and designed $\bar{\nu}$ (solid line) versus time.

Figure H.42: I-control to reject a perturbation: step length, step duration, and average walking rate versus time. Circles represent steps taken by the outer leg, squares represent steps taken by the inner leg.

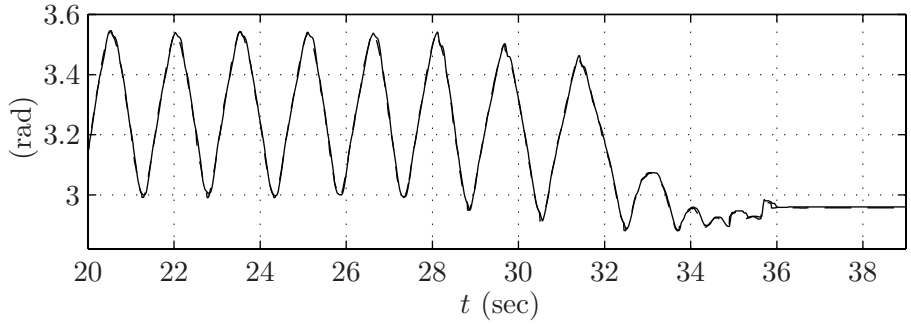

(a) q_1 (solid) and $h_{d,1}$ (dashed) versus time.

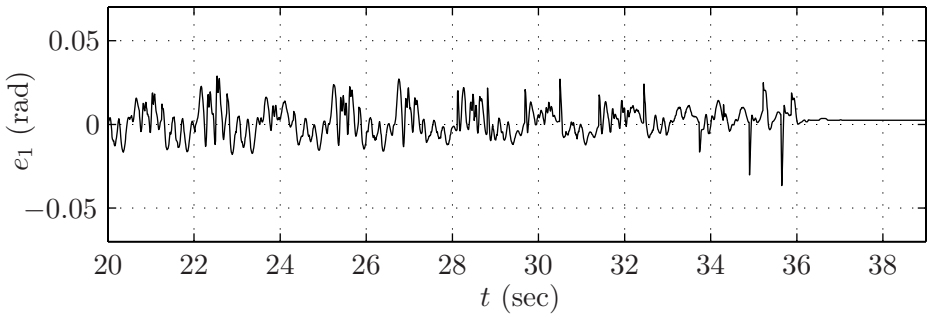

(b) $e_1 = q_1 - h_{d,1}$ versus time.

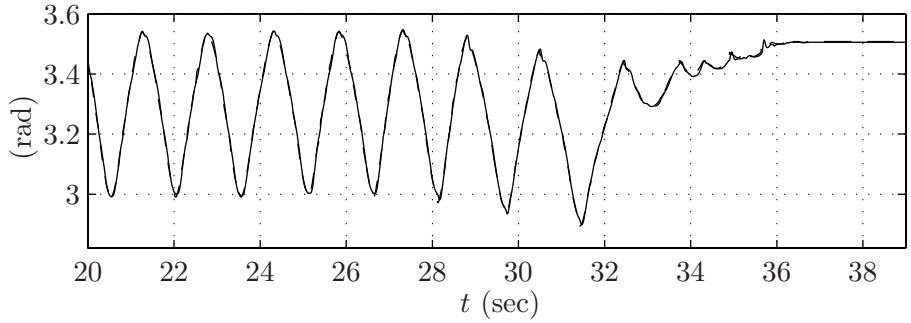

(c) q_2 (solid) and $h_{d,2}$ (dashed) versus time.

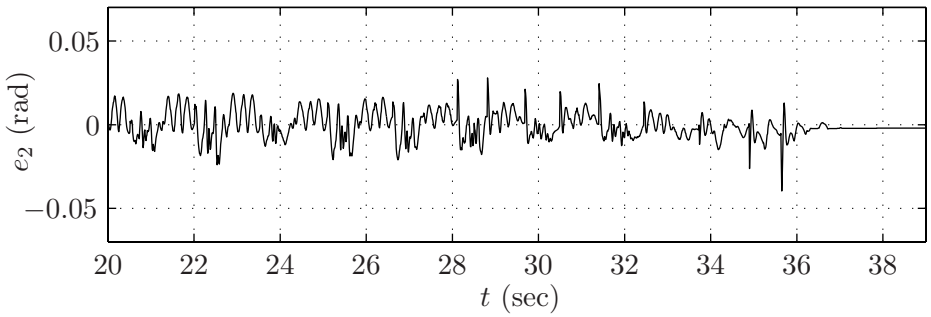

(d) $e_2 = q_2 - h_{d,2}$ versus time.

Figure H.43: I-control to stop the robot: q_1, e_1, q_2, and e_2 versus time.

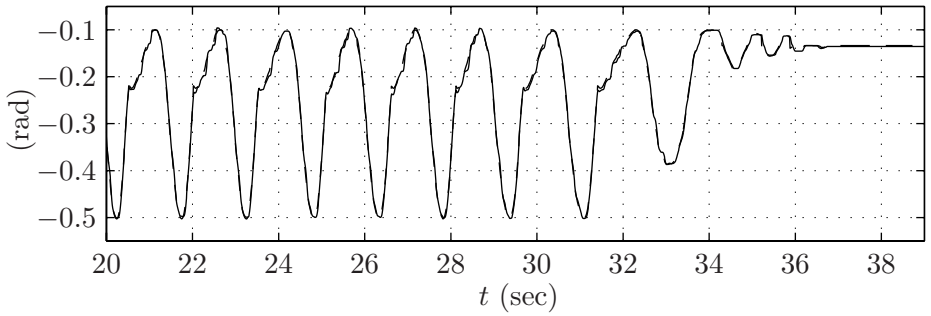

(a) q_3 (solid) and $h_{d,3}$ (dashed) versus time.

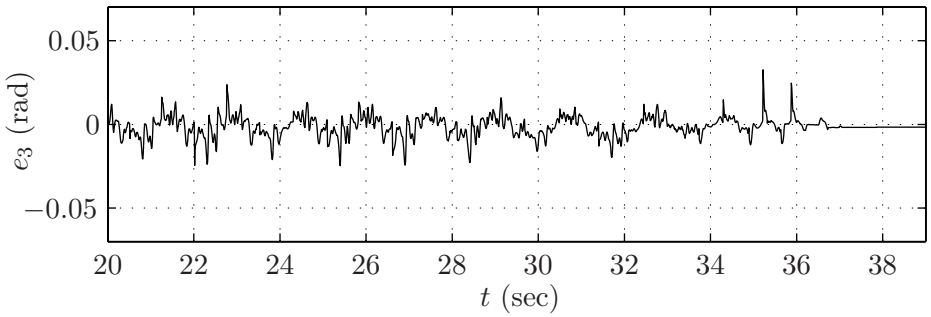

(b) $e_3 = q_3 - h_{d,3}$ versus time.

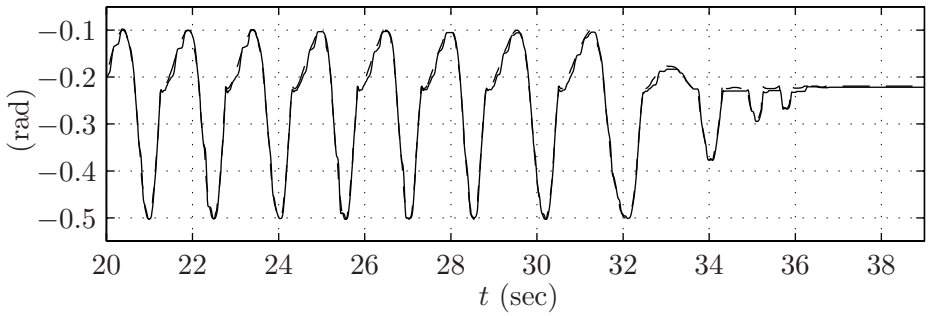

(c) q_4 (solid) and $h_{d,4}$ (dashed) versus time.

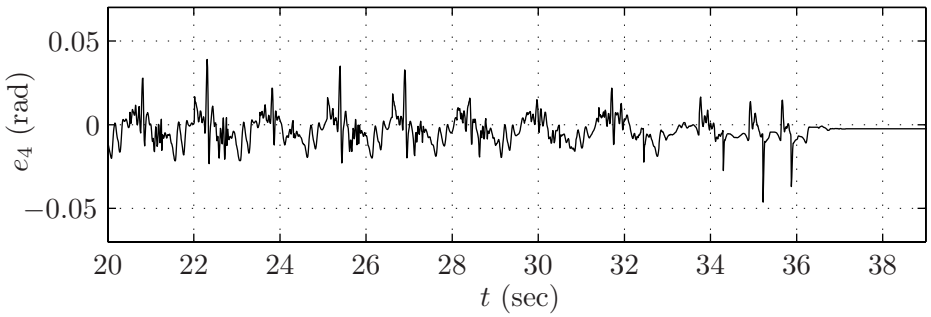

(d) $e_4 = q_4 - h_{d,4}$ versus time.

Figure H.44: I-control to stop the robot: q_3, e_3, q_4, and e_4 versus time.

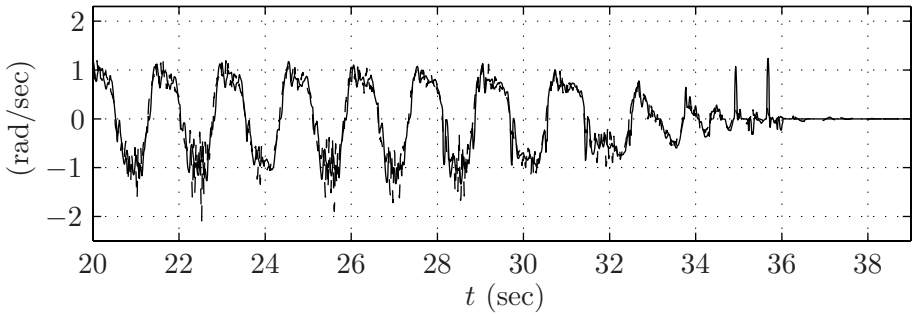

(a) $\dot{q}_1$ (solid) and $(\partial h_{d,1}/\partial\hat{\theta})\dot{\hat{\theta}}$ (dashed) versus time.

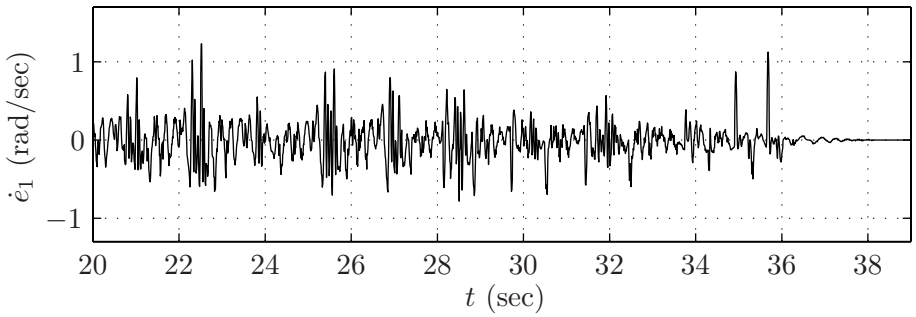

(b) $\dot{e}_1 = \dot{q}_1 - (\partial h_{d,1}/\partial\hat{\theta})\dot{\hat{\theta}}$ versus time.

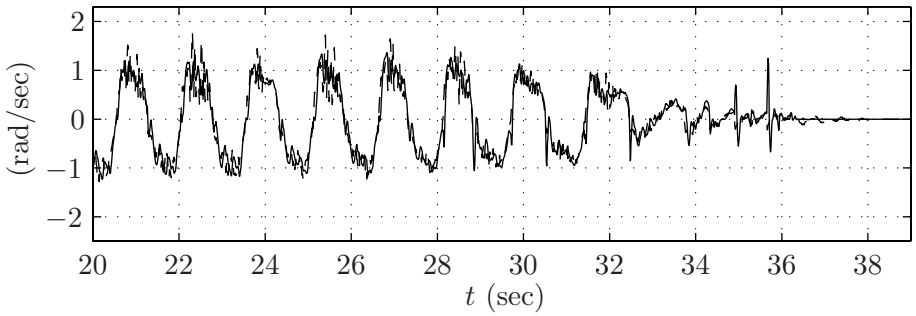

(c) $\dot{q}_2$ (solid) and $(\partial h_{d,2}/\partial\hat{\theta})\dot{\hat{\theta}}$ (dashed) versus time.

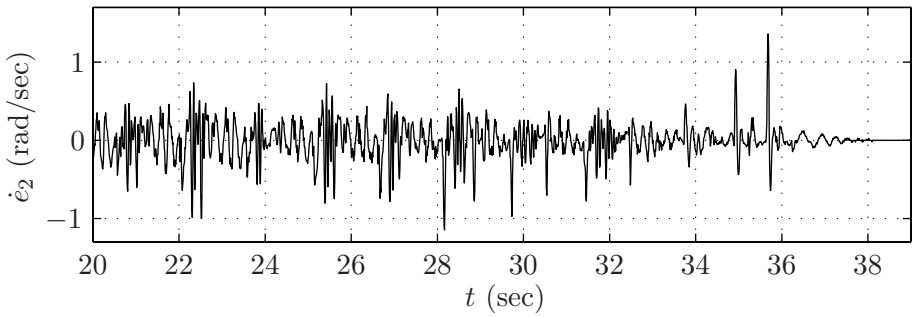

(d) $\dot{e}_2 = \dot{q}_2 - (\partial h_{d,2}/\partial\hat{\theta})\dot{\hat{\theta}}$ versus time.

Figure H.45: I-control to stop the robot: $\dot{q}_1$, $\dot{e}_1$, $\dot{q}_2$, and $\dot{e}_2$ versus time.

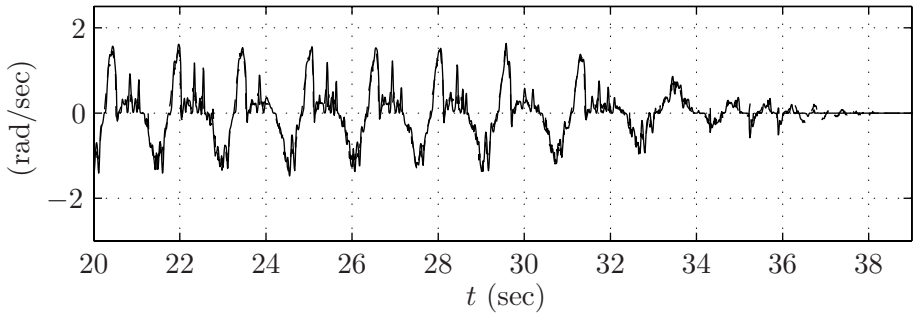

(a) $\dot{q}_3$ (solid) and $(\partial h_{d,3}/\partial\hat{\theta})\dot{\hat{\theta}}$ (dashed) versus time.

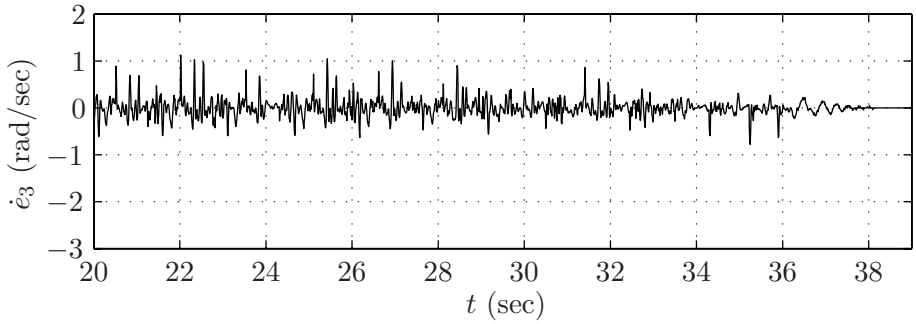

(b) $\dot{e}_3 = \dot{q}_3 - (\partial h_{d,3}/\partial\hat{\theta})\dot{\hat{\theta}}$ versus time.

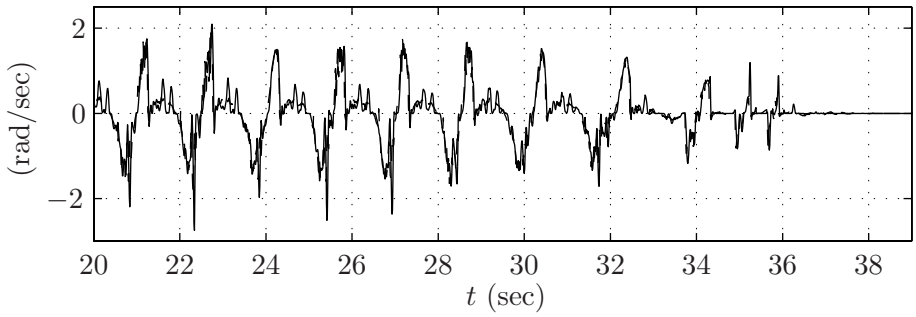

(c) $\dot{q}_4$ (solid) and $(\partial h_{d,4}/\partial\hat{\theta})\dot{\hat{\theta}}$ (dashed) versus time.

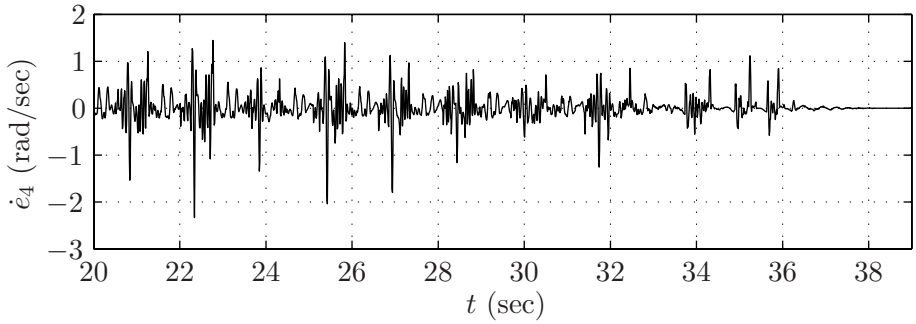

(d) $\dot{e}_4 = \dot{q}_4 - (\partial h_{d,4}/\partial\hat{\theta})\dot{\hat{\theta}}$ versus time.

Figure H.46: I-control to stop the robot: $\dot{q}_3$, $\dot{e}_3$, $\dot{q}_4$, and $\dot{e}_4$ versus time.

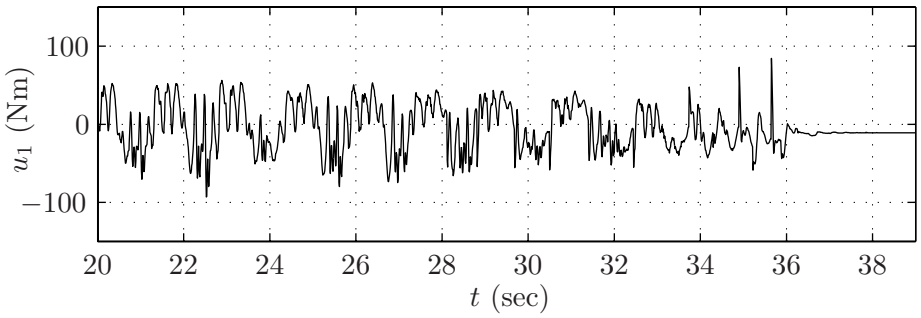

(a) u_1 versus time.

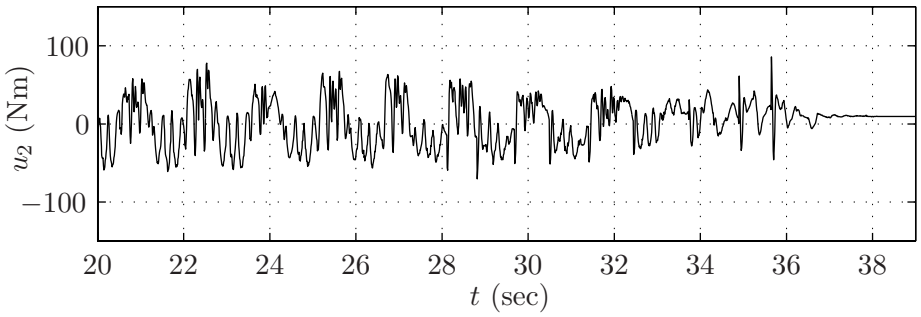

(b) u_2 versus time.

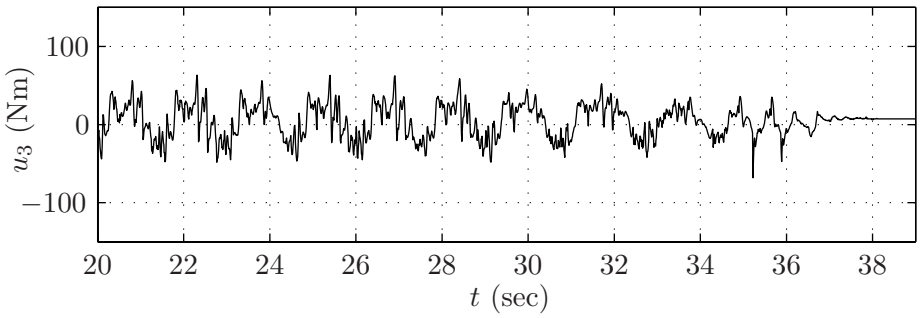

(c) u_3 versus time.

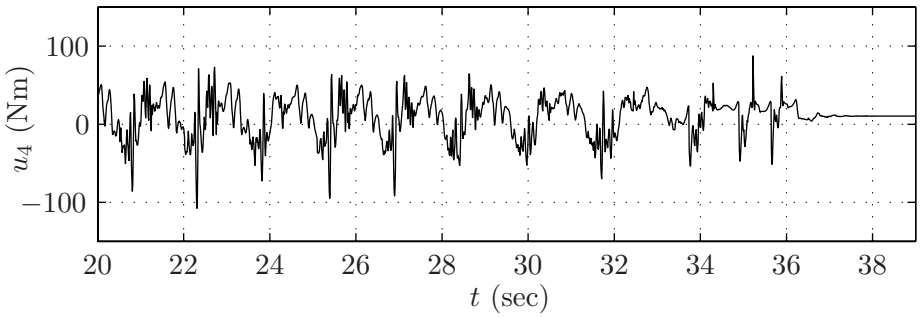

(d) u_4 versus time.

Figure H.47: I-control to stop the robot: u_1, u_2, u_3, and u_4 versus time.

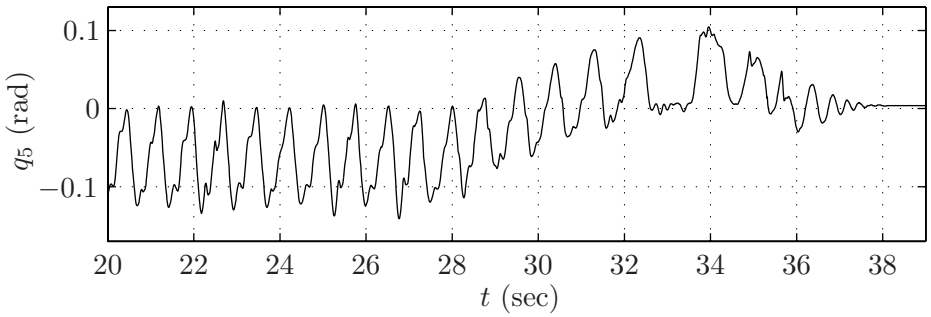

(a) q_5 versus time.

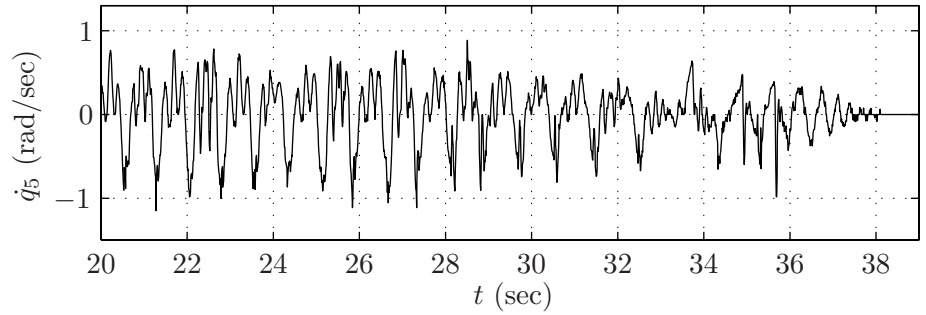

(b) $\dot{q}_5$ versus time.

Figure H.48: I-control to stop the robot: q_5, $\dot{q}_5$ versus time.

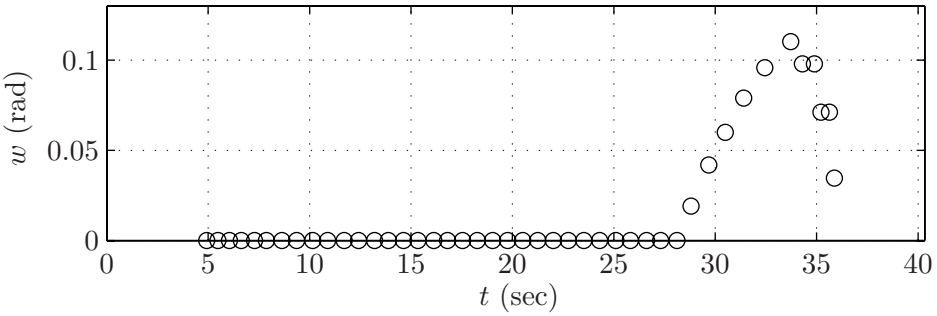

Figure H.49: I-control to stop the robot: w versus time.

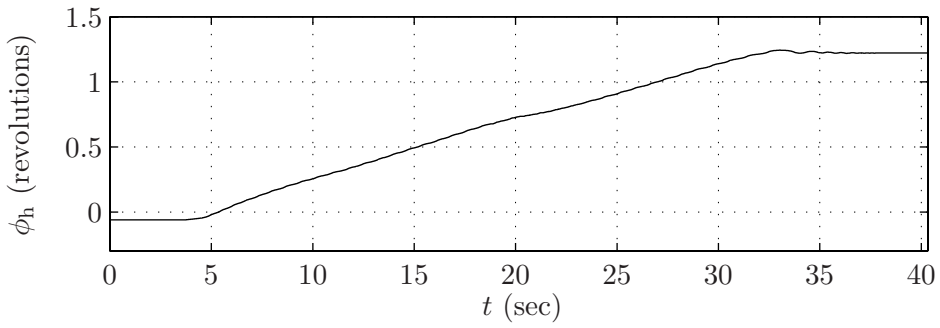

(a) ϕ_h versus time.

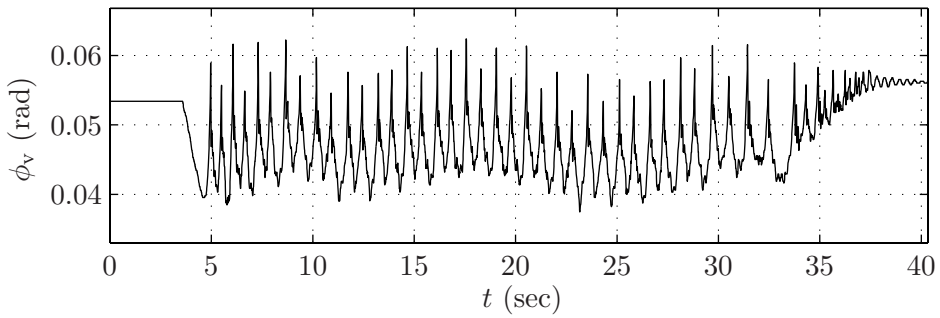

(b) ϕ_v versus time (portion of trace).

Figure H.50: I-control to stop the robot: ϕ_h and ϕ_v versus time.

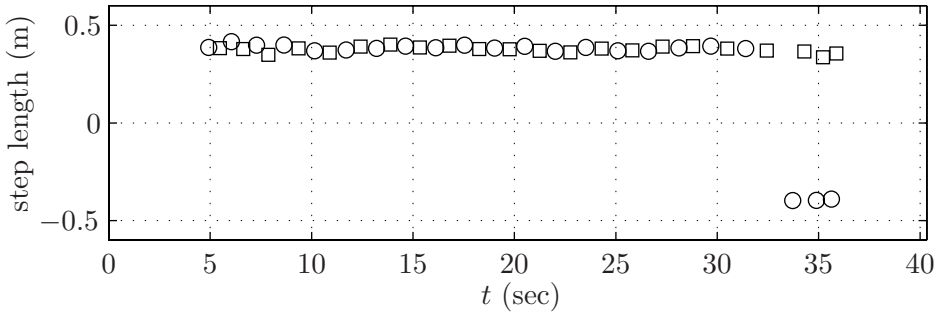

(a) step length versus time.

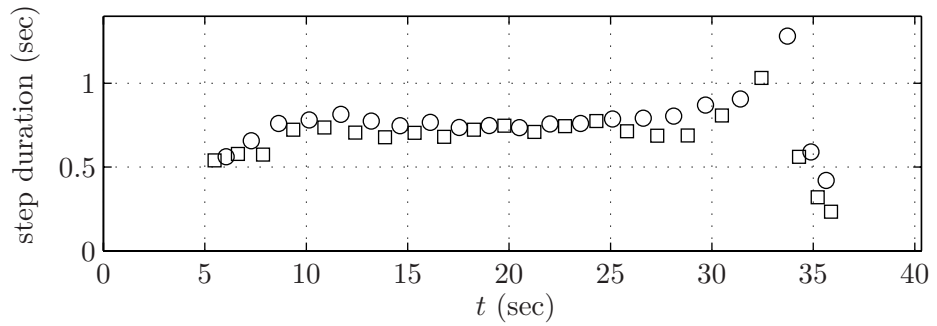

(b) step duration versus time.

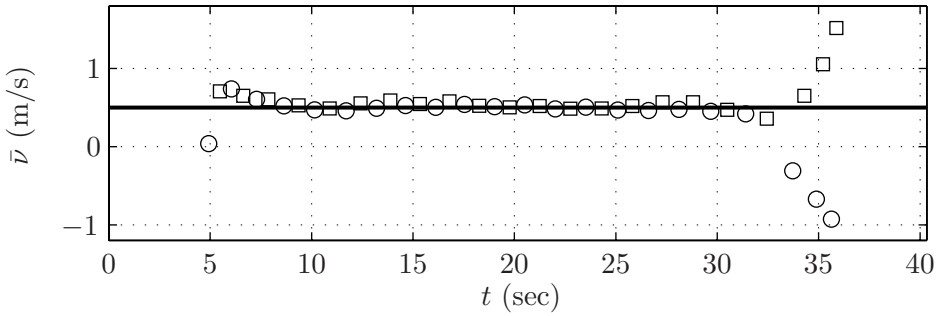

(c) $\bar{\nu}$ = (step length)/(step duration) (circles and squares) and designed $\bar{\nu}$ (solid line) versus time.

Figure H.51: I-control to stop the robot: step length, step duration, and average walking rate versus time. Circles represent steps taken by the outer leg, squares represent steps taken by the inner leg.

APPENDIX I

Extensions to running

This appendix sketches some initial work toward the development of a framework for the control of running in planar biped robots satisfying RH1)–RH5). The approach to the control of running taken here follows the approach to the control of walking taken in the main body of the dissertation. That approach is to impose virtual constrains on the biped's posture to regulate the biped's state to a low dimensional surface within the biped's state space, that is, to design outputs such that the resulting zero dynamics has an asymptotically stable periodic orbit. The appendix begins with a model for running, then continues with the definition of outputs and their corresponding zero dynamics, and concludes with a Poincaré analysis and a comment on the next steps in the development of the framework begun here.

I.1 The model for running

The model for running considered differs from the model for walking given in Chapter 2 in that 1) running has an additional phase of motion, the *flight phase*, when no part of the biped is in contact with the ground, and 2) running does not have a phase of double support. The model of running consists of two phases: the stance phase and the flight phase; and *running* is informally defined as alternating stance and flight phases.

This section gives the models for the stance and flight phases and for the impact that occurs upon leg touchdown at the end of the flight phase. To distinguish objects associated with the models of the stance and flight phases, the labels "s" and "f" will be used as

subscripts.

I.1.1 The stance phase model

The model for the stance phase is the same for running as it is for walking. See Section 2.1 for details of that model.

I.1.2 The flight phase model

The model for the flight phase is similar to the extended model used in the impact model given in Section 2.2. It differs from the extended model in coordinate choice. Here, $q_e := (q', p^{\mathrm{h}}_{\mathrm{COM}}, p^{\mathrm{v}}_{\mathrm{COM}})'$, i.e., q_e is q appended with the Cartesian position of the robot's center of mass (COM) with respect to some world coordinate frame. Note that by coordinate choice, D_e depends only on the shape coordinates, q, and partitions into

$$D_e(q) = \begin{bmatrix} D_{e,11}(q) & 0 \\ 0 & D_{e,22} \end{bmatrix} \tag{I.1}$$

where $D_{e,22}$ is a constant matrix.

The state space of the model is taken as $T\mathcal{Q}_{\mathrm{f}} := \{x_e := (q_e', \dot{q}_e')' \mid q_e \in \mathcal{Q}_{\mathrm{f}},\ \dot{q}_e \in \mathbb{R}^{N+2}\}$, where $\mathcal{Q}_{\mathrm{f}}$ is a simply-connected, open subset of $[0, 2\pi)^N \times \mathbb{R}^2$ corresponding to physically reasonable configurations of the robot such that $p^{\mathrm{v}}_1 \geq 0$ and $p^{\mathrm{v}}_2 \geq 0$, i.e., the leg ends are above the walking surface. The model is written in state space form by defining

$$\dot{x}_e = \begin{bmatrix} \dot{q}_e \\ D_e^{-1}(q_e)\left[-C_e(q_e, \dot{q}_e)\dot{q}_e - G_e(q_e) + B_e u\right] \end{bmatrix} \tag{I.2}$$

$$=: f_{\mathrm{f}}(x_e) + g_{\mathrm{f}}(x_e)u. \tag{I.3}$$

I.1.3 The impact model

The impact model presented in Section 2.2 expressed in the coordinates of Section I.1.2 is used to model the impact that occurs when the end of what was the swing leg during the previous stance phase touches down.

I.1.4 The hybrid model of running

Adopting the notation for hybrid dynamical systems given in [GJ95], the overall biped robot model is expressed as a nonlinear hybrid system containing two charts

$$\Sigma_{\mathrm{s}}: \begin{cases} \mathcal{X}_{\mathrm{s}} &= T\mathcal{Q}_{\mathrm{s}} \\ \mathcal{F}_{\mathrm{s}}: (\dot{x}) &= f_{\mathrm{s}}(x) + g_{\mathrm{s}}(x)u \\ S_{\mathrm{s}}^{\mathrm{f}} &= \{(q,\dot{q}) \in T\mathcal{Q}_{\mathrm{s}} \mid F_1^{\mathrm{N}} = 0\} \\ \mathcal{T}_{\mathrm{s}}^{\mathrm{f}}: (x_e) &= \pi^{-1}(x) \end{cases} \tag{I.4}$$

$$\Sigma_{\mathrm{f}}: \begin{cases} \mathcal{X}_{\mathrm{f}} &= T\mathcal{Q}_{\mathrm{f}} \\ \mathcal{F}_{\mathrm{f}}: (\dot{x}_e) &= f_{\mathrm{f}}(x_e) + g_{\mathrm{f}}(x_e)u \\ S_{\mathrm{f}}^{\mathrm{s}} &= \{(q_e,\dot{q}_e) \in T\mathcal{Q}_{\mathrm{f}} \mid p_2^{\mathrm{v}} = 0,\ p_1^{\mathrm{v}} > 0\} \\ \mathcal{T}_{\mathrm{f}}^{\mathrm{s}}: (x^+) &= \pi \circ \Delta(x_e^-) \end{cases} \tag{I.5}$$

where, $\mathcal{F}_i$ is the flow on chart $\mathcal{X}_i$, S_i^j is the switching surface for transitions between chart i and chart j, $\mathcal{T}_i^j$ is the transition function applied when $x \in S_i^j$,

$$\pi(x_e) := \begin{bmatrix} \pi_q(q_e) \\ \pi_{\dot{q}}\ \dot{q}_e \end{bmatrix}, \tag{I.6}$$

$$\pi^{-1}(x) := \begin{bmatrix} \pi_q^{-1}(q) \\ \pi_{\dot{q}}^{-1}(q)\,\dot{q} \end{bmatrix}, \tag{I.7}$$

and

$$\pi_q(q_e) := q \tag{I.8}$$

$$\pi_{\dot{q}} := \frac{\partial \pi_q}{\partial q_e} \tag{I.9}$$

$$\pi_q^{-1}(q) := (q', p_{\mathrm{COM}}^{\mathrm{h}}(q), p_{\mathrm{COM}}^{\mathrm{v}}(q))' \tag{I.10}$$

$$\pi_{\dot{q}}^{-1}(q) := \frac{\partial \pi_q^{-1}}{\partial q}. \tag{I.11}$$

A transition from chart $\mathcal{X}_{\mathrm{s}}$ to chart $\mathcal{X}_{\mathrm{f}}$ occurs when the normal force on the stance leg end vanishes. A transition from chart $\mathcal{X}_{\mathrm{f}}$ to chart $\mathcal{X}_{\mathrm{s}}$ occurs when the end of what was the swing leg during the previous stance phase touches down. It is assumed that the control signals are continuous upon switching from chart $\mathcal{X}_{\mathrm{s}}$ to chart $\mathcal{X}_{\mathrm{f}}$.

I.2 Stance phase zero dynamics

Following the development in Chapter 4, define an output on (2.4) as

$$y_{\mathrm{s}} = h_{\mathrm{s}}(q) := h_{\mathrm{s},0}(q) - h_{\mathrm{s},d} \circ \theta_{\mathrm{s}}(q) \tag{I.12}$$

where $h_{\mathrm{s},0}(q)$ specifies $(N-1)$ independent quantities that are to be controlled and $h_{\mathrm{s},d} \circ \theta_{\mathrm{s}}(q)$ specifies the desired evolution of these quantities as a function of the monotonic quantity

$$\theta_{\mathrm{s}}(q) := cq. \tag{I.13}$$

Let $h_{\mathrm{s},d}$ be as in (4.8) so that $h(q)$ is finitely parameterized by α_{s}, the output's Bézier polynomial's coefficients. Define

$$\gamma_{\mathrm{s}}(q, \dot{q}) := \gamma_{0,\mathrm{s}}(q)\dot{q} \tag{I.14}$$

where $\gamma_{0,\mathrm{s}}(q)$ is the last row of D, and assume that h_{s} satisfies HH2)–HH4). Then, the stance phase zero dynamics manifold is

$$Z_{\mathrm{s}} := \{x \in T\tilde{\mathcal{Q}}_{\mathrm{s}} \mid h_{\mathrm{s}}(x) = 0, L_{f_{\mathrm{s}}} h_{\mathrm{s}}(x) = 0\}. \tag{I.15}$$

where $\tilde{\mathcal{Q}}_{\mathrm{s}}$ is defined in HH2), and

$$\begin{aligned} \eta_{\mathrm{s},1} &:= h_{\mathrm{s}}(q), \quad \eta_{\mathrm{s},2} := L_{f_{\mathrm{s}}} h_{\mathrm{s}}(q, \dot{q}), \\ \xi_{1,\mathrm{s}} &:= \theta_{\mathrm{s}}(q), \quad \xi_{2,\mathrm{s}} := \gamma_{\mathrm{s}}(q, \dot{q}), \end{aligned} \tag{I.16}$$

is a valid coordinate transformation on Z_{s}. Since $L_{g_{\mathrm{s}}}\theta_{\mathrm{s}} = 0$ and $L_{g_{\mathrm{s}}}\gamma_{\mathrm{s}} = 0$, the zero dynamics of the stance phase are

$$\begin{aligned} \dot{\xi}_{1,\mathrm{s}} &= L_{f_{\mathrm{s}}}\theta_{\mathrm{s}} \\ \dot{\xi}_{2,\mathrm{s}} &= L_{f_{\mathrm{s}}}\gamma_{\mathrm{s}} \end{aligned} \tag{I.17}$$

where the right hand side is evaluated at

$$q = \Phi_{\mathrm{s}}^{-1}(0, \xi_{1,\mathrm{s}}) \tag{I.18}$$

$$\dot{q} = \Psi_{\mathrm{s}}^{-1}(q) \begin{bmatrix} 0 \\ \\ \xi_{2,\mathrm{s}} \end{bmatrix} \tag{I.19}$$

with

$$\Phi_{\mathrm{s}}(q) := \begin{bmatrix} h_{\mathrm{s}} \\ \theta_{\mathrm{s}} \end{bmatrix} \tag{I.20}$$

$$\Psi_{\mathrm{s}}(q) := \begin{bmatrix} \frac{\partial h_{\mathrm{s}}}{\partial q} \\ \gamma_{0,\mathrm{s}} \end{bmatrix}. \tag{I.21}$$

From Theorem 3.1, zero dynamics of the stance phase are known to have the form

$$\dot{\xi}_{1,\mathrm{s}} = \kappa_{1,\mathrm{s}}(\xi_{1,\mathrm{s}})\xi_{2,\mathrm{s}} \tag{I.22}$$

$$\dot{\xi}_{2,\mathrm{s}} = \kappa_{2,\mathrm{s}}(\xi_{2,\mathrm{s}}), \tag{I.23}$$

and, from the results in Section 3.5, may be integrated to obtain

$$\xi^2_{2,\mathrm{s}}(t) = \xi^2_{2,\mathrm{s}}(0) + 2\int_{\theta_{\mathrm{s}}^+}^{\theta_{\mathrm{s}}^-} \frac{\kappa_{2,\mathrm{s}}(\theta)}{\kappa_{1,\mathrm{s}}(\theta)} d\theta \tag{I.24}$$

where θ_{s}^+ and θ_{s}^- are, respectively, the values of θ_{s} at the beginning and end of the stance phase.

I.3 Flight phase zero dynamics

Paralleling the development for the stance phase zero dynamics, define an output on (I.3)

$$y_{\mathrm{f}} = h_{\mathrm{f}}(q_e) := h_{\mathrm{f},0}(q_e) - h_{\mathrm{f},d} \circ \theta_{\mathrm{f}}(q_e) \tag{I.25}$$

with $h_{\mathrm{f},0}$ and $h_{\mathrm{f},d}$ defined analogously to $h_{\mathrm{f},0}$ and $h_{\mathrm{f},d}$ with

$$\theta_{\mathrm{f}}(q_e) := p^{\mathrm{h}}_{\mathrm{COM}} \tag{I.26}$$

Here, $h_{\mathrm{f},d}$ is finitely parameterized by α_{f}. Assume that h_{f} satisfies HH2)–HH4) and define

$$\gamma_{\mathrm{f}}(q_e, \dot{q}_e) := \gamma_{0,\mathrm{f}}(q_e)\dot{q}_e \tag{I.27}$$

where $\gamma_{0,\mathrm{f}}(q_e)$ is the N^{th} row of D_e. Then, the flight phase zero dynamics manifold is

$$Z_{\mathrm{f}} := \{x_e \in T\tilde{\mathcal{Q}}_{\mathrm{f}} \mid h_{\mathrm{f}}(x_e) = 0, L_{f_{\mathrm{f}}} h_{\mathrm{f}}(x_e) = 0\}. \tag{I.28}$$

where $\tilde{\mathcal{Q}}_{\mathrm{f}}$ is defined in HH2), and

$$\begin{aligned}
\eta_{\mathrm{f},1} &:= h_{\mathrm{f}}(q), \quad & \eta_{\mathrm{f},2} &:= L_{f_{\mathrm{f}}} h_{\mathrm{f}}(q,\dot{q}), \\
\xi_{1,\mathrm{f}} &:= q_N, & \xi_{4,\mathrm{f}} &:= \gamma_{\mathrm{f}}, \\
\xi_{2,\mathrm{f}} &:= p^{\mathrm{h}}_{\mathrm{COM}}, & \xi_{5,\mathrm{f}} &:= \dot{p}^{\mathrm{h}}_{\mathrm{COM}}, \\
\xi_{3,\mathrm{f}} &:= p^{\mathrm{v}}_{\mathrm{COM}}, & \xi_{6,\mathrm{f}} &:= \dot{p}^{\mathrm{v}}_{\mathrm{COM}},
\end{aligned} \tag{I.29}$$

is a valid coordinate transformation on Z_{f}. Since

$$\begin{aligned}
L_{g_{\mathrm{f}}} q_N &= 0, & L_{g_{\mathrm{f}}} \gamma_{\mathrm{f}} &= 0, \\
L_{g_{\mathrm{f}}} p^{\mathrm{h}}_{\mathrm{COM}} &= 0, & L_{g_{\mathrm{f}}} \dot{p}^{\mathrm{h}}_{\mathrm{COM}} &= 0, \\
L_{g_{\mathrm{f}}} p^{\mathrm{v}}_{\mathrm{COM}} &= 0, & L_{g_{\mathrm{f}}} \dot{p}^{\mathrm{v}}_{\mathrm{COM}} &= 0,
\end{aligned} \tag{I.30}$$

the zero dynamics of the flight phase are

$$\begin{aligned}
\dot{\xi}_{1,\mathrm{f}} &= L_{f_{\mathrm{f}}} q_N, & \dot{\xi}_{4,\mathrm{f}} &= 0, \\
\dot{\xi}_{2,\mathrm{f}} &= \xi_{5,\mathrm{f}}, & \dot{\xi}_{5,\mathrm{f}} &= 0, \\
\dot{\xi}_{3,\mathrm{f}} &= \xi_{6,\mathrm{f}}, & \dot{\xi}_{6,\mathrm{f}} &= -g_0,
\end{aligned} \tag{I.31}$$

where $L_{f_{\mathrm{f}}} q_N$ is evaluated at

$$q_e = \Phi_{\mathrm{f}}^{-1}(0, \xi_{1,\mathrm{f}}, \xi_{3,\mathrm{f}}, \xi_{5,\mathrm{f}}) \tag{I.32}$$

$$\dot{q}_e = \Psi_{\mathrm{f}}^{-1}(q_e) \begin{bmatrix} 0 \\ \xi_{2,\mathrm{f}} \\ \xi_{4,\mathrm{f}} \\ \xi_{6,\mathrm{f}} \end{bmatrix}. \tag{I.33}$$

with

$$\Phi_{\mathrm{f}}(q_e) := \begin{bmatrix} h_{\mathrm{f}} \\ q_N \\ \theta_{\mathrm{f}} \\ p^{\mathrm{v}}_{\mathrm{COM}} \end{bmatrix} \tag{I.34}$$

$$\Psi_{\mathrm{f}}(q_e) := \begin{bmatrix} \frac{\partial h_{\mathrm{f}}}{\partial q_e} \\ \gamma_{0,\mathrm{f}} \\ \begin{bmatrix} 0 & I \end{bmatrix} \end{bmatrix}. \tag{I.35}$$

The zero dynamics of the flight phase take the form

$$\dot{\xi}_{1,\mathrm{f}} = \kappa_{1,\mathrm{f}}(\xi_{4,\mathrm{f}}, \xi_{2,\mathrm{f}}, \xi_{5,\mathrm{f}}, \xi_{6,\mathrm{f}}) \tag{I.36}$$

$$\dot{\xi}_{4,\mathrm{f}} = 0 \tag{I.37}$$

$$\ddot{\xi}_{2,\mathrm{f}} = 0 \tag{I.38}$$

$$\ddot{\xi}_{3,\mathrm{f}} = -g_0 \tag{I.39}$$

Equation (I.36) is the dynamics of the absolute coordinate. Equation (I.37) reflects a nonholonomic constraint, conservation of the angular momentum γ_{f}. Equations (I.38) and (I.39) correspond to the ballistic COM dynamics.

Aside from the absolute coordinate's dynamics, integration of the flight phase zero dynamics is trivial. Integration of (I.37) yields the expected conservation law

$$\xi_{4,\mathrm{f}}(t) = \gamma_{\mathrm{f}}(0). \tag{I.40}$$

Integration of the the COM dynamics yields

$$\xi_{5,\mathrm{f}}(t) = \dot{p}^{\mathrm{h}}_{\mathrm{COM}}(0) \tag{I.41}$$

$$\xi_{6,\mathrm{f}}(t) = -g_0 t + \dot{p}^{\mathrm{v}}_{\mathrm{COM}}(0) \tag{I.42}$$

$$\xi_{2,\mathrm{f}}(t) = (\dot{p}^{\mathrm{h}}_{\mathrm{COM}}(0))t + p^{\mathrm{h}}_{\mathrm{COM}}(0) \tag{I.43}$$

$$\xi_{3,\mathrm{f}}(t) = -\frac{g_0}{2}t^2 + (\dot{p}^{\mathrm{v}}_{\mathrm{COM}}(0))t + p^{\mathrm{v}}_{\mathrm{COM}}(0) \tag{I.44}$$

These results along with the observation that $\kappa_{1,\mathrm{f}}$ is independent of $\xi_{6,\mathrm{f}}$ allows (I.36) to be written as

$$\dot{\xi}_{1,\mathrm{f}} = \kappa_{1,\mathrm{f}}(\gamma_{\mathrm{f}}(0), \xi_{2,\mathrm{f}}, \dot{p}^{\mathrm{h}}_{\mathrm{COM}}(0)). \tag{I.45}$$

Since $\xi_{2,\mathrm{f}}$ is monotonic whenever the robot is moving forward, (I.45) may be written as

$$\frac{d\xi_{1,\mathrm{f}}}{dt}\frac{dt}{d\xi_{2,\mathrm{f}}} = \kappa_{1,\mathrm{f}}(\gamma_{\mathrm{f}}(0), \xi_{2,\mathrm{f}}, \dot{p}^{\mathrm{h}}_{\mathrm{COM}}(0))\frac{1}{\dot{p}^{\mathrm{h}}_{\mathrm{COM}}(0)} \tag{I.46}$$

so that integration yields

$$\int_{q_N(0)}^{\xi_{1,\mathrm{f}}(t)} d\xi_{1,\mathrm{f}} = \frac{1}{\dot{p}^{\mathrm{h}}_{\mathrm{COM}}(0)} \int_{p^{\mathrm{h}}_{\mathrm{COM}}(0)}^{p^{\mathrm{h}}_{\mathrm{COM}}(t)} \kappa_{1,\mathrm{f}}(\gamma_{\mathrm{f}}(0), \xi_{2,\mathrm{f}}, \dot{p}^{\mathrm{h}}_{\mathrm{COM}}(0)) d\xi_{2,\mathrm{f}} \tag{I.47}$$

which yields

$$\xi_{1,\mathrm{f}}(t) = q_N(0) + \frac{1}{\dot{p}^{\mathrm{h}}_{\mathrm{COM}}(0)} \int_{p^{\mathrm{h}}_{\mathrm{COM}}(0)}^{p^{\mathrm{h}}_{\mathrm{COM}}(t)} \kappa_{1,\mathrm{f}}(\gamma_{\mathrm{f}}(0), \xi_{2,\mathrm{f}}, \dot{p}^{\mathrm{h}}_{\mathrm{COM}}(0)) d\xi_{2,\mathrm{f}}. \tag{I.48}$$

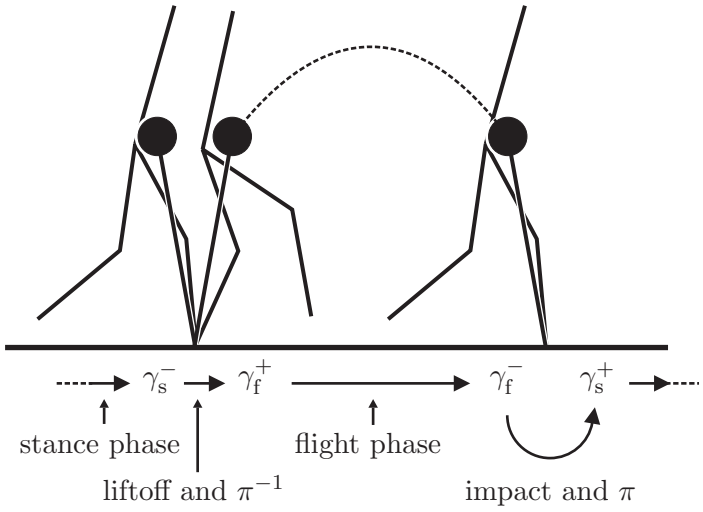

Figure I.1: Sketch of the running cycle

I.4 Achieving boundary conditions via deadbeat control

Assume that the output parameters α_s and α_f are chosen such that there exists a periodic orbit corresponding to $y_s \equiv 0$ and $y_f \equiv 0$, i.e., the periodic orbit evolves on Z_s and Z_f. In particular, assume the following orbit conditions hold,

OC1) at the boundary of the stance and flight phases $F_1^N = 0$,

OC2) at the boundary of the stance and flight phases the shape coordinates $q_1, \ldots, q_{N-1}$ are continuous up to their second derivatives (ensuring that the control signals will be continuous), and

OC3) upon impact (upon transition from the flight phase to the stance phase), the state is mapped from a point in Z_f to a point in Z_s.

It is assumed that the parameters α_s can be made differentiable functions of γ_f^+ (the value of γ_f at the end of the flight phase; see Figure I.1) and that the parameters α_f can be made differentiable functions of γ_s^- (the value of γ_s at the end of the stance phase; see Figure I.1) such that the following conditions on the parameters hold

PC1) $Z_s \cap S_s^f$ is a one-dimensional smooth embedded submanifold of $T\mathcal{Q}_s$ and can be parameterized by γ_s^-,

PC2) $Z_{\rm f} \cap S_{\rm f}^{\rm s}$ is a one-dimensional smooth embedded submanifold of $T\mathcal{Q}_{\rm f}$ and can be parameterized by $\gamma_{\rm f}^-$, and

PC3) the orbit conditions OC1)–OC3) are met in an open set of $Z_{\rm s} \cap S_{\rm s}^{\rm f}$.

I.4.1 Flight phase duration

The desired landing configuration at the end of the flight phase depends only on $\xi_{1,\rm f}$ and $\xi_{3,\rm f}$ (if the constraints encoded in $h_{\rm f}$ are scaled according to the flight time). The parameters $\alpha_{\rm f}$ are chosen so that $\xi_{1,\rm f}$ and $\xi_{3,\rm f}$ at the end of the flight phase are some desired, fixed values,

$$\xi_{1,\rm f}(t_f) = q_N^{\rm d} \tag{I.49}$$

$$\xi_{3,\rm f}(t_f) = p_{\rm COM}^{\rm v,d} \tag{I.50}$$

where t_f is the flight time which may be calculated from (I.44) to be

$$t_f = \frac{\dot{p}_{\rm COM}^{\rm v}(0)}{g_0} + \frac{1}{g_0}\sqrt{\left(\dot{p}_{\rm COM}^{\rm v}(0)\right)^2 + 2g_0\left(p_{\rm COM}^{\rm v}(0) - p_{\rm COM}^{\rm v,d}\right)}. \tag{I.51}$$

If $p_{\rm COM}^{\rm v,d}$ is chosen to be equal to $p_{\rm COM}^{\rm v}(0)$ (i.e., the COM height at the end of the flight phase be the same as at the beginning of the of the flight phase) then the calculation of t_f simplifies to

$$t_f = \frac{2}{g_0}\,\dot{p}_{\rm COM}^{\rm h}(0). \tag{I.52}$$

I.5 A Poincaré analysis

The Poincaré section will be chosen as $S_{\rm s}^{\rm f}$, corresponding to the set where $F_{\rm 1}^{\rm N} = 0$ at the end of the stance phase. Under the assumptions of Section I.4, the Poincaré map is a map from real line back to itself: At the end of the stance phase the velocity is given by

$$\dot{q}_{\rm s}^- = \Psi_{\rm s}^{-1}(q_{\rm s}^-)\begin{bmatrix} 0 \\ \\ 1 \end{bmatrix}\gamma_{\rm s}^-. \tag{I.53}$$

At the beginning of the flight phase the velocity is given by

$$\dot{q}_{e,\rm f}^+ = \pi_{\dot{q}}^{-1}(q_{\rm s}^-)\,\Psi_{\rm s}^{-1}(q_{\rm s}^-)\begin{bmatrix} 0 \\ \\ 1 \end{bmatrix}\gamma_{\rm s}^-. \tag{I.54}$$

At the end of the flight phase the velocity is given by

$$\dot{q}_{e,\mathrm{f}}^{-} = \Psi_{\mathrm{f}}^{-1}(Rq_{\mathrm{s}}^{+})\,\Theta\gamma_{\mathrm{s}}^{-} \tag{I.55}$$

where

$$\Theta := \begin{bmatrix} 0 \\ \begin{bmatrix} \gamma_{0,\mathrm{f}} \\ \frac{\partial p_{\mathrm{COM}}^{\mathrm{h}}}{\partial q} \\ -\sqrt{\left(\dot{p}_{\mathrm{COM}}^{\mathrm{v}}(0)\right)^2 + 2g_0\left(p_{\mathrm{COM}}^{\mathrm{v}}(0) - p_{\mathrm{COM}}^{\mathrm{v,d}}\right)} \end{bmatrix} \Big|_{q_{\mathrm{s}}^{-}} \Psi_{\mathrm{s}}^{-1}(q_{\mathrm{s}}^{-}) \begin{bmatrix} 0 \\ 1 \end{bmatrix} \end{bmatrix}. \tag{I.56}$$

As a consequence of the rigid impact model, the velocity at the beginning of the stance phase is

$$q_{\mathrm{s}}^{+} := R\pi_{\dot{q}}\,\Pi(q_{e,\mathrm{f}}^{-}) \begin{bmatrix} D_e(q_{e,\mathrm{f}}^{-}) \\ 0 \end{bmatrix} \Psi_{\mathrm{f}}^{-1}(Rq_{\mathrm{s}}^{+})\,\Theta\gamma_{\mathrm{s}}^{-}. \tag{I.57}$$

where $\Pi(q_e)$ is defined in (2.15). Hence,

$$\gamma_{\mathrm{s}}^{+} = \delta_{\mathrm{zero}}\gamma_{\mathrm{s}}^{-} \tag{I.58}$$

where

$$\delta_{\mathrm{zero}} := \gamma_{0,\mathrm{s}}\,R\,\pi_{\dot{q}}\,\Pi(q_{e,\mathrm{f}}^{-}) \begin{bmatrix} D_e(q_{e,\mathrm{f}}^{-}) \\ 0 \end{bmatrix} \Psi_{\mathrm{f}}^{-1}(Rq_{\mathrm{s}}^{+})\,\Theta. \tag{I.59}$$

Define $\zeta_{\mathrm{s},2} := \frac{1}{2}(\gamma_{\mathrm{s}})^2$. The Poincaré map is

$$\rho(\zeta_{\mathrm{s},2}^{-}) := \delta_{\mathrm{zero}}^2\zeta_{\mathrm{s},2}^{-} - V_{\mathrm{zero}}(\zeta_{\mathrm{s},2}^{-}) \tag{I.60}$$

where

$$V_{\mathrm{zero}}(\zeta_{\mathrm{s},2}^{-}) := -\int_{\theta_{\mathrm{s}}^{+}}^{\theta_{\mathrm{s}}^{-}} \frac{\kappa_{2,\mathrm{s}}(\theta, \alpha_{\mathrm{s}}(\sqrt{2\zeta_{\mathrm{s},2}^{-}}))}{\kappa_{1,\mathrm{s}}(\theta, \alpha_{\mathrm{s}}(\sqrt{2\zeta_{\mathrm{s},2}^{-}}))}\,d\theta. \tag{I.61}$$

Unfortunately, this map is not LTI as it was in walking since V_{zero} depends upon $\zeta_{\mathrm{s},2}^{-}$. The existence of a fixed point $\zeta_{\mathrm{s},2}^{*}$ of (I.60) is guaranteed by the assumption of periodicity. The fixed point satisfies

$$\zeta_{\mathrm{s},2}^{*} = -\frac{V_{\mathrm{zero}}\left(\zeta_{\mathrm{s},2}^{*}\right)}{1 - \delta_{\mathrm{zero}}^2} \tag{I.62}$$

and may be calculated numerically. Linearization about the fixed point yields

$$\left.\frac{d\rho}{d\zeta_{\mathrm{s},2}^{-}}\right|_{\zeta_{\mathrm{s},2}^{*}} = \delta_{\mathrm{zero}}^{2} - \left.\frac{\partial V_{\mathrm{zero}}(\zeta_{\mathrm{s},2}^{-})}{\partial \zeta_{\mathrm{s},2}^{-}}\right|_{\zeta_{\mathrm{s},2}^{*}}. \tag{I.63}$$

Hence, the fixed point (I.62) will be locally asymptotically stable if

$$\left|\left.\frac{d\rho}{d\zeta_{\mathrm{s},2}^{-}}\right|_{\zeta_{\mathrm{s},2}^{*}}\right| < 1. \tag{I.64}$$

I.6 Technical issues to be addressed

The work of this appendix represents the beginnings of a framework for the control of running in a class of planar biped robots. The next key steps in the development will include 1) careful definition of a solution to the system as modeled by Σ_{s} and Σ_{f} and 2) investigation of the assumptions on the output parameters α_{s} and α_{f} given by PC1)–PC3). Other technical issues will likely arise as these issues are addressed.

BIBLIOGRAPHY

BIBLIOGRAPHY

[ADN01] J. Adolfsson, H. Dankowicz, and A. Nordmark, *3D passive walkers: finding periodic gaits in the presence of discontinuities*, Nonlinear Dynamics **24** (2001), no. 2, 205–229.

[AF99] Y. Aoustin and A Formal'sky, *Design of reference trajectory to stabilize desired nominal cyclic gait of a biped*, Proc. of the First Workshop on Robot Motion and Control, Kiekrz, Poland, June 1999, pp. 159–164.

[Åst03] K.J. Åström, *Åström's homepage*, 2003, `http://www.control.lth.se/~kja/`.

[Bab98] V. I. Babitsky, *Theory of vibro-impact systems and applications*, Foundations of Engineering Mechanics, Springer, Berlin, 1998.

[BAK99] R. Burridge, Rizzi A., and D. Koditschek, *Sequential composition of dynamically dexterous robot behaviors*, International Journal of Robotics Research **18** (1999), no. 6, 534–555.

[Ban86] S.P. Banks, *Control systems engineering*, Prentice Hall, Englewood Cliffs, 1986.

[Bar84] Jonathan Barnes (ed.), *The complete works of aristotle: the revised oxford translation*, Bollingen Series LXXI, vol. 1, ch. Progression of Animals, Princeton University Press, 1984.

[BB98] S.P. Bhat and D.S. Bernstein, *Continuous finite-time stabilization of the translational and rotational double integrators*, IEEE Transactions on Automatic Control **43** (1998), no. 5, 678–682.

[BB00] ———, *Finite-time stability of continuous autonomous systems*, SIAM J. Contr. Optim. **38** (2000), 751–766.

[Ber03] K. Berns, *The walking machine catalogue*, 2003, `http://www.clawar.com/`.

[Béz72] P. Bézier, *Numerical control: Mathematics and applications*, John Wiley & Sons, New York, 1972.

[BF98] M.D. Berkemeier and R.S. Fearing, *Sliding and hopping gaits for the underactuated acrobot*, IEEE Transactions on Robotics and Automation **14** (1998), no. 4, 629–634.

[BF99] ———, *Tracking fast inverted trajectories of the underactuated acrobot*, IEEE Transactions on Robotics and Automation **15** (1999), no. 4, 740–750.

[BH95] G. Boone and J. Hodgins, *Reflexive responses to slipping in bipedal running robots*, Proc. of the IEEE/RSJ International Conference on Intelligent Robots and Systems, Pittsburgh, PA, 1995, pp. 158–164.

[BK00] C.E. Bauby and A.D. Kuo, *Active control of lateral balance in human walking*, Journal of Biomechanics **33** (2000), no. 11, 1433–1440.

[BKK90] M. Bühler, D. E. Koditschek, and P.J. Kindlmann, *A family of robot control strategies for intermittent dynamical environments*, IEEE Control Systems Magazine **10** (1990), no. 2, 16–22.

[Boo75] W.M. Boothby, *An introduction to differentiable manifolds and riemannian geometry*, Academic Press, New York, 1975.

[BRM92] A.M. Bloch, M. Reyhanoglu, and N.H. McClamroch, *Control and stabilization of nonholonomic dynamic systems*, IEEE Transactions on Automatic Control **37** (1992), no. 11, 1746–1757.

[Bro96] B. Brogliato, *Nonsmooth impact dynamics: Models, dynamics and control*, Lecture Notes in Control and Information Sciences, vol. 220, Springer, London, 1996.

[BT86] G. Bekey and R. Tomovic, *Robot control by reflex actions*, Proc. of the IEEE International Conference on Robotics and Automation, San Francisco, CA, April 1986, pp. 240–247.

[CA97] G. Cabodevilla and G. Abba, *Quasi optimal gait for a biped robot using genetic algorithm*, Proc. of the IEEE International Conference on Systems, Man and Cybernetics, Computational Cybernetics and Simulations, Orlando, FL, October 1997, pp. 3960–3965.

[CA01] C. Chevallereau and Y. Aoustin, *Optimal reference trajectories for walking and running of a biped robot*, Robotica **19** (2001), no. 5, 557–569.

[CAA+02] C. Chevallereau, G. Abba, Y. Aoustin, F. Plestan, E.R. Westervelt, C. Canduas-de Wit, and J.W. Grizzle, *Rabbit: A testbed for advanced control theory*, To appear in IEEE Control Systems Magazine; submitted September, 2002. (2002).

[CB87] R.E. Carlton and S.J. Bartholet, *The evolution of the application of mobile robotics to nuclear facility operations and maintenance*, Proc. of the IEEE International Conference on Robotics and Automation, Raleigh, NC, April 1987, pp. 720–726.

[CCS00] L. Chong, E. Culotta, and A. Sugden, *On the move*, Science **288** (2000), 79–106.

[Che84] C.T. Chen, *Linear system theory and design*, Oxford, New York, 1984.

[Che03a] C. Chevallereau, *ROBEA: Robotics and artificial entities*, 2003, `http://www-lag.ensieg.inpg.fr/PRC-Bipedes/English/`.

[Che03b] ———, *Time-scaling control for an underactuated biped robot*, IEEE Transactions on Robotics and Automation **19** (2003), no. 2, 362–368.

[CJ71] C.K. Chow and D.H. Jacobson, *Studies of human locomotion via optimal programming*, Mathematical Biosciences **10** (1971), 239–306.

[CMI99] M. Conditt and F. Mussa-Ivaldi, *Central representation of time during motor learning*, Proceedings of the National Academy of Sciences of the United States of America **96** (1999), 11625–11630.

[Cra89] J.J. Craig, *Introduction to robotics: mechanics and control*, Addison-Wesley, Reading, MA, 1989.

[CS93] C.K. Chen and N. Sreenath, *Control of coupled spatial two-body system with nonholonomic constraints*, Proc. IEEE International Conference on Decision and Control, San Antonio, TX, 1993, pp. 949–954.

[CS00] C. Chevallereau and P. Sardain, *Design and actuation optimization of a 4 axes biped robot for walking and running*, Proc. of the IEEE International Conference on Robotics and Automation, San Francisco, CA, April 2000, pp. 3365–3370.

[CWR01] S.H. Collins, M. Wisse, and A. Ruina, *A three-dimensional passive-dynamic walking robot with two legs and knees*, International Journal of Robotics Research **20** (2001), no. 7, 607–615.

[DFF+00] M. Dickinson, C. Farley, R. Full, M. Koehel, R. Kram, and S. Lehman, *How animals move: An integrative view*, Science **288** (2000), 100–106.

[DGMS94] S. Diop, J.W. Grizzle, P.E. Moraal, and A. Stefanopoulou, *Interpolation and numerical differentiation for observer design*, Proc. of the American Control Conference, Baltimore, MD, June 1994, pp. 1329–1333.

[EG94] B. Espiau and A. Goswami, *Compass gait revisited*, Proc. of the IFAC Symposium on Robot Control, Capri, Italy, September 1994, pp. 745–846.

[Esp97] B. Espiau, *Bip: a joint project for the development of an anthropomorphic biped robot*, Proc. of the International Conference on Advanced Robotics, Monterey, CA, July 1997, pp. 267–272.

[FGL94] C. Fernandes, L. Gurvits, and Z. Li, *Near-optimal nonholonomic motion planning for a system of coupled rigid bodies*, IEEE Transactions on Automatic Control **39** (1994), no. 3, 450–463.

[FK98] Y. Fujimoto and A. Kawamura, *Simulation of an autonomous biped walking robot including environmental force interaction*, IEEE Robotics and Automation Magazine (1998), 33–42.

[FK99] R. Full and D. Koditschek, *Templates and anchors: Neuromechanical hypotheses of legged locomotion on land*, Journal of Experimental Biology **202** (1999), 3325–3332.

[FM86] J. Furusho and M. Masubuchi, *Control of a dynamical biped locomotion system for steady walking*, Journal of Dynamic Systems, Measurement, and Control **108** (1986), 111–118.

[FOK98] Y. Fujimoto, S. Obata, and A. Kawamura, *Robust biped walking with active interaction control between foot and ground*, Proc. of the IEEE International Conference on Robotics and Automation, Leuven, Belgium, May 1998, pp. 2030–2035.

[FS90] J. Furusho and A. Sano, *Sensor-based control of a nine-link biped*, International Journal of Robotics Research **9** (1990), no. 2, 83–98.

[GAP99] J.W. Grizzle, G. Abba, and F. Plestan, *Proving asymptotic stability of a walking cycle for a five dof biped robot model*, 2nd Int. Conf. on Climbing and Walking Robots, CLAWAR-99, Portsmouth, U.K., September 1999, pp. 69–81.

[GAP01] ———, *Asymptotically stable walking for biped robots: Analysis via systems with impulse effects*, IEEE Transactions on Automatic Control **46** (2001), 51–64.

[GCR00] M. Garcia, A. Chatterjee, and A. Ruina, *Efficiency, speed, and scaling of two-dimensional passive-dynamic walking*, Dynamics and Stability of Systems **15** (2000), no. 2, 75–99.

[GCRC98] M. Garcia, A. Chatterjee, A. Ruina, and M. Coleman, *The simplest walking model: stability, complexity and scaling*, ASME Journal of Biomechanical Engineering **120** (1998), no. 2, 281–288.

[GEK96] A. Goswami, B. Espiau, and A. Keramane, *Limit cycles and their stability in a passive bipedal gait*, Proc. of the IEEE International Conference on Robotics and Automation, Minneapolis, MN., April 1996, pp. 246–251.

[GFLZ94] A.A. Grishin, A.M. Formal'sky, A.V. Lensky, and S.V. Zhitomirsky, *Dynamical walking of a vehicle with two telescopic legs controlled by two drives*, International Journal of Robotics Research **13** (1994), no. 2, 137–147.

[GJ95] J. Guckenheimer and S. Johnson, *Planar hybird systems*, Hybrid Systems II, Lecture Notes in Computer Science, Springer-Verlag, 1995, pp. 203–225.

[GLP00] M. Gienger, K. Löffler, and F. Pfeiffer, *A biped robot that jogs*, Proc. of the IEEE International Conference on Robotics and Automation, San Francisco, CA, April 2000, pp. 3334–3339.

[Gol60] W. Goldsmith, *Impact: the theory and physical behaviour of colliding solids*, Arnold, London, 1960.

[Gos99] A. Goswami, *Postural stability of biped robots and the foot-rotation indicator (FRI) point*, International Journal of Robotics Research **18** (1999), no. 6, 523–533.

[GPS02] H. Goldstein, C. Poole, and J. Safko, *Classical mechanics*, third ed., Addison-Wesley, San Francisco, 2002.

[Gri03] J.W. Grizzle, *Jessy Grizzle's publications*, 2003, `http://www.eecs.umich.edu/~grizzle/papers/robotics.html`.

[HAF00] Y. Hasegawa, T. Arakawa, and T. Fukuda, *Trajectory generation for biped locomotion*, Mechatronics **10** (2000), no. 1–2, 67–89.

[Hai86] V.T. Haimo, *Finite time controllers*, SIAM J. Contr. Optim. **24** (1986), no. 4, 760–770.

[Har99] M.W. Hardt, *Multibody dynamical algorithms, numerical optimal control, with detailed studies in the control of jet engine compressors and biped walking*, Ph.D. thesis, University of California, San Diego, 1999.

[Hat76] H. Hatze, *The complete optimization of a human motion*, Mathematical Biosciences **28** (1976), 99–135.

[HB98] G.W. Howell and J. Baillieul, *Simple controllable walking mechanisms which exhibit bifurcations*, Proc. IEEE International Conference on Decision and Control, Tampa, FL, December 1998, pp. 3027–3032.

[HHHT98] K. Hirai, M. Hirose, Y. Haikawa, and T. Takenake, *The development of Honda humanoid robot*, Proc. of the IEEE International Conference on Robotics and Automation, Leuven, Belgium, May 1998, pp. 1321–1326.

[HKK+99] Q. Huang, S. Kajita, N. Koyachi, K. Kaneko, K. Yokoi, H. Arai, Komoriya K., and K. Tanie, *A high stability, smooth walking pattern for a biped robot*, Proc. of the IEEE International Conference on Robotics and Automation, Detroit, MI, May 1999, pp. 65–71.

[HM94] Y. Hürmüzlü and D.B. Marghitu, *Rigid body collisions of planar kinematic chains with multiple contact points*, International Journal of Robotics Research **13** (1994), no. 1, 82–92.

[HNK+98] S. Hashimoto, S. Narita, H. Kasahara, K. Shirai, T. Kobayashi, A. Takanishi, S. Sugano, J. Yamaguchi, H. Sawada, H. Takanobu, K. Shibuya, T. Morita, T. Kurata, N. Onoe, K. Ouchi, T. Noguchi, Y. Niwa, S. Nagayama, H. Tabayashi, I. Matsui, M. Obata, H. Matsuzaki, A. Murasugi, T. Kobayashi, S. Haruyama, T. Okada, Y. Hidaki, Y. Taguchi, K. Hoashi, E. Morikawa, Y. Iwano, D. Araki, J. Suzuki, M. Yokoyama, I. Dawa, D. Nishino, S. Inoue, T. Hirano, E. Soga, S. Gen, T. Yanada, K. Kato, S. Sakamoto, Y. Ishii, S. Matsuo, Y. Yamamoto, K. Sato, T. Hagiwara, T. Ueda, N. Honda, K. Hashimoto, T. Hanamoto, S. Kayaba, T. Kojima, H. Iwata, H. Kubodera, R. Matsuki, T. Nakajima, K. Nitto, D. Yamamoto, Y. Kamizaki, S. Nagaike, Y. Kunitake, and S. Morita, *Humanoid robots in Waseda University-Hadaly-2 and WABIAN*, Autonomous Robots **12** (1998), no. 1, 25–38.

[Hon03] Honda Corporation, *ASIMO website*, 2003, `http://world.honda.com/ASIMO/`.

[Hür93a] Y. Hürmüzlü, *Dynamics of bipedal gait—part 1: objective functions and the contact event of a planar five-link biped*, Journal of Applied Mechanics **60** (1993), 331–336.

[Hür93b] ———, *Dynamics of bipedal gait—part 2: stability analysis of a planar five-link biped*, Journal of Applied Mechanics **60** (1993), 337–343.

[IM88] A. Isidori and C. Moog, *On the nonlinear equivalent of the notion of transmission zeros*, Proc. of the IIASA Conference: Modeling and Adaptive Control (Berlin) (Byrnes C. and A. Kurzhanski, eds.), Springer-Verlag, 1988, pp. 146–157.

[IMT00] K. Ito, F. Matsuno, and R. Takahashi, *Underactuated crawling robot*, Proc. of the IEEE International Conference on Intelligent Robotos and Systems, Takamatsu, Japan., October–November 2000, pp. 1684–1689.

[Isi95] A. Isidori, *Nonlinear control systems: An introduction*, third ed., Springer-Verlag, Berlin, 1995.

[Jua00] J.G. Juang, *Fuzzy neural network approaches for robotic gait synthesis*, IEEE Transactions on Systems, Man, and Cybernetics **30** (2000), no. 4, 594–601.

[Kaw99] M. Kawato, *Internal models for motor control and trajectory planning*, Current Opinion in Neurobiology **9** (1999), 718–727.

[KB91] D.D. Koditschek and M. Buhler, *Analysis of a simplified hopping robot*, International Journal of Robotics Research **10** (1991), no. 6, 587–605.

[Kha96] H.K. Khalil, *Nonlinear systems - 2nd edition*, Prentice Hall, Upper Saddle River, 1996.

[KKK+01] S. Kajita, F. Kanehiro, K. Kaneko, K. Yokoi, and H. Hirukawa, *The 3D linear inverted pendulum mode: a simple modeling for a biped walking pattern generation*, Proc. of the IEEE/RSJ International Conference on Intelligent Robots and Systems, Maui, HI, November 2001, pp. 239–246.

[KKK+02a] S. Kajita, F. Kanehiro, K. Kaneko, K. Fujiwara, K. Yokoi, and H. Hirukawa, *A realtime pattern generator for biped walking*, Proc. of the IEEE International Conference on Robotics and Automation, Washington, D.C., May 2002, pp. 31–37.

[KKK+02b] K. Kaneko, F. Kanehiro, S. Kajita, K. Yokoyama, K. Akachi, T. Kawasaki, S. Ota, and T. Isozumi, *Design of prototype humanoid robotics platform for HRP*, Proc. of the IEEE/RSJ International Conference on Intelligent Robots and Systems, Lausanne, Switzerland, October 2002, pp. 2431–2436.

[KM84] R. Katoh and M. Mori, *Control method of biped locomotion giving asymptotic stability of trajectory*, Automatica **20** (1984), no. 4, 405–414.

[Kri90] P.S. Krishnaprasad, *Geometric phases and optimal reconfiguration for multibody systems*, Proc. of the American Control Conference, Philadelphia, PA, 1990, pp. 2440–2444.

[KT72] I. Kato and H. Tsuiki, *The hydraulically powered biped walking machine with a high carrying capacity*, Proc. of the fourth International Symposium on External Control of Human Extremities, Dubrovnik, Yugoslavia, September 1972, pp. 410–421.

[KT96] S. Kajita and K. Tani, *Experimental study of biped dynamic walking*, IEEE Control Systems Magazine **16** (1996), no. 1, 13–19.

[Kuo99] A.D. Kuo, *Stabilization of lateral motion in passive dynamic walking*, International Journal of Robotics Research **18** (1999), no. 9, 917–930.

[KW89] V.R. Kumar and K.J. Waldron, *A review of research on walking vehicles*, The robotics review 1 (O. Khatib, J.J. Craig, and T. Lozano-Pérez, eds.), MIT Press, 1989, pp. 243–266.

[KYK92] S. Kajita, T. Yamaura, and A. Kobayashi, *Dynamic walking control of biped robot along a potential energy conserving orbit*, IEEE Transactions on Robotics and Automation **8** (1992), no. 4, 431–437.

[LR68] R.A. Liston and Mosher R.S., *A versatile walking truck*, Proceedings of the Transportation Engineering Conference., Institution of Civil Engineers, London, 1968.

[LYT00] H. Lim, Y. Yamamoto, and A. Takanishi, *Control to realize human-like walking of a biped humanoid robot*, Proc. of the IEEE International Conference on Systems, Man and Cybernetics, Computational Cybernetics and Simulations, Nashville, TN, June 2000, pp. 3271–3276.

[McG90] T. McGeer, *Passive dynamic walking*, International Journal of Robotics Research **9** (1990), no. 2, 62–82.

[McG93] ———, *Dynamics and control of bipedal locomotion*, Journal of Theoretical Biology **166** (1993), no. 3, 277–314.

[Mil94] W.T. Miller, *Real-time neural network control of a biped walking robot*, IEEE Control Systems Magazine **14** (1994), no. 1.

[MLS93] R.M. Murray, Z. Li, and S. Sastry, *A mathematical introduction to robotic manipulation*, CRC Press, Boca Raton, 1993.

[MM94] L. Magdalena and F. Monasterio, *Learning gait patterns for the fuzzy synthesis of piped walk*, NAFIPS/IFIS/NASA '94, December 1994, pp. 248–250.

[MMAN95] K. Mitobe, N. Mori, K. Aida, and Y. Nasu, *Nonlinear feedback control of a biped walking robot*, Proc. of the IEEE International Conference on Robotics and Automation, Nagoya, Japan, May 1995, pp. 2865–2870.

[MO96] D.W. Marhefka and D. Orin, *Simulation of contact using a nonlinear damping model*, Proc. of the IEEE International Conference on Robotics and Automation, Minneapolis, MN., April 1996, pp. 1662–1668.

[MS84] H. Miura and I. Shimoyama, *Dynamic walk of a biped*, International Journal of Robotics Research **3** (1984), no. 2, 60–74.

[MS01] T.G. McGee and M.W. Spong, *Trajectory planning and control of a novel walking biped*, IEEE International Conference on Control Applications, Mexico City, Mexico, September 2001, pp. 1099–1104.

[NFK00] J. Nakanishi, T. Fukuda, and D. Koditschek, *A brachiating robot controller*, IEEE Transactions on Robotics and Automation **16** (2000), no. 2, 109–123.

[Nv89] H. Nijmeijer and van der Schaft,A. J., *Nonlinear dynamical control systems*, Springer-Verlag, Berlin, 1989.

[OTS01] K. Ono, R. Takahashi, and T. Shimada, *Self-excited walking of a biped mechanism*, International Journal of Robotics Research **20** (2001), no. 12, 953–966.

[OYI01] K. Ono, K. Yamamoto, and A. Imadu, *Control of giant swing motion of a two-link horizontal bar gymnastic robot*, Advanced Robotics **15** (2001), no. 4, 449–465.

[PCT+01] J.E. Pratt, M.C. Chee, A. Torres, P. Dilworth, and G.A. Pratt, *Virtual model control: an intuitive approach for bipedal locomotion*, International Journal of Robotics Research **20** (2001), no. 2, 129–143.

[PGWA01] F. Plestan, J.W. Grizzle, E.R. Westervelt, and G. Abba, *Stable walking of a 7-dof biped robot*, Accepted for publication in IEEE Transactions on Robotics and Automation, Submitted February 2001, See [Gri03] for a preprint.

[PK98] J.H. Park and K.D. Kim, *Biped robot walking using gravity-compensated inverted pendulum mode and computed torque control*, Proc. of the IEEE International Conference on Robotics and Automation, Leuven, Belgium, May 1998, pp. 3528–3533.

[PLG02] F. Pfeiffer, K. Löffler, and M. Gienger, *The concept of Jogging JOHNNIE*, Proc. of the IEEE International Conference on Robotics and Automation, Washington, D.C., May 2002, pp. 3129–3135.

[PP98] J.E. Pratt and G.A. Pratt, *Intuitive control of a planar bipedal walking robot*, Proc. of the IEEE International Conference on Robotics and Automation, Leuven, Belgium, May 1998, pp. 2014–2021.

[Pra00] J.E. Pratt, *Exploiting inherent robustness and natural dynamics in the control of bipedal walking robots*, Ph.D. thesis, MIT, June 2000.

[PW95] G.A. Pratt and M.M. Williamson, *Series elastic actuators*, Proc. of the IEEE/RSJ International Conference on Intelligent Robots and Systems, Pittsburgh, PA, August 1995, pp. 399–406.

[RA90] D.F. Rogers and J.A. Adams, *Mathematical elements for computer graphics*, second ed., McGraw-Hill, New York, 1990.

[Rai84] M.H. Raibert, *Hopping in legged systems—modeling and simulation for the two-dimensional one-legged case*, IEEE Transactions on Systems, Man, and Cybernetics **14** (1984), no. 3, 451–463.

[Rai86] ———, *Legged robots that balance*, MIT Press, Mass., 1986.

[RB01a] M. Rostami and G. Bessonnet, *Sagittal gait of a biped robot during the single support phase. part 1: passive motion*, Robotica **19** (2001), 163–176.

[RB01b] ———, *Sagittal gait of a biped robot during the single support phase. part 2: optimal motion*, Robotica **19** (2001), 241–253.

[RCdWG98] L. Roussel, C. Canudas-de Wit, and A. Goswami, *Generation of energy optimal complete gait cycles for biped robots*, Proc. of the IEEE International Conference on Robotics and Automation, Leuven, Belgium, May 1998, pp. 2036–2041.

[RFAGCL00] J.A. Rosas-Flores, J. Alvarez-Gallegos, and R. Castro-Linares, *Stabilization of a class of underactuated systems*, Proc. IEEE International Conference on Decision and Control, Sydney, Australia, December 2000, pp. 2168–2173.

[RK96] A. Rizzi and D. Koditschek, *An active visual estimator for dexterous manipulation*, IEEE Transactions on Robotics and Automation **12** (1996), no. 5, 697–713.

[Ros94] M.E. Rosheim, *Robot evolution: the development of anthrobotics*, Wiley, New York, 1994.

[Rou98] L. Roussel, *Génération de trajectoires de marche optimales pour un robot bipède*, Ph.D. thesis, Institut National Polytechnique - Grenoble - France, November 1998.

[RP] A. Ruina and R. Pratap, *Introduction to statics and dynamics*, Oxford University Press, to be published, available at `http://www.tam.cornell.edu/~ruina/Book/`.

[RTT93] M.H. Raibert, S. Tzafestas, and C. Tzafestas, *Comparative simulation study of three control techniques applied to a biped robot*, Proc. of the IEEE International Conference on Systems, Man and Cybernetics Systems Engineering in the Service of Humans, Le Touquet, France, October 1993, pp. 494–502.

[Rus83] M. Russell, *ODEX I: the first functionoid*, Robotics Age **5** (1983), no. 5, 12–18.

[RvdSMK99] M. Reyhanoglu, A. van der Schaft, N.H. McClamroch, and I. Kolmanovsky, *Dynamics and control of a class of underactuated mechanical systems*, IEEE Transactions on Automatic Control **44** (1999), no. 9, 1663–1671.

[Ryg93] L.A. Rygg, *Mechanical horse*, US Patent (1893), #491,927.

[SB98] A.C. Smith and M.D. Berkemeier, *The motion of a finite-width wheel in 3d*, Proc. of the IEEE International Conference on Robotics and Automation, Leuven, Belgium, May 1998, pp. 2345–2350.

[SB02] M.W. Spong and F. Bullo, *Controlled symmetries and passive walking*, IFAC 2002, Barcelona, Spain, July 2002.

[Sch98] W.J. Schwind, *Spring loaded inverted pendulum running: A plant model*, Ph.D. thesis, University of Michigan, 1998.

[SF90] A. Sano and J. Furusho, *Realization of natural dynamic walking using the angular momentum information*, Proc. of the IEEE International Conference on Robotics and Automation, Cincinnati, OH., May 1990, pp. 1476–1481.

[SG92] C.L. Shih and W.A. Gruver, *Control of a biped robot in the double-support phase*, IEEE Transactions on Systems, Man, and Cybernetics **22** (1992), no. 4, 729–735.

[SKI99] M. Sampei, H. Kiyota, and M. Ishikawa, *Control strategies for mechanical systems with various constraints-control of non-holonomic systems*, Proc. of the IEEE International Conference on Systems, Man and Cybernetics, Tokyo, Japan, October 1999, pp. 158–165.

[Spo95] M.W. Spong, *The swing up control problem for the acrobot*, IEEE Control Systems Magazine **15** (1995), no. 1, 49–55.

[Spo99] _____, *Passivity based control of the compass gait biped*, Proc. of IFAC World Congress, Beijing, China, July 1999.

[SSK98] U. Saranli, W. Schwind, and D. Koditschek, *Toward the control of a multi-jointed, monoped runner*, Proc. of the IEEE International Conference on Robotics and Automation, Leuven, Belgium, May 1998, pp. 2676–2682.

[SV89] M.W. Spong and M. Vidyasagar, *Robot dynamics and control*, John Wiley & Sons, New York, 1989.

[SW89] S. Song and K.J. Waldron, *Machines that walk: The adaptive suspension vehicle*, MIT Press Series in Artificial Intelligence, MIT Press, 1989.

[TGE97] B. Thuilot, A. Goswami, and B. Espiau, *Bifurcation and chaos in a simple passive bipedal gait*, Proc. of the IEEE International Conference on Robotics and Automation, Albuquerque, N.M., April 1997, pp. 792–798.

[TIYK85] A. Takanishi, M. Ishida, Y. Yamazaki, and I. Kato, *The realization of dynamic walking by the biped walking robot WL-10RD*, Proc. of the International Conference on Advanced Robotics, September 1985, pp. 459–466.

[Tod85] D.J. Todd, *Walking machines: an introduction to legged robotics*, Kogan Page, 1985.

[TTN+99] H. Takanobu, H. Tabayashi, S. Narita, A. Takanishi, E. Guglielmelli, and P. Dario, *Remote interaction between human and humanoid robot*, Autonomous Robots **25** (1999), no. 4, 371–385.

[van98] R.Q. van der Linde, *Active leg compliance for passive walking*, Proc. of the IEEE International Conference on Robotics and Automation, Leuven, Belgium, May 1998, pp. 2339–2344.

[VBSS90] M. Vukobratović, B. Borovac, D. Surla, and D. Stokic, *Biped locomotion*, Springer-Verlag, Berlin, 1990.

[vE01] W. van Egmond, *Amoebas are more than just blobs*, Micscape Magazine (2001), availble at `http://www.microscopy-uk.org.uk/mag/artsep01/amoeba.html`.

[vS99] O. von Stryk, *Dircol user's guide*, Technische Universität Müchen, Zentrum Mathematik (SCB), Lehrstuhl M2 Höhere Mathematik und Numerische Mathematik, D-80290, Müchen, Germany, 2.1 ed., 1999.

[WGCdW03] E.R. Westervelt, J.W. Grizzle, and C. Canudas de Wit, *Switching and PI control of walking motions of planar biped walkers*, IEEE Transactions on Automatic Control **48** (2003), no. 2, 308–312.

[WGK03] E.R. Westervelt, J.W. Grizzle, and D. Koditschek, *Hybrid zero dynamics of planar biped walkers*, IEEE Transactions on Automatic Control **48** (2003), no. 1, 42–56.

[YMH98] H. Ye, A.N. Michel, and L. Hou, *Stability theory for hybrid dynamical systems*, IEEE Transactions on Automatic Control **43** (1998), no. 4, 461–474.

[YSIT99] J. Yamaguchi, E. Soga, S. Inoue, and A. Takanishi, *Development of a bipedial humanoid robot: control method of whole body cooperative dynamic biped walking*, Proc. of the IEEE International Conference on Robotics and Automation, Detroit, MI, May 1999, pp. 368–374.